INVESTIGATION OF AIRFOIL DYNAMIC STALL AND ITS INFLUENCE ON HELICOPTER CONTROL LOADS

Franklin O. Carta, et al

United Aircraft Research Laboratories

Prepared for:

Army Air Mobility Research and Development Laboratory

September 1972

AD

USAAMRDL TECHNICAL REPORT 72-51

INVESTIGATION OF AIRFOIL DYNAMIC STALL AND ITS INFLUENCE ON HELICOPTER CONTROL LOADS

By

F. O. Carta
G. L. Commerford
R. G. Carlson
R. H. Blackwell

September 1972

EUSTIS DIRECTORATE
U. S. ARMY AIR MOBILITY RESEARCH AND DEVELOPMENT LABORATORY
FORT EUSTIS, VIRGINIA

CONTRACT DAAJ02-71-C-0003
UNITED AIRCRAFT CORPORATION RESEARCH LABORATORIES
EAST HARTFORD, CONNECTICUT

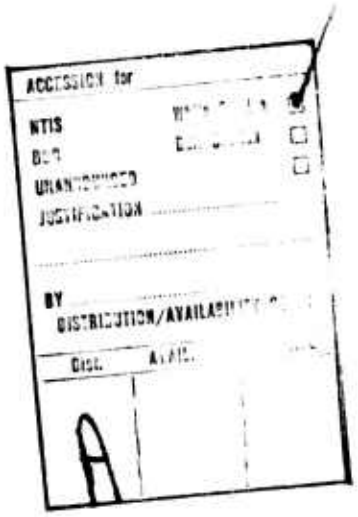

DISCLAIMERS

The findings in this report are not to be construed as an official Department of the Army position unless so designated by other authorized documents.

When Government drawings, specifications, or other data are used for any purpose other than in connection with a definitely related Government procurement operation, the United States Government thereby incurs no responsibility nor any obligation whatsoever; and the fact that the Government may have formulated, furnished, or in any way supplied the said drawings, specifications, or other data is not to be regarded by implication or otherwise as in any manner licensing the holder or any other person or corporation, or conveying any rights or permission, to manufacture, use, or sell any patented invention that may in any way be related thereto.

Trade names cited in this report do not constitute an official endorsement or approval of the use of such commercial hardware or software.

DISPOSITION INSTRUCTIONS

Destroy this report when no longer needed. Do not return it to the originator.

Unclassified
Security Classification

DOCUMENT CONTROL DATA - R & D

(Security classification of title, body of abstract and indexing annotation must be entered when the overall report is classified)

1. ORIGINATING ACTIVITY (Corporate author)	2a. REPORT SECURITY CLASSIFICATION
United Aircraft Research Laboratories United Aircraft Corporation East Hartford, Connecticut	Unclassified 2b. GROUP

3. REPORT TITLE

INVESTIGATION OF AIRFOIL DYNAMIC STALL AND ITS INFLUENCE ON HELICOPTER CONTROL LOADS

4. DESCRIPTIVE NOTES (Type of report and inclusive dates)

Final Report

5. AUTHOR(S) (First name, middle initial, last name)

Franklin O. Carta — Raymond G. Carlson
Gerard L. Commerford — Robert H. Blackwell

6. REPORT DATE	7a. TOTAL NO. OF PAGES	7b. NO. OF REFS
September 1972	206	31

8a. CONTRACT OR GRANT NO.	9a. ORIGINATOR'S REPORT NUMBER(S)
DAAJ02-71-C-0003 b. PROJECT NO. c. Task 1F162204A13904 d.	USAAMRDL Technical Report 72-51 9b. OTHER REPORT NO(S) (Any other numbers that may be assigned this report)

10. DISTRIBUTION STATEMENT

Approved for public release; distribution unlimited.

11. SUPPLEMENTARY NOTES	12. SPONSORING MILITARY ACTIVITY
	Eustis Directorate U.S. Army Air Mobility R&D Laboratory Fort Eustis, Virginia

13. ABSTRACT

Measurements were made of the unsteady normal force and pitching moment on an NACA 0012 airfoil model oscillated both sinusoidally and nonsinusoidally over a range of incidence angles, including a substantial penetration into stall. The sinusoidal normal force and pitching moment data were reduced and tabulated as functions of the angle of attack, the angular velocity parameter, and the angular acceleration parameter. This generalized form of the data was used to reconstruct the measured sinusoidal aerodynamic response of the model airfoil with excellent results. Additional correlations were made using nonsinusoidal pitch schedules which included periodic ramp changes in angle of attack and a flexured angular blade response to a one-per-rev sinusoidal incidence angle change typical of that for a helicopter blade. The agreement between predicted and measured normal force and moment loops was very good for the ramp motion. Integration of the nonsinusoidal moment loops to calculate aerodynamic damping in pitch has produced good agreement between predicted and measured results. Good agreement was also obtained between predicted and measured flexible blade response.

Scaling procedures describing aspect ratio and compressibility effects were derived and used to calculate full-scale unsteady normal force and moment coefficients from the unsteady model data. Correlation studies were performed to determine whether the incorporation of the unsteady aerodynamic data into an existing rotor aeroelastic analysis would provide an adequate method for predicting stall-flutter-induced control loads. The analysis was carried out for the NH-3A (S-61F) and CH-53A helicopter rotors and for a wind tunnel model rotor. Use of variable rotor inflow model and unsteady aerodynamics provided good correlation with torsional oscillations observed in test.

DD FORM 1 NOV 68 1473 REPLACES DD FORM 1473, 1 JAN 64, WHICH IS OBSOLETE FOR ARMY USE.

Ia

Unclassified
Security Classification

14. KEY WORDS	LINK A		LINK B		LINK C	
	ROLE	WT	ROLE	WT	ROLE	WT
Dynamic Stall Stall Flutter Rotor Blade Control Loads Rotor Aeroelasticity Unsteady Aerodynamics Oscillating Airfoil Experiment Helicopter Rotor Blades						

Tab

DEPARTMENT OF THE ARMY
U. S. ARMY AIR MOBILITY RESEARCH & DEVELOPMENT LABORATORY
EUSTIS DIRECTORATE
FORT EUSTIS, VIRGINIA 23604

This report has been reviewed by the Eustis Directorate, U.S. Army Air Mobility Research and Development Laboratory and is considered to be technically sound.

This research was performed to investigate airfoil dynamic stall and to study its influence on helicopter control loads. In reporting the results of this research, the authors have carefully defined the assumptions made to produce a reasonably tractable problem and have thoroughly documented the analytical and experimental procedures and results. The published results are thought to be among the most advanced practical treatments of the problem of stall-induced dynamic loading in the helicopter rotor.

The report is published for the dissemination of the results of the investigation and for the stimulation of research relative to stall phenomena. The program was conducted under the technical management of Mr. W. E. Nettles of the Aeromechanics Division of this Directorate.

IC

Task 1F162204A13904
Contract DAAJ02-71-C-0003
USAAMRDL Technical Report 72-51
September 1972

INVESTIGATION OF AIRFOIL DYNAMIC STALL AND ITS INFLUENCE ON HELICOPTER CONTROL LOADS

Final Report

by

F. O. Carta
G. L. Commerford
R. G. Carlson
R. H. Blackwell

Prepared by

United Aircraft Corporation
Research Laboratories
East Hartford, Connecticut

for

EUSTIS DIRECTORATE
U. S. ARMY AIR MOBILITY RESEARCH AND DEVELOPMENT LABORATORY
FORT EUSTIS, VIRGINIA

II

SUMMARY

Measurements were made of the unsteady normal force and pitching moment on an NACA 0012 airfoil model oscillated both sinusoidally and nonsinusoidally over a range of incidence angles, including a substantial penetration into stall. The sinusoidal normal force and pitching moment data were reduced and tabulated as functions of the angle of attack, the angular velocity parameter, and the angular acceleration parameter. This generalized form of the data was used to reconstruct the measured sinusoidal aerodynamic response of the model airfoil with excellent results. Additional correlations were made using nonsinusoidal pitch schedules which included periodic ramp changes in angle of attack and a flexured angular blade response to a one-per-rev sinusoidal incidence angle change typical of that for a helicopter blade. The agreement between predicted and measured normal force and moment loops was very good for the ramp motion. Integration of the nonsinusoidal moment loops to calculate aerodynamic damping in pitch has produced good agreement between predicted and measured results. Good agreement was also obtained between predicted and measured flexible blade response.

Scaling procedures describing aspect ratio and compressibility effects were derived and used to calculate full-scale unsteady normal force and moment coefficients from the unsteady model data. Correlation studies were performed to determine whether the incorporation of the unsteady aerodynamic data into an existing rotor aeroelastic analysis would provide an adequate method for predicting stall-flutter-induced control loads. The analysis was carried out for the NH-3A (S-61F) and CH-53A helicopter rotors and for a wind tunnel model rotor. Use of variable rotor inflow model and unsteady aerodynamics provided good correlation with torsional oscillations observed in test.

FOREWORD

This work was performed for the Eustis Directorate, U. S. Army Air Mobility Research and Development Laboratory, Fort Eustis, Virginia, under Contract DAAJ02-71-C-0003, DA Task 1F162204A13904. Technical monitor for the Army was Mr. William Nettles. The experimental work and the unsteady airfoil data analysis were performed at the United Aircraft Research Laboratories, East Hartford, Connecticut, by Messrs. F. O. Carta and G. L. Commerford. The helicopter rotor control load correlations were performed at the Sikorsky Aircraft Division of United Aircraft Corporation, Stratford, Connecticut, by Dr. R. G. Carlson and Mr. R. H. Blackwell.

TABLE OF CONTENTS

LIST OF ILLUSTRATIONS

LIST OF TABLES

LIST OF SYMBOLS

a	pitch axis location aft of leading edge, ft, Equation (3)
A	dimensionless angular velocity, Equation (4), or area under integral Equation (10)
b	airfoil semichord, ft, Equation (4)
B	dimensionless angular acceleration, Equation (5)
B_w	bandwidth, cps, Equation (28)
C	airfoil chord, ft, Equation (2), or mechanical damping per unit span, (ft-lb-sec/rad)/ft, Equation (34)
$C_{A,B,C}$	constants, Equation (16)
C_m	pitching moment coefficient, Equation (3)
$C_{m_{model}}$	model pitching moment coefficient
C_{m_o}	starting value of C_m, Equation (45)
C_{m_R}	real part of moment coefficient, Equation (6)
C_n	normal force coefficient, Equation (2)
C_n'	intermediate normal force scaling curve
$C_{n_{MAX}}$	maximum normal force coefficient
$C_{n_{model}}$	model normal force coefficient
$C_{n_{stall}}$	normal force coefficient at the stall angle
$C_{n_{stall,ss,model}}$	steady-state model normal force coefficient at the stall angle

$C_p = \frac{\Delta p}{q}$	pressure coefficient, Equation (11)
C_T/σ	rotor thrust coefficient-solidity ratio
f	frequency, cps
$f(\xi)$	dummy function, Equation (10)
f_{max}	highest harmonic frequency of interest, Equation (27)
F( )	function, Equation (20)
h_R	sampling rate of original data, samples/sec, Equation (23)
$h_{R_{ABS}}$	absolute sampling rate, samples/sec, Equation (22)
i	index, Equation (10)
I	airfoil mass moment of inertia in pitch per unit span, (ft-lb-sec^2/rad)/ft, Equation (34)
I_α	inertia parameter, rad^{-1}, Equation (36)
$k = b\omega/V$	reduced frequency, Equation (7)
k_1	reduced frequency of first harmonic
K	pitch spring stiffness per unit span, (ft-lb/rad)/ft, Equation (34)
K_n	normal force scaling parameter, Figure 45
L	number of samples per cycle of highest harmonic, Equation (27)
L_{ACT}	actual number of samples per cycle of highest harmonic, Equation (33)
m	total number of samples per channel, Equation (25)

M	Mach number, or applied aerodynamic moment per unit span, ft-lb/ft, Equation(34)
M_T	root torsional moment, in.-lb
n	index, Equation (51)
N	number, Equation (10)
N_c	number of channels, Equation (22)
p_L	lower surface static pressure, lb/ft^2 or $lb/in.^2$, Equation (2)
p_u	upper surface static pressure, lb/ft^2 or $lb/in.^2$, Equation (2)
$\Delta p = p_u - p_L$	static pressure difference, lb/ft^2 or $lb/in.^2$
$q = \frac{1}{2}\rho V^2$	dynamic pressure, lb/ft^2, Equation (2)
$\bar{r}$	dimensionless radial coordinate, local radius/R
R	rotor blade radius, ft
S_R	recording speed, in./sec, Equation (23)
S_P	playback speed, in./sec, Equation (23)
t	time, sec, Equation (1)
T	recording time, sec, Equation (26)
ΔT	time between samples, sec, Equation (23)
ΔT_{ABS}	absolute time between samples, sec, Equation (22)
T_o	applied torque per unit span, ft-lb/ft, Equation (34)
V	velocity, ft/sec, Equation (4)
W_i	Gaussian weighting factors, Equation (10)
x	chordwise coordinate, ft, Equation (2)

z	dimensionless chordwise station, Equation (12)
α	angle of attack, deg or rad, Equation (1)
α_M	mean angle of attack, deg or rad, Equation (1)
α_{OL}	angle of attack for zero lift, deg or rad, Equation (8)
α_R	real part of angle of attack, rad, Equation (6)
α_{sm}	steady-state stall angle for pitching moment coefficient, deg or rad, Equation (9)
α_{sn}	steady-state stall angle for normal force coefficient, deg or rad, Equation (8)
α_{TPP}	rotor tip-path-plane angle of attack, positive for rotor tilted back, Figure 68
$\bar{\alpha}$	angular amplitude, deg or rad, Equation (1)
$\beta = \dot{\alpha}$	angular velocity, rad/sec, Equation (41)
δ	logarithmic decrement, Equation (37)
δ_m	additive correction curve for pitching moment scaling, Figure 49
δ_n	additive correction curve for normal force scaling, Figure 47
Δ	determinant, Equation (18)
η	dimensionless chordwise variable, Equation (12)
θ_{75}	blade collective pitch angle at 0.75 span, deg, Figure 1
μ	rotor advance ratio
ξ	dimensionless chordwise variable, Equation (10)
Ξ_{α_2}	two-dimensional aerodynamic damping in pitch, Equation (6)

ρ	air density, lb sec^2/ft^4, Equation (35)
σ_E	edgewise stress, $lb/in.^2$, Figure 58
σ_F	flatwise stress, $lb/in.^2$, Figure 58
σ_m	pitching moment stall angle parameter, Equation (9)
σ_n	normal force stall angle parameter, Equation (8)
χ_{TPP}	wake skew angle, positive for streamlines below tip path plane, Figure 68
ψ	azimuth angle measured from downstream blade position, deg
ω	oscillatory frequency, rad/sec, Equation (1)
ω_α	natural torsional airfoil frequency, rad/sec, Equation (37)
$(\dot{\ })$	first derivative with respect to time
$(\ddot{\ })$	second derivative with respect to time

INTRODUCTION

Classical rotor theories are incapable of accurately predicting overall rotor performance characteristics in stall (References 1 through 7), nor can they predict the details of the rotor loading required for the definition of critical high-frequency vibratory loads. Such theories generally assume that two-dimensional, steady-state airfoil data are applicable and, further, that the inflow velocities induced at the rotor blades by the vortex system of the rotor are constant with respect to time and space. In an attempt to provide a more suitable analysis for application to the rotor stall situation, a study was performed at the United Aircraft Corporation (UAC), under USAAMRDL sponsorship, to integrate available two-dimensional, unsteady airfoil data into an existing rotor aeroelastic-variable inflow analysis (Reference 8). The data available for this purpose were those obtained from Reference 9 for airfoils executing pure sinusoidal pitch motion. Since rotor blades do not normally execute pure sinusoidal motion as they penetrate the stall regime, a unique feature of the expanded UAC analysis was the conversion of the available sinusoidal results to a more general nonsinusoidal form in which local section forces and moments are expressed in terms of instantaneous Mach number, angle of attack, α, angular velocity, A, and angular acceleration parameter, B. This conversion is required before section forces and moments associated with typical rotor blade angle-of-attack variations can be computed in a rational manner. Figure 1 shows a typical angle-of-attack variation for one rotor blade station along with the associated variation in angular velocity parameter. The angular velocity parameter has been shown (References 10 and 11, for example) to have an important influence on airfoil stall characteristics. The departure from pure sinusoidal motion is evident, particularly in the critical angular velocity parameter.

Reference 7 contained data similar to those of Reference 9 but at higher subsonic Mach numbers. Attempts were made to recast these compressible data in a more general form dependent on α, A, and B. However, the range of parameters tested in Reference 7 was too limited to permit this transformation. For this reason, the UAC rotor analysis developed in Reference 8 used the incompressible data of Reference 9 in conjunction with scaling laws to account approximately for compressibility. Although the accuracy of the analysis was compromised to a certain degree, its ability to predict a stall flutter type of response was successfully demonstrated. However, correlation of analytical and flight test data on the NH-3A helicopter indicated that the predicted stall flutter response occurred at rotor lifts higher than those measured in flight. Although

this correlation with NH-3A flight data was not good, a comparable correlation, using the same α, A, B technique, with model scale rotor data yielded excellent agreement (see Figure 12 of Reference 12).

To achieve good correlation between the predicted response from the analysis of Reference 8 and the measured response on a full-scale helicopter rotor, it is necessary that (1) reliable detailed flight test data be available, (2) all facets of the aeroelastic analysis (e.g., prediction of rotor inflow, applicability of the sinusoidal unsteady data, scaling of data to account for compressibility effects, representation of blade flexibility, etc.) be accurate, and (3) factors neglected in the correlation (e.g., effects of blade three-dimensional flow, wake geometry distortions, or fuselage/wing interference) be, in fact, negligible.

It was decided to examine the effects of each of these factors singly if possible. A logical starting point for this examination concerned the fundamental assumption that unsteady sinusoidal data, tabulated as a function of α, A, and B, can be used to predict the aerodynamic response of an airfoil executing a nonsinusoidal motion. To test this assumption, a group of proof-of-theory experiments was devised and carried out as reported herein. Concurrently, an analysis was carried out in an attempt to improve the correlation of predicted and measured control loads. The new unsteady data tables were incorporated into the UAC aeroelastic blade response program, and correlation studies were carried out for the NH-3A and the CH-53A rotor systems and for a dynamically scaled model rotor. The effect of rotor inflow upon torsional response prediction was assessed by repeating the analysis for several inflow distributions. Slight modifications were made to the unsteady data tabulations of Reference 8 to smooth out regions of irregular data. This modified original unsteady data and the new model data were then compared by running some of the correlation cases with both tabulations.

EXPERIMENTAL PROCEDURES

MODEL AIRFOIL AND TEST FACILITY

As stated before, one of the primary objectives of this experimental program was to test the validity of the hypothesis that sinusoidal data could be generalized by the UAC α, A, B, method (References 8 and 9) to predict the aerodynamic response of an airfoil to a nonsinusoidal motion. This was designed to be a completely self-contained program in which a single airfoil would be tested in the same facility with both sinusoidal and nonsinusoidal motions to eliminate as many extraneous variables as possible in the course of this proof-of-theory test.

In view of the multitude of tasks required of the model airfoil, there were a number of design constraints imposed on its internal and external configuration. First, it was required that the test program be performed in a convenient test facility in which a large number of varied tests could be run over a long period of time without incurring occupancy conflicts. The facility chosen to satisfy these requirements was the UAC two-dimensional, high-speed cascade wind tunnel (shown in Figure 2) modified substantially for the performance of this isolated airfoil test. This tunnel received air from a large pressurized plenum chamber. After passing through a series of fine mesh screens to reduce turbulence, the air entered the test section through a rectangular bellmouth. The test section was 4 inches wide, and the adjustable sidewall quadrants were rotated to provide a test section height of 14 inches between the horizontal floor and ceiling pieces. Sidewall extension pieces were added to the tunnel, and the air exhausted to atmosphere four chordlengths downstream of the model airfoil trailing-edge location.

The specific tasks required of the airfoil model each placed additional constraints on the model design. The maximum 4-inch width of the tunnel and the need for sidewall boundary layer fences (see below) restricted the total model span to 3.73 inches. The chord of the model was chosen to be 5 inches to permit the insertion of 10 miniature pressure transducers. The need for pressure transducers located along the entire chord produced a high strength requirement along the entire chord, but the need for a flexured oscillating airfoil scaled to simulate a full-scale rotor blade section produced a low inertia requirement. Accordingly, the model was constructed as described below to fulfill as many of these requirements as possible.

The basic building blocks of this model were the steel spar and the magnesium ribs, shown partially assembled in Figure 3. The large magnesium rib contained all of the pressure instrumentation. In the upper half of Figure 3, this portion of the rib is seen to contain 10 transverse holes into which the 10 miniature pressure transducers were inserted. In addition, two alignment and drive pins are seen which were matched to holes on the narrow rib; this constituted the driving half of the model. The lower half of Figure 3 shows the back side of the large rib, which also contained 20 static pressure taps, 10 for each surface. Also shown here is the steel spar, hollowed out to compensate for the model weight aft of the 25 percent chord pivot axis. Instrumentation leads and hypo tubing were passed through the hollow center of the spar, and the round shaft ends were later inserted into support bearings in both sidewalls.

Balsa filler pieces were then placed fore and aft of the shaft as shown in Figure 4. Balsa wood was specifically chosen to provide a light-weight rigid core. Next, the two model halves were assembled and four layers of carbon-epoxy skin were wrapped around the airfoil: two with fibers in the chordwise direction, and two with fibers in the spanwise direction. The static pressure tubing which can be seen protruding from the surface of the rib in Figure 4 was partially buried in the skin and then machined flush with the surface. After the surface was smoothed, the skin was sliced chordwise at the joint between the two ribs, the mating faces were machined flush, and the model was painted. Static holes were then drilled from both airfoil surfaces into the transducer cavities. This is shown in Figure 5.

The miniature differential pressure transducers were supplied by Sensotec (model no. SA-SD, Type 8J-6H) and had a working range of ± 15 psi. Their sensitivity at unit gain varied from 1 mv/psi to 2.3 mv/psi, and the actual values as calibrated are given in Table I. Although the transducers showed some deviation with temperature change, these deviations were small, and the characteristic was linear at constant temperature. This is shown in Figure 6 for a typical transducer at a gain factor of 20. It will be shown later that the mode of operation chosen avoided all possible thermal problems.

One of the transducers is pictured in the upper half of Figure 7. The transducer consisted of a circular metal diaphragm 1/8 inch in diameter, with bonded semiconductor strain gages. The diaphragm was mounted at one end of a cylindrical tube, which was partially open at the far end and capped by an overhanging end piece. An O-ring on the cylinder served to isolate the two ends of the transducer when it was inserted into its

ity in the model. A typical installation is shown schematically in the lower half of Figure 7. Pictured here is a sketch of a spanwise section through the large rib, looking aft. The figure is largely self-explanatory. The epoxy plugs at the two surfaces were poured in place to prevent pressure leakage through the layers of skin. All but the last three transducers were configured in this manner. Because of space limitations, the three rearmost transducers were placed forward of their measuring stations and were connected to them by means of short surface tunnels buried under the skin. These are seen in Figures 3 and 4 as short chordwise streaks in the large rib. Both the transducer and static tap orifices were distributed along the airfoil chord according to the normalized roots of a Legendre polynomial to take advantage of the inherent accuracy of the Gaussian integration method (References 13 and 14). This is discussed in a later section and in Appendix I.

Sidewall boundary layer end plates were used in an attempt to reduce sidewall interaction effects on such a short span model. The end plates were 9.25 inches long and 3 inches high, with a circular leading edge, as shown in Figure 8. They were located 0.188 inches from the sidewalls, with their leading edges 2 inches forward of the airfoil leading edge. Installation of the end plates produced an effective aspect ratio, based on reduction of lift curve slope, of approximately 9.5 (see page 84 of Reference 15).

The airfoil model was mounted in the wind tunnel between thrust bearings which were loaded to keep the two airfoil halves together. The airfoil was oscillated either sinusoidally or nonsinusoidally by the drive system shown schematically in Figure 9. In this system, a variable-speed 6.5-hp electric motor drove an eccentric cam, located in a transmission box, in a circular motion by means of a drive belt and pulleys. A double follower within the transmission converted the circular cam motion to a periodic shaft motion, which was transmitted to the blade through a shaft coupler. For most of the tests, this coupler was rigid and the airfoil motion was completely prescribed by the angular schedule of the cam-follower system. For a small portion of the test program, the coupler was flexible. In these cases, the model was driven at low frequency (e.g., approximately 10 cps) to simulate a one-per-rev cyclic change in angle of attack of a typical rotor blade, and the coupler flexibility was chosen to simulate the torsional response of a typical rotor blade at frequencies between three-per-rev and ten-per-rev. Most of the tests were conducted with a sinusoidal cam which imparted an angular amplitude of ± 8 degrees to the blade. For a portion of these tests, the pitching oscillation either approximated the time history of a helicopter rotor blade or executed a ramp-like motion, both at ± 8 degrees. A very small number of sinusoidal tests were conducted at an amplitude of ± 3 degrees.

Further descriptions of each test condition are given later in the text, and an overall summary of the test points actually run is given in Table II.

Angular deflections were measured using a cylindrical electrical capacitor on each side of the airfoil. One part was mounted on the airfoil shaft and rotated with the same motion as the shaft. The other part was stationary and its cylindrical surface was made concentric with the shaft center line. This is shown schematically in Figure 10. Both cylindrical surfaces were coated with conducting paint and were excited by means of a capacitive signal conditioner. An initial setting was chosen with the faces staggered by some amount, as shown in the sketch of Figure 10. As the shaft rotated in either direction, there would be more or less capacitive area in opposition, which was manifested as a variable output voltage. This voltage was found to be a linear function of the angular displacement from rest with sufficient sensitivity to ensure a reading error of less than 0.1 degree.

One of these capacitive transducers was mounted at the free end of the blade and always measured blade motion. The other transducer was mounted between the transmission and the shaft coupler and always measured the motion input to the coupler. For a rigid coupling, the two transducers yielded the same angular motions, and only one was recorded. For the flexible coupling tests, the coupler transducer still measured the input motion, but the blade transducer measured the effects of blade inertia, blade stiffness, and aerodynamic forces and moments. Hence, the blade transducer produced a response that was measurably different from that of the coupler transducer during a flexible test, and both responses were recorded.

TEST PROCEDURE AND RAW DATA REDUCTION

The instantaneous angle of attack α at time t during a sinusoidal oscillation of frequency ω rad/sec can be expressed as

$$\alpha = \alpha_M + \bar{\alpha} \sin \omega t \qquad (1)$$

where α_M and $\bar{\alpha}$ are the mean angle of attack and the angular amplitude of oscillation, respectively. If simultaneous time-varying measurements of α and Δp from the chordwise pressure transducers described in the

preceding section are made, the time-varying lift and moment versus angle of attack can be obtained. The normal force coefficient (positive up) at any instant is given by

$$C_n = -\int_0^c (p_u - p_L) \frac{dx}{qc} \tag{2}$$

and the corresponding moment coefficient about an axis at a (positive nose up) is given by

$$C_m = \int_0^c (x - a)(p_u - p_L) \frac{dx}{qc^2} \tag{3}$$

where p_u and p_L are the static pressures on the upper and lower surfaces, respectively ($\Delta p = p_u - p_L$), c is the blade chord, and q is the free-stream dynamic pressure.

The initial portion of this program was concerned with the formulation of a tabulation of unsteady normal force and moment for an airfoil oscillating sinusoidally in pitch. The normal force and moment were to be tabulated as functions of angular position, α, angular velocity parameter,

$$A = \frac{b\dot{\alpha}}{V} \tag{4}$$

and angular acceleration parameter,

$$B = \frac{b^2\ddot{\alpha}}{V^2} \tag{5}$$

as the independent variables. Using Equations (1) through (3), it was possible to obtain unsteady normal force and moment data in terms of the experimental variables α, α_M, $\bar{\alpha}$, and ω. As shown in Reference 8, the required tabulation can be constructed from these data.

The oscillatory portions of the unsteady pressures were measured separately from steady or mean pressures. The steady pressures were obtained directly from the 20 static surface taps. The oscillatory pressures were obtained from the 10 differential transducers by (a) first setting the tunnel speed at the desired value with the model airfoil set at its mean angle of attack, (b) electronically nulling the voltage output of the transducers, and (c) oscillating the airfoil and recording the oscillatory pressures only (see below for further details). This procedure was followed for two reasons. First, as shown in Figure 6, the transducers were found to be temperature sensitive. Although this sensitivity was small, it could have led to measurement errors because the air temperature with flow was different from the ambient temperature of the room air. By nulling the signal under full flow conditions with the tunnel at its equilibrium temperature, the thermal drift problem was eliminated. Second, by nulling out the steady portion of the signal, it was possible to use the entire voltage range of the transducers to measure the oscillatory portion of the unsteady pressure, which increased the accuracy and sensitivity of these measurements.

The steady-state tests were run with the airfoil restrained at the transmission. The steady pressure difference distribution was obtained from the static pressure taps. Although the differential pressure transducers were not used for measuring the steady portion (mean value) of the pressure during the oscillatory tests, it is noteworthy that they were indeed capable of measuring the steady portion accurately if the transducers were initially balanced at the operating temperature of the tunnel. This can be shown by comparing a typical steady-state pressure difference distribution obtained from the pressure transducers (with proper thermal compensation and calibration) to that obtained directly from the static pressure taps. These data are shown in Figure 11.

The steady-state normal force and moment at the angles of attack listed in Table II were obtained by integrating the static pressure distributions over the airfoil. The details and results of this integration will be covered in a later section. The pressures were recorded both from a manometer board and from a pressure scanner system. The pressure scanner (scanivalve) mode of operation allowed the sequential monitoring of the static pressures. Each pressure input was scanned in sequence and converted to an analog voltage with a single pressure transducer external to the model. The voltage output was displayed on a digital voltmeter.

The remainder and bulk of the test program was concerned with obtaining unsteady normal force and moment data on the airfoil while it was undergoing either sinusoidal or nonsinusoidal pitch oscillations. These different motions were produced by changing cams in the transmission or by replacing the rigid coupler with one of three separate Bendix flexures (series 5000). The test procedure used with each of these changes was essentially the same and is described below.

First, the airfoil mean angle of attack was set to some desired value, corresponding to the mean position of the transmission output shaft. All angles were measured with a Model B Ailger and Watts Vernier Angle Gage (Clinometer) which was calibrated to within one minute (1') of angular deviation. A special block was machined to fit closely over the airfoil with its upper surface parallel to the airfoil center line (see Figure 12). Angular measurements were made with the Clinometer positioned on this block as shown.

With the airfoil positioned as described, the wind tunnel was started. The test section Mach number was set nominally for M = 0.325 (actual velocity at operating temperature was V = 390 ±6 ft/sec). The tunnel was run long enough for the airfoil to reach a thermal equilibrium. At this point, the tunnel was shut down quickly and all the transducers were balanced to zero output with temperatures at or very close to their operating temperatures. The tunnel was restarted and the Mach number was set. This procedure eliminated all or most of the DC-bias in the transducer output due to temperature. It also allowed the gages to be balanced without thermal offset so that the output signal could be amplified as much as possible without risk of saturating the recording equipment due to thermal drift. The transmission locking mechanism was released, and the motor which oscillated the airfoil was started. The required frequencies were set by monitoring the position gage output on a Beckman Universal Model 8370 EPUT (Events Per Unit Time) Meter and adjusting the variable speed control. The basic system used for recording the data is discussed in Reference 16 and is referred to as the WISARD (Wideband System for Acquiring and Recording Data). The various components of the WISARD and the peripheral equipment used throughout this program are shown in the block diagram of Figure 13. The pressure transducer signals were amplified to a maximum level without exceeding 1.0v output (by a gain of 50 near the leading edge and 200 near the trailing edge). High-frequency noise was minimized by filtering the amplifier output above 10,000 cps. Since this frequency was two orders of magnitude higher than the highest oscillatory test frequency, no signal attenuation in the frequency range of interest was possible. The amplified, filtered pressure transducer

signals together with the balanced position gage signals were recorded directly on FM tape using a CEC (model VR-3400) 14-channel variable-speed tape recorder. Ten channels were used for the pressure data, and two were used for the angle-of-attack data from the position gages. (The other two channels were used for identification and internal mode control of the WISARD.)

Typical raw data output from a pressure transducer near the leading edge (Δp) and the position gage (α) are shown in Figure 14. All the panels shown in this figure are for ± 8 degrees sinusoidal motion at a frequency of 25 cps and a Mach number of 0.325. The left-hand panels are for a mean angle of attack of 6 degrees, where no dynamic stall is observed. The right-hand panels are for a mean angle of attack of 11 degrees, where considerable penetration into stall can be observed. Both lower panels are oscilloscope photographs of the pressure and position time histories directly from the tape recorder playback. The upper panels are Lissajous figures of these same time histories in which the position signal was used as the horizontal base. The characteristic separation loop is evident in the right-hand panel.

To compute the unsteady normal force and moment, the raw pressure data were multiplied by their respective sensitivities and divided by the gains used in the amplifiers. The mean value of the pressure time histories was subtracted from the actual value at each instant of time so that the resulting normal force and moment were purely the unsteady portions. The steady-state normal force and moment for a given angle of attack obtained earlier were then added to these unsteady data to obtain the total normal force and moment.

The data processing procedure required that analog signals from the FM tape be converted to digital form. This conversion was also done on the WISARD and is shown schematically in the lower portion of the block diagram of Figure 13. Here the operating flexibility of the data system permitted us to maximize the frequency resolution of each unsteady signal, regardless of the oscillatory frequency. By recording the data at any of a number of selected tape speeds and playing the tape back at a slower speed, it was possible to obtain test information at higher frequencies than would otherwise be possible if recording and playback speeds were equal. Once the recording speed was selected, the amount of record which would fill the computer storage could be established directly from the samping rate of the WISARD digitizing process. A detailed description of the logic used in selecting tape recorder speeds and record lengths is given in Appendix II. The results of this study are shown in Table III.

These settings were established so that if a Fourier analysis of the signals was required, there would be at least four samples/cycle in the tenth harmonic of the oscillatory frequency.

TEST RESULTS

DATA PROCESSING

The digitized magnetic tape produced by the data system was processed on a UNIVAC 1108 digital computer. First, the millivolt equivalents of pressure difference, Δp, and angular position, α, were arranged in the computer core as functions of time. The pressures, suitably multiplied by conversion factors, were integrated to yield normal force and moment coefficient time histories, $C_n(t)$ and $C_m(t)$, using the nondimensional versions of Equations (2) and (3). Because the pressure orifices were arranged in a Gaussian net over the forward 90 percent of the blade chord, it was possible to take advantage of the Gaussian integration method, as discussed in Appendix I. By this means, a greater degree of accuracy was attained than would be possible using standard numerical quadrature formulas. Time histories representing 50 or more cycles of motion were converted and stored for each test point.

These data contained some noncoherent noise in addition to the desired unsteady information, particularly during flow separation. A typical time history for separated flow is shown in Figure 15. To minimize the effects of this superimposed noise and to enhance the coherent or repeatable elements of the time history, a 40-cycle signal averaging process was used. This reduced the noise level relative to the desired signal level by a factor of $\sqrt{40} \cong 6.3$ (see pages 116-118 of Reference 17). The resulting smoothed cycle for each component was then normalized with respect to its period to occupy 100 units of nondimensional time to provide a uniform data set for further processing. A sample of the smoothed time histories is shown in Figure 16 for the same conditions that produced Figure 15.

The normal force and moment time histories for each test point were then interpolated at integral values of incidence angle, and the results were stored in the computer. From this point, the process described in Reference 8 to convert the normal force and moment into tabular functions of angular position, α, angular velocity parameter, A, and angular acceleration parameter, B, was followed. For convenience, the schematic outline of the process, from Figure 70 of Reference 8, is reproduced herein as Figure 17. Reference 8 describes the conversion process in detail, and this description will not be repeated herein. The generalized unsteady normal force coefficient is contained in Table IV, and the moment coefficient is in Table V. Within each table the data are arranged in blocks for each integral value of geometric angle of attack.

STEADY-STATE NORMAL FORCE AND MOMENT

The oscillatory tests were designed to provide only the unsteady portions of the normal force and moment. Therefore, it was important throughout this program that an accurate measurement of the steady portion of the force and moment be available. This was particularly true because of the small span of the model, which made it impossible to use results of previous investigators. Furthermore, at high angles of attack, the steady portions of the total signals were considerably greater than the unsteady portions.

To ensure the accuracy of the steady force and moment, these data were checked in as many ways as possible. First, the pressure measurements were made at chordwise grid locations corresponding to a modified Gaussian net (see Appendix I). Second, the measurements were made using both direct manometer board pressure readings and pressure transducer readings which were sequentially converted to analog voltages and displayed on a digital voltmeter. Third, at each mean angle of attack setting made during the oscillatory tests, the thermally soaked differential pressure transducer outputs were also used to check previously obtained results. The steady-state normal force and pitching moment coefficients versus angle of attack shown in Figures 18 and 19 are the final result of all these measurements. The fact that the normal force at $\alpha = 0$ degrees was not zero for the symmetrical NACA 0012 airfoil merely reflects the fact that the mean airflow angle in the tunnel differed from the local horizontal by the noted angle of zero lift ($\alpha_{0L} = 0.6$ degrees). All angles used in this report are referenced to local horizontal, not the angle of zero lift.

NORMAL FORCE AND MOMENT HYSTERESIS LOOPS

The smoothed data described in an earlier section (e.g., that shown in Figure 16) were time histories of the unsteady normal force, pitching moment, and angle of attack. Additional information can be obtained from such data when explicit time dependency is removed. This was accomplished conveniently by replotting the normal force and moment as functions of instantaneous angle of attack. Since one complete cycle of data is considered, the angle-of-attack variation begins and ends at the same point, and the resulting curves are closed. The nature of these closed curves is best understood by considering the case of sinusoidal motion first.

Sinusoidal Time Histories

When an airfoil is sinusoidally oscillated quasi-steadily over a small amplitude range at zero mean angle of attack, the resultant normal force and moment versus angle of attack retrace the steady-state force and moment curves for that airfoil. Typical data of this sort are shown in Figure 20a. If only the frequency is increased, a phase shift between the force or moment and the angle of attack begins to manifest itself. Now the unsteady force and moment versus angle of attack curves enclose a finite area as depicted in Figure 20b (arrows denote the direction of increasing time). When the mean angle of attack of the motion is increased such that the maximum angle of attack of the oscillation exceeds the steady-state stall angle, the stall phenomenon is delayed. This behavior is shown in Figure 20c, where no stall actually occurs despite the fact that the steady-state stall angle is exceeded. A further increase in mean angle of attack results in a deep stall and recovery usually referred to as dynamic stall. Figure 20d shows force and moment loops of this latter kind. In the classical or potential flow region the unsteady loops are elliptical, while in the separated flow region they can be severely distorted. This discussion represents an oversimplification of the dynamic stall phenomenon. Actually the magnitude and character of the dynamic stall delay are dependent on the reduced frequency, the penetration beyond static stall, and other related factors. For a more complete understanding, the reader is referred to the previous literature on this subject (References 7, 8, 9, 11, 18, 19, 20, and 21, to name but a few).

Additional knowledge of the behavior of oscillating airfoils can be gained from observing the manner in which moment loop areas are enclosed. Reference 20 has shown that aerodynamic damping of an airfoil is proportional to the total area enclosed by these moment loops. Specifically, the following expression for damping is taken from this reference:

$$\Xi_{a_2} = - \frac{\oint C_{m_R} \, d\alpha_R}{\pi \bar{\alpha}^2} \tag{6}$$

where Ξ_{a_2} is the two-dimensional aerodynamic damping
$\oint C_{m_R} d\alpha_R$ is the area enclosed by the moment loop and
$\bar{\alpha}$ is the oscillatory amplitude

It was also shown in Reference 20 that counterclockwise enclosures of the moment loop are stabilizing while clockwise enclosures are destabilizing.

Thus, as the mean angle of attack is increased from Figure 20c to 20d, it can be seen that a portion of the moment loop becomes unstable (i.e., the lower portion of the figure eight loop in Figure 20d is clockwise) and the overall aerodynamic damping is decreased. The aerodynamic damping is of the utmost importance in investigations of dynamic stall or stall flutter.

The characteristics of the normal force and moment hysteresis loops discussed above were found consistently throughout the sinusoidal tests conducted in this program.

Nonsinusoidal Time Histories

The cam-follower system used in these tests made it possible to obtain a wide variety of airfoil angle-of-attack time histories. An extreme example of nonsinusoidal motion was obtained from a ramp cam, which produced regions of constant or nearly constant angular velocity connected by small regions in which the direction of motion was reversed. Figure 21 is a plot of the theoretical nondimensional time history of the angle of attack and its first two time derivatives as designed into the ramp cam. The solid curves represent the forward motion of the cam. Under these circumstances the angular velocity during the upstroke was twice the angular velocity during the downstroke. This cam could also be operated in reverse (denoted by backward ramp motion), which is depicted in Figure 21 by the dashed curves. Here the angular velocity during the downstroke was twice the angular velocity during the upstroke. The angular acceleration was zero everywhere except over the regions of maximum and minimum angle of attack, where it pulsed rapidly to a minimum and a maximum value, respectively.

One objective of this portion of the experiment was to examine the effect of varying the time rate of change of α from one part of the cycle to another. This is indicated in Table VI, in which values of A are listed for the constant portions of the motions for the four frequencies tested, for both forward and backward motions. For example, it is seen that the forward cam at 10 cps and the backward cam at 20 cps will have identical values of A over the upstroke but will have different values over the downstroke. The normal force response for these conditions is shown in Figure 22. The solid curve labeled F-10 was measured with the forward cam at 10 cps, and the dashed curve labeled B-20 was measured with the backward cam at 20 cps, for oscillations of ± 8 degrees about a mean angle of attack of 11 degrees. It is seen that during the upstroke, both of these loops coincide over most of the α range. However, after the maximum angle of attack was reached, the angular velocity on the downstroke

was four times greater for the backward ramp (B-20) than for the forward ramp (F-10). The higher negative A in the backward ramp appears to have caused the flow to remain separated over a wider range of angle of attack than the smaller negative A of the forward ramp, although a small portion of this difference between the two curves may be attributable to increased phase shift due to a larger value of reduced frequency. Conversely, the lower negative value of A on the downstroke of the forward ramp appears to have allowed the flow to reattach close to the mean angle of attack.

A different trend can be observed on the upstroke by comparing two loops for two different frequencies for the forward ramp. In addition to the 10-cps condition (F-10), another solid curve has been plotted for a 20-cps oscillation of the forward ramp about a mean angle of attack of 11 degrees (F-20). Here the doubling of A at 20 cps (F-20) relative to the 10-cps condition (F-10) for both the upstroke and the downstroke caused an overall enlargement of the loop; the maximum normal force attained was greater, and the delay in normal force recovery over the downstroke was also greater for curve F-20 relative to curve F-10. Additional cases for normal force were examined and they showed a comparable trend, consistent with the results shown above.

Similar families of loops were obtained for pitching moment. A sample is shown in Figure 23 for the forward ramp at 10 cps (solid curve, F-10) and the backward ramp at 20 cps (dashed curve, B-20). Once again, the curves coincide over the region where the values of A are identical and diverge where the values of A are not equal. However, the differences on the return stroke are not so accentuated here as in the case of normal force, until after recovery from stall appears to have taken place. Similar trends were observed for the moment curves obtained at other frequencies.

An additional nonsinusoidal cam was built to simulate the cyclic pitch variation of a helicopter rotor blade. However, when tests were run with this cam, it was found that surface irregularities caused the airfoil to respond erratically and imposed large loads on the follower bearings, producing results which were difficult to interpret. These tests were discontinued after a short time, and other tests with the sinusoidal cam were substituted.

UNSTEADY PRESSURE INVESTIGATION

During the rigid sinusoidal portion of the test program, a few cases were run at a mean angle of attack of 11 degrees and at frequencies of 50 and 75 cps in which single surface pressure measurements were made

(see item 4 in Table II). These data were obtained by taping the upper and lower surfaces of the airfoil, respectively, so that the differential pressure transducers were sensing the individual surface pressures. The purpose of this test was to establish whether a wave type fluctuation in pressure could be observed on either or both sides of the airfoil during the oscillations.

Figure 24 shows the original chordwise variation in differential pressure measured directly from the transducers with both sides active compared with the same differential distribution reconstructed from the single surface measurements, both taken at an instantaneous incidence angle of 3 degrees during a sinusoidal oscillation. Note that these pressure differentials are measured relative to the pressure at the mean angle of attack; i.e., the Δp (x) plotted here is taken to be zero along the chord at $\alpha = \alpha_M$. This result is presented here to verify the ability of the single surface measurements to reproduce faithfully the results obtained from the differential transducers.

The pressure and suction surfaces of the airfoil are considered separately in Figures 25 and 26, respectively. Here the instantaneous chordwise pressure distributions on each side of the airfoil are plotted at various instantaneous angles of attack during a cycle of motion. Again the pressures are measured relative to the pressure at the mean angle of attack. The solid lines represent the conditions of incidence angle increasing relative to α_M = 11 degrees ($\dot{\alpha} > 0$), and the dashed lines represent the conditions of incidence angle decreasing relative to α_M = 11 degrees ($\dot{\alpha} < 0$).

In Figure 25, it is seen that the pressure distribution along the pressure surface changed very little over much of the cycle, either in magnitude or in shape, although it changed sign relative to the mean pressure, as expected. In contrast, the pressure distribution over the suction surface changed drastically as incidence angle was changed (Figure 26). Here it is seen that for the angles decreasing from the mean angle, a potential flow condition was established and the pressure distributions are well behaved and exhibit the usual leading-edge peak. However, for the angles increasing from the mean angle, it appears that a dynamic stall condition was encountered. Note that in Figure 26 the potential behavior of the curve for α = 13.7 degrees becomes distorted for α = 16.3 degrees and appears to have developed a propagating wave for α = 19.0 degrees. Additional pressure curves were examined for α decreasing from the peak value of 19 degrees (not shown here to avoid the confusion of overlapping curves), and it was found that a distinct pressure wave could be discerned

propagating rearward along the chord until it became too small to identify at approximately the 40 or 50 percent chord station. Almost identical results were observed for the higher frequency (f = 75 cps) case.

The rearward propagation of a pressure wave strongly suggests a vortex shedding phenomenon as described by Ham in Reference 19. Furthermore, the relative lack of response on the pressure surface (Figure 25) indicates that the bulk of the dynamic stall activity occurs on the suction surface. This phenomenon can also be inferred from the figures in Reference 22, and it was clearly evident in the motion picture (Reference 23) of the animated pressure distributions which accompanied Reference 22. Thus, it should be possible to use even the unsteady differential pressure data to examine some of the details of the dynamic stall phenomenon. This work will be undertaken in the future.

UNSTEADY AIRFOIL DATA

GENERALIZATION OF UNSTEADY SINUSOIDAL DATA

The process used to generalize these results has already been briefly described in a previous section and has been thoroughly discussed in Reference 8. As in the past, the normal force and moment coefficient data were tabulated as functions of α, A, and B, and these tabulations were stored in the computer. (They are also found in this report in Tables IV and V for C_n and C_m, respectively.) The differences between this tabulation and our previous tabulation (Reference 8) were many and varied. We shall be concerned here only with a few of the more important differences. First, the model scale was considerably different; this time the chord was 5 inches and in Reference 8 it was 24 inches. Another important difference lay in the method of extracting points from the original time histories. Previously, a single cycle, chosen at random, was analyzed and manual procedures were used to interpolate the normal force and moment values, cross-plot the results, and extract the final values for tabulation. In the present study, the single cycle was replaced by a time-averaged cycle and most of the intermediate steps were performed by a computer. This led to a self-consistent set of data which was smoother than that obtained previously. Finally, the parameters chosen for this experiment were specifically picked to extend the useful tabulated range beyond that of the previous table.

It is instructive to examine the α, A, B table generated by the present test and to compare its range with the required parameter ranges of typical conditions experienced in flight. To accomplish this, we can combine Equations (12) and (13) of Reference 8 to eliminate the angular displacement from the mean, and after some manipulations, we obtain

$$\frac{A^2}{k^2 \bar{\alpha}^2} + \frac{B^2}{k^4 \bar{\alpha}^2} = 1 \qquad (7)$$

This equation shows that contours of constant k and $\bar{\alpha}$ will be ellipses in the A, B plane. Furthermore, the major and minor axes of any given ellipse will be directly governed by the size of both the reduced frequency and the angular amplitude, being large when $k\bar{\alpha}$ is large and small when $k\bar{\alpha}$ is small. This is clearly illustrated in Figure 27. The solid outside ellipse is the limit of the conditions tested in this study, and the data

tabulation (presented in Tables IV and V) is arranged roughly in the same pattern. (Note that the moment data in Table V extend farther into the corners of the table than do the normal force data in Table IV, because the C_m data were extrapolated through a series of cross-plots to increase their useful range.) For comparison, the large solid rectangle represents the tabular limits of the old data used in Reference 8. The dashed curves labeled a through d are the anticipated limits for various application requirements. Curves a and b represent the bounds of typical helicopter rotor blades executing one-per-rev motions at ± 8 degrees amplitudes for high and low aspect ratios, respectively (the differences in the curves being associated with differences in blade chord length). Curve c represents a sinusoidal stall flutter limit of eight-per-rev at ± 4 degrees, and curve d represents the maximum frequency boundary of the nonsinusoidal ramp motion during the present program. It is clear from this figure that the sinusoidal data obtained is adequate for the analysis of the typical cases shown here.

One of our major objectives in this program was to examine the ability of the generalized data taken from a sinusoidal test to predict the aerodynamic response of the airfoil as it executed a more general periodic (nonsinusoidal) motion. Therefore, an obvious first requirement of the tabulated data is that for a sinusoidal motion, the predicted normal force and moment loops must faithfully reproduce the original loops. It is seen from Figures 28 and 29 that this condition is essentially satisfied. These figures represent a sampling of the normal force and moment comparisons (respectively) made between the original data and the reproduced loops. The left panels in each figure show the effect of mean angle-of-attack variation for a frequency of approximately 50 cps. The right panels in each figure show the effect of frequency at a constant mean angle of attack of 11 degrees. In almost all cases, the agreement between the original data and the reproduced loops is excellent, particularly at the higher frequencies. In a few instances, the agreement at low frequency shows some deterioration, but it is still acceptable for our present purposes. This is shown in Figure 29c, which is typical of the maximum deviation of a reproduced loop from the original observed during this study. Thus, the present force and moment tabulation has been shown to be an extremely accurate duplication of the experimental data. This accuracy appears to be significantly greater than that demonstrated by any other method for which results have been presented in the literature.

A few cases of sinusoidal motion were also run at an oscillatory amplitude of ±3 degrees. Once again, the unsteady normal force and moment were predicted using the α, A, and B tabulation generated from the ±8 degree sinusoidal tests. Figures 30 and 31 show the results of comparing the original ±3 degree experimental normal force and moment to that predicted by the tabulation. Both figures are for a mean angle of attack of 14 degrees. Figure 30 is for an oscillatory frequency of 12.6 cps and shows very good agreement in both normal force and pitching moment. Figure 31 is for an oscillatory frequency of 31.1 cps, and the agreement is only fair for the decreasing incidence branch, although it is good for increasing incidence.

USE OF DATA TABULATION TO PREDICT GENERAL RESPONSE

It was stated in an earlier section that one object of the ramp motion tests was to examine the effect of variable $\dot{\alpha}$ within a cycle of motion on the blade aerodynamic response. A more important object was to test the validity of the hypothesis that sinusoidal data could be generalized by the UAC α, A, B method to predict the aerodynamic response of an airfoil to a nonsinusoidal motion. The abrupt changes in angular velocity and acceleration provided an extreme environment in which to test this hypothesis.

Figure 32 is a plot of the actual nondimensional time history of the angle of attack produced by the ramp cam when it was rotated in the forward direction. When this time history was analyzed for use with the tabulation, it was found that there were minor deviations between the true (or measured) angular position and the ideal (constant $\dot{\alpha}$) trajectory. These irregularities resulted from small errors in the cam surfaces. Although these anomalies were within acceptable limits, they did cause some spurious oscillations when the angle of attack was numerically differentiated to obtain the angular rate term, A, and the angular acceleration term, B. This problem was avoided in the present application by fitting the angle-of-attack time histories with high-order polynomials (up to fourteenth order), which were then differentiated exactly rather than numerically. The polynomial fits produced the actual time histories with good accuracy.

Figures 33 and 34 show some typical comparisons between measured force and moment loops for the forward ramp motion and those predicted from the α, A, and B tabulation of sinusoidal data. In all cases, the predicted $C_{n_{MAX}}$ was within 5 percent of the measured value in magnitude but did tend to occur at a slightly lower angle of attack. After stall,

the predicted normal force decreased more rapidly and tended to remain stalled over a greater angle of attack range than did the measured normal force. The overall agreement of normal force is considered to be very good. The moment loops of Figure 33 also appear to be in good agreement with regard to shape (including crossover points), although a small shift in magnitude is apparent. Since stall flutter is primarily a torsional problem, the moment loops are somewhat more important than the normal force loops. A measure of how well the measured and predicted moment loops agree can be obtained by comparing the aerodynamic damping calculated from each set of loops. An analysis of aerodynamic damping is presented in Reference 20 and is discussed briefly in a preceding section of this report. The expression for aerodynamic damping given by Equation (6) was used to obtain the damping for both the measured and predicted moment loops for all tests with the ramp time history of Figure 32. These results are shown in Figure 35. The agreement at low reduced frequency and low mean angle of attack is excellent. At higher reduced frequencies, the damping for the predicted moment loops is consistently less (i.e., more negative or tending more toward negative) than the damping for measured moment loops, particularly for oscillatory motions which penetrate and return from stalled flow. Similar results were obtained for the backward ramp, as shown in Figure 36 for the normal force, in Figure 37 for the moment, and in Figure 38 for the aerodynamic damping.

FLEXURED TEST RESULTS

The bulk of the tests conducted in this program were with a rigid coupler between the transmission shaft and the airfoil. It was possible to simulate the stall flutter problem two-dimensionally by replacing this rigid coupler with flexible ones. Three different Bendix flexures were used which resulted in natural frequencies of the airfoil of 41.5, 52 and 75 cps. It was stated earlier that the airfoil was constructed in two parts and was mounted in thrust bearings in the sidewalls of the wind tunnel. These thrust bearings, which were required to hold the two model parts together, introduced more mechanical damping in the system than is normally desirable for a stall flutter test. Typical values of the no-flow damping obtained from the decay rate of the plucked spring-mounted airfoil were between 3.9 and 10.2 percent of critical damping. Despite this amount of damping, it was felt that a stall flutter test was still meaningful, particularly when it was observed that significant flutter response still occurred.

The airfoil as described was oscillated sinusoidally at an amplitude of ±8 degrees about mean angles of attack of 6, 11, and 16 degrees. At each mean angle of attack, three different excitation drive frequencies were used to simulate the one-per-rev cyclic pitch of a helicopter blade. The combinations of natural frequencies and excitation drive frequencies resulted in a range of frequency ratios from 2.76 to 10.0 cycles-per-rev, which is within the typical range of most helicopters. The oscillatory amplitude of ±8 degrees was also representative of typical helicopter motion.

Use of flexures did not change any of the test procedures described earlier. Both position gages were required for these tests; one measured the excitation output of the transmission (one-per-rev), while the other measured the response of the airfoil (many-per-rev).

In addition to the direct measurement of the airfoil response, an analysis was performed in which the generalized α, A, B tabulation for the moment (Table V) was used to predict the airfoil response. Details of the numerical procedure used are given in Appendix III. The various physical characteristics of the airfoil required in this analysis are given in Table VII. Several values of the logarithmic decrement of the mechanical damping were used in the analysis since the actual value of this damping during testing was not known. This was because the differential pressure across the sidewalls during the tests caused additional thrust loadings on the bearings, which in turn caused an unknown increase in mechanical damping. However, it was felt that the total mechanical damping of the system did not exceed the values used in the analysis.

Some typical results of these tests are shown in Figures 39 and 40 for different combinations of frequency and angle of attack. The solid curves denote the experimental data, while the dashed curves denote the results of the numerical solution for the same conditions using the tabulated values of C_m. Each of the test results shown is one cycle of time-averaged motion. The time-averaging process was applied to 40 cycles of motion as in other parts of this study. To verify the fact that this averaging procedure did not wash out important features of the motion, it was also done for five cycles, and no essential difference was found.

Although the agreement between test and analysis is not perfect, the results indicate that the α, A, B method does yield results which contain all the essential characteristics of the test results. Each graph in Figures 39 and 40 shows three pairs of curves, one pair for each mean angle of attack. For convenience, each curve was plotted as a deviation

from the mean angle of attack, and on these figures each pair of curves is drawn from its own origin on the ordinate. Figure 39 plots three different excitation frequencies for an airfoil natural frequency of 41.5 cps, while Figure 40 shows the same three excitation frequencies for an airfoil natural frequency of 52 cps. In all six plots, it should be observed that the occurrences of natural blade oscillations at high angle of attack which typify stall flutter were all predicted. Note also that the initial cycle of predicted blade response always coincided with the measured response. Since these blade oscillations and their inception points are the most important aspects of stall flutter, these results are particularly significant. At the lowest angle of attack (α_M = 6 deg) and the lower blade natural frequency (41.5 cps) shown in Figure 39, the analytical solution behaved almost sinusoidally while the test data exhibited a broadened cycle on the upstroke (i.e., the test angle-of-attack time history on the upper half of the cycle extended over a time greater than one-half the period of the excitation frequency). This phenomenon was not nearly as severe for the α_M = 6 degrees cases at an airfoil natural frequency of 52 cps (see Figure 40). For all other cases, the agreement between theory and test results was considered to be excellent.

PROCESSING OF THE UNSTEADY DATA FOR USE IN HELICOPTER CONTROL LOAD CORRELATION STUDIES

MODIFICATION OF THE ORIGINAL UNSTEADY DATA TABLES

The unsteady data tabulations presented in Reference 8 were reexamined, and modifications were made in an attempt to improve correlation with hysteresis loops for sinusoidal motion. The procedure used was to examine the cross-plots of normal force and pitching moment coefficients versus α, A, and B and to smooth out irregular variations. Examples of the original and the smoothed cross-plots are shown in Figures 41 and 42. The effect of these changes on the ability to reconstruct the original hysteresis loops was evaluated, and those modifications which led to general improvement in correlation were incorporated into the tables. Because of the scatter in the data, alterations which improved correlation of some loops at times deteriorated that of others. Samples of some of the improvements in correlation are shown in Figure 43.

SCALING OF THE NEW UNSTEADY DATA

Application of the unsteady data to rotor blade operating conditions requires that the measured data for Mach number 0.325 be scaled to obtain approximations of higher Mach number unsteady characteristics. As in Reference 8, scaling procedures based on the steady-state stall angle were chosen which transformed the steady-state C_n and C_m data obtained for the wind tunnel model to steady normal force and moment curves for a 0012 airfoil over a range of Mach numbers. These steady-state scaling laws were then assumed to apply to the unsteady blade characteristics as well. It was shown in Reference 8 that normal force and pitching moment coefficient hysteresis loops measured at M = 0.4 and M = 0.6 could be predicted with reasonable accuracy by scaling the measured data for M = 0.2. The agreement between measured and scaled data was good for M = 0.4 but was less favorable for M = 0.6. Although it would be desirable to have experimental unsteady data at high Mach numbers, it is felt that the present data can be adequately scaled to the Mach numbers typical of the retreating-blade portion of the rotor disk where stall-related unsteady effects are significant.

Other factors included in the data transformation process are a correction for the finite effective aspect ratio of the model and a correction for the slight difference between the chosen α = 0 degrees reference line and the measured angle of zero normal force. For the

steady-state model data shown in Figure 18, the normal force curve slope is only about 0.0836/degree and the measured angle of zero normal force is 0.6 degrees. The treatment of these two factors led to a data scaling technique slightly different from that used in Reference 8. This will now be discussed.

Normal Force

To scale the measured unsteady normal force data for Mach number effects using a process based on steady-state stall angle, it was first necessary to replot the steady model C_n data versus the relative stall angle parameter

$$\sigma_n = \frac{\alpha - \alpha_{0L}}{\alpha_{sn} - \alpha_{0L}} \tag{8}$$

The normal force stall angle or point of departure from a linear normal force curve, α_{sn}, and the angle of zero normal force, α_{0L}, are taken from Figure 18 to be 12.0 degrees and 0.6 degree, respectively. The resulting plot, shown in Figure 44, is then the basic curve from which all normal force data are scaled. The unsteady data tables used in the following correlation studies also use this calculated σ_n as an independent variable in place of measured angle of attack.

The process for mapping the steady model data onto an arbitrary steady normal force curve is depicted in Figure 45 and is described as follows:

(1) Choose the point of departure from linearity, α_{sn}, and replot the given normal force curve versus $\sigma_n = \alpha/\alpha_{sn}$.

(2) Calculate the ratio K_n where $K_n = C_{n_{stall}}/C_{n_{stall,ss,model}}$ where $C_{n_{stall}} = C_n(\alpha_{sn})$.

(3) Plot an intermediate scaling curve $C_n'(\sigma_n)$ where $C_n'(\sigma_n) = K_n\, C_{n_{model}}(\sigma_n)$.

(4) Determine an additive correction curve $\delta_n(\sigma_n)$ such that $C_n(\sigma_n) = C_n'(\sigma_n) + \delta_n(\sigma_n)$.

This procedure was carried out for full-scale NACA 0012 C_n data. The steady-state data taken from Reference 24 were obtained from a Sikorsky-built 16-inch-chord airfoil section which was tested in the UAC 8-foot Subsonic Wind Tunnel at Reynolds numbers from 2.6 to 5.3 million. The C_n characteristics are shown in Figure 46. The scaling curves used to transform the model data to the full-scale curves are shown in Figure 47.

After the three quantities α_{sn}, K_n and $\delta_n(\sigma_n)$ are chosen for each Mach number and the assumption is made that the same scaling laws can be applied to the unsteady normal force coefficients, the following computation procedure is used to arrive at unsteady C_n coefficients:

(1) Compute the rotor blade section conditions σ_n, M, A, B.

(2) Compute the dimensionless stall angle parameter, $\sigma_n = \alpha/\alpha_{sn}$.

(3) Enter the tabulation of the unsteady C_n coefficients with σ_n, A, B and extract $C_{n_{model}}(\sigma_n, A, B)$.

(4) Calculate $C_n'(\sigma_n, A, B) = K_n(M)\, C_{n_{model}}(\sigma_n, A, B)$.

(5) Calculate $C_n(\sigma_n, A, B) = C_n'(\sigma_n, A, B) + \delta_n(\sigma_n)$.

The scaling parameters used in this Mach number scaling procedure are given in Table VIII.

Pitching Moment

As in the case of the normal force, the Mach number scaling procedure used for the pitching moment is based on the steady-state stall angle. Figure 48 shows the NACA 0012 steady-state pitching moment curves used in Reference 8. For each Mach number, the pseudo-stall angle parameter, α_{sm}, is chosen to scale the measured M = 0.325 model data to the appropriate full-scale curve. The dimensionless pitching moment parameter

$$\sigma_m = \frac{\alpha - \alpha_{OL}}{\alpha_{sm} - \alpha_{OL}} \tag{9}$$

defines the relative degree of pitching moment stall of the model. From Figure 19, α_{sm} is taken to be 14 degrees, while α_{OL} = 0.6 degree as before.

In a manner analogous to that used for the normal force coefficients, the parameter α_{sm} and an additive pitching moment correction curve $\delta_m(\sigma_m)$ were chosen to scale the full-scale C_m characteristics from the steady model data. The best values of α_{sm} and $\delta_m(\sigma_m)$ for each Mach number are chosen as follows:

(1) Choose the stall angle parameter, α_{sm}, which best maps the stall region of the full-scale curve from the model data, and replot the pitching moment curve versus $\sigma_m = \alpha/\alpha_{sm}$.

(2) Determine the additive correction curve $\delta_m(\sigma_m)$ such that $C_m(\sigma_m) = C_{m_{model}}(\sigma_m) + \delta_m(\sigma_m)$.

Figure 49 shows some of the results obtained with this procedure. The α_{sm} and $\delta_m(\sigma_m)$ values were used in the following calculation procedure for pitching moment coefficient:

(1) Compute the following two-dimensional conditions at a rotor blade section α, M, A, B.

(2) Compute the dimensionless stall angle parameter $\sigma_m = \alpha/\alpha_{sm}$ where α_{sm} corresponds to the blade section Mach number M.

(3) Enter the pitching moment tabulation with σ_m, A, B and extract $C_{m_{model}}(\sigma_m, A, B)$.

(4) Calculate $C_m(\sigma_m, A, B) = C_{m_{model}}(\sigma_m, A, B) + \delta_m(\sigma_m)$.

Table VIII lists the moment stall angles, α_{sm}, used in the present calculations.

CORRELATION STUDY

The purpose of the correlation study was to evaluate the analytical capability for predicting stall-flutter-induced control loads using the unsteady aerodynamic model described herein. Three rotor systems having large retreating blade control loads were chosen for this study: the NH-3A (S-61F) compound helicopter rotor at high speed, the CH-53A helicopter rotor under heavy loading, and a dynamically scaled model rotor. Each rotor system had been extensively instrumented to measure the required blade loads and responses. References 25, 26, and 27 are the sources of the test data for the NH-3A, the CH-53A, and the model rotor, respectively. The cases chosen for the present study are summarized in Table IX with designations from the appropriate reference.

The Normal Modes Blade Aeroelastic Analysis was used to calculate the blade elastic response for each of the flight conditions. This program, which is described in Reference 28, represents blade flatwise, edgewise, and torsional elastic deformation by a summation of normal mode responses. A timewise integration of the equations of motion for a coupled rotor aerodynamic and dynamic system is used to solve for the modal response. Using this analysis, the effect of unsteady aerodynamics on the blade dynamic response was studied. As detailed in Reference 8, the unsteady airfoil data were incorporated into the blade response calculations. At each azimuthal and radial blade station the blade angle of attack and its first two time derivatives were computed and used to look up the C_n and C_m coefficients from the unsteady tables. These coefficients were then scaled to the local blade Mach number using the procedure outlined in the previous section. The importance of variable rotor inflow was evaluated using the UAC Prescribed Wake Analysis, which calculates the induced velocity distribution over the rotor disk due to the rotor shed wake. This procedure is described in Reference 29. The results of the correlation study should indicate the importance of unsteady aerodynamic and variable inflow effects in modelling rotor blade torsional excitation.

NH-3A FLIGHT TEST CORRELATION

The five-bladed NH-3A compound helicopter exhibits pronounced high-frequency torsional oscillations over a range of high-speed flight conditions. Four conditions were chosen for investigation: a 186-knot case with $C_T/\sigma = 0.0579$, two cases at approximately 160 knots and $C_T/\sigma = 0.073$, and a 138-knot 60-degree angle of bank coordinated turn at $C_T/\sigma = 0.0854$. These cases were chosen because their C_T/σ values were among the highest

experienced for this aircraft. Because of the auxiliary propulsion from the jets, the rotor trim conditions are generally not typical of pure helicopter operation. Table IX shows small tip-path-plane inclinations for two of the correlation cases and suggests that wake effects may have an important influence upon blade response. For a small tip-path-plane inclination, the wake remains close to the rotor and hence can affect it more than it would for a large tip-path-plane inclination.

The rotor blades were modelled using rigid-body flapping and lagging degrees of freedom and five flatwise, two edgewise, and two torsional elastic modes. In all cases, rotor shaft angle and cyclic pitch were taken from test measurements, and collective pitch was incremented to match measured lift. The use of two-dimensional lifting line theory has consistently underpredicted rotor lift, making it necessary to augment collective pitch in the analytical solution.

EFFECT OF MODIFICATIONS TO ORIGINAL UNSTEADY DATA

The investigation was begun by running NH-3A case 43 with the original unsteady aerodynamic tables (Reference 8) which were modified to smooth regions of irregular data. In this calculation, a small fourth-quadrant oscillation was predicted. Figure 50 shows the analytical response with and without the data modifications. The level of calculated response is lower than the measured value and does not initiate over the nose of the aircraft.

The possibility that rotor trim might be critical in determining stall flutter susceptibility was examined. The computer program was run with incremental changes in cyclic and collective pitch. These cases generally resulted in calculated lifts and propulsive forces different from test data. Figure 51 demonstrates that variations in longitudinal cyclic pitch do modify the fourth-quadrant torsional response for constant C_T/σ but do not change the basic character of the results. Figure 52 shows that increasing collective pitch can induce higher levels of analytic response but not the proper azimuthal distribution. In this case, C_T/σ varied from 0.0475 at θ_{75} = 7.29 degrees to 0.067 at θ_{75} = 9.29 degrees, as shown.

In the compound mode, nonuniform rotor inflow can be expected to be a significant factor in determining blade angles of attack and, therefore, aerodynamic forces and moments. Three forms of nonuniform rotor inflow were examined. First, the UAC Prescribed Wake Analysis was used to calculate the induced velocities caused by a nondistorted helical wake. When case 43 was rerun with this inflow, there was an improvement both in

amplitude and azimuthal character correlation. As seen in Figure 53 (note change in scale in this figure), the unsteady aerodynamic model predicts a torsional oscillation beginning at about azimuth angle ψ = 160 degrees and persisting over the retreating side of the rotor disk. Second, the Prescribed Wake Analysis was used to calculate a rotor inflow in which the distortions of the rotor wake due to interactions between vortex elements were included. The resulting normal modes solution for case 43 using this distorted wake inflow was not significantly different from the nondistorted wake solution. Examination of the small change in calculated trajectories of tip filaments indicates that distortion does not significantly affect rotor inflow for this thrust, advance ratio, and tip-path-plane inclination. Finally, the effect of the aircraft wing on induced velocity in the plane of the rotor was examined. Wing lift was estimated from aircraft gross weight and main rotor shaft tension. The UAC Rotor Wake Interference Program was used to describe induced velocities in the plane of the rotor caused by the wing circulation. The effect on rotor inflow was determined to be small for the low-wing S-61F configuration. The torsional response prediction taking into account distorted wake and wing inflow effects was essentially the same as that using the nondistorted wake.

EFFECT OF NEW UNSTEADY DATA

When the new unsteady model data became available, the analysis was carried out for NH-3A cases 28, 39, 43, and 72. Figures 54 through 57 compare the steady and unsteady solutions obtained for these cases using constant inflow. The level of torsional excitation is significantly underpredicted by both the steady and unsteady solutions. The reason for the discrepancy in the steady components of the response is not known. This may be the result of changes in blade steady pitching moment introduced by trim tabs and tip weights used to achieve proper balancing and tracking. Also, there may be a bias applied to the data during the signal acquisition and conditioning process. Figure 58 shows a sample of flatwise and edgewise stress correlation obtained with constant inflow. The level of edgewise vibratory stress calculated with unsteady aerodynamics and constant inflow is much less than that measured in test. Compared to calculations using steady aerodynamics, unsteady aerodynamic solutions generally require lower collective pitch angles to match test values of lift. This results in lower edgewise drag loads and stresses. The lack of reliable unsteady drag data adds to the difficulties involved in predicting dynamic response.

To study the combined effects of the new unsteady data and variable inflow, two of the NH-3A cases were rerun with nondistorted wake inflow distributions. As was found with the original unsteady data, greater torsional moment oscillations were achieved. The calculated results were very sensitive to small changes in rotor tip-path-plane orientation. Figure 59 for case 43 shows that the peak-to-peak torsional moment is well matched by the analysis. The advancing blade oscillations are the result of calculated vortex-blade passage distances that are much smaller than those experienced in flight. The calculation was repeated with a $\frac{1}{2}$-degree change in tip-path-plane angle, and the advancing blade oscillation was diminished. The final result is shown in Figure 60. The same sensitivity to rotor inflow was found for case 39. Inflows were calculated for the measured tip-path-plane angle and for a tip-path-plane angle perturbed by 1 degree. The results do not show as good phase correlation, but the sensitivity of the calculation to inflow variations is similar to that shown for case 43. Figure 61 shows the flatwise and edgewise stress correlation obtained for case 43 with the modified nondistorted wake. In this case, the flatwise vibratory stress is overestimated but the edgewise response is near the level measured in test. The nature of the edgewise response lends support to the feeling that proper modelling of wake effects is important for these flight conditions.

DISCUSSION OF THE NH-3A CORRELATION

The determination of the important effect of the nonuniform inflow is a major result of the NH-3A correlation study. For these cases, small tip-path-plane inclinations and fairly small rotor loading lead to small wake skew angles. Examination of a group of NH-3A cases which had greater negative tip-path-plane angles of attack bears out the general conclusion that high levels of torsional response are related to blade-wake interaction. Induced velocity fluctuations on the forward portion of the rotor disk cause oscillations in blade pitching moment well before the blade enters deep stall. Examination of the blade dynamic equations indicates that for these cases, the aerodynamic moments applied to the advancing blade can result in small torsional oscillations over the nose of the aircraft which serve to define initial conditions for retreating blade response. In the third and fourth quadrants of rotor azimuth, the blade acts in torsion like a simple oscillator with very small or even negative aerodynamic damping. Unsteady aerodynamics are needed to model the growth rate of the retreating blade oscillation. The lack of phase correlation seen in some of the torsional response calculations and the overprediction of flatwise and edgewise stress shown in Figure 61 point out the difficulties involved in combining a discrete wake analysis and a lifting-line

aerodynamic model. Calculation of blade aerodynamics at a set of radial locations can be a poor representation of distributed aerodynamic loading for abruptly varying inflow. Representation of the blade as a lifting surface rather than a lifting line would appear to be necessary in regions where vortices are passing close to blades. Unsteady drag data are also necessary for proper modelling of edgewise response. (Steady-state drag data were used in this analysis.)

MODEL ROTOR TEST CORRELATION

The analytical unsteady model was applied to the problem of predicting torsional oscillations obtained under controlled wind tunnel conditions. Reference 27 reports the results of a series of tests performed with a 9-foot-diameter articulated model rotor. The four untwisted blades had 0.353-foot chords, giving the rotor a solidity of 0.1. The airfoil section was NACA 0012. The blades were dynamically scaled replicas of full-scale blades having comparable mass and stiffness distributions. At each of a series of advance ratios, blade collective pitch was incremented until high retreating blade torsional stress levels were encountered. For this rotor system, the large torsional response generally initiated in the third quadrant, increased in amplitude through the fourth quadrant, and was damped out before azimuth angle $\psi = 90$ degrees was reached. Two of the more extreme conditions were chosen for analytical study: case 51-11, which had an advance ratio of $\mu = 0.504$ and $C_T/\sigma = 0.081$, and case 68-6, which had $\mu = 0.294$ and $C_T/\sigma = 0.105$.

In the Normal Modes Program, four flatwise, two edgewise, and two torsional elastic modes were used to describe the blades. Examination of low Reynolds number aerodynamic data indicated that lift and moment stall angles are reduced by about 20 percent from the high Reynolds number data characteristic of full-scale rotor operation. Accordingly, the unsteady data were scaled to lift and moment curves with stall angles reduced 20 percent. The program was run using measured cyclic pitch and shaft angle. Attempts to increase collective pitch to attain measured lift values were generally not successful. The two conditions studied were heavily stalled, so increases in collective pitch did not significantly increase calculated lift. Analytic lift was up to 15 percent below test lift for the same collective pitch settings.

When the new unsteady data tables were used in the prediction of model rotor stall flutter, too little torsional excitation was calculated. Figure 62 shows only a small fourth-quadrant oscillation for case 68-6. To study the reason for the small rate of growth of the oscillation, the

two cases were rerun with the original modified unsteady tables. Figures 63 and 64 show that the original unsteady aerodynamic tables predict less fourth-quadrant aerodynamic damping and more nearly match the magnitude of the stall flutter oscillation.

DISCUSSION OF THE MODEL ROTOR CORRELATION

Unlike the NH-3A, the model rotor seems to exhibit pure stall flutter. Significant torsional excitation grows quickly in the fourth quadrant, where the blade angles of attack penetrate into stall. Examination of the applied aerodynamic pitching moment and the torsional response shows definite regions of negative damping in the fourth quadrant. A better prediction of response is obtained with the original unsteady data than with the new data because the original data predicts larger negative damping regions. This may be due to the low aspect ratio of the model described earlier in this report.

CH-53A FLIGHT TEST CORRELATION

In heavily loaded flight conditions, the CH-53A experiences large torsional oscillations at the blade torsional natural frequency (approximately 6.5/rev). These oscillations generally start over the nose of the aircraft and grow in amplitude in the third and fourth quadrants of rotor azimuth. Case 55 of the CH-53A rotor loads report (Reference 26) was selected for analysis. This is a 137-knot flight condition with C_T/σ = 0.069. Three flatwise, two edgewise, and one torsional mode were found to be sufficient in describing the blade aeroelastic response. This case was studied using test values of shaft angle and cyclic pitch while iterating to the proper lift with collective pitch angle. Based on the model rotor results, it was decided to use only the modified original unsteady data for the CH-53A correlation.

First, a series of cases was run with constant inflow. As in the case of the NH-3A, predicted torsional response was much too small. Two more constant inflow cases were run in which the blade stall angle was reduced by 10 and 20 percent. Figure 65 shows the effect of reducing the stall angle 20 percent. Deeper stall and higher levels of torsional excitation are calculated, but the response does not initiate over the nose of the helicopter and the amplitude of oscillation is not matched.

The importance of nonuniform rotor inflow for this case was studied by repeating the analysis using the variable inflow distribution consistent with a nondistorted rotor wake and the original blade stall angle values

(Table VIII). One of the difficulties encountered with the lifting-line analysis is that for very close vortex-blade passages, unrealistically large induced velocities can be calculated. Accordingly, the rotor inflow distribution calculated from the analysis was modified to smooth out an induced velocity spike calculated at ψ = 140 degrees and $\bar{r}$ = 0.75. Figure 66 shows the torsional signature resulting from this calculation. Although the peak-to-peak torsional moment is not quite matched, the phasing and frequency content of the solution are good. Figure 67 compares the root torsional moment calculated with steady and unsteady aerodynamics for the same modified nondistorted wake inflow. With steady-state aerodynamic data, the oscillation begins similarly in the region of ψ = 180 degrees but damps out over the retreating side of the rotor disk.

DISCUSSION OF THE CH-53A CORRELATION

The analytical results for the CH-53A are similar to those for the NH-3A. Even at this forward speed, a rotor tip-path-plane angle of attack of only -2 to -3 degrees existed. The wake deflection angle (angle between the rotor disk and wake streamlines) was calculated in the Prescribed Wake Analysis to be 5.0 degrees. As seen schematically in Figure 68, if the rotor skew angle is less than or equal to the coning angle, tip vortices trailed from the forward portion of the rotor disk can intersect inboard blade segments. Also shown in this figure is the pattern of trailing vortices at one instant of time for case 55. Several potentially strong vortex-blade interactions over the front half of the rotor disk are shown. As in the case of the NH-3A, the observed torsional response is a hybrid made up of wake-induced effects and retreating blade stall flutter. Blade torsion is excited over the nose of the aircraft, and the retreating blade oscillates in undamped motion at the blade natural frequency. The failure to match the amplitude of the test moment may be due to difficulties in scaling the unsteady pitching moment data to high Mach numbers. Compared to the NH-3A cases, this condition has lower forward speed and higher tip speed, both of which increase retreating blade Mach numbers. Mach number is known to have significant effects upon unsteady characteristics, and correlation of high-Mach-number hysteresis loops using the present scaling technique has been only fair.

GENERAL DISCUSSION OF CORRELATION

The complexity of the rotor unsteady three-dimensional aerodynamic environment suggests that complete understanding of blade torsional response and control load buildup will require further fundamental study. Blade-wake interaction, blade dynamic response and dynamic stall effects

all contribute to the retreating blade torsional loads. The rotor trailing wake was found to be an important source of torsional excitation not only for the NH-3A compound but also for the CH-53A in the pure helicopter mode. Any lift or propulsive force condition which has a rotor coning angle greater than or approximately equal to the wake skew angle can result in inboard blade-vortex intersections. The CH-53A results indicate that for the large coning angles and small tip path plane angles characteristic of high lift flight, blade-vortex interference effects can become significant. The effect of blade-wake intersection on blade torsional response is an excitation of the blade first torsional mode by the large aerodynamic pitching moments resulting from vortex-induced local stall as the blade passes over the nose of the aircraft. In response to this applied moment the retreating blade acts like a simple spring-inertia torsional system with small damping. The negative pitch damping associated with dynamic stall serves to further increase the amplitude of retreating blade oscillations.

Blade aerodynamics were best described with the original unsteady data tables apparently because of the lower effective aspect ratio of the more recently tested model airfoil. Although the analysis generally underpredicted peak-to-peak control loads, good correlation of the azimuthal load distribution indicates that blade aerodynamic/dynamic effects are being reasonably well modelled. For this reason it is felt that qualitative predictions of control load trends can be obtained with the present analytical methods. However, continued correlation studies are, of course, desirable to examine other parameters and to increase the confidence level in the analysis. In addition, in applying the analysis, its assumptions should always be kept in mind. In particular, refinements to the blade lifting-line model used in the analysis should be considered to permit more accurate predictions of the loads induced by a vortex passing close to the blade.

CONCLUSIONS

The conclusions listed below were reached in the course of this investigation. Although conclusions 1, 2, and 3 derive from the current data, it is believed that these conclusions apply to the use of generalized data obtained from other sinusoidal experiments as well. Conclusions 4 and 5 were reached upon performing correlation studies with various rotor configurations involving the use of both the new generalized unsteady data and the original generalized unsteady data from Reference 8.

1. The generalized normal force and moment data can be used to reconstruct accurately the aerodynamic response of an airfoil oscillating either sinusoidally or nonsinusoidally.

2. The generalized moment data can be used to predict the stall flutter response of a flexured airfoil periodically driven into the stall region at low frequency.

3. Pressure waves which may be associated with dynamic stall vortex shedding appear to move rearward along the blade chord. Most of the dynamic stall activity appears to be confined to the airfoil suction surface.

4. Greatly improved correlation between measured rotor control loads and those predicted by the Normal Modes Blade Aeroelastic Analysis was achieved relative to the results obtained in Reference 8.

5. High-amplitude oscillatory control loads on rotor blades generally result from a combination of moments produced by local stall induced by blade-vortex interaction, stall flutter, and blade torsional dynamic response. The relative importance of these moment sources depends on the rotor operating condition. Best results were obtained with a smoothed version of the original unsteady data tables and variable rotor inflow.

RECOMMENDATIONS

The recommendations listed below are included here to provide a framework for the formulation of future programs in the study of dynamic stall aerodynamics and its relation to rotor blade control instabilities.

1. Analyses should be conducted to systematically define the rotor design factors influencing the buildup in control loads.

2. Additional stall flutter tests should be conducted on a flexured model with low mechanical damping driven at low frequency to simulate cyclic pitch changes. Use should be made of the techniques developed herein and a companion analysis performed to predict the motion.

3. Additional detailed pressure measurements should be made on instrumented models at higher Mach numbers to determine the effects of compressibility on dynamic stall.

4. The possibility of developing alternate methods for representing rotor blade unsteady aerodynamics should be investigated. These methods should strive to retain the general accuracy demonstrated by the α, A, B method while at the same time avoiding its associated large data acquisition and reduction requirements.

5. Unsteady drag characteristics should be measured and incorporated into the blade response calculations.

6. Improved procedures for accurately predicting lifts and moments on a blade as it passes near a trailing vortex should be developed.

7. Parametric stall flutter analyses of a two-dimensional airfoil should be performed using the analytical techniques developed herein to determine the governing parameters and their effects on stall flutter.

8. Pressure data obtained in this investigation should be further analyzed to study in detail the apparent pressure wave associated with dynamic stall.

9. Additional stall flutter tests should be conducted with the object of visualizing the flow over the airfoil during the motion. This could range in sophistication from tuft and oil spray studies to high-speed Schlieren motion pictures.

10. Additional studies should be undertaken to further evaluate the ramp data obtained during this program. Particular attention should be paid to comparisons of force and moment response over regions of constant A.

LITERATURE CITED

1. Fink, M. R., TARE, INTERFERENCE AND PERFORMANCE DATA FOR THE UAC HELICOPTER ROTOR TEST APPARATUS, United Aircraft Research Laboratories Report R-0941-1, October 1956.

2. Arcidiacono, P. J., AERODYNAMIC CHARACTERISTICS OF A MODEL HELICOPTER ROTOR OPERATING UNDER NOMINALLY STALLED CONDITIONS IN FORWARD FLIGHT, Journal of the American Helicopter Society, Vol. 9, No. 3, July 1964.

3. Rabbott, J. P., Jr., COMPARISON OF THEORETICAL AND EXPERIMENTAL MODEL HELICOPTER ROTOR PERFORMANCE IN FORWARD FLIGHT, United Aircraft Corporation, Sikorsky Aircraft Division; TCREC Technical Report 61-103, U. S. Army Transportation Research Command, Fort Eustis, Virginia, July 1961.

4. McCloud III, J. L. and McCullough, G. B., COMPARISON OF CALCULATED AND MEASURED STALL BOUNDARIES OF A HELICOPTER ROTOR AT ADVANCE RATIOS FROM 0.3 TO 0.4, NASA TN D-73, September 1959.

5. Sweet, G. E. and Jenkins, J. L., Jr., RESULTS OF WIND TUNNEL MEASUREMENTS ON A HELICOPTER ROTOR OPERATING AT EXTREME THRUST COEFFICIENTS AND HIGH TIP SPEED RATIOS, Journal of the American Helicopter Society, Vol. 8, No. 3, July 1963.

6. Harris, F. D. and Pruyn, R. R., BLADE STALL - HALF FACT, HALF FICTION. American Helicopter Society, 23rd Annual National Forum Proceedings, AHS Preprint No. 101, May 1967.

7. Liiva, J., et al., TWO-DIMENSIONAL TESTS OF AIRFOILS OSCILLATING NEAR STALL, Vol. I, Summary and Evaluation of Results, The Boeing Company, Vertol Division; USAAVLABS TR 68-13A, U. S. Army Aviation Materiel Laboratories, Fort Eustis, Virginia, April 1968, AD 670957.

8. Arcidiacono, P. J., et al., INVESTIGATION OF HELICOPTER CONTROL LOADS INDUCED BY STALL FLUTTER, United Aircraft Corporation, Sikorsky Aircraft Division; USAAVALABS Technical Report 70-2, U. S. Army Aviation Materiel Laboratories, Fort Eustis, Virginia, March 1970, AD 869823.

9. Carta, F. O., EXPERIMENTAL INVESTIGATION OF THE UNSTEADY AERODYNAMIC CHARACTERISTICS OF AN NACA 0012 AIRFOIL, United Aircraft Research Laboratories Report M-1283-1, August 1960.

10. Fung, Y. C., THE THEORY OF AEROELASTICITY, John Wiley & Sons, Inc., New York, 1955.

11. Ham, N. D. and Garelick, M. S., DYNAMIC STALL CONSIDERATIONS IN HELICOPTER ROTORS, Journal of the American Helicopter Society, Vol. 13, No. 2, April 1968, pp. 49-55.

12. Carta, F.O., et al., ANALYTICAL STUDY OF HELICOPTER ROTOR STALL FLUTTER, American Helicopter Society, 26th Annual National Forum, AHS Preprint No. 413, June 1970.

13. Davis, E. L., THE MEASUREMENT OF UNSTEADY PRESSURES IN WIND TUNNELS, AGARD Report 169, March 1958.

14. Milne, W. E., NUMERICAL CALCULUS, Princeton University Press, 1949, pp. 285-290.

15. Perkins, C. D. and Hage, R. E., AIRPLANE PERFORMANCE STABILITY AND CONTROL, John Wiley & Sons, Inc., New York, 1949, p. 84.

16. Ward, D. and Cohen, W., WIDE BAND SYSTEM FOR ACQUIRING AND RECORDING DATA (WISARD), United Aircraft Research Laboratories Report H-076944-1, October 1969.

17. Oliver, B. M. and Cage, J. M., editors, ELECTRONIC MEASUREMENTS AND INSTRUMENTATION, McGraw-Hill Book Compnay, Inc., New York, 1971, pp. 116-118.

18. Halfman, R. L., et al., EVALUATION OF HIGH-ANGLE-OF-ATTACK AERODYNAMIC -DERIVATIVE DATA AND STALL-FLUTTER PREDICTION TECHNIQUES, NACA Technical Note 2533, November 1951.

19. Ham, N. D, AERODYNAMIC LOADING ON A TWO-DIMENSIONAL AIRFOIL DURING DYNAMIC STALL, AIAA Journal, Vol. 6, No. 10, October 1968, pp. 1927-1934.

20. Carta, F. O., and Niebanck, C. F., PREDICTION OF ROTOR INSTABILITY AT HIGH FORWARD SPEEDS, Vol. III, Stall Flutter, United Aircraft Corporation, Sikorsky Aircraft Division; USAAVLABS Technical Report 68-18C, U. S. Army Aviation Materiel Laboratories, Fort Eustis, Virginia, February 1969, AD 687322.

21. Carta, F. O., EFFECT OF UNSTEADY PRESSURE GRADIENT REDUCTION ON DYNAMIC STALL DELAY, AIAA Journal of Aircraft, Vol. 8, No. 10, October 1971, pp. 839-841.

22. Fisher, R. K. and McCroskey, W. J., DETAILED AERODYNAMIC MEASUREMENTS ON A MODEL ROTOR IN THE BLADE STALL REGIME, American Helicopter Society, 27th Annual National Forum, AHS Preprint No. 521, May 1971.

23. McCroskey, W. J., MOTION PICTURE SHOWN AS PART OF Ref. 22.

24. Crockett, C., TWO-DIMENSIONAL TESTS OF EIGHT SYMMETRICAL AIRFOIL SECTIONS WITH THICKNESS RATIOS FROM 5 TO 12 PERCENT, United Aircraft Research Laboratories Report B430113-1, July 1963.

25. Fenaughty, R. and Beno, E., NH-3A VIBRATORY AIRLOADS AND VIBRATORY ROTOR LOADS, United Aircraft Corporation, Sikorsky Aircraft Division Report SER 611493, NASC Report, Naval Air Systems Command, Washington, D. C., January 1970.

26. Beno, E., CH-53A MAIN ROTOR AND STABILIZER VIBRATORY AIRLOADS AND FORCES, United Aircraft Corporation, Sikorsky Aircraft Division Report SER 65593, NASC Report, Naval Air Systems Command, Washington, D. C., June 1970.

27. Niebanck, C. F. and Bain, L. J., ROTOR AEROELASTIC INSTABILITY AND TRANSIENT CHRACTERISTICS, United Aircraft Corporation, Sikorsky Aircraft Division; USAAVLABS Technical Report 69-88, U. S. Army Aviation Materiel Laboratories, Fort Eustis, Virginia, February 1970, AD 869035.

28. Arcidiacono, P. J., PREDICTION OF ROTOR INSTABILITY AT HIGH FORWARD SPEEDS, Vol. I, Steady Flight Differential Equations of Motion for a Flexible Helicopter Blade With Chordwise Mass Unbalance, United Aircraft Corporation, Sikorsky Aircraft Division; USAAVLABS Technical Report 68-18A, U. S. Army Aviation Materiel Laboratories, Fort Eustis, Virginia, February 1969, AD 685860.

29. Landgrebe, A. J., AN ANALYTICAL METHOD FOR PREDICTING ROTOR WAKE GEOMETRY, United Aircraft Research Laboratories, Journal of the American Helicopter Society, Vol. 14, No. 4, October 1969, pp. 20-32.

30. Blackman, R. B. and Tukey, J. W., THE MEASUREMENT OF POWER SPECTRA FROM THE POINT OF VIEW OF COMMUNICATIONS ENGINEERING, Part I, Bell System Technical Journal, Vol. 37, 1958, pp. 185-282.

31. Milne, W. E., NUMERICAL SOLUTION OF DIFFERENTIAL EQUATIONS, John Wiley & Sons, Inc., New York, 1953.

APPENDIX I
USE OF GAUSSIAN QUADRATURE

An excellent discussion of the use of the Gaussian quadrature technique to integrate experimentally measured chordwise pressures is given by Davis in Reference 13. An attempt will be made here to summarize it briefly before describing the application of this technique to the present study.

First, the pressure orifices must be located at a series of coordinate points corresponding to the roots of a Legendre polynomial, suitably normalized over the region of integration. According to Davis, the method has the advantage that for n pressure stations, an exact integration is possible if the pressure distribution can be represented by a polynomial of (2n-1)th degree. If the measured pressure distribution can only be approximated by a polynomial, Gauss's method will always lead to a higher order of accuracy for the same number of pressure stations than other numerical integration procedures, such as trapezoidal or Simpson's rule integration. It is shown in Figure 10 of Reference 13 that the probable error in computing the chordwise normal force using 10 or more Gaussian stations is 1 percent or less.

It was necessary to adapt the Gaussian method to apply it to the present experiment. In ordinary usage, the formula for the area under a curve $f(\xi)$ over the normalized interval $0 \leq \xi \leq 1$ is computed from the formula

$$A = \int_0^1 f(\xi)\,d\xi = \sum_{i=1}^{N} W_i f(\xi_i) \qquad (0 \leq \xi \leq 1) \tag{10}$$

where the W_i in the right-hand expression are the Gaussian weighting coefficients. The N values of ξ_i are located at the zeroes of the Nth degree Legendre polynomial. For 10 chordwise stations, the values of ξ_i and W_i are given in Table X. It is seen from the second column of this table that the last ξ value is located 1.3 percent from the end of the interval, and the next to last ξ value is located 6.7 percent from the end of the interval. However, there was insufficient room in the trailing-edge region of the model rib to place transducers aft of the 80 percent chord station. As a compromise solution, it was decided to place the transducers where there was room ahead of the 80 percent chord station, and to connect the three rearmost transducers to their measuring stations by means

of surface tunnels (described earlier), but to restrict the rearmost measuring station to be no farther aft than the 90 percent chord station. Thus it was necessary to extrapolate over the last 10 percent of the chord to complete the chordwise integrations.

The actual procedure is indicated schematically in Figure 69 and is described below. Let η be a dimensionless chordwise coordinate, $0 \leq \eta \leq 1$, and let $z < \eta$ be some point near the trailing edge. If $C_p(\eta)$ is the chordwise pressure coefficient, then the normal force will be given by the integral

$$C_n = \int_0^1 C_p(\eta)\, d\eta = \int_0^z C_p(\eta)\, d\eta + \int_z^1 C_p(\eta)\, d\eta \qquad (11)$$

where the right-hand formulation represents the Gaussian integration over $0 \leq \eta \leq z$ and the extrapolated integration over $z \leq \eta \leq 1$. If we let

$$\eta = z\,\xi \qquad (12)$$

Equation (11) becomes

$$C_n = z \int_0^1 C_p(\xi)\, d\xi + \int_z^1 C_p(\eta)\, d\eta \qquad (13)$$

Replace the first integral of Equation (13) by its Gaussian equivalent from Equation (10),

$$C_n = z \sum_{i=1}^{N} W_i\, C_p(\xi_i) + \int_z^1 C_p(\eta)\, d\eta \qquad (14)$$

The rearmost orifice was chosen to be located at the 90 percent chord station (see Table X, right-hand column), so $\xi_i = 0.98695$ corresponds to $\eta = 0.90$. Hence, from Equation (12), we can solve for z to obtain $z = 0.912$. Equation (14) then becomes

$$C_n = 0.912 \sum_{i=1}^{10} W_i C_p(\xi_i) + \int_{.912}^{1} C_p(\eta)\, d\eta \tag{15}$$

To evaluate the last integral, assume a parabolic form to $C_p(\eta)$,

$$C_p(\eta) = C_A + C_B \eta + C_C \eta^2 \tag{16}$$

and require that the curve pass through the coordinates (η_9, C_{p9}), $(\eta_{10}, C_{p_{10}})$ and (1, 0). The final result for this integral will then be

$$\int_z^1 C_p(\eta) d\eta = C_A(1-z) + \frac{1}{2} C_B(1-z^2) + \frac{1}{3} C_C(1-z^3) \tag{17}$$

where

$$\left.\begin{aligned} C_A &= \frac{1}{\Delta}\left[C_{p_9}\eta_{10}(1-\eta_{10}) - C_{p_{10}}\eta_9(1-\eta_9)\right] \\ C_B &= \frac{1}{\Delta}\left[C_{p_{10}}(1-\eta_9^2) - C_{p_9}(1-\eta_{10}^2)\right] \\ C_C &= \frac{1}{\Delta}\left[C_{p_9}(1-\eta_{10}) - C_{p_{10}}(1-\eta_9)\right] \end{aligned}\right\} \tag{18}$$

$$\Delta = (\eta_{10}-\eta_9)(1-\eta_{10})(1-\eta_9)$$

and where

$$\left.\begin{aligned} z &= 0.9119 \\ \eta_9 &= 0.850374 \\ \eta_{10} &= 0.90 \end{aligned}\right\} \tag{19}$$

The moment coefficient about the 25 percent chord station is obtained from these equations by replacing $C_p(\xi_1)$ and $C_p(\eta)$ by

$$F(\xi_i) = (0.25 - \xi_i)\, C_p(\xi_i) \tag{20}$$

and

$$F(\eta) = (0.25 - \eta)\, C_p(\eta) \tag{21}$$

respectively.

APPENDIX II
OPTIMUM RECORDING CONDITIONS FOR WISARD

Fourier spectral methods were not directly used in the analysis of the unsteady data. However, the ability of the data system to extract information with sufficient frequency resolution to ensure accuracy and repeatability was dependent on many of the same parameters that govern the resolving capabilities of the spectral analysis technique (Reference 30). Hence, the parameter values selected for the data recording mode were the same as those that would be required for a spectral analysis.

In this brief analysis, we seek to establish the criteria which were used to select the tape speed at which data were recorded (S_R in in./sec) and total record time (T in sec). To do this, we must first note that the absolute sampling rate of WISARD during data playback (which is the rate at which data were digitized and stored on digital tape) was 15,000 samples/sec. This rate was divided by the number of channels being sampled, N_C, to obtain the absolute sampling rate per channel during playback,

$$h_{R_{ABS}} = \frac{1}{\Delta T_{ABS}} = \frac{15{,}000}{N_C} \quad (\text{samples/sec}) \tag{22}$$

where ΔT_{ABS} is the absolute time between samples.

In general during this test program, the recording speed, S_R, was greater than the playback speed, S_p. In this case, the effective sampling rate of the original data, within the time frame of the original data, was greater by the ratio S_R/S_p, or

$$h_R = h_{R_{ABS}} \times \frac{S_R}{S_p} = \frac{1}{\Delta T} = \frac{1}{\Delta T_{ABS}} \times \frac{S_R}{S_p} \tag{23}$$

where h_R is the effective sampling rate and ΔT is the time between samples in the original time domain. Hence, from Equations (22) and (23),

$$h_R = \frac{1}{\Delta T} = \frac{15{,}000}{N_c} \times \frac{S_R}{S_p} \quad \text{(samples / sec)} \tag{24}$$

In many cases, the core storage capacity of the computing machine was a limiting factor. In the spectral analysis procedure outlined in Reference 30, a specific parameter, m, is denoted as the total number of samples to be processed per channel. This is most conveniently chosen to be some integral power of 2, the most useful of which are

$$m = \begin{cases} 512 = 2^9 \\ 1024 = 2^{10} \\ 2048 = 2^{11} \\ 4096 = 2^{12} \\ 8192 = 2^{13} \end{cases} \quad \text{samples /channel} \tag{25}$$

Thus the minimum recording time to obtain m samples per channel is obtained by dividing Equation (25) by Equation (24), or

$$T = \frac{m}{h_R} = \frac{m N_c}{15{,}000\,(S_R/S_p)} \quad \text{(sec)} \tag{26}$$

In Reference 30, it is pointed out that an important parameter in the analysis is the minimum number of samples per cycle of the highest harmonic of interest; this parameter is denoted as L in the present work. A criterion is established in Reference 30 that when L = 2 samples/cycle, a maximum frequency can be determined from Equation (24),

$$f_{max} = \frac{h_R}{L} = \frac{h_R}{2} \quad \text{(cps)} \tag{27}$$

which sets an upper limit for meaningful results. This is the highest frequency attainable before aliasing takes place, in which higher frequency information (at $f > f_{max}$) is folded into the low-frequency domain

(see Reference 30 for more details on aliasing). Use of a minimum value of L = 4 samples/cycle in the present analysis and a low-pass filter to block the high-frequency noise ensured the accuracy of the data to well beyond the highest harmonic specified as f_{max}.

A final parameter of interest is the bandwidth which defines the frequency resolution of the computation. This is defined in Reference 30 as twice the maximum frequency of interest divided by the number of samples being analyzed, or

$$B_w = \frac{2 f_{max}}{m} \tag{28}$$

When Equations (24) and (27) (with L = 4) are substituted into Equation (28), the result is

$$B_w = \frac{7500}{mN_c}\left(\frac{S_R}{S_p}\right) \tag{29}$$

The number of channels in this application was $N_c = 12$, and the number of samples per channel chosen for analysis was m = 4096. With the introduction of these numbers, Equations (26), (28), and (29) can be rearranged to yield

$$\frac{S_R}{S_p} = \frac{f_{max}}{312.5} \tag{30}$$

$$B_w = 0.15259\left(\frac{S_R}{S_p}\right) \tag{31}$$

$$T = \frac{3.2768}{(S_R/S_p)} \tag{32}$$

These equations were used to construct Table III. The highest harmonic of interest, f_{max}, was chosen to be 10 times the test frequency, and S_R/S_p was computed from Equation (30). Use of a fixed value, $S_p = 1.875$ in./sec, fixed the calculated value of S_R. However, the tape recorder could operate only at fixed multiples of the playback speed, so the next highest value of S_R was chosen and the actual speed ratio S_R/S_p was computed. This was then introduced into Equations (31) and (32) to compute the frequency resolution and record time. Finally, the actual number of samples per cycle in the 10th harmonic, L_{ACT}, was obtained by solving Equation (27) for L, substituting Equation (24) for h_R, and using $N_c = 12$ and the actual tape speed ratio,

$$L_{ACT} = \frac{1250}{f_{max}} \left(\frac{S_R}{S_p} \right)_{ACT} \tag{33}$$

APPENDIX III
NUMERICAL SOLUTION OF AIRFOIL RESPONSE EQUATION

The single-degree-of-freedom system consisting of the NACA 0012 airfoil mounted in the wind tunnel on a torsional spring was analyzed using the α, A, B tabulation of unsteady moment. In the test, the airfoil was held in the tunnel sidewall plates by thrust bearings which introduced a significant amount of damping. As mentioned in the text, the airfoil was excited sinusoidally.

The equation of motion of the mechanical system described is the same as that for a single-degree-of-freedom torsional forced vibration problem with damping but also with an added external moment resulting from the airflow over the airfoil. The equation of motion may be written as

$$I\ddot{\alpha} + C\dot{\alpha} + K(\alpha - \alpha_M) = M(t, \alpha, \dot{\alpha}, \ddot{\alpha}, \ldots) + T_o \cos \omega t \qquad (34)$$

where I = airfoil mass moment of inertia in pitch

C = equivalent viscous damping

K = torsional spring constant

$M(\ )$ = aerodynamic moment

T_o = magnitude of the applied torque

ω = frequency of applied moment

t = time

α = instantaneous angle of attack

α_M = mean angle of attack of the oscillation

The primary purpose of this program was to test the ability of the sinusoidally generated unsteady force and moment data to predict non-sinusoidal unsteady force and moment. Accordingly, the aerodynamic moment used in the differential equation (Equation (34)) was assumed to be a function of angle of attack and its first two time derivatives only, and it was expressed as $M(\alpha, A, B)$. Equation (34) may be divided through by $2\rho V^2 b^2$ to convert the moment to the moment coefficient, with the result

$$\frac{I}{2\rho V^2 b^2}\left[\ddot{\alpha} + \frac{C}{I}\dot{\alpha} + \frac{K}{I}(\alpha - \alpha_M)\right] = C_m(\alpha, A, B) + \frac{T_0 \cos \omega t}{2\rho V^2 b^2} \qquad (35)$$

If we define the quantities

$$I_\alpha = \frac{I}{2\rho b^4} \qquad (36)$$

$$\frac{C}{I} = \frac{\omega_\alpha \delta}{\pi} \qquad (37)$$

$$\frac{K}{I} = \omega_\alpha^2 \qquad (38)$$

where ω_α is the torsional natural frequency and δ is the logarithmic decrement of the damped oscillation, then Equation (35) may be rewritten as

$$I_\alpha \left(\frac{b}{V}\right)^2 \left[\ddot{\alpha} + \frac{\omega_\alpha \delta}{\pi}\dot{\alpha} + \omega_\alpha^2 (\alpha - \alpha_M)\right] = C_M(\alpha, A, B) + \frac{T_0 \cos \omega t}{2\rho V^2 b^2} \qquad (39)$$

Dividing through by $I_\alpha (b/V)^2$ yields

$$\ddot{\alpha} + \left(\frac{\omega_\alpha \delta}{\pi}\right)\dot{\alpha} + \omega_\alpha^2 (\alpha - \alpha_M) = \frac{C_m(\alpha, A, B)}{I_\alpha (b/V)^2} + \frac{T_0 \cos \omega t}{I} \qquad (40)$$

This second-order differential equation can be converted to two first-order equations for solution on the computer by assuming that

$$\dot{\alpha} = \beta \tag{41}$$

Now Equation (40) may be written as

$$\dot{\beta} = -\left(\frac{\omega_\alpha \delta}{\pi}\right)\beta - \omega_\alpha^2(\alpha - \alpha_M) + \frac{C_m(\alpha, A, B)}{I_\alpha(b/V)^2} + \frac{T_0 \cos \omega t}{I} \tag{42}$$

Equations (41) and (42) are a pair of first-order differential equations suitable for solution on the computer. It should be noted that since $A = b\dot{\alpha}/V$ and $B = b^2\dot{\beta}/V^2$, the moment coefficient is a function of the parameters being solved for. The assumption has been made in the solution that if a sufficiently short time step is taken, the moment coefficient is adequately represented by using past values of A and B when interpolating Table V for C_m.

The initial conditions are taken at the peak of a cycle of motion as

$$\alpha_0 = \alpha(0) = \alpha_M + \bar{\alpha} \tag{43}$$

$$\beta_0 = \beta(0) = 0 \tag{44}$$

The solution was started with the best estimate of the actual C_m, namely,

$$C_{m_0} = C_m(\alpha_M + \bar{\alpha},\ 0,\ -b^2\omega^2\bar{\alpha}/V^2) \tag{45}$$

It was also necessary to estimate the angle of attack and its derivative at the end of the first time step, $\alpha_1 = \alpha(\Delta t)$ and $\beta_1 = \beta(\Delta t)$. This was accomplished by using the first three terms of Taylor's series as

$$\alpha_1 = \alpha_0 + \dot{\alpha}_0 \Delta t + \ddot{\alpha}_0 \frac{\Delta t^2}{2} + \ldots \tag{46}$$

$$\beta_1 = \beta_0 + \dot{\beta}_0 \Delta t + \ddot{\beta}_0 \frac{\Delta t^2}{2} + \ldots \tag{47}$$

where Δt is the time increment of the solution. In applying Equations (46) and (47), it was necessary to revert to the original differential equations to obtain

$$\ddot{\alpha}_0 = \dot{\beta}_0 = -\omega_\alpha^2 (\alpha - \alpha_M) + \frac{C_{m_0}}{I_\alpha (b/V)^2} + \frac{T_0}{I} \tag{48}$$

and

$$\ddot{\beta}_0 = -\left(\frac{\omega_\alpha \delta}{\pi}\right) \dot{\beta}_0 - \omega_\alpha^2 \dot{\alpha}_0 \tag{49}$$

However, since $\dot{\alpha}_0 = \beta_0 = 0$, Equation (49) reduces to

$$\ddot{\beta}_0 = -\frac{\omega_\alpha \delta}{\pi} \dot{\beta}_0 \tag{50}$$

By substituting Equations (48) and (50) into Equations (46) and (47) together with the initial conditions, the quantities α_0, β_0, α_1, and β_1 are completely defined.

The numerical integration routine can now be started to obtain the complete solution. A simple trapezoidal formula (see Reference 31) was used with the following recursion relationships:

$$\alpha_{n+1} = \alpha_n + \frac{\Delta t}{2}(\beta_{n+1} + \beta_n) \tag{51}$$

$$\beta_{n+1} = \beta_n + \frac{\Delta t}{2}(\dot{\beta}_{n+1} + \dot{\beta}_n) \tag{52}$$

where $\dot{\beta}_{n+1}$ was obtained from the original differential equation (Equation (42)) with continually updated values of C_m.

The numerical integration was continued until two consecutive cycles of motion had converged to within an angle of attack discrepancy of 0.5 percent. Original computations were made to a tolerance of 0.1 percent, but the added accuracy occasionally caused convergence difficulties. These problems were most probably caused because the tabulated moment coefficients had small fluctuations and were not completely smooth mathematical functions. The larger tolerance amounted to a maximum of only 0.1 degree, which was roughly the plotting accuracy of the data and therefore was not significant.

TABLE I. TRANSDUCER SENSITIVITIES

Position Number	Percent Chord Behind L.E.	Sensitivity (mv/psi)
1	1.19	1.81
2	6.15	2.06
3	14.62	1.23
4	25.83	1.385
5	38.81	2.385
6	52.38	1.85
7	65.36	1.58
8	76.57	1.295
9	85.03	0.98
10	90.00	1.76

TABLE II. TEST PROGRAM OUTLINE

Item No.	Cam Description and Angular Amplitude	Type of Coupler	Primary* Drive Frequency (cps)	Mean Angle* of Attack (deg)
1	none	rigid	0 (steady state)	0,3,7,9,10,11, 12,13,14,16, 18,20,22
2	sinusoidal, ±8	rigid	12.5, 31, 50, 75 100	3,6,9,11,12, 14,16,18
3	sinusoidal, ±8	rigid	120	3
4	sinusoidal, ±8	rigid	50,75	11 (single surface meas.)
5	sinusoidal, ±3	rigid	10,25,50,75	14
6	helicopter, ±8	rigid	10,16.7,33	6,11,14
7	forward ramp, ±8	rigid	7.5,10,15,20	6,11,14
8	backward ramp, ±8	rigid	7.5,10,15,20	6,11,14
9	sinusoidal, ±8	flexible (3 springs)	7.5,10,15	6,11,16
10	none	flexible (3 springs)	0 (free vibration)	6,11,16 + α for max. oscillation
11	none	flexible (3 springs)	impulsive loading, $\Delta\alpha \sim 3$	6,11,16

*Note: Each item represents test points taken at all possible combinations of frequency and angle of attack.

TABLE III. TAPE RECORDING PARAMETERS FOR WISARD

Test Frequency f (cps)	10th Harmonic Frequency f_{max} (cps)	Calculated Speed Ratio Eq. (30) S_R/S_P	Calculated Record Speed S_R (in./sec)	Actual Record Speed S_R (in./sec)	Actual Speed Ratio $(S_R/S_P)_{ACT}$	Frequency Resolution Eq. (31) B_w (cps)	Record Time Eq. (32) T (sec)	Actual Samples Per Cycle in 10th Harmonic L_{ACT}
12.5	125	0.4	0.75	1.875	1.0	0.1526	3.28	10.0
31.25	312.5	1.0	1.875	1.875	1.0	0.1526	3.28	4.0
50.0	500	1.6	3.0	7.5	4.0	0.6104	0.82	10.0
75.0	750	2.4	4.5	7.5	4.0	0.6104	0.82	6.67
100.0	1000	3.2	6.0	7.5	4.0	0.6104	0.82	5.0

TABLE IV. UNSTEADY NORMAL FORCE COEFFICIENT C_n FOR M = 0.325
α = 1 DEGREE

β \ α	-.048	-.040	-.032	-.024	-.016	-.012	-.008	-.006	-.004	-.002	0	.002	.004	.006	.008	.012	.016	.024	.032	.040	.048
.[illegible]	-.1[illegible]	-.057	-.015	.025	.063	.077	.050	.027	.006	-.011	-.023	-.031	-.033	-.030	-.023	-.004	.020	.080	.142	.205	.260
.[illegible]	-.08[illegible]	-.064	-.035	.013	.071	.088	.095	.094	.090	.083	.074	.070	.070	.072	.074	.080	.090	.117	.143	.175	.217
.[illegible]	-.057	-.035	-.005	.030	.056	.063	.070	.073	.075	.077	.080	.082	.084	.085	.085	.089	.095	.111	.132	.158	.198
.[illegible]	-.03[illegible]	-.014	-.001	.015	.034	.[illegible]	.060	.068	.075	.080	.085	.090	.093	.095	.098	.104	.110	.125	.145	.174	.216
.[illegible]	-.02[illegible]	-.02[illegible]	-.010	.010	.030	.051	.068	.075	.082	.087	.093	.096	.099	.103	.105	.113	.120	.140	.170	.197	.246
.[illegible]		-.007	.007	.033	.058	.07[illegible]	.08[illegible]	.086	.090	.097	.100	.108	.112	.118	.122	.133	.144	.165	.185	.207	
.[illegible]		.010	.021	.040	.06[illegible]	.07[illegible]	.08[illegible]	.090	.09[illegible]	.102	.10[illegible]	.113	.120	.125	.126	.140	.153	.175	.199	.220	
.[illegible]			.015	.04[illegible]	.06[illegible]	.075	.087	.095	.100	.10[illegible]	.110	.115	.120	.124	.131	.140	.164	.195	.245		
.[illegible]					.05[illegible]	.0[illegible]7	.0[illegible]1	.08[illegible]	.095	.100	.105	.111	.118	.122	.129	.145	.160				

TABLE IV - Continued
α = 2 DEGREES

B \ A	-.048	-.040	-.032	-.024	-.016	-.012	-.008	-.006	-.004	-.002	0	.002	.004	.006	.008	.012	.016	.024	.032	.040	.048
0	0	.035	.070	.104	.140	.155	.144	.127	.111	.100	.090	.080	.070	.065	.068	.089	.114	.163	.212	.265	.312
.001	-.013	.037	.077	.116	.147	.160	.164	.170	.170	.165	.160	.155	.153	.151	.150	.152	.157	.176	.205	.236	.278
.002	.003	.040	.059	.083	.113	.132	.155	.160	.167	.170	.173	.174	.173	.171	.170	.167	.170	.189	.224	.270	.325
.003	-.015	.015	.045	.079	.107	.130	.134	.140	.146	.153	.159	.164	.170	.175	.180	.189	.196	.204	.205	.211	.215
.004	.042	.054	.067	.080	.095	.102	.115	.123	.130	.140	.150	.160	.170	.180	.187	.202	.210	.220	.227	.235	.241
.006		.079	.082	.090	.096	.100	.105	.113	.131	.143	.156	.170	.183	.198	.210	.229	.239	.250	.262	.275	
.008		.090	.093	.098	.100	.101	.110	.118	.134	.146	.154	.170	.184	.199	.212	.234	.250	.270	.286	.302	
.012			.094	.093	.112	.115	.140	.150	.159	.167	.171	.180	.189	.197	.201	.218	.232	.260	.289		
.016					.133	.150	.170	.175	.180	.182	.185	.186	.188	.191	.195	.203	.212				

TABLE IV - Continued
α = 3 DEGREES

B \ A	-.048	-.040	-.032	-.024	-.016	-.012	-.008	-.006	-.004	-.002	0	.002	.004	.006	.008	.012	.016	.024	.032	.040	.048
0	.089	.135	.160	.173	.240	.242	.200	.180	.180	.100	.202	.145	.165	.153	.156	.193	.232	.265	.285	.320	.405
.001	.027	.077	.10	.173	.224	.245	.255	.254	.246	.233	.225	.228	.234	.238	.241	.245	.245	.240	.267	.313	.360
.002	.085	.100	.120	.163	.201	.214	.222	.223	.223	.222	.224	.226	.232	.240	.248	.261	.270	.280	.285	.287	.286
.003	.134	.143	.144	.157	.170	.180	.191	.199	.20	.215	.225	.234	.244	.255	.263	.276	.286	.299	.305	.305	.305
.004	.187	.16	.145	.134	.147	.157	.177	.190	.204	.217	.232	.245	.256	.267	.277	.292	.303	.319	.328	.332	.335
.00		.145	.13	.125	.134	.148	.170	.185	.200	.215	.232	.248	.260	.273	.284	.305	.322	.350	.370	.388	
.00		.105	.11	.128	.152	.16	.185	.190	.202	.210	.223	.230	.244	.265	.263	.287	.308	.351	.397	.442	
.01			.124	.145	.166	.178	.188	.193	.200	.203	.212	.217	.223	.230	.236	.252	.269	.305	.351		
.01					.180	.185	.190	.192	.196	.200	.200	.203	.208	.210	.210	.221	.230				

TABLE IV - Continued
α = 4 DEGREES

B \ A	-.048	-.040	-.032	-.024	-.016	-.012	-.008	-.006	-.004	-.002	0	.002	.004	.006	.008	.012	.016	.024	.032	.040	.048
-.003	.175	.190	.210	.225	.250	.285	.300	.310	.320	.330	.340	.350	360	.375	.370	.380	.385	.400	.430	.460	.515
-.002	.180	.195	.215	.240	.267	.281	.295	.300	.307	.314	.320	.327	.334	.340	.347	.360	.373	.390	.415	.450	.505
-.001	.190	.205	.225	.250	.280	.240	.280	.284	.288	.293	.297	.300	.305	.309	.313	.315	.340	.360	.400	.440	.490
0	.200	.210	.230	.270	.330	.350	.310	.300	.285	.277	.270	.263	.260	.260	.260	.270	.285	.320	.370	.420	.480
.001	.213	.213	.223	.244	.297	.328	.326	.317	.306	.299	.296	.298	.304	.312	.320	.335	.343	.350	.355	.355	.345
.002	.242	.220	.223	.235	.255	.269	.286	.293	.297	.298	.297	.295	.296	.301	.309	.332	.351	.372	.380	.380	.370
.003	.268	.223	.195	.190	.218	.245	.272	.285	.296	.300	.298	.292	.290	.295	.303	.332	.358	.392	.410	.418	.420
.004	.231	.190	.169	.174	.213	.232	.253	.263	.273	.282	.292	.302	.312	.321	.331	.350	.368	.401	.433	.457	.476
.006		.170	.160	.180	.210	.226	.240	.250	.258	.265	.274	.280	.291	.300	.310	.331	.352	.405	.465	.520	
.008		.185	.170	.178	.200	.213	.230	.240	.249	.260	.267	.275	.287	.300	.309	.315	.354	.400	.449	.498	
.012			.174	.172	.186	.200	.212	.220	.230	.240	.246	.255	.265	.275	.288	.310	.330	.380	.429		
.016					.175	.155	.157	.165	.185	.200	.215	.220	.245	.255	.268	.280	.297				

TABLE IV - Continued

α = 5 DEGREES

B \ A	-.048	-.040	-.032	-.024	-.016	-.012	-.008	-.006	-.004	-.002	0	.002	.004	.006	.008	.012	.016	.024	.032	.040	.048
-.006		.240	.250	.320	.350	.355	.360	.370	.375	.385	.395	.410	.425	.440	.465	.480	.490	.525	.555	.580	
-.004	.232	.255	.286	.313	.341	.355	.368	.375	.382	.388	.396	.403	.409	.417	.423	.436	.450	.487	.504	.533	.560
-.003	.250	.285	.295	.315	.340	.355	.372	.376	.381	.385	.391	.395	.400	.406	.410	.420	.432	.465	.475	.490	.530
-.002	.285	.300	.310	.315	.342	.352	.361	.365	[illegible]	.374	.379	.383	.387	.392	.397	.406	.414	.445	.450	.465	.525
-.001	.29[illegible]	.305	.315	.320	.37[illegible]	.350	.358	.363	.367	.372	.377	.382	.386	.391	.394	.400	.395	.430	.440	.465	.540
0	.2[illegible]	.29[illegible]	.31[illegible]	.36[illegible]	.4[illegible]	.42[illegible]	.40[illegible]	.35[illegible]	.37[illegible]	.365	.355	.350	.350	.355	.360	.370	.388	.410	.450	.490	.570
.001	.283	.288	.304	.332	.363	.377	.387	.372	.364	.372	388	.384	.382	.387	.394	.407	.418	.435	.448	.470	.482
.002	.287	.256	.240	.248	.305	.338	.357	[illegible]	.366	.369	.371	.373	.376	.381	.387	.400	.415	.450	.488	.532	.576
.003	.230	.200	.192	.230	.280	.308	.317	.325	.332	.344	.360	.376	.387	.395	.401	.410	.413	.463	.515	.545	.565
.004	.285	.220	.205	.237	[illegible]	.277	.290	.300	.313	.327	.340	.352	.366	.378	.391	.411	.418	.457	.527	.570	.620
.006		.227	.215	.220	.242	[illegible]	.285	.300	[illegible]	.320	.330	.345	.355	.365	.368	.403	.425	.470	.520	.560	
.008		.233	.205	.202	.224	.243	.264	.275	.284	[illegible]	.307	.320	.330	.340	.353	.377	.402	.454	.505	.560	
.012			.213	.192	.184	.204	.222	.230	.240	.250	.260	.270	.285	.295	.310	.375	.363	.422	.485		
.016					.1[illegible]	.185	.1[illegible]	.1[illegible]	.1[illegible]	[illegible]	.21	.2[illegible]	.23	.245	.265	.29	.32[illegible]				

TABLE IV - Continued
α = 6 DEGREES

B \ A	-.048	-.040	-.032	-.024	-.016	-.012	-.008	-.006	-.004	-.002	0	.002	.004	.006	.008	.012	.016	.024	.032	.040	.048
-.008		.345	.355	.372	.389	.407	.420	.426	.434	.452	.470	.480	.488	.500	.507	.532	.550	.570	.584	.596	
-.006		.333	.383	[illegible]	.413	[illegible]	.442	.448	.455	.462	.470	.477	.483	.489	.498	.513	.525	.545	.565	.610	
-.004	.352	[illegible]	[illegible]	.410	.430	[illegible]	.450	.455	.460	.465	.469	.476	.479	.484	.488	.498	.508	.528	.548	.568	.588
-.003	.345	.350	[illegible]	[illegible]	.423	.433	.444	.448	.454	.459	.464	.468	.473	.478	.484	.495	.505	.524	.544	.567	.586
-.002	.340	.355	.364	.388	.412	.423	.435	.442	.447	.453	.458	.464	.469	.476	.482	.492	.505	.527	.550	.570	.590
-.001	.338	.355	.355	[illegible]	.450	.454	.458	.459	.462	.464	.466	.467	.469	.471	.473	.476	.480	.438	.530	.567	.592
0	.346	.358	.377	.411	.471	[illegible]	.495	.485	.468	.456	.450	.454	.456	.458	.462	[illegible]	.476	.496	.525	.569	.655
.001	.300	.310	.325	.353	.402	.432	.455	.463	[illegible]	[illegible]	.455	.449	.453	.462	.470	.485	.497	.518	.548	.598	.666
.002	.197	.217	.245	.288	.365	.392	.413	.421	.428	.434	.437	.442	.447	.455	.461	.477	.494	.534	.577	.630	.707
.003	.225	.230	.258	.298	.335	.358	.378	[illegible]	.398	.408	.417	.427	.437	.447	.457	.477	.497	.537	.577	.617	.657
.004	.352	.339	.254	.256	.301	.324	.347	.358	.370	.373	.393	.405	.416	.427	.440	.462	.485	.532	.578	.624	.672
.006		.262	.233	.230	.259	.269	.304	.317	.333	.345	.359	.373	.385	.400	.415	.440	.470	.523	.575	.632	
.008		[illegible]	.225	.213	.232	[illegible]	[illegible]	[illegible]	[illegible]	.305	[illegible]	.337	.354	.370	.386	.418	.426	.507	.563	.620	
.012			[illegible]	.150	.175	[illegible]	[illegible]	[illegible]	[illegible]	.152	.270	[illegible]	[illegible]	.315	.334	.367	.400	.465	.532		
.016					[illegible]	[illegible]	.15	[illegible]	[illegible]	[illegible]	[illegible]	.245	[illegible]	[illegible]	[illegible]	.335	.370				

TABLE IV - Continued
α = 7 DEGREES

B \ A	-.048	-.040	-.032	-.024	-.016	-.012	-.008	-.006	-.004	-.002	0	.002	.004	.006	.008	.012	.016	.024	.032	.040	.048
-.016																					
-.012			.350	.375	.425	.450	.470	[illegible]	.500	.510	.530	.540	.550	.565	.580	.595	.610	.650	.690		
-.008		[illegible]	[illegible]	[illegible]	[illegible]	[illegible]	.517	[illegible]	.533	.540	[illegible]	.555	[illegible]	.570	[illegible]	.592	.605	.637	.667	.697	
-.006		[illegible]	[illegible]	[illegible]	[illegible]	[illegible]	[illegible]	[illegible]	[illegible]	.545	[illegible]	.555	[illegible]	.567	.574	.587	.598	.620	.650	.670	
-.004	[illegible]	[illegible]	[illegible]	[illegible]	[illegible]	.507	[illegible]	.524	[illegible]	.535	.540	.545	.551	.556	.562	.572	.583	.603	.624	.645	.667
-.003	[illegible]	[illegible]	[illegible]	[illegible]	[illegible]	[illegible]	.511	[illegible]	[illegible]	[illegible]	.533	[illegible]	.543	.550	.555	.560	.575	.600	.630	.660	.690
-.002	[illegible]	[illegible]	[illegible]	.477	[illegible]	[illegible]	.497	[illegible]	.503	.507	.511	.515	.520	[illegible]	.532	.545	.560	.598	.640	.685	.733
-.001	.425	[illegible]	.453	[illegible]	[illegible]	[illegible]	.547	[illegible]	[illegible]	.545	[illegible]	[illegible]	[illegible]	.528	.527	.535	.545	.572	.605	.642	.683
0	.375	[illegible]	.420	.453	.515	.557	.525	[illegible]	[illegible]	.548	[illegible]	.537	.538	.540	.544	.553	.567	.596	.625	.652	.676
.001	[illegible]	[illegible]	[illegible]	[illegible]	.435	[illegible]	[illegible]	[illegible]	[illegible]	[illegible]	[illegible]	[illegible]	.547	.553	.554	.560	.573	.615	.656	.697	.758
.002	.357	[illegible]	[illegible]	[illegible]	[illegible]	.417	[illegible]	[illegible]	[illegible]	.477	[illegible]	[illegible]	.512	.520	.530	.548	.567	.603	.640	.677	.713
.003	[illegible]	.345	.305	[illegible]	[illegible]	[illegible]	[illegible]	.404	[illegible]	.454	.470	[illegible]	.492	.498	.504	.520	.544	.593	.645	.695	.745
.004	[illegible]	[illegible]	[illegible]	[illegible]	[illegible]	[illegible]	[illegible]	[illegible]	[illegible]	[illegible]	[illegible]	[illegible]	.470	[illegible]	.490	.510	.533	.592	.653	[illegible]	.772
[illegible]		[illegible]	[illegible]	[illegible]	[illegible]	[illegible]	[illegible]	.330	[illegible]	.365	[illegible]	[illegible]	.417	.435	.450	.485	.520	.585	.635	.675	
[illegible]		[illegible]	[illegible]	[illegible]	[illegible]	[illegible]	[illegible]	[illegible]	.317	.335	[illegible]	[illegible]	[illegible]	.400	[illegible]	.453	.485	.551	.619	[illegible]	
[illegible]			[illegible]	[illegible]	[illegible]	[illegible]	[illegible]	[illegible]	[illegible]	[illegible]	[illegible]	[illegible]	.340	.355	.372	[illegible]	[illegible]	.490	[illegible]		
[illegible]					[illegible]	[illegible]	[illegible]	[illegible]	[illegible]	.253	.271	[illegible]	.300	.313	[illegible]	.355	.393				

TABLE IV - Continued

α = 8 DEGREES

B \ A	-.048	-.040	-.032	-.024	-.016	-.012	-.008	-.006	-.004	-.002	0	.002	.004	.006	.008	.012	.016	.024	.032	.040	.048
-.016																					
-.012			[illegible]	.535	[illegible]	.575	[illegible]	.545	.600	.610	.615	.620	.630	.635	.640	.655	.690	.695	.725		
-.008		[illegible]	[illegible]	[illegible]	[illegible]	.541	.605	[illegible]	[illegible]	.625	.630	.635	.643	.650	.657	.669	.682	.708	.734	.760	
-.006		[illegible]	[illegible]	[illegible]	.550	[illegible]	[illegible]	[illegible]	[illegible]	[illegible]	.625	.632	.639	.645	.650	.661	.672	.695	.722	.772	
-.004	[illegible]	[illegible]	.524	[illegible]	[illegible]	[illegible]	[illegible]	.577	[illegible]	.587	[illegible]	.597	.602	.607	.614	.626	.639	.672	.712	.763	.818
-.003	[illegible]	[illegible]	[illegible]	[illegible]	.555	[illegible]	[illegible]	[illegible]	[illegible]	.580	.585	.589	.595	.600	.607	.620	.633	.663	.695	.730	.768
-.002	[illegible]	.485	[illegible]	[illegible]	[illegible]	.547	[illegible]	[illegible]	[illegible]	[illegible]	[illegible]	.601	.605	.609	.613	.623	.634	.660	.685	.716	.743
-.001	[illegible]	.480	[illegible]	[illegible]	[illegible]	.617	[illegible]	[illegible]	[illegible]	.623	.613	.604	.600	.600	.602	.610	.626	.672	.725	.796	.847
0	[illegible]	.430	[illegible]	[illegible]	[illegible]	[illegible]	[illegible]	[illegible]	[illegible]	.625	.620	.620	.625	.630	.640	.650	.660	.685	.710	.750	.830
.001	[illegible]	.457	[illegible]	[illegible]	[illegible]	[illegible]	[illegible]	[illegible]	.573	[illegible]	.642	.643	.644	.645	.646	.648	.650	.675	.723	.770	.820
.002	.417	.374	[illegible]	[illegible]	[illegible]	[illegible]	[illegible]	.447	.514	.570	.587	.594	.601	.608	.615	.629	.643	.570	.707	.770	.857
.003	[illegible]	.333	[illegible]	[illegible]	[illegible]	.377	[illegible]	[illegible]	[illegible]	.529	.540	.551	.562	.571	.576	.602	.623	.663	.703	.744	.777
.004	[illegible]	.362	[illegible]	[illegible]	.337	[illegible]	[illegible]	[illegible]	[illegible]	[illegible]	.502	.514	.529	.543	.556	.583	.608	.662	.704	.735	.760
.006		.315	[illegible]	[illegible]	[illegible]	[illegible]	[illegible]	[illegible]	[illegible]	[illegible]	.430	.448	.465	.485	.502	.538	.570	.635	.695	.755	
.008		[illegible]	[illegible]	[illegible]	[illegible]	[illegible]	[illegible]	[illegible]	[illegible]	.355	.379	.405	.430	.450	.475	.515	.552	.614	.670	.718	
.012			[illegible]	[illegible]	[illegible]	[illegible]	[illegible]	[illegible]	[illegible]	[illegible]	.310	.330	.350	.365	.380	.420	.455	.520	.565		
.016					[illegible]	[illegible]	[illegible]	[illegible]	[illegible]	[illegible]	.275	.295	.312	.330	.342	.370	.395				

TABLE IV - Continued
α = 9 DEGREES

B \ A	-.048	-.040	-.032	-.024	-.016	-.012	-.008	-.006	-.004	-.002	0	.002	.004	.006	.008	.012	.016	.024	.032	.040	.048
-.016					.580	.600	.625	.645	.660	.680	.697	.70[illegible]	.713	.725	.735	.755	.770				
-.012			.585	.613	.644	.658	.672	.680	.690	.696	.703	.710	.718	.725	.733	.748	.762	.793	.822		
-.008		.602	.624	.645	.668	.678	.690	.694	.700	.705	.710	.715	.720	.725	.733	.742	.753	.774	.797	.819	
-.006		.593	.613	.632	.654	.662	.675	.678	.683	.690	.695	.700	.703	.710	.714	.724	.733	.758	.790	.840	
-.004	560	.600	.612	.621	.632	.638	.643	.647	.650	.655	.658	.662	.668	.673	.678	.690	.704	.727	.765	.810	.870
-.003	.550	.586	.612	.627	.640	.650	.657	.661	.665	.668	.672	.676	.680	.684	.688	.695	.703	.727	.772	.820	.870
-.002	.495	.538	.581	.627	.668	.682	.694	.697	.699	.700	.699	.695	.690	.688	.689	.693	.710	.753	.806	.858	.908
-.001	.500	.546	.593	.640	.678	.690	.698	.700	.701	.699	.695	.688	.678	.675	.677	.697	.718	.775	.830	.887	.940
0	.478	.478	.480	.481	.585	.652	.694	.698	.702	.706	.712	.716	.720	.726	.732	.743	.755	.782	.814	.852	.917
.001	.430	.412	.393	.405	.474	.450	.503	.560	.613	.662	.700	.725	.744	.748	.740	.727	.728	.766	.804	.802	.784
.002	.450	.403	.370	.358	.372	.395	.435	.474	.515	.570	.650	.695	.709	.714	.714	.711	.715	.754	.775	.760	.797
.003	.307	.392	.312	.320	.353	.372	.407	.434	.471	.523	.602	.666	.681	.689	.694	.695	.700	.732	.788	.828	.910
.004	.555	.331	.281	.278	.318	.354	.412	.444	.485	.532	.587	.598	.620	.639	.654	.675	.687	.719	.764	.824	.885
.006		.275	.205	.215	.289	.344	.368	.403	.446	.468	.490	.510	.530	.550	.567	.601	.634	.695	.750	.800	
.008		.174	.183	.216	.266	.297	.334	.345	.383	.330	.400	.420	.438	.460	.478	.520	.560	.640	.705	.766	
.012			.132	.180	.247	.275	.304	.320	.333	.348	.361	.377	.390	.405	.420	.450	.478	.535	.592		
.016					.241	.27[illegible]	.29[illegible]	.31	.32[illegible]	.33[illegible]	.350	.365	.380	.395	.41	.435	.465				

TABLE IV - Continued
α = 10 DEGREES

B \ A	-.048	-.040	-.032	-.024	-.016	-.012	-.008	-.006	-.004	-.002	0	.002	.004	.006	.008	.012	.016	.024	.032	.040	.048
-.016					.670	.680	.700	.710	.720	.730	.735	.745	.755	.765	.780	.795	.810				
-.012			.688	.710	.731	.742	.754	.760	.765	.770	.775	.782	.788	.793	.800	.810	.822	.844	.868		
-.008		.665	.705	.735	.751	.758	.764	.770	.772	.775	.778	.780	.785	.790	.792	.799	.804	.828	.873	.932	
-.006		.653	.688	.720	.743	.753	.760	.760	.761	.760	.762	.765	.768	.770	.772	.782	.795	.825	.865	.915	
-.004	.600	.625	.667	.702	.732	.745	.754	.756	.758	.760	.763	.764	.766	.770	.774	.784	.797	.828	.864	.903	.948
-.003	.535	.590	.642	.693	.735	.750	.763	.765	.767	.769	.768	.768	.770	.772	.777	.788	.803	.840	.886	.935	.988
-.002	.555	.600	.643	.688	.727	.754	.775	.777	.776	.768	.762	.760	.761	.765	.769	.785	.805	.858	.910	.965	1.018
-.001	.545	.512	.562	.672	.755	.770	.768	.755	.742	.734	.727	.725	.730	.745	.763	.793	.820	.860	.892	.947	.996
0	.570	.540	.490	.490	.590	.680	.740	.750	.770	.780	.784	.800	.800	.810	.820	.820	.830	.850	.880	.920	.980
.001	.570	.468	.440	.432	.424	.428	.505	.587	.665	.734	.786	.823	.845	.854	.852	.854	.824	.830	.862	.864	.883
.002	.550	.405	.358	.357	.355	.357	.410	.493	.562	.621	.670	.710	.742	.767	.788	.820	.813	.826	.872	.913	.954
.003	.456	.368	.316	.298	.355	.403	.455	.476	.510	.537	.568	.598	.626	.657	.686	.748	.806	.805	.833	.893	.990
.004	.477	.296	.240	.285	.353	.386	.420	.436	.453	.470	.486	.506	.527	.544	.575	.640	.764	.788	.818	.869	.939
.006		.190	.232	.272	.314	.333	.355	.365	.376	.385	.399	.410	.427	.450	.486	.575	.660	.735	.783	.825	
.008		.265	.232	.232	.268	.276	.300	.315	.327	.340	.358	.380	.410	.440	.478	.540	.593	.675	.739	.792	
.012			.248	.211	.218	.232	.252	.265	.280	.295	.308	.330	.345	.365	.383	.428	.472	.568	.670		
.016					.195	.210	.220	.230	.235	.240	.245	.250	.250	.255	.260	.280	.310				

TABLE IV - Continued

α = 11 DEGREES

	-.048	-.040	-.032	-.024	-.016	-.012	-.008	-.006	-.004	-.002	0	.002	.004	.006	.008	.012	.016	.024	.032	.040	.048
-.016					.760	.780	.790	.800	.815	.830	.840	.855	.870	.880	.890	.905	.918				
-.012			.745	.762	.782	.800	.810	.820	.825	.833	.840	.848	.853	.860	.868	.882	.898	.928	.958		
-.008		.735	.747	.763	.785	.798	.810	.818	.824	.833	.838	.848	.853	.861	.869	.883	.900	.929	.960	.990	
-.006		.670	.740	.770	.797	.808	.820	.825	.834	.840	.845	.850	.858	.865	.871	.882	.895	.920	.955	1.035	
-.004	.642	.687	.728	.766	.801	.816	.830	.837	.842	.848	.852	.857	.858	.860	.862	.867	.878	.914	.968	1.035	1.113
-.003	.610	.668	.720	.768	.808	.825	.838	.845	.850	.854	.857	.860	.863	.866	.870	.879	.890	.920	.966	1.023	1.088
-.002	.617	.600	.644	.754	.821	.841	.852	.854	.855	.856	.857	.858	.860	.863	.868	.879	.894	.932	.980	1.035	1.090
-.001	.630	.588	.565	.590	.810	.850	.853	.841	.834	.830	.828	.831	.838	.853	.868	.894	.917	.961	1.003	1.054	1.110
0	[illegible]	.600	.513	.504	[illegible]	[illegible]	.770	.802	.828	.850	.865	.885	.896	.907	.910	.906	.906	.919	.948	.989	1.035
.001	.450	.413	.420	.426	.421	.418	.450	.550	.625	.700	.769	.835	.897	.930	.936	.927	.900	.910	.950	1.004	1.057
.002	.507	.403	[illegible]	[illegible]	.383	.374	.352	.379	.460	.575	.658	.717	.768	.808	.839	.885	.912	.908	.912	.955	1.028
.003	[illegible]	.238	.362	.334	[illegible]	.347	.368	.388	.437	.471	.518	.567	.616	.662	.709	.798	.855	.904	.898	.882	.916
.004	.460	.265	.265	.319	.314	.335	.400	.431	.462	.492	.522	.555	.588	.617	.648	.709	.772	.870	.896	.898	.890
.006		.313	.272	.257	.271	.295	.332	.350	.375	.398	.425	.450	.479	.510	.539	.605	.675	.780	.847	.893	
.008		.325	.254	.222	.217	.230	.255	.273	.300	.337	.370	.404	.425	.468	.498	.556	.612	.708	.790	.868	
.012			[illegible]	.151	.222	.255	[illegible]	.304	.320	.338	.353	.370	.388	.402	.418	.452	.484	.550	.615		
.016					.345	.360	.370	.380	.390	.395	.405	.410	.415	.425	.430	.435	.440				

TABLE IV - Continued
α = 12 DEGREES

B \ A	-.048	-.040	-.032	-.024	-.016	-.012	-.008	-.006	-.004	-.002	0	.002	.004	.006	.008	.012	.016	.024	.032	.040	.048
-.016					.890	.905	.920	.930	.940	.947	.955	.962	.970	.980	.990	1.010	1.030				
-.012			.845	.871	.900	.915	.929	.935	.942	.950	.957	.964	.970	.978	.984	1.000	1.013	1.040	1.070		
-.008		.822	.846	.870	.894	.905	.918	.925	.930	.935	.940	.946	.953	.958	.964	.978	.989	1.012	1.037	1.060	
-.006		.778	.820	.856	.891	.905	.918	.922	.926	.930	.932	.933	.930	.932	.938	.948	.962	1.008	1.065	1.134	
-.004	.700	.729	.799	.842	.883	.899	.912	.916	.920	.924	.925	.927	.930	.934	.939	.952	.968	1.010	1.062	1.121	1.180
-.003	.653	.679	.726	.818	.890	.915	.935	.942	.948	.952	.954	.955	.955	.955	.956	.962	.975	1.015	1.075	1.134	1.178
-.002	.728	.714	.705	.708	.900	.920	.927	.933	.937	.942	.948	.954	.960	.966	.971	.981	.998	1.028	1.058	1.090	1.122
-.001	.630	.605	.593	.622	.767	.897	.945	.948	.952	.955	.960	.964	.967	.973	.977	.987	.997	1.017	1.038	1.060	1.085
0	.594	.514	.477	.508	.620	.690	.770	.810	.854	.900	.946	.983	.994	.995	.995	.994	.996	1.010	1.035	1.067	1.105
.001	.458	.440	.422	.406	.405	.422	.506	.610	.710	.800	.873	.940	.995	1.026	1.032	1.020	[illegible]	[illegible]	1.000	1.030	1.073
.002	.291	.295	.322	.372	.380	.354	.367	.457	.550	.640	.713	.772	.820	.860	.893	.941	[illegible]	1.0[illegible]	[illegible]	.994	1.031
.003	.353	.330	.342	.345	.337	.335	.381	.430	.477	.526	.573	.620	.665	.707	.747	.823	.888	.917	.992	.998	1.013
.004	.445	.367	.316	.295	.327	.363	.426	.464	.506	.550	.587	.624	.657	.686	.715	.768	.817	.900	.962	1.000	1.015
.006		.328	.270	.250	.285	.342	.400	.430	.460	.490	.519	.547	.573	.600	.627	.679	.726	.815	.882	.930	
.008		.345	.322	.210	.269	.322	.374	.400	.426	.452	.478	.500	.524	.548	.570	.614	.657	.740	.821	.900	
.012			.295	.197	.316	.340	.358	.374	.392	.408	.423	.440	.457	.472	.490	.522	.557	.635	.720		
.016					.150	.155	.160	.165	.170	.175	.180	.185	.190	.195	.200	.220	.230				

TABLE IV - Continued
α = 13 DEGREES

B \ A	-.048	-.040	-.032	-.024	-.016	-.012	-.008	-.006	-.004	-.002	0	.002	.004	.006	.008	.012	.016	.024	.032	.040	.048
-.016					.995	1.005	1.015	1.025	1.030	1.045	1.050	1.060	1.070	1.085	1.100	1.120	1.130				
-.012			.931	.954	.978	.988	.999	1.005	1.010	1.018	1.021	1.029	1.034	1.039	1.046	1.057	1.068	1.090	1.114		
-.008		.862	.908	.949	.981	.995	1.002	1.006	1.009	1.010	1.010	1.010	1.011	1.013	1.016	1.027	1.043	1.090	1.155	1.228	
-.006		.845	.900	.944	.983	1.000	1.013	1.019	1.022	1.027	1.030	1.030	1.031	1.032	1.034	1.041	1.053	1.093	1.149	1.215	
-.004	.842	.837	.835	.930	.994	.996	.999	1.001	1.005	1.008	1.013	1.018	1.025	1.031	1.038	1.053	1.071	1.111	1.152	1.184	1.208
-.003	.779	.785	.790	.805	.970	1.003	1.011	1.007	1.006	1.010	1.013	1.018	1.025	1 033	1.042	1.065	1.087	1.125	1.151	1.159	1.242
-.002	.692	.685	.693	.728	.929	.992	1.020	1.023	1.023	1.024	1.026	1.030	1.035	1.041	1.049	1.075	1.104	1.118	1.127	1.150	1.201
-.001	.575	.562	.568	.608	.787	.879	.972	1.015	1.032	1.038	1.040	1.040	1.041	1.046	1.052	1.094	1.100	1.099	1.123	1.165	1.222
0	.590	.490	.440	.480	.575	.650	.720	.775	.890	.960	1.009	1.030	1.050	1.060	1.060	1.070	1.060	1.070	1.110	1.120	1.140
.001	.397	.370	.378	.401	.424	.435	.550	.655	.750	.865	.972	1.070	1.093	1.102	1.107	1.108	1.105	1.093	1.078	1.064	1.055
.002	.514	.467	.425	.389	.365	.382	.477	.526	.575	.622	.668	.716	.762	.809	.854	.945	1.020	1.089	1.111	1.115	1.109
.003	.437	.380	.344	.330	.344	.380	.440	.474	.510	.547	.591	.640	.687	.732	.775	.855	.923	1.007	1.055	1.090	1.110
.004	.460	.347	.313	.296	.305	.332	.387	.421	.456	.497	.536	.579	.621	.662	.703	.782	.864	.955	1.006	1.041	1.067
.006		.356	.261	.246	.330	.450	.513	.540	.569	.594	.618	.640	.665	.687	.707	.750	.790	.868	.940	1.010	
.008		.178	.251	.325	.400	.436	.472	.490	.509	.528	.546	.564	.584	.600	.619	.655	.692	.765	.839	.912	
.012			.403	.355	.343	.345	.355	.365	.365	.380	.380	.403	.410	.420	.435	.450	.460	.480	.495		

TABLE IV - Continued
α = 14 DEGREES

B \ A	-.048	-.040	-.032	-.024	-.016	-.012	-.008	-.006	-.004	-.002	0	.002	.004	.006	.008	.012	.016	.024	.032	.040	.048
-.016					1.080	1.090	1.105	1.110	1.120	1.125	1.140	1.150	1.155	1.165	1.175	1.190	1.200				
-.012			.990	1.015	1.043	1.057	1.070	1.076	1.083	1.090	1.100	1.102	1.111	1.118	1.125	1.138	1.150	1.180	1.205		
-.008		.950	.979	1.005	1.030	1.045	1.060	1.065	1.072	1.080	1.085	1.096	1.102	1.110	1.120	1.137	1.155	1.199	1.251	1.315	
-.006		.950	.960	.991	1.020	1.045	1.062	1.071	1.080	1.090	1.120	1.107	1.138	1.124	1.155	1.173	1.190	1.202	1.240	1.271	
-.004	.772	.844	.895	.	1.020	1.050	1.072	.082	1.089	1.097	1.105	1.114	1.122	1.129	1.136	1.152	1.167	1.196	1.226	1.256	1.286
-.003	.788	.736	.783	.865	.946	.987	1.029	1.050	1.070	1.090	1.111	1.126	1.134	1.138	1.141	1.149	1.163	1.200	1.224	1.231	1.234
-.002	.755	.657	.657	.731	.923	1.013	1.065	1.077	1.097	1.110	1.122	1.133	1.143	1.150	1.159	1.170	1.180	1.197	1.209	1.220	1.228
-.001	.742	.645	.586	.605	.770	.904	.993	1.028	1.059	1.085	1.108	1.128	1.145	1.159	1.172	1.186	1.170	1.200	1.285	1.252	1.260
0	.617	.491	.445	.470	.540	.587	.651	.725	.925	1.010	1.063	1.095	1.123	1.135	1.150	1.160	1.156	1.151	1.157	1.174	1.195
.001	.758	.634	.526	.455	.440	.444	.493	.560	.635	.715	.790	.866	.943	1.017	1.093	1.161	1.183	1.231	1.239	1.256	1.273
.002	.574	.469	.386	.367	.385	.437	.552	.595	.638	.683	.727	.772	.817	.861	.905	.988	1.050	1.147	1.177	1.184	1.195
.003	.494	.405	.340	.312	.381	.450	.518	.553	.587	.623	.657	.692	.726	.761	.795	.863	.932	1.051	1.108	1.143	1.169
.004	.552	.400	.300	.263	.326	.390	.451	.498	.535	.570	.606	.642	.676	.711	.744	.810	.873	.987	1.080	1.148	1.178
.006		.330	.242	.210	.273	.267	.310	.336	.365	.398	.431	.467	.502	.540	.580	.663	.739	.869	.960	1.040	
.009		.317	.231	.183	.196	.218	.246	.265	.285	.309	.329	.353	.380	.410	.440	.505	.572	.700	.810	.900	
.012			.170	.115	.105	.105	.110	.115	.125	.130	.140	.145	.150	.165	.180	.215	.255	.355	.480		

TABLE IV - Continued
α = 15 DEGREES

B \ A	-.048	-.040	-.032	-.024	-.016	-.012	-.008	-.006	-.004	-.002	0	.002	.004	.006	.008	.012	.016	.024	.032	.040	.048
-.016					1.140	1.155	1.170	1.180	1.190	1.200	1.210	1.220	1.230	1.240	1.250	1.265	1.280				
-.012			1.038	1.074	1.111	1.130	1.150	1.158	1.168	1.178	1.187	1.197	1.204	1.214	1.222	1.241	1.260	1.299	1.337		
-.008		1.070	1.075	1.090	1.113	1.127	1.140	1.150	1.158	1.166	1.174	1.181	1.190	1.200	1.208	1.226	1.242	1.279	1.314	1.350	
-.006		.970	1.036	1.072	1.109	1.127	1.143	1.150	1.160	1.169	1.178	1.185	1.194	1.201	1.210	1.228	1.244	1.278	1.311	1.346	
-.004	.700	.780	.870	.977	1.058	1.091	1.118	1.131	1.143	1.155	1.165	1.176	1.186	1.196	1.205	1.223	1.239	1.272	1.303	1.329	1.364
-.003	.785	.743	.752	.835	.998	1.125	1.165	1.178	1.190	1.201	1.210	1.217	1.224	1.231	1.236	1.244	1.250	1.273	1.307	1.318	1.303
-.002	.719	.683	.680	.705	.908	1.050	1.163	1.198	1.224	1.246	1.262	1.272	1.279	1.281	1.288	1.264	1.253	1.284	1.305	1.300	1.281
-.001	.577	.535	.528	.602	.744	.862	1.060	1.12	1.165	1.200	1.226	1.245	1.260	1.264	1.263	1.247	1.247	1.261	1.248	1.230	1.213
0	.650	.500	.470	.480	.530	.560	.620	.680	.910	1.030	1.112	1.230	1.270	1.280	1.280	1.280	1.270	1.290	1.280	1.260	1.310
.001	.578	.485	.430	.427	.464	.507	.585	.642	.697	.752	.807	.863	.920	.975	1.032	1.144	1.231	1.251	1.262	1.270	1.27[illegible]
.002	.598	.451	.369	.357	.424	.560	.635	.674	.711	.747	.783	.818	.855	.891	.925	.994	1.055	1.168	1.242	1.278	1.28[illegible]
.003	.560	.430	.325	.312	.390	.464	.544	.583	.624	.662	.700	.740	.775	.811	.845	.910	.970	1.093	1.166	1.220	1.24[illegible]
.004	.550	.372	.290	.254	.332	.388	.457	.497	.535	.573	.613	.650	.689	.722	.754	.819	.880	1.000	1.090	1.160	1.19[illegible]
.006		.320	.233	.210	.260	.310	.370	.400	.430	.461	.494	.522	.550	.579	.607	.658	.710	.813	.910	.997	
.008		.20	.17	.1[illegible]	.22[illegible]	.250	.29[illegible]	.31[illegible]	.33[illegible]	.355	.380	.400	.420	.445	.470	.515	.560	.650	.740	.835	

TABLE IV - Continued
α = 16 DEGREES

B \ A	-.048	-.040	-.032	-.024	-.016	-.012	-.008	-.006	-.004	-.002	0	.002	.004	.006	.008	.012	.016	.024	.032	.040	.048
-.016					1.160	1.190	1.220	1.235	1.250	1.260	1.270	1.288	1.305	1.330	1.345	1.367	1.390				
-.012			1.133	1.162	1.195	1.210	1.225	1.232	1.240	1.249	1.247	1.264	1.273	1.280	1.288	1.303	1.320	1.353	1.383		
-.008		1.054	1.191	1.212	1.211	1.215	1.223	1.228	1.233	1.239	1.244	1.250	1.260	1.265	1.272	1.288	1.306	1.346	1.387	1.428	
-.006		.895	1.052	1.259	1.205	1.214	1.225	1.230	1.227	1.246	1.253	1.260	1.278	1.277	1.284	1.303	1.323	1.363	1.402	1.445	
-.004	.833	.834	.857	.934	1.081	1.196	1.269	1.284	1.294	1.302	1.308	1.313	1.317	1.319	1.320	1.323	1.327	1.360	1.400	1.391	1.355
-.003	.762	.717	.773	.810	.962	1.103	1.262	1.298	1.323	1.337	1.344	1.345	1.343	1.338	1.334	1.325	1.325	1.365	1.372	1.337	1.320
-.002	.660	.607	.613	.690	.850	.988	1.185	1.254	1.292	1.316	1.332	1.337	1.336	1.335	1.333	1.325	1.318	1.349	1.327	1.310	1.315
-.001	.577	.528	.520	.550	.687	.836	.960	1.100	1.314	1.329	1.334	1.335	1.331	1.325	1.318	1.318	1.328	1.320	1.312	1.320	1.330
0	.485	.515	.509	.515	.530	.547	.596	.665	.820	.970	1.127	1.125	1.329	1.342	1.347	1.355	1.365	1.383	1.351	1.355	1.386
.001	.430	.443	.420	.423	.446	.417	.408	.525	.575	.700	.817	.945	1.065	1.185	1.260	1.290	1.305	1.315	1.319	1.323	1.326
.002	.406	.370	.355	.355	.370	.389	.415	.430	.446	.468	.497	.550	.670	.795	.920	1.100	1.217	1.250	1.259	1.266	1.273
.003	.420	.379	.352	.366	.435	.447	.488	.515	.545	.580	.620	.667	.722	.777	.837	.958	1.060	1.172	1.197	1.208	1.220
.004	.435	.453	.477	.510	.566	.607	.656	.683	.713	.740	.767	.795	.825	.852	.893	.929	.973	1.043	1.096	1.137	1.170
.006		.655	.677	.693	.730	.756	.790	.810	.830	.850	.870	.888	.905	.916	.925	.937	.945	.965	.980	.993	

TABLE IV - Continued
α = 17 DEGREES

B \ A	-.048	-.040	-.032	-.024	-.016	-.012	-.008	-.006	-.004	-.002	0	.002	.004	.006	.008	.012	.016	.024	.032	.040	.048
-.016					1.350	1.352	1.355	1.356	1.358	1.359	1.360	1.362	1.365	1.367	1.370	1.375	1.380				
-.012			1.343	1.343	1.348	1.350	1.353	1.354	1.357	1.359	1.362	1.365	1.368	1.372	1.377	1.387	1.399	1.432	1.485		
-.008		.955	1.167	1.318	1.343	1.341	1.341	1.343	1.347	1.351	1.359	1.363	1.370	1.377	1.383	1.400	1.418	1.455	1.498	1.535	
-.006		.967	1.021	1.140	1.275	1.310	1.323	1.332	1.338	1.344	1.348	1.353	1.359	1.364	1.350	1.384	1.410	1.450	1.484	1.470	
-.004	.900	.795	.805	.900	1.071	1.176	1.263	1.302	1.333	1.359	1.371	1.375	1.374	1.371	1.368	1.368	1.382	1.449	1.439	1.396	1.364
-.003	.890	.715	.697	.786	.938	1.044	1.170	1.241	1.313	1.383	1.405	1.405	1.396	1.385	1.377	1.373	1.391	1.428	1.417	1.430	1.465
-.002	.834	.662	.610	.656	.828	.932	1.068	1.150	1.238	1.328	1.418	1.435	1.437	1.428	1.401	1.385	1.405	1.411	1.426	1.453	1.488
-.001	.753	.600	.552	.565	.704	.830	.930	.995	1.095	1.275	1.344	1.365	1.370	1.390	1.399	1.405	1.402	1.407	1.441	1.464	1.473
0	.660	.520	.510	.520	.540	.580	.620	.670	.780	.950	1.093	1.250	1.320	1.380	1.420	1.440	1.450	1.440	1.410	1.400	1.390
.001	.523	.443	.409	.417	.459	.488	.524	548	.580	.635	.750	.905	1.090	1.218	1.273	1.320	1.346	1.367	1.365	1.352	1.356
.002	.510	.452	.431	.430	.443	.455	.475	.490	.508	.531	.562	.600	.646	.700	.785	1.005	1.193	1.280	1.295	1.295	1.283
.003	.540	.490	.470	.478	.490	.498	.510	.520	.530	.544	.560	.579	.600	.630	.660	.772	.970	1.093	1.117	1.123	1.120

TABLE IV - Continued
α = 18 DEGREES

B \ A	-.048	-.040	-.032	-.024	-.016	-.012	-.008	-.006	-.004	-.002	0	.002	.004	.006	.008	.012	.016	.024	.032	.040	.048
-.016					1.580	1.575	1.570	1.570	1.570	1.570	1.570	1.570	1.570	1.570	1.570	1.565	1.540				
-.012			1.300	1.428	1.510	1.533	1.542	1.544	1.541	1.538	1.536	1.533	1.534	1.535	1.536	1.539	1.543	1.557	1.572		
-.008		1.095	1.181	1.288	1.437	1.477	1.498	1.501	1.504	1.503	1.501	1.496	1.490	1.487	1.487	1.493	1.513	1.559	1.564	1.539	
-.006		.923	.995	1.117	1.288	1.388	1.455	1.472	1.477	1.470	1.465	1.460	1.458	1.459	1.462	1.475	1.503	1.543	1.545	1.513	
-.004	.984	.850	.803	.850	1.047	1.193	1.330	1.417	1.447	1.462	1.465	1.463	1.462	1.462	1.463	1.475	1.502	1.498	1.515	1.548	1.592
-.003	.930	.770	.740	.786	.900	1.045	1.168	1.222	1.270	1.312	1.350	1.383	1.413	1.441	1.461	1.487	1.498	1.496	1.502	1.547	1.570
-.002	.71:	.663	.645	.660	.797	.915	1.047	1.116	1.185	1.250	1.311	1.364	1.407	1.447	1.480	1.504	1.494	1.497	1.540	1.566	1.575
-.001	.680	.610	.570	.590	.660	.765	.915	.994	1.067	1.140	1.215	1.293	1.365	1.445	1.478	1.500	1.490	1.565	1.580	1.540	1.490
0	.580	.520	.487	.493	.568	.640	.672	.690	.758	.900	1.034	1.168	1.295	1.425	1.503	1.538	1.540	1.505	1.454	1.420	1.392
.001	.460	.390	.330	.300	.340	.390	.470	.520	.570	.720	.870	1.050	1.235	1.390	1.540	1.595	1.580	1.530	1.490	1.460	1.440

TABLE IV - Continued
α = 19 DEGREES

B \ A	-.048	-.040	-.032	-.024	-.016	-.012	-.008	-.006	-.004	-.002	0	.002	.004	.006	.008	.012	.016	.024	.032	.040	.048
-.016					1.490	1.490	1.490	1.490	1.490	1.490	1.490	1.495	1.500	1.505	1.510	1.520	1.540				
-.012			1.502	1.502	1.508	1.509	1.510	1.510	1.511	1.513	1.515	1.520	1.524	1.530	1.535	1.553	1.580	1.656	1.807		
-.008		.885	1.135	1.322	1.428	1.462	1.488	1.500	1.514	1.524	1.534	1.545	1.555	1.563	1.570	1.583	1.595	1.613	1.628	1.636	
-.004		1.017	.961	1.047	1.248	1.374	1.461	1.489	1.522	1.529	1.542	1.552	1.562	1.568	1.572	1.578	1.583	1.598	1.617	1.650	
-.004	.965	.870	.839	.841	.920	1.148	1.300	1.370	1.425	1.463	1.497	1.523	1.545	1.562	1.573	1.575	1.563	1.573	1.628	1.673	1.76
-.003	.804	.764	.745	.755	.883	.995	1.128	1.183	1.278	1.352	1.428	1.479	1.516	1.544	1.565	1.586	1.575	1.576	1.657	1.695	1.715
-.002	.661	.653	.657	.681	.756	.850	1.014	1.090	1.170	1.251	1.330	1.418	1.500	1.559	1.581	1.586	1.579	1.561	1.538	1.513	1.485
-.001	.570	.535	.551	.600	.667	.718	.825	.922	1.038	1.150	1.258	1.358	1.433	1.482	1.505	1.564	1.638	1.639	1.562	1.450	1.305
0	.522	.455	.430	.469	.575	.646	.720	.767	.815	.870	.940	1.048	1.225	1.430	1.528	1.609	1.624	1.540	1.473	1.425	1.382

TABLE IV - Continued
α = 20 DEGREES

B \ A	-.048	-.040	-.032	-.024	-.016	-.012	-.008	-.006	-.004	-.002	0	.002	.004	.006	.008	.012	.016	.024	.032	.040	.048
-.016					1.545	1.555	1.575	1.585	1.595	1.605	1.610	1.625	1.630	1.640	1.645	1.650	1.645				
-.012			1.385	1.404	1.480	1.540	1.580	1.598	1.610	1.620	1.630	1.638	1.641	1.648	1.650	1.651	1.657	1.677	1.700		
-.008		1.237	1.198	1.199	1.343	1.468	1.564	1.596	1.614	1.620	1.620	1.620	1.621	1.623	1.625	1.631	1.641	1.672	1.720	1.779	
-.006		1.039	1.030	1.052	1.140	1.320	1.505	1.561	1.597	1.601	1.597	1.590	1.590	1.590	1.590	1.600	1.619	1.670	1.740	1.810	
-.004	.749	.794	.838	.882	.930	1.080	1.267	1.360	1.455	1.489	1.500	1.512	1.520	1.530	1.542	1.570	1.605	1.704	1.740	1.674	1.53E
-.003	.660	.690	.740	.794	.852	.918	1.100	1.190	1.280	1.368	1.415	1.440	1.470	1.500	1.528	1.580	1.625	1.719	1.740	1.627	1.425
-.002	.515	.555	.617	.698	.770	.828	.935	1.030	1.115	1.209	1.283	1.350	1.414	1.472	1.525	1.618	1.685	1.712	1.656	1.557	1.455
-.001	.400	.435	.485	.563	.674	.736	.817	.900	.980	1.070	1.156	1.240	1.325	1.408	1.493	1.646	1.705	1.670	1.563	1.452	1.358
0	.150	.260	.370	.480	.590	.650	.720	.780	.860	.910	.952	1.090	1.220	1.330	1.430	1.61	1.710	1.660	1.470	1.290	1.140

TABLE IV - Continued
α = 21 DEGREES

B \ A	-.048	-.040	-.032	-.024	-.016	-.012	-.008	-.006	-.004	-.002	0	.002	.004	.006	.008	.012	.016	.024	.032	.040	.048
-.016					1.575	1.586	1.590	1.597	1.605	1.610	1.615	1.617	1.620	1.625	1.630	1.637	1.645				
-.012			1.488	1.520	1.550	1.568	1.583	1.591	1.600	1.609	1.616	1.624	1.632	1.640	1.649	1.660	1.680	1.713	1.748		
-.008		1.190	1.240	1.302	1.385	1.415	1.455	1.473	1.494	1.511	1.532	1.550	1.570	1.590	1.609	1.646	1.684	1.760	1.839	1.913	
-.006		.920	1.019	1.114	1.210	1.258	1.310	1.337	1.363	1.393	1.423	1.455	1.487	1.523	1.560	1.649	1.730	1.820	1.824	1.760	
-.004	.679	.727	.786	.863	.970	1.041	1.143	1.205	1.265	1.339	1.383	1.440	1.495	1.548	1.600	1.700	1.768	1.800	1.780	1.726	1.645
-.003	.469	.572	.680	.780	.895	.947	1.012	1.080	1.153	1.221	1.295	1.366	1.433	1.505	1.576	1.710	1.773	1.790	1.750	1.670	1.550
-.002	.353	.449	.550	.675	.791	.853	.915	.956	1.040	1.082	1.175	1.273	1.367	1.462	1.553	1.684	1.766	1.759	1.670	1.546	1.402
-.001	.408	.459	.518	.586	.690	.747	.795	.825	.854	.895	.968	1.083	1.227	1.381	1.515	1.665	1.743	1.772	1.694	1.560	1.380
0	.360	.420	.500	.580	.660	.700	.740	.765	.800	.850	.921	.985	1.080	1.215	1.470	1.660	1.720	1.755	1.720	1.615	1.415

TABLE IV - Continued
α = 22 DEGREES

B \ A	-.048	-.040	-.032	-.024	-.016	-.012	-.008	-.006	-.004	-.002	0	.002	.004	.006	.008	.012	.016	.024	.032	.040	.048
-.016					1.715	1.722	1.730	1.735	1.740	1.743	1.747	1.751	1.755	1.763	1.770	1.778	1.785				
-.012			1.579	1.620	1.662	1.682	1.703	1.713	1.723	1.734	1.744	1.753	1.764	1.774	1.783	1.805	1.825	1.867	1.908		
-.008		1.017	1.175	1.333	1.472	1.530	1.583	1.610	1.632	1.658	1.680	1.702	1.725	1.745	1.765	1.802	1.830	1.868	1.871	1.828	
-.006		.790	.950	1.110	1.270	1.352	1.431	1.470	1.512	1.550	1.590	1.629	1.666	1.700	1.732	1.787	1.832	1.889	1.880	1.791	
-.004	.490	.597	.718	.863	1.010	1.085	1.173	1.225	1.280	1.366	1.425	1.525	1.608	1.677	1.734	1.823	1.871	1.876	1.823	1.745	1.642
-.003	.403	.497	.605	.742	.889	.966	1.055	1.105	1.163	1.225	1.301	1.386	1.471	1.555	1.638	1.785	1.840	1.838	1.790	1.705	1.600
-.002	.344	.434	.531	.649	.775	.829	.930	.977	1.026	1.100	1.152	1.234	1.314	1.464	1.572	1.703	1.776	1.812	1.760	1.670	1.542
-.001	.310	.410	.560	.609	.707	.755	.806	.838	.878	.926	1.009	1.122	1.258	1.340	1.442	1.582	1.752	1.783	1.733	1.642	1.520
0	.675	.630	.610	.600	.625	.655	.690	.715	.740	.780	.893	1.095	1.210	1.295	1.370	1.540	1.740	1.790	1.720	1.610	1.550

TABLE IV - Continued
α = 23 DEGREES

B \ A	-.048	-.040	-.032	-.024	-.016	-.012	-.008	-.006	-.004	-.002	0	.002	.004	.006	.008	.012	.016	.024	.032	.040	.048
-.016					1.850	1.850	1.850	1.850	1.850	1.850	1.850	1.850	1.850	1.850	1.850	1.850	1.850				
-.012			1.385	1.630	1.820	1.870	1.895	1.896	1.898	1.899	1.900	1.901	1.902	1.903	1.904	1.907	1.910	1.915	1.920		
-.008		.825	1.064	1.302	1.527	1.661	1.760	1.797	1.827	1.852	1.872	1.885	1.896	1.901	1.903	1.903	1.903	1.899	1.897	1.892	
-.006		.647	.825	1.057	1.288	1.403	1.513	1.565	1.612	1.660	1.705	1.750	1.788	1.828	1.857	1.883	1.897	1.906	1.908	1.903	
-.004	.400	.502	.625	.806	1.000	1.097	1.202	1.263	1.322	1.391	1.460	1.542	1.605	1.677	1.783	1.814	1.860	1.923	1.959	1.984	2.007
-.003	.337	.435	.565	.715	.875	.960	1.056	1.110	1.168	1.245	1.322	1.404	1.480	1.560	1.627	1.742	1.818	1.930	1.988	2.018	2.028
-.002	.405	.495	.580	.673	.790	.854	.929	.970	1.019	1.070	1.132	1.200	1.282	1.379	1.492	1.651	1.764	1.900	1.966	2.006	2.023
-.001	.647	.670	.695	.730	.777	.805	.825	.844	.868	.942	1.007	1.105	1.200	1.298	1.385	1.570	1.708	1.860	1.938	1.980	2.003
0	.790	.775	.760	.755	.760	.767	.780	.795	.810	.835	.867	.940	1.130	1.240	1.310	1.535	1.670	1.795	1.870	1.920	1.975

TABLE V. UNSTEADY MOMENT COEFFICIENT C_m FOR M = 0.325
α = 3 DEGREES

B \ A	-.048	-.040	-.032	-.024	-.016	-.012	-.008	-.006	-.004	-.002	0	.002	.004	.006	.008	.012	.016	.024	.032	.040	.048
-.001	.053	.042	.032	.022	.014	.010	.004	.001	-.002	-.006	-.007	-.009	-.012	-.015	-.018	-.024	-.042	-.052	-.062	-.072	-.084
0	.055	.041	.030	.025	.020	.016	.011	.008	.006	.003	0	-.002	-.005	-.008	-.011	-.016	-.021	-.033	-.045	-.058	-.072
.001	.063	.051	.040	.030	.015	.006	-.002	-.006	-.009	-.013	-.016	-.018	-.021	-.023	-.025	-.026	-.026	-.029	-.039	-.052	-.066
.002	.061	.048	.035	.022	.009	.003	-.003	-.006	-.009	-.012	-.014	-.017	-.020	-.022	-.025	-.029	-.033	-.039	-.045	-.059	-.074
.003	.065	.049	.034	.016	.003	-.003	-.008	-.010	-.012	-.014	-.017	-.018	-.020	-.023	-.026	-.030	-.034	-.042	-.049	-.060	-.071
.004	.075	.052	.028	.011	0	-.004	-.009	-.011	-.014	-.016	-.018	-.020	-.023	-.025	-.028	-.032	-.036	-.046	-.053	-.060	-.066
.006	.058	.041	.025	.010	-.003	-.008	-.013	-.014	-.016	-.017	-.018	-.020	-.022	-.024	-.026	-.032	-.040	-.052	-.060	-.067	-.072
.008	.039	.029	.021	.010	.002	-.003	-.008	-.011	-.014	-.017	-.019	-.022	-.026	-.028	-.032	-.038	-.044	-.057	-.070	-.084	-.096
.012	.051	.039	.027	.015	.003	-.003	-.009	-.012	-.015	-.018	-.022	-.024	-.027	-.030	-.034	-.040	-.046	-.068	-.070	-.083	-.095
.016	.044	.032	.021	.010	.001	-.007	-.014	-.016	-.018	-.021	-.024	-.027	-.030	-.032	-.034	-.039	-.044	-.053	-.063	-.073	-.083

TABLE V - Continued
α = 4 DEGREES

B \ A	-.048	-.040	-.032	-.024	-.016	-.012	-.008	-.006	-.004	-.002	0	.002	.004	.006	.008	.012	.016	.024	.032	.040	.048
-.004	.065	.054	.042	.031	.020	.016	.010	.008	.005	.002	-.001	-.004	-.006	-.009	-.011	-.018	-.021	-.024	-.032	-.042	-.053
-.003	.062	.052	.040	.029	.018	.014	.008	.006	.003	.001	-.003	-.005	-.008	-.011	-.013	-.019	-.024	-.029	-.038	-.048	-.060
-.002	.059	.049	.038	.028	.017	.012	.006	.004	.002	-.001	-.004	-.006	-.009	-.012	-.014	-.020	-.025	-.037	-.046	-.056	-.067
-.001	.055	.045	.035	.025	.015	.010	.005	.002	0	-.003	-.005	-.008	-.010	-.013	-.016	-.020	-.038	-.048	-.058	-.068	-.079
0	.058	.046	.035	.028	.020	.016	.011	.008	.006	.002	.001	-.003	-.006	-.008	-.011	-.015	-.021	-.032	-.043	-.055	-.068
.001	.090	.071	.050	.029	.013	.006	-.002	-.005	-.008	-.011	-.014	-.017	-.019	-.022	-.024	-.028	-.031	-.034	-.037	-.042	-.048
.002	.081	.056	.037	.019	.008	.002	-.002	-.005	-.008	-.010	-.012	-.015	-.018	-.020	-.023	-.028	-.033	-.042	-.047	-.055	-.064
.003	.068	.047	.028	.014	.004	0	-.005	-.007	-.010	-.012	-.014	-.016	-.019	-.021	-.024	-.028	-.033	-.042	-.051	-.060	-.071
.004	.058	.039	.025	.014	.004	-.001	-.006	-.008	-.010	-.013	-.015	-.018	-.020	-.022	-.025	-.030	-.035	-.045	-.055	-.064	-.075
.006	.049	.038	.026	.015	.004	-.001	-.006	-.009	-.012	-.015	-.017	-.020	-.023	-.025	-.028	-.034	-.040	-.050	-.061	-.072	-.083
.008	.049	.037	.026	.015	.004	-.002	-.007	-.010	-.013	-.016	-.018	-.021	-.024	-.027	-.030	-.036	-.042	-.053	-.064	-.076	-.087
.012	.044	.034	.024	.013	.004	0	-.006	-.008	-.011	-.013	-.016	-.019	-.022	-.025	-.028	-.035	-.043	-.062	-.073	-.085	-.096
.016	.046	.037	.027	.018	.004	.002	-.004	-.008	-.011	-.015	-.017	-.021	-.024	-.025	-.027	-.037	-.043	-.067	-.082	-.097	-.110

TABLE V - Continued
α = 5 DEGREES

B \ A	-.048	-.040	-.032	-.024	-.016	-.012	-.008	-.006	-.004	-.002	0	.002	.004	.006	.008	.012	.016	.024	.032	.040	.048
-.006	.072	.059	.048	.036	.031	.025	.020	.016	.013	.009	.006	.003	.001	-.002	-.006	-.009	-.014	-.030	-.044	-.056	-.060
-.004	.065	.054	.043	.032	.022	.016	.012	.008	.006	.003	0	-.002	-.005	-.008	-.011	-.016	-.021	-.032	-.043	-.054	-.065
-.003	.060	.050	.040	.029	.019	.014	.008	.006	.003	0	-.002	-.005	-.008	-.010	-.013	-.018	-.023	-.034	-.045	-.055	-.066
-.002	.059	.049	.039	.028	.017	.012	.007	.004	.002	-.001	-.004	-.006	-.009	-.012	-.014	-.020	-.025	-.036	-.046	-.057	-.068
-.001	.060	.049	.038	.028	.018	.012	.007	.004	.002	-.001	-.004	-.006	-.009	-.012	-.014	-.020	-.025	-.035	-.047	-.057	-.068
0	.060	.048	.038	.030	.020	.016	.010	.007	.005	.002	.002	-.003	-.006	-.008	-.011	-.015	-.021	-.031	-.042	-.053	-.066
.001	.056	.047	.037	.027	.014	.007	-.001	-.005	-.009	-.012	-.015	-.018	-.020	-.022	-.024	-.027	-.030	-.037	-.044	-.050	-.056
.002	.060	.047	.034	.021	.009	.004	-.001	-.004	-.006	-.009	-.011	-.014	-.016	-.019	-.021	-.026	-.031	-.041	-.051	-.061	-.071
.003	.070	.054	.037	.021	.006	.003	0	-.002	-.005	-.007	-.009	-.012	-.014	-.017	-.020	-.025	-.031	-.042	-.053	-.064	-.075
.004	.056	.046	.036	.015	.006	.004	.001	-.001	-.004	-.006	-.009	-.012	-.014	-.017	-.020	-.026	-.033	-.045	-.052	-.057	-.064
.006	.062	.044	.027	.016	.010	.008	.005	.003	0	-.003	-.006	-.009	-.012	-.016	-.019	-.027	-.035	-.052	-.062	-.066	-.068
.008	.052	.038	.026	.018	.010	.004	-.001	-.004	-.006	-.009	-.012	-.015	-.018	-.021	-.024	-.030	-.037	-.055	-.070	-.076	-.078
.012	.049	.038	.030	.018	.007	.001	-.005	-.007	-.011	-.013	-.016	-.020	-.022	-.025	-.029	-.035	-.041	-.055	-.070	-.084	-.094
.016	.050	.041	.035	.018	.006	-.003	-.011	-.012	-.014	-.017	-.018	-.023	-.026	-.031	-.033	-.040	-.044	-.050	-.064	-.084	-.098

TABLE V - Continued
α = 6 DEGREES

B \ A	-.048	-.040	-.032	-.024	-.016	-.012	-.008	-.006	-.004	-.002	0	.002	.004	.006	.008	.012	.016	.024	.032	.040	.048
-.008	.078	.068	.057	.046	.034	.028	.026	.021	.019	.016	.012	.010	.007	.004	0	-.007	-.011	-.022	-.031	-.042	-.055
-.006	.071	.060	.049	.038	.027	.021	.016	.013	.010	.008	.004	.002	-.001	-.004	-.007	-.013	-.018	-.029	-.040	-.051	-.063
-.004	.065	.053	.042	.031	.020	.016	.010	.007	.004	.001	-.001	-.004	-.007	-.010	-.013	-.018	-.024	-.035	-.046	-.057	-.068
-.003	.063	.052	.041	.030	.020	.014	.008	.006	.003	0	-.003	-.005	-.008	-.011	-.014	-.019	-.025	-.035	-.046	-.058	-.068
-.002	.060	.050	.039	.028	.018	.013	.007	.004	.002	-.001	-.004	-.006	-.008	-.012	-.014	-.020	-.028	-.035	-.046	-.057	-.067
-.001	.061	.050	.040	.030	.020	.015	.010	.007	.005	.002	-.001	-.003	-.006	-.008	-.011	-.016	-.021	-.032	-.041	-.052	-.062
0	.060	.050	.040	.030	.020	.015	.010	.007	.005	.002	0	-.003	-.006	-.008	-.011	-.016	-.021	-.031	-.041	-.052	-.065
.001	.057	.048	.038	.028	.016	.009	-.001	-.006	-.010	-.014	-.016	-.018	-.020	-.021	-.023	-.026	-.029	-.036	-.042	-.053	-.065
.002	.056	.047	.038	.025	.012	.007	-.001	-.005	-.009	-.013	-.015	-.017	-.019	-.021	-.023	-.027	-.031	-.040	-.047	-.055	-.066
.003	.054	.044	.035	.021	.010	.005	-.002	-.006	-.010	-.012	-.015	-.017	-.019	-.021	-.024	-.028	-.033	-.042	-.051	-.060	-.072
.004	.052	.042	.031	.020	.009	.004	-.002	-.005	-.007	-.010	-.013	-.016	-.018	-.021	-.024	-.030	-.035	-.046	-.057	-.068	-.078
.006	.042	.040	.033	.022	.010	.004	-.002	-.005	-.008	-.010	-.014	-.016	-.019	-.022	-.025	-.031	-.037	-.049	-.060	-.072	-.083
.008	.046	.035	.032	.023	.010	.004	-.002	-.005	-.008	-.011	-.014	-.017	-.020	-.024	-.027	-.033	-.040	-.052	-.065	-.077	-.090
.012	.039	.034	[illegible]	.021	.012	.006	0	-.003	-.007	-.010	-.013	-.016	-.019	-.023	-.026	-.032	-.039	-.052	-.064	-.077	-.090
.016	.034	.029	.024	.020	.012	.006	.002	-.002	-.007	-.010	-.015	-.017	-.019	-.022	-.024	-.030	-.039	-.049	-.057	-.074	-.089

TABLE V - Continued
α = 7 DEGREES

B \ A	-.048	-.040	-.032	-.024	-.016	-.012	-.008	-.006	-.004	-.002	0	.002	.004	.006	.008	.012	.016	.024	.032	.040	.048
-.012	.078	.064	.054	.044	.034	.027	.023	.018	.015	.012	.009	.007	.004	.002	-.001	-.007	-.012	-.021	-.032	-.038	-.048
-.008	.074	.062	.051	.040	.029	.024	.018	.016	.013	.010	.007	.005	.002	-.001	-.004	-.010	-.016	-.025	-.038	-.048	-.060
-.006	.072	.061	.049	.038	.026	.021	.015	.013	.009	.006	.004	.001	-.002	-.005	-.008	-.014	-.020	-.031	-.042	-.054	-.065
-.004	.066	.054	.044	.032	.022	.016	.010	.008	.005	002	-.001	-.004	-.006	-.009	-.012	-.018	-.024	-.035	-.046	-.057	-.068
-.003	.064	.053	.042	.032	.021	.016	.010	.008	.005	.002	0	-.003	-.006	-.009	-.011	-.017	-.022	-.033	-.043	-.054	-.065
-.002	.063	.052	.042	.031	.021	.016	.011	.008	.006	.003	0	-.002	-.005	-.007	-.010	-.015	-.020	-.030	-.041	-.051	-.062
-.001	.048	.043	.039	.033	.023	.018	.013	.010	.008	.005	.003	0	-.003	-.005	-.008	-.013	-.018	-.029	-.039	-.050	-.060
0	.055	.046	.039	.030	.019	.014	.009	.007	.003	.001	0	-.004	-.006	-.009	-.012	-.016	-.021	-.032	-.042	-.053	-.064
.001	.047	.044	.038	.028	.017	.009	0	-.004	-.007	-.011	-.013	-.016	-.019	-.021	-.023	-.026	-.028	-.036	-.050	-.064	-.079
.002	.054	.046	.036	.025	.014	.008	.003	0	-.002	-.005	-.008	-.010	-.013	-.016	-.019	-.024	-.030	-.041	-.052	-.063	-.077
.003	.042	.040	.036	.027	.016	.010	.005	.002	-.001	-.004	-.007	-.009	-.012	-.015	-.018	-.024	-.030	-.041	-.052	-.064	-.075
.004	.040	.040	.036	.026	.014	.008	.003	0	-.003	-.006	-.009	-.012	-.014	-.017	-.020	-.026	-.032	-.043	-.054	-.066	-.078
.006	.036	.036	.035	.025	.014	.008	.002	-.001	-.004	-.007	-.010	-.013	-.016	-.019	-.022	-.028	-.034	-.046	-.058	-.070	-.084
.008	.025	.033	.032	.020	.008	.003	-.003	-.006	-.009	-.012	-.014	-.017	-.020	-.023	-.026	-.032	-.038	-.050	-.062	-.073	-.086
.012	.020	.026	.022	.012	.002	-.003	-.008	-.011	-.013	-.016	-.019	-.021	-.024	-.027	-.029	-.034	-.040	-.050	-.061	-.072	-.083
.016	.011	.015	.011	.007	0	-.004	-.008	-.011	-.014	-.016	-.020	-.022	-.024	-.027	-.030	-.035	-.040	-.050	-.058	-.066	-.075

TABLE V - Continued
α = 8 DEGREES

B \ A	-.048	-.040	-.032	-.024	-.016	-.012	-.008	-.006	-.004	-.002	0	.002	.004	.006	.008	.012	.016	.024	.032	.040	.048
-.012	.068	.059	.050	.042	.032	.027	.022	.019	.016	.013	.010	.006	.004	.002	-.001	-.005	-.012	-.018	-.032	-.038	-.057
-.008	.076	.064	.053	.042	.031	.025	.020	.017	.014	.011	.008	.005	.002	0	-.003	-.009	-.015	-.026	-.037	-.048	-.060
-.006	.075	.063	.052	.040	.029	.023	.017	.015	.012	.009	.006	.003	0	-.003	-.006	-.012	-.017	-.029	-.040	-.052	-.061
-.004	.068	.057	.047	.036	.025	.020	.014	.011	.008	.006	.003	0	-.002	-.005	-.008	-.013	-.019	-.030	-.041	-.050	-.056
-.003	.063	.052	.042	.032	.022	.017	.012	.009	.007	.004	.002	0	-.003	-.006	-.008	-.014	-.019	-.029	-.039	-.049	-.059
-.002	.060	.050	.040	.030	.020	.015	.011	.008	.005	.003	0	-.002	-.004	-.007	-.009	-.014	-.019	-.029	-.039	-.048	-.058
-.001	.051	.044	.037	.030	.024	.021	.016	.014	.012	.010	.007	.004	.001	-.002	-.004	-.010	-.016	-.028	-.040	-.052	-.063
0	.048	.039	.037	.029	.018	.014	.008	.006	.003	0	0	-.005	-.007	-.010	-.013	-.016	-.022	-.033	-.043	-.054	-.064
.001	.042	.039	.03[illegible]	.030	.021	.014	.006	0	-.004	-.008	-.012	-.016	-.019	-.021	-.024	-.028	-.029	-.034	-.044	-.056	-.066
.002	.038	.038	.035	.030	.020	.013	.004	0	-.004	-.008	-.012	-.015	-.018	-.021	-.024	-.028	-.031	-.038	-.051	-.063	-.072
.003	.034	.036	.036	.032	.015	.005	-.002	-.005	-.008	-.011	-.012	-.017	-.020	-.022	-.024	-.028	-.032	-.039	-.051	-.066	-.076
.004	.024	.033	.036	.028	.008	0	-.005	-.008	-.011	-.013	-.016	-.018	-.020	-.023	-.025	-.029	-.034	-.041	-.051	-.070	-.090
.006	.020	.033	.031	.020	.008	.003	-.003	-.005	-.008	-.011	-.014	-.016	-.019	-.022	-.024	-.030	-.036	-.047	-.058	-.069	-.080
.008	.020	.030	.024	.014	.006	.002	-.002	-.004	-.006	-.008	-.010	-.012	-.015	-.017	-.020	-.027	-.036	-.050	-.062	-.069	-.076
.012	.013	.018	.016	.011	.004	0	-.004	-.007	-.009	-.011	-.014	-.017	-.019	-.022	-.025	-.031	-.036	-.048	-.060	-.071	-.083
.016	.013	.013	.016	.012	.003	-.003	-.009	-.013	-.017	-.021	-.025	-.029	-.031	-.033	-.034	-.035	-.036	-.044	-.052	-.072	-.087

TABLE V - Continued
α = 9 DEGREES

B \ A	-.048	-.040	-.032	-.024	-.016	-.012	-.080	-.060	-.04	-.02	0	.002	.004	.006	.008	.012	.016	.024	.032	.040	.048
-.016	.066	.060	.050	.040	.033	.035	.022	.020	.018	.016	.015	.013	.011	.008	.006	.002	-.004	-.013	-.024	-.034	-.042
-.012	.070	.061	.051	.041	.032	.037	.022	.020	.017	.015	.013	.010	.008	.005	.003	-.001	-.006	-.016	-.026	-.035	-.044
-.008	.074	.062	.052	.041	.031	.026	.021	.018	.016	.015	.011	.008	.006	.003	0	-.005	-.010	-.020	-.030	-.040	-.050
-.006	.072	.062	.051	.040	.030	.024	.019	.016	.014	.011	.009	.006	.003	.001	-.002	-.007	-.012	-.023	-.033	-.043	-.054
-.004	.062	.054	.044	.035	.026	.021	.016	.014	.011	.009	.007	.004	.002	0	-.003	-.008	-.014	-.026	-.038	-.053	-.072
-.003	.060	.051	.042	.033	.024	.019	.014	.012	.010	.008	.005	.003	0	-.002	-.004	-.010	-.017	-.027	-.040	-.056	-.076
-.002	.059	.050	.040	.032	.022	.017	.013	.011	.008	.006	.004	.001	-.001	-.003	-.006	-.009	-.015	-.027	-.038	-.052	-.069
-.001	.047	.040	.036	.032	.023	.019	.014	.012	.010	.008	.006	.004	.001	-.001	-.004	-.009	-.014	-.027	-.038	-.051	-.062
0	.040	.030	.032	.028	.018	.012	.007	.005	.002	0	-.003	-.006	-.008	-.011	-.013	-.018	-.024	-.034	-.044	-.054	-.064
.001	.039	.032	.030	.027	.017	.007	.007	.006	.004	-.002	-.006	-.010	-.015	-.019	-.022	-.027	-.029	-.037	-.048	-.059	-.070
.002	.037	.033	.030	.029	.012	.010	.011	.010	.007	.003	-.002	-.007	-.012	-.017	-.022	-.026	-.031	-.037	-.049	-.061	-.070
.003	.035	.030	.036	.025	.009	.009	.008	.006	.003	-.001	-.005	-.010	-.014	-.019	-.024	-.031	-.034	-.039	-.050	-.061	-.073
.004	.024	.034	.028	.014	.006	.002	-.004	-.006	-.009	-.011	-.014	-.016	-.019	-.021	-.025	-.031	-.036	-.044	-.052	-.064	-.080
.006	.027	.028	.022	.011	-.002	-.006	-.011	-.013	-.015	-.018	-.020	-.022	-.024	-.026	-.029	-.034	-.038	-.047	-.056	-.065	-.077
.008	.038	.029	.014	-.001	-.013	-.016	-.018	-.020	-.021	-.022	-.024	-.025	-.027	-.028	-.029	-.032	-.035	-.045	-.058	-.071	-.081
.012	0	-.004	-.009	-.014	-.018	-.020	-.022	-.023	-.024	-.025	-.026	-.028	-.029	-.030	-.031	-.033	-.035	-.040	-.044	-.048	-.052
.016	.006	.006	-.017	-.016	-.018	-.019	-.023	-.024	-.025	-.026	-.027	-.028	-.029	-.030	-.032	-.033	-.035	-.040	-.037	-.067	-.080

TABLE V - Continued
α = 10 DEGREES

B \ A	-.048	-.040	-.032	-.024	-.016	-.012	-.008	-.006	-.004	-.002	0	.002	.004	.006	.008	.012	.016	.024	.032	.040	.048
-.016	.056	.052	.050	.042	.038	.032	.022	.019	.017	.015	.014	.011	.008	.006	.004	.002	-.001	-.007	-.015	-.020	-.026
-.012	.061	.054	.045	.037	.030	.027	.021	.019	.017	.015	.013	.011	.009	.007	.005	.001	-.003	-.010	-.019	-.026	-.034
-.008	.064	.064	.047	.035	.024	.021	.017	.016	.014	.012	.011	.009	.007	.005	.003	-.002	-.007	-.018	-.029	-.039	-.051
-.006	.074	.064	.052	.039	.025	.019	.014	.011	.009	.007	.005	.004	.002	0	-.002	-.007	-.011	-.021	-.034	-.050	-.067
-.004	.069	.058	.048	.036	.026	.020	.014	.012	.009	.006	.004	.001	-.002	-.004	-.008	-.013	-.018	-.029	-.040	-.051	-.062
-.003	.042	.041	.039	.034	.024	.019	.014	.011	.008	.006	.004	.001	-.002	-.004	-.007	-.012	-.017	-.027	-.037	-.048	-.058
-.002	.036	.038	.038	.035	.026	.020	.014	.012	.009	.006	.004	.001	-.002	-.004	-.007	-.012	-.018	-.029	-.040	-.050	-.061
-.001	.028	.026	.026	.030	.028	.023	.018	.015	.013	.010	.008	.005	.002	0	-.003	-.008	-.013	-.026	-.040	-.053	-.067
0	.028	.021	.027	.024	.017	.011	.007	.006	.003	.001	-.002	-.006	-.008	-.013	-.015	-.020	-.025	-.035	-.044	-.055	-.066
.001	.021	.023	.025	.026	0	.003	.002	-.001	-.005	-.008	-.012	-.015	-.018	-.020	-.023	-.027	-.030	-.034	-.046	-.061	-.079
.002	.019	.036	.033	.017	.005	0	-.004	-.006	-.007	-.008	-.008	-.010	-.014	-.018	-.025	-.030	-.032	-.037	-.044	-.055	-.075
.003	.020	.032	.030	.015	-.007	-.009	-.010	-.009	-.009	-.008	-.008	-.008	-.010	-.016	-.024	-.031	-.039	-.041	-.048	-.059	-.074
.004	.020	.028	.025	.006	-.018	-.020	-.015	-.012	-.008	-.007	-.007	-.009	-.012	-.016	-.021	-.034	-.042	-.046	-.052	-.062	-.076
.006	.023	.020	.010	-.008	-.012	-.011	-.009	-.007	-.006	-.006	-.008	-.010	-.012	-.015	-.018	-.026	-.036	-.051	-.059	-.064	-.073
.008	.016	.008	-.006	-.010	-.004	-.003	-.004	-.005	-.006	-.008	-.010	-.012	-.015	-.018	-.021	-.028	-.036	-.050	-.061	-.069	-.073
.012	-.002	-.005	-.000	-.004	-.006	-.007	-.010	-.012	-.012	-.015	-.014	-.019	-.021	-.023	-.025	-.030	-.035	-.046	-.058	-.068	-.077
.016	-.004	-.006	-.008	-.002	-.010	-.012	-.021	-.024	-.025	-.026	-.025	-.027	-.029	-.031	-.032	-.030	-.033	-.042	-.049	-.058	-.070

TABLE V - Continued
α = 11 DEGREES

F \ A	-.048	-.040	-.032	-.024	-.016	-.012	-.008	-.006	-.004	-.002	0	.002	.004	.006	.008	.012	.016	.024	.032	.040	.048
-.016	.090	.078	.066	.054	.041	.035	.029	.026	.023	.020	.017	.013	.010	.007	.004	-.002	-.007	-.017	-.026	-.033	-.037
-.012	.086	.074	.062	.050	.037	.031	.025	.022	.019	.016	.012	.010	.007	.003	0	-.006	-.011	-.021	-.029	-.036	-.039
-.008	.084	.072	.059	.046	.034	.028	.021	.018	.016	.012	.009	.006	.003	0	-.003	-.009	-.014	-.024	-.032	-.038	-.042
-.006	.056	.059	.056	.045	.033	.026	.020	.017	.014	.011	.008	.005	.002	-.001	-.004	-.010	-.016	-.026	-.036	-.046	-.055
-.004	.029	.041	.046	.038	.028	.022	.017	.014	.012	.009	.006	.004	.001	-.002	-.004	-.010	-.015	-.026	-.037	-.047	-.058
-.003	.006	.022	.032	.034	.025	.020	.015	.013	.010	.008	.006	.004	.001	-.001	-.004	-.009	-.014	-.024	-.035	-.052	-.070
-.002	-.005	.008	.021	.029	.024	.020	.016	.013	.011	.008	.006	.004	.002	-.001	-.003	-.008	-.013	-.027	-.043	-.059	-.079
-.001	.004	.009	.012	.019	.024	.024	.019	.016	.014	.011	.008	.006	.003	0	-.002	-.007	-.016	-.034	-.047	-.060	-.076
0	.016	.016	.019	.019	.014	.010	.006	.006	.004	.002	0	-.003	-.009	-.014	-.016	-.022	-.026	-.034	-.043	-.054	-.068
.001	.020	.024	.026	.014	-.008	-.011	-.003	.001	.002	-.002	-.008	-.013	-.017	-.021	-.023	-.027	-.030	-.037	-.042	-.051	-.062
.002	.017	.027	.030	.010	-.015	-.016	.001	.004	.006	.004	-.002	-.007	-.012	-.017	-.022	-.032	-.038	-.040	-.043	-.054	-.073
.003	.023	.023	.019	-.004	-.017	-.009	.002	.006	.008	.007	.004	-.001	-.008	-.014	-.020	-.030	-.039	-.048	-.050	-.052	-.062
.004	.025	.020	.004	-.012	-.016	-.008	.002	.004	.006	.006	.004	.002	-.004	-.012	-.018	-.029	-.039	-.051	-.058	-.058	-.065
.006	.007	0	-.006	-.010	-.010	-.008	-.005	-.003	-.002	-.002	-.002	-.004	-.006	-.009	-.012	-.024	-.033	-.049	-.062	-.071	-.074
.008	-.001	-.006	-.008	-.009	-.008	-.007	-.006	-.006	-.007	-.007	-.008	-.009	-.011	-.012	-.013	-.021	-.032	-.048	-.060	-.072	-.079
.012	-.001	-.002	-.004	-.008	-.010	-.010	-.011	-.012	-.012	-.012	-.013	-.014	-.016	-.013	-.020	-.023	-.027	-.038	-.049	-.060	-.069
.016		.002	-.002	-.008	-.010	-.010	-.013	-.014	-.015	-.016	-.017	-.018	-.022	-.025	-.028	-.023	-.026	-.033	-.040	-.049	

TABLE V - Continued
α = 12 DEGREES

B \ A	-.048	-.040	-.032	-.024	-.016	-.012	-.008	-.006	-.004	-.002	0	.002	.004	.006	.008	.012	.016	.024	.032	.040	.048
-.016	.056	.058	.056	.047	.038	.033	.029	.028	.026	.024	.022	.020	.018	.016	.014	.006	.002	-.008	-.018	-.027	-.037
-.012	.054	.058	.056	.047	.038	.033	.028	.026	.024	.022	.019	.017	.014	.012	.010	.005	0	-.009	-.018	-.028	-.039
-.008	.048	.055	.055	.047	.037	.032	.027	.024	.021	.019	.016	.014	.011	.008	.006	.001	-.005	-.015	-.025	-.035	-.046
-.006	.028	.036	.041	.042	.038	.033	.028	.025	.022	.019	.016	.013	.010	.007	.004	-.001	-.007	-.019	-.031	-.043	-.054
-.004	0	.011	.021	.028	.031	.031	.030	.028	.027	.025	.021	.018	.014	.010	.006	-.001	-.009	-.025	-.040	-.056	-.071
-.003	-.006	.004	.013	.021	.026	.026	.026	.025	.024	.022	.020	.017	.013	.009	.005	-.003	-.012	-.028	-.044	-.060	-.077
-.002	.009	.009	.010	.013	.019	.022	.022	.021	.020	.018	.015	.013	.009	.006	.002	-.007	-.015	-.031	-.045	-.057	-.065
-.001	.010	.014	.010	.005	.006	.011	.020	.020	.019	.017	.014	.010	.006	.002	-.002	-.012	-.021	-.036	-.045	-.053	-.064
0	.011	.017	.020	.020	.007	.004	.004	.006	.004	.003	0	-.003	-.007	-.011	-.016	-.022	-.027	-.033	-.041	-.052	-.067
.001	.012	.017	.018	.010	-.019	-.015	-.006	-.006	-.008	-.011	-.013	-.016	-.018	-.021	-.023	-.027	-.031	-.036	-.043	-.053	-.066
.002	.013	.016	.012	-.009	-.019	-.012	-.009	-.010	-.011	-.013	-.015	-.017	-.020	-.022	-.025	-.031	-.038	-.048	-.050	-.057	-.070
.003	.015	.005	-.005	-.013	-.019	-.021	-.022	-.023	-.022	-.022	-.024	-.025	-.026	-.027	-.029	-.032	-.039	-.052	-.060	-.062	-.064
.004	-.010	-.002	-.004	-.014	-.022	-.024	-.025	-.026	-.026	-.027	-.028	-.029	-.030	-.032	-.033	-.036	-.040	-.051	-.060	-.069	-.075
.006	-.011	-.006	-.009	-.014	-.020	-.022	-.025	-.027	-.028	-.030	-.031	-.033	-.034	-.035	-.037	-.040	-.043	-.049	-.059	-.069	-.078
.008	-.021	-.017	-.014	-.013	-.015	-.017	-.020	-.021	-.023	-.025	-.026	-.028	-.029	-.031	-.033	-.036	-.040	-.047	-.057	-.067	-.077
.012	-.021	-.016	-.015	-.019	-.023	-.025	-.027	-.028	-.029	-.030	-.031	-.032	-.033	-.034	-.035	-.037	-.039	-.043	-.047	-.051	-.055
.016			-.016	-.024	-.026	-.028	-.039	-.040	-.041	-.041	-.042	-.042	-.043	-.044	-.044	-.035	-.036	-.040	-.038		

TABLE V - Continued
α = 13 DEGREES

B \ A	-.048	-.040	-.032	-.024	-.016	-.012	-.008	-.006	-.004	-.002	0	.002	.004	.006	.008	.012	.016	.024	.032	.040	.048
-.016	.062	.058	.056	.048	.036	.032	.027	.025	.023	.021	.019	.017	.015	.013	.011	.008	.004	-.00	-.010	-.023	-.036
-.012	.052	.050	.047	.042	.035	.031	.027	.025	.023	.021	.019	.017	.015	.013	.011	.007	.003	-.005	-.015	-.027	-.038
-.008	.034	.034	.033	.032	.030	.028	.026	.024	.023	.021	.020	.017	.015	.012	.010	.004	-.002	-.014	-.026	-.038	-.049
-.006	.010	.018	.020	.023	.024	.024	.023	.022	.021	.020	.018	.016	.014	.010	.007	0	-.007	-.022	-.036	-.050	-.060
-.004	-.001	.003	.008	.012	.018	.020	.022	.022	.022	.020	.018	.014	.010	.006	.002	-.006	-.014	-.028	-.042	-.054	-.062
-.003	-.011	-.005	.002	.008	.015	.019	.021	.021	.019	.016	.013	.01	.006	.003	-.001	-.008	-.015	-.028	-.042	-.057	-.066
-.002	.004	.002	.001	.003	.009	.014	.020	.021	.021	.019	.015	.011	.007	.003	-.001	-.009	-.016	-.031	-.045	-.056	-.062
-.001	.004	.006	.010	.010	-.001	.002	.016	.020	.021	.020	.018	.014	.009	.002	-.005	-.015	-.023	-.034	-.042	-.049	-.054
0	.004	.006	.013	.014	-.008	-.015	-.002	.002	.002	.002	-.001	-.002	-.008	-.012	-.016	-.023	-.032	-.034	-.042	-.054	-.068
.001	.012	.012	.002	-.017	-.026	-.024	-.019	-.017	-.015	-.014	-.014	-.015	-.016	-.017	-.020	-.026	-.032	-.042	-.047	-.052	-.056
.002	-.017	-.014	-.014	-.018	-.024	-.026	-.029	-.030	-.031	-.032	-.033	-.033	-.034	-.034	-.034	-.035	-.036	-.050	-.060	-.068	-.073
.003	-.014	-.006	-.008	-.021	-.027	-.029	-.031	-.032	-.034	-.034	-.035	-.037	-.038	-.039	-.04	-.042	-.044	-.050	-.061	-.071	-.076
.004	-.016	-.007	-.011	-.022	-.027	-.029	-.032	-.033	-.034	-.035	-.036	-.037	-.039	-.040	-.041	-.044	-.046	-.051	-.058	-.071	-.088
.006	-.031	-.020	-.016	-.016	-.020	-.023	-.026	-.028	-.030	-.031	-.033	-.034	-.036	-.037	-.039	-.042	-.044	-.049	-.056	-.068	-.087
.008	-.019	-.016	-.017	-.021	-.026	-.028	-.031	-.032	-.033	-.034	-.035	-.037	-.038	-.039	-.040	-.043	-.045	-.050	-.055	-.064	-.074

TABLE V - Continued
α = 14 DEGREES

B \ A	-.048	-.040	-.032	-.024	-.016	-.012	-.008	-.006	-.004	-.002	0	.002	.004	.006	.008	.012	.016	.024	.032	.040	.048
-.016	.020	.040	.042	.044	.037	.027	.022	.020	.015	.023	.022	.020	.018	.017	.016	.012	-.003	-.014	-.005	-.016	-.024
-.012	.016	.030	.035	.038	.034	.025	.022	.019	.015	.018	.017	.014	.011	.010	.007	.002	-.008	-.018	-.015	-.028	-.037
-.008	.003	016	.022	.026	.026	.024	.020	.018	.015	.012	.010	.007	.004	.002	0	-.006	-.013	-.022	-.032	-.043	-.054
-.004	-.015	-.003	.007	.015	.019	.019	.018	.017	.015	.013	.010	.007	.004	0	-.002	-.008	-.014	-.025	-.039	-.051	-.062
-.002	-.003	-.012	-.008	.001	.007	.009	.010	.010	.010	.010	.009	.008	.007	.006	.004	0	-.006	-.026	-.046	-.057	-.056
-.003	-.007	-.012	-.008	-.004	0	.004	.006	.006	.007	.008	.008	.008	.007	.006	.005	0	-.010	-.031	-.045	-.052	-.052
-.002	-.014	-.009	-.004	0	-.006	-.011	-.009	-.004	.004	.009	.010	.009	.007	.004	0	-.008	-.018	-.034	-.042	-.050	-.058
-.001	-.004	.004	.010	.010	-.003	-.007	-.010	-.011	-.011	-.002	.012	.006	.001	-.004	-.008	-.016	-.023	-.031	-.038	-.047	-.057
0	-.028	-.014	-.004	-.002	-.024	-.036	-.048	-.049	-.040	-.015	0	-.004	-.009	-.012	-.016	-.022	-.037	-.036	-.044	-.056	-.071
.001	-.030	-.024	-.022	-.036	-.032	-.035	-.038	-.040	-.042	-.040	-.029	-.016	-.016	-.018	-.021	-.026	-.032	-.047	-.058	-.071	-.087
.002	-.010	-.011	-.012	-.022	-.031	-.035	-.040	-.042	-.043	-.043	-.039	-.034	-.031	-.031	-.032	-.036	-.040	-.049	-.058	-.069	-.080
.003	-.022	-.017	-.018	-.022	-.025	-.027	-.028	-.029	-.030	-.031	-.032	-.034	-.035	-.036	-.037	-.040	-.043	-.051	-.060	-.069	-.078
.004	-.036	-.028	-.020	-.015	-.013	-.014	-.016	-.017	-.018	-.020	-.022	-.024	-.026	-.028	-.030	-.034	-.039	-.048	-.059	-.070	-.082
.006	-.030	-.024	-.020	-.019	-.018	-.019	-.019	-.020	-.020	-.020	-.021	-.022	-.023	-.024	-.025	-.028	-.031	-.040	-.054	-.070	-.084
.008	-.035	-.031	-.030	-.030	-.029	-.030	-.030	-.030	-.031	-.031	-.032	-.032	-.032	-.033	-.034	-.036	-.038	-.044	-.053	-.067	-.086

TABLE V - Continued
α = 15 DEGREES

B \ A	-.048	-.040	-.032	-.024	-.016	-.012	-.008	-.006	-.004	-.002	0	.002	.004	.006	.008	.012	.016	.024	.032	.040	.048
-.016	.044	.053	.053	.049	.045	.042	.036	.034	.032	.029	.026	.024	.023	.021	.020	.015	.009	-.003	-.010	-.020	-.030
-.012	.016	.030	.036	.036	.032	.030	.027	.026	.024	.022	.020	.018	.016	.014	.012	.008	.003	-.007	-.018	-.029	-.042
-.008	-.037	-.014	.005	.017	.020	.020	.018	.016	.015	.013	.011	.009	.007	.005	.003	-.002	-.007	-.016	-.032	-.048	-.063
-.006	-.016	-.021	-.01	-.003	.016	.018	.01	015	.017	.015	.014	.012	.009	.007	.004	-.002	-.008	-.025	-.044	-.054	-.056
-.004	-.032	-.025	-.020	-.013	-.007	-.004	-.002	-.001	0	0	.001	.001	.001	0	0	-.004	-.010	-.032	-.046	-.054	-.057
-.003	-.034	-.024	-.017	-.014	-.012	-.011	-.010	-.00	-.00	-.00	-.008	-.008	-.007	-.007	-.010	-.009	-.016	-.033	-.042	-.051	-.061
-.002	-.03	-.021	-.010	-.006	-.012	-.016	-.017	-.017	-.016	-.015	-.014	-.013	-.012	-.012	-.013	-.016	-.021	-.032	-.043	-.055	-.067
-.001	-.050	-.032	-.015	-.004	-.00	-.014	-.01	-.022	-.024	-.026	-.023	-.015	-.008	-.008	-.011	-.016	-.022	-.033	-.044	-.056	-.068
0	-.045	-.034	-.025	-.023	-.036	-.044	-.051	-.053	-.050	-.037	-.020	-.010	-.013	-.012	-.014	-.018	-.032	-.040	-.051	-.060	-.074
.001	-.034	-.024	-.021	-.02	-.036	-.040	-.039	-.03	-.036	-.034	-.032	-.030	-.029	-.028	-.028	-.029	-.034	-.045	-.056	-.067	-.078
.002	-.043	-.037	-.031	-.024	-.024	-.026	-.02	-.02	-.030	-.032	-.033	-.034	-.035	-.037	-.039	-.041	-.044	-.050	-.060	-.070	-.080
.003	-.030	-.023	-.020	-.024	-.02	-.031	-.034	-.034	-.036	-.037	-.03	-.040	-.041	-.042	-.044	-.046	-.048	-.054	-.060	-.067	-.076
.004	-.030	-.022	-.022	-.027	-.032	-.034	-.036	-.03	-.039	-.040	-.041	-.042	-.044	-.045	-.046	-.048	-.050	-.055	-.060	-.064	-.070
.00	-.03	-.041	-.044	-.047	-.050	-.051	-.053	-.05	.054	-.055	-.056	-.056	-.058	-.058	-.059	-.060	-.062	-.066	-.068	-.072	-.075
.00	-.04	-.06	-.06	-.06	-.07	-.06	-.06	-.06	-.070	-.070	-.071	-.072	-.073	-.075	-.076	-.077	-.073	-.075	-.077	-.079	-.082

TABLE V - Continued
α = 16 DEGREES

B \ A	-.048	-.040	-.032	-.024	-.016	-.012	-.008	-.006	-.004	-.002	0	.002	.004	.006	.008	.012	.016	.024	.032	.040	.048
-.016	.018	.030	.040	.040	.028	.021	.016	.015	.013	.011	.010	.008	.006	.005	.003	.001	-.002	-.009	-.018	-.027	-.034
-.012	.003	.006	.017	.026	.023	.020	.016	.015	.013	.011	.010	.008	.006	.005	.003	0	-.004	-.012	-.024	-.036	-.045
-.008	-.025	-.031	-.030	-.012	.010	.013	.013	.013	.012	.011	.010	.009	.006	.004	.002	-.004	-.010	-.024	-.038	-.048	-.058
-.006	-.045	-.039	-.034	-.025	-.005	0	.002	.003	.003	.003	.002	.001	-.001	-.002	-.004	-.008	-.014	-.028	-.042	-.053	-.057
-.004	-.050	-.047	-.034	-.026	-.018	-.015	-.011	-.010	-.008	-.008	-.008	-.008	-.008	-.009	-.010	-.014	-.018	-.030	-.045	-.058	-.062
-.003	-.060	-.048	-.030	-.021	-.027	-.025	-.012	-.008	-.007	-.006	-.007	-.008	-.009	-.010	-.012	-.016	-.020	-.030	-.042	-.056	-.067
-.002	-.065	-.050	-.031	-.028	-.024	-.031	-.021	-.009	-.008	-.008	-.008	-.009	-.010	-.011	-.013	-.017	-.021	-.032	-.045	-.060	-.075
-.001	-.062	-.045	-.037	-.018	-.019	-.021	-.024	-.026	-.029	-.037	-.016	-.006	-.003	-.004	-.008	-.016	-.024	-.036	-.046	-.058	-.073
0	-.058	-.047	-.039	-.034	-.044	-.050	-.057	-.060	-.060	-.055	-.043	-.031	-.028	-.012	-.011	-.016	-.028	-.046	-.057	-.063	-.077
.001	-.046	-.035	-.032	-.034	-.041	-.046	-.050	-.052	-.052	-.048	-.044	-.039	-.034	-.030	-.028	-.030	-.035	-.048	-.057	-.063	-.074
.002	-.032	-.027	-.026	-.030	-.036	-.040	-.044	-.044	-.044	-.044	-.043	-.042	-.041	-.041	-.041	-.042	-.044	-.052	-.059	-.066	-.073
.003	-.028	-.031	-.034	-.038	-.042	-.044	-.045	-.046	-.047	-.048	-.049	-.050	-.051	-.052	-.053	-.055	-.056	-.060	-.063	-.067	-.071
.004	-.047	-.049	-.052	-.054	-.056	-.058	-.059	-.060	-.060	-.061	-.061	-.062	-.062	-.063	-.064	-.065	-.066	-.068	-.071	-.073	-.075

TABLE V - Continued
α = 17 DEGREES

B \ A	-.048	-.040	-.032	-.024	-.016	-.012	-.008	-.006	-.004	-.002	0	.002	.004	.006	.008	.012	.016	.024	.032	.040	.048
-.016	-.022	-.024	-.022	-.020	.002	0	.011	.016	.020	.019	.018	.016	.013	.011	.008	0	-.012	-.018	-.026	-.030	-.038
-.012	-.035	-.035	-.035	-.035	-.019	-.007	.005	.010	.011	.010	.009	.007	.005	.003	0	-.004	-.009	-.018	-.028	-.037	-.046
-.008	-.060	-.048	-.046	-.044	-.033	-.017	.001	.006	.008	.008	.008	.007	.006	.004	.002	-.003	-.008	-.022	-.037	-.055	-.074
-.006	-.071	-.055	-.045	-.042	-.037	-.026	-.009	.002	.006	.008	.006	.004	.002	-.001	-.004	-.009	-.014	-.026	-.040	-.053	-.067
-.004	-.087	-.068	-.048	-.034	-.039	-.040	-.027	-.015	-.004	-.001	-.001	-.002	-.004	-.005	-.007	-.011	-.016	-.030	-.045	-.061	-.079
-.003	-.087	-.068	-.048	-.032	-.031	-.038	-.032	-.024	-.017	-.013	-.012	-.012	-.012	-.012	-.013	-.015	-.018	-.031	-.049	-.067	-.086
-.002	-.074	-.054	-.038	-.028	-.028	-.034	-.033	-.031	-.028	-.026	-.024	-.021	-.018	-.014	-.016	-.016	-.019	-.035	-.055	-.066	-.072
-.001	-.066	-.050	-.040	-.038	-.036	-.035	-.034	-.033	-.032	-.032	-.030	-.029	-.024	-.015	-.012	-.017	-.023	-.039	-.056	-.071	-.080
0	-.067	-.054	-.044	-.040	-.050	-.058	-.064	-.067	-.070	-.071	-.063	-.055	-.048	-.033	-.027	-.022	-.026	-.048	-.058	-.065	-.078
.001	-.029	-.032	-.035	-.038	-.042	-.043	-.044	-.045	-.046	-.047	-.048	-.048	-.049	-.050	-.050	-.052	-.053	-.056	-.059	-.062	-.065
.002	-.057	-.058	-.060	-.062	-.063	-.064	-.065	-.065	-.066	-.066	-.066	-.067	-.068	-.068	-.068	-.069	-.070	-.072	-.073	-.074	-.076

TABLE V - Continued
α = 18 DEGREES

B \ A	-.048	-.040	-.032	-.024	-.016	-.012	-.008	-.006	-.004	-.002	0	.002	.004	.006	.008	.012	.016	.024	.032	.040	.048
-.016	-.076	-.055	-.030	-.016	-.003	.002	.004	.006	.007	.008	.012	.014	.016	.017	.019	.015	.008	-.008	-.022	-.040	-.060
-.012	-.081	-.066	-.054	-.043	-.033	-.028	-.024	-.021	-.019	-.017	-.014	-.012	-.009	-.007	-.005	-.002	-.003	-.014	-.028	-.044	-.062
-.008	-.086	-.074	-.068	-.063	-.058	-.055	-.051	-.048	-.044	-.040	-.035	-.030	-.025	-.021	-.018	-.013	-.010	-.020	-.036	-.052	-.067
-.006	-.099	-.081	-.068	-.060	-.060	-.062	-.059	-.056	-.053	-.048	-.042	-.036	-.030	-.026	-.021	-.015	-.012	-.025	-.044	-.060	-.076
-.004	-.096	-.080	-.064	-.050	-.048	-.057	-.060	-.059	-.057	-.053	-.049	-.044	-.038	-.031	-.024	-.015	-.015	-.034	-.051	-.062	-.071
-.003	-.091	-.075	-.060	-.048	-.042	-.047	-.057	-.057	-.056	-.053	-.048	-.043	-.037	-.029	-.022	-.014	-.017	-.037	-.054	-.066	-.074
-.002	-.085	-.070	-.056	-.046	-.043	-.044	-.048	-.050	-.049	-.046	-.041	-.035	-.029	-.022	-.017	-.014	-.019	-.042	-.058	-.070	-.082
-.001	-.078	-.063	-.050	-.046	-.056	-.050	-.045	-.045	-.047	-.047	-.044	-.040	-.033	-.026	-.021	-.020	-.024	-.046	-.060	-.070	-.081
0	-.071	-.056	-.046	-.043	-.054	-.067	-.075	-.078	-.080	-.081	-.081	-.077	-.068	-.060	-.050	-.031	-.026	-.048	-.058	-.065	-.077

TABLE V - Continued
α = 19 DEGREES

B \ A	-.048	-.040	-.032	-.024	-.016	-.012	-.008	-.006	-.004	-.002	0	.002	.004	.006	.008	.012	.016	.024	.032	.040	.048
-.016	-.094	-.090	-.088	-.078	-.050	-.028	-.003	-.002	-.001	0	.001	.002	.004	.005	.006	.006	.006	-.010	-.032	-.050	-.06
-.012	-.094	-.089	-.086	-.078	-.057	-.039	-.024	-.018	-.013	-.009	-.005	-.003	-.001	0	0	0	-.004	-.016	-.035	-.057	-.08
-.008	-.094	-.089	-.085	-.082	-.081	-.076	-.062	-.053	-.045	-.036	-.027	-.021	-.015	-.011	-.010	-.009	-.012	-.023	-.042	-.068	-.09
-.006	-.102	-.083	-.066	-.058	-.058	-.063	-.066	-.064	-.060	-.053	-.047	-.040	-.034	-.027	-.022	-.014	-.013	-.022	-.041	-.066	-.09
-.004	-.113	-.097	-.080	-.064	-.060	-.067	-.074	-.074	-.073	-.069	-.063	-.056	-.049	-.043	-.037	-.029	-.024	-.032	-.052	-.074	-.09
-.003	-.104	-.089	-.075	-.062	-.058	-.061	-.067	-.070	-.073	-.073	-.070	-.065	-.059	-.053	-.047	-.035	-.026	-.037	-.058	-.069	-.07
-.002	-.085	-.069	-.061	-.058	-.059	-.060	-.062	-.064	-.069	-.075	-.073	-.068	-.063	-.057	-.050	-.042	-.032	-.047	-.062	-.070	-.07
-.001	-.064	-.060	-.058	-.058	-.063	-.067	-.065	-.057	-.060	-.067	-.071	-.068	-.062	-.058	-.053	-.043	-.039	-.044	-.058	-.068	-.07
0	-.068	-.060	-.056	-.058	-.068	-.078	-.081	-.084	-.088	-.090	-.098	-.090	-.080	-.068	-.061	-.053	-.049	-.053	-.063	-.069	-.07

TABLE V - Continued
α = 20 DEGREES

B \ A	-.048	-.040	-.032	-.024	-.016	-.012	-.008	-.006	-.004	-.002	0	.002	.004	.006	.008	.012	.016	.024	.032	.040	.048
-.016	-.136	-.113	-.097	-.080	-.062	-.057	-.044	-.037	-.025	-.018	-.012	-.008	-.006	-.002	0	.005	.001	-.020	-.030	-.047	-.062
-.012	-.151	-.128	-.107	-.087	-.069	-.059	-.050	-.045	-.040	-.035	-.030	-.027	-.025	-.023	-.022	-.020	-.019	-.023	-.035	-.050	-.064
-.008	-.159	-.136	-.114	-.094	-.077	-.071	-.065	-.063	-.061	-.060	-.059	-.058	-.057	-.055	-.053	-.049	-.042	-.028	-.044	-.058	-.071
-.006	-.141	-.123	-.105	-.090	-.080	-.077	-.076	-.076	-.076	-.076	-.076	-.075	-.073	-.070	-.063	-.048	-.033	-.033	-.054	-.071	-.089
-.004	-.098	-.085	-.080	-.084	-.074	-.079	-.082	-.084	-.086	-.088	-.090	-.084	-.075	-.066	-.057	-.039	-.028	-.045	-.058	-.067	-.072
-.003	-.094	-.086	-.080	-.075	-.072	-.072	-.074	-.072	-.080	-.084	-.090	-.093	-.092	-.084	-.074	-.053	-.040	-.047	-.056	-.068	-.081
-.002	-.086	-.075	-.071	-.069	-.072	-.074	-.071	-.080	-.082	-.084	-.086	-.089	-.089	-.087	-.083	-.068	-.056	-.051	-.059	-.072	-.087
-.001	-.077	-.068	-.061	-.060	-.072	-.076	-.074	-.074	-.079	-.078	-.075	-.072	-.075	-.066	-.062	-.080	-.069	-.056	-.059	-.071	-.089
0	-.072	-.065	-.061	-.063	-.072	-.080	-.083	-.087	-.092	-.096	-.112	-.100	-.090	-.076	-.099	-.094	-.081	-.069	-.072	-.075	-.075

TABLE V - Continued
α = 21 DEGREES

B \ A	-.048	-.040	-.032	-.024	-.016	-.012	-.008	-.006	-.004	-.002	0	.002	.004	.006	.008	.012	.016	.024	.032	.040	.048
-.016	-.174	-.160	-.140	-.116	-.090	-.080	-.066	-.062	-.057	-.047	-.033	-.031	-.028	-.024	-.013	-.010	.003	.004	-.006	-.014	-.029
-.012	-.166	-.155	-.143	-.130	-.115	-.108	-.095	-.088	-.083	-.077	-.072	-.063	-.057	-.050	-.044	-.033	-.025	-.019	-.025	-.037	-.053
-.008	-.148	-.143	-.137	-.133	-.123	-.113	-.104	-.094	-.091	-.085	-.077	-.070	-.062	-.054	-.048	-.039	-.035	-.043	-.056	-.069	-.081
-.004	-.112	-.110	-.110	-.114	-.112	-.104	-.104	-.100	-.096	-.092	-.087	-.082	-.078	-.073	-.069	-.064	-.060	-.057	-.059	-.064	-.073
-.004	-.105	-.097	-.094	-.093	-.095	-.097	-.099	-.100	-.101	-.102	-.103	-.104	-.104	-.104	-.104	-.096	-.077	-.056	-.063	-.074	-.087
-.003	-.091	-.085	-.084	-.084	-.086	-.090	-.090	-.092	-.093	-.094	-.096	-.098	-.100	-.103	-.106	-.106	-.082	-.060	-.067	-.079	-.094
-.002	-.077	-.071	-.070	-.074	-.081	-.085	-.090	-.093	-.096	-.100	-.104	-.104	-.114	-.117	-.116	-.100	-.088	-.071	-.060	-.074	-.082
-.001	-.069	-.062	-.062	-.066	-.074	-.080	-.086	-.086	-.092	-.094	-.097	-.100	-.103	-.106	-.109	-.114	-.103	-.084	-.078	-.079	-.085
0	-.072	-.062	-.054	-.060	-.070	-.075	-.083	-.086	-.094	-.104	-.122	-.106	-.106	-.110	-.131	-.134	-.118	-.099	-.095	-.095	-.089

TABLE V - Continued
α = 22 DEGREES

β \ γ	-.040	-.032	-.024	-.016	-.012	-.008	-.006	-.004	-.002	0	.002	.004	.006	.008	.012	.016	.024	.032	.040	.048
-.016	-.253	-.233	-.212	-.192	-.180	-.171	-.164	-.085	-.046	-.077	-.061	-.055	-.052	-.046	-.040	-.037	-.034	-.039	-.046	-.056	-.074
-.012	-.240	-.230	-.217	-.171	-.154	-.143	-.131	-.123	-.115	-.107	-.096	-.086	-.082	-.076	-.072	-.066	-.061	-.056	-.054	-.060	-.075
-.008	-.230	-.234	-.137	-.145	-.152	-.154	-.150	-.145	-.134	-.132	-.122	-.113	-.104	-.096	-.086	-.076	-.065	-.053	-.055	-.066	-.083
-.004	-.218	-.210	-.115	-.125	-.140	-.147	-.154	-.154	-.145	-.140	-.130	-.121	-.113	-.105	-.099	-.087	-.077	-.066	-.067	-.076	-.092
.004	-.[illegible]	-.[illegible]	-.094	-.100	-.[illegible]	-.[illegible]	-.120	-.123	-.126	-.124	-.132	-.132	-.124	-.124	-.118	-.109	-.101	-.087	-.078	-.079	-.085
-.003	-.092	-.092	-.[illegible]	-.[illegible]	-.097	-.[illegible]	-.111	-.115	-.111	-.124	-.124	-.134	-.137	-.136	-.135	-.127	-.117	-.094	-.081	-.077	-.077
-.012	-.[illegible]	-.[illegible]	-.072	-.077	-.[illegible]	-.[illegible]	-.102	-.[illegible]	-.111	-.116	-.121	-.126	-.132	-.137	-.134	-.135	-.123	-.104	-.095	-.091	-.090
-.020	-.[illegible]	-.[illegible]	-.064	-.[illegible]	-.077	-.[illegible]	-.[illegible]	-.[illegible]	-.097	-.102	-.106	-.111	-.117	-.123	-.128	-.137	-.134	-.118	-.109	-.105	-.103
	-.[illegible]	-.[illegible]	-.050	-.[illegible]	-.[illegible]	-.[illegible]	-.[illegible]	-.[illegible]	-.[illegible]	-.110	-.130	-.114	-.120	-.133	-.142	-.140	-.136	-.127	-.121	-.116	-.111

TABLE V - Continued
α = 23 DEGREES

B \ A	-.048	-.040	-.032	-.024	-.016	-.012	-.008	-.006	-.004	-.002	0	.002	.004	.006	.008	.012	.016	.024	.032	.040	.048
-.016		-.212	-.25[illegible]	-.21[illegible]	-.175	-.157	-.143	-.136	-.130	-.11[illegible]	-.102	-.0[illegible]4	-.0[illegible]0	-.065	-.078	-.068	-.054	-.031	-.016	0	
-.012		-.167	-.223	-.212	-.1[illegible]6	-.17[illegible]	-.157	-.151	-.143	-.137	-.130	-.123	-.116	-.109	-.102	-.088	-.074	-.049	-.039	-.031	
-.008	-.040	-.067	-.144	-.1[illegible]3	-.1[illegible]	-.1[illegible]0	-.1[illegible]2	-.151	-.141	-.131	-.124	-.117	-.112	-.107	-.102	-.095	-.089	-.080	-.074	-.069	-.067
-.006	-.03[illegible]	-.05[illegible]	-.102	-.13[illegible]	-.1[illegible]1	-.167	-.16[illegible]	-.16[illegible]	-.167	-.165	-.163	-.15[illegible]	-.157	-.154	-.150	-.141	-.130	-.104	-.074	-.040	-.032
-.004	-.03[illegible]	-.0[illegible]2	-.062	-.102	-.122	-.133	-.143	-.148	-.153	-.15[illegible]	-.163	-.167	-.171	-.175	-.178	-.178	-.161	-.117	-.080	-.051	-.028
-.003	-.056	-.0[illegible]5	-.077	-.0[illegible]4	-.105	-.1[illegible]3	-.122	-.127	-.133	-.13[illegible]	-.144	-.152	-.159	-.167	-.173	-.177	-.157	-.120	-.089	-.063	-.040
-.002	-.056	-.0[illegible]3	-.071	-.0[illegible]1	-.0[illegible]2	-.1[illegible]0	-.1[illegible]5	-.1[illegible]2	-.117	-.123	-.12[illegible]	-.136	-.144	-.154	-.159	-.160	-.154	-.127	-.101	-.080	-.060
-.001	-.0[illegible]3	-.0[illegible]7	-.073	-.07[illegible]	-.0[illegible]4	-.0[illegible]	-.0[illegible]3	-.0[illegible]7	-.101	-.1[illegible]0	-.1[illegible]1	-.116	-.123	-.1[illegible]4	-.1[illegible]3	-.156	-.164	-.158	-.137	-.109	-.081
0	-.071	-.073	-.[illegible]	-.[illegible]	-.[illegible]	-.[illegible]	-.0[illegible]7	-.1[illegible]5	-.116	-.1[illegible]0	-.135	-.124	-.1[illegible]	-.118	-.133	-.157	-.175	-.181	-.157	-.1[illegible]2	-.098

TABLE V - Continued
α = 24 DEGREES

B \ A	-.048	-.040	-.032	-.024	-.016	-.012	-.008	-.006	-.004	-.002	0	.002	.004	.006	.008	.012	.016	.024	.032	.040	.048
-.016		-.214	-.218	-.221	-.211	-.198	-.186	-.179	-.172	-.164	-.154	-.152	-.148	-.144	-.140	-.130	-.126	-.128	-.116	-.108	
-.012		-.158	-.184	-.195	-.198	-.196	-.193	-.191	-.189	-.187	-.184	-.181	-.177	-.173	-.169	-.159	-.148	-.121	-.089	-.055	
-.008		-.083	-.126	-.155	-.176	-.184	-.191	-.193	-.195	-.196	-.197	-.196	-.194	-.191	-.187	-.176	-.161	-.118	-.063	-.050	
-.006		-.056	-.084	-.123	-.156	-.170	-.180	-.184	-.188	-.191	-.193	-.193	-.191	-.187	-.184	-.174	-.161	-.128	-.086	-.037	
-.004		-.019	-.055	-.070	-.123	-.138	-.153	-.160	-.166	-.172	-.177	-.180	-.183	-.184	-.185	-.184	-.177	-.152	-.120	-.085	
-.003		-.015	-.030	-.069	-.105	-.121	-.136	-.142	-.148	-.154	-.160	-.164	-.169	-.172	-.176	-.181	-.184	-.180	-.168	-.122	
-.002		-.027	-.056	-.073	-.093	-.104	-.115	-.121	-.126	-.132	-.139	-.145	-.151	-.157	-.164	-.177	-.192	-.212	-.220	-.166	
-.001			-.078	-.083	-.091	-.094	-.099	-.101	-.105	-.110	-.116	-.123	-.131	-.141	-.151	-.178	-.200	-.226	-.246		
0			-.100	-.096	-.090	-.096	-.102	-.107	-.116	-.125	-.140	-.136	-.140	-.142	-.146	-.179	-.211	-.235	-.263		

TABLE V - Continued
α = 25 DEGREES

B \ A	-.048	-.040	-.032	-.024	-.016	-.012	-.008	-.006	-.004	-.002	0	.002	.004	.006	.008	.012	.016	.024	.032	.040	.048
-.016			-.252	-.241	-.218	-.215	-.209	-.207	-.204	-.202	-.199	-.185	-.180	-.173	-.166	-.157	-.142	-.120	-.103		
-.012			-.253	-.220	-.206	-.200	-.193	-.190	-.186	-.183	-.180	-.176	-.173	-.169	-.166	-.159	-.153	-.140	-.126		
-.008			-.185	-.154	-.142	-.142	-.141	-.181	-.180	-.180	-.180	-.179	-.179	-.178	-.178	-.178	-.177	-.176	-.174		
-.006			-.125	-.142	-.156	-.162	-.168	-.172	-.175	-.179	-.182	-.185	-.188	-.192	-.195	-.202	-.208	-.221	-.234		
-.004			-.055	-.085	-.116	-.131	-.146	-.154	-.162	-.169	-.177	-.185	-.192	-.200	-.207	-.223	-.238	-.268	-.299		
-.003				-.062	-.087	-.115	-.132	-.141	-.150	-.159	-.168	-.176	-.185	-.194	-.202	-.220	-.238	-.273			
-.002				-.051	-.064	-.101	-.117	-.125	-.134	-.142	-.151	-.159	-.167	-.175	-.184	-.200	-.216	-.250			
-.001				-.045	-.073	-.087	-.101	-.108	-.115	-.122	-.129	-.136	-.143	-.148	-.156	-.170	-.184	-.211			
0											-.144										

TABLE VI. VALUES OF CONSTANT ANGULAR VELOCITY A FOR RAMP CAM TIME HISTORIES

Frequency f (cps)	Forward		Backward	
	Upstroke	Downstroke	Upstroke	Downstroke
7.5	0.0021	-0.00105	0.00105	-0.0021
10.0	0.0028	-0.0014	0.0014	-0.0028
14.3	0.0040	-0.0020	0.0020	-0.0040
20.0	0.0056	-0.0028	0.0028	-0.0056

TABLE VII. PARAMETER VALUES FOR NUMERICAL SOLUTION

I	=	0.000529 (ft-lb-sec^2/rad)/ft	
b	=	0.2il ft	
V	=	390 ft/sec	
ρ	=	0.0022 lb sec^2/ft^4	
T_o	=	$I\omega_n\bar{\alpha} = 0.739\ \omega_n^2 \times 10^{-4}$ ft-lb/ft	
δ	=	various values from 0.25 to 1.00	
ω	=	47.1, 62.8, and 92.4 rad/sec	All Combinations
ω_n	=	260.5, 326, and 471 rad/sec	
α_M	=	6, 11, and 16 deg	
$\bar{\alpha}$	=	8 deg	
Δt	=	$\frac{0.002\omega}{2\pi} = 3.19\omega \times 10^{-4}$ sec	
Tolerance	=	$\left\lvert \frac{\alpha_{in+1} - \alpha_{in}}{\alpha_{in+1}} \right\rvert < 0.005$	

TABLE VIII. SCALING PARAMETERS USED FOR MODEL AIRFOIL DATA

Mach Number M	Normal Force Stall Angle, α_{sn} (deg)	Normal Force Coefficient at Stall, K_n	Pitching Moment Stall Angle, α_{sm} (deg)
0	11.0	1.17	13.5
0.2	11.0	1.17	14.0
0.3	11.0	1.248	14.0
0.4	9.0	1.078	12.4
0.5	6.8	0.845	9.0
0.6	5.6	0.740	8.0
0.7	4.0	0.528	7.0
0.80	2.0	0.418	7.0

TABLE IX. SUMMARY OF TEST CASES USED FOR CORRELATION STUDY

Case	Velocity (kt)	Nominal Advance Ratio	Nominal Thrust Coefficient - Solidity Ratio	Shaft Angle (deg)	Tip Path Plane Angle (deg)	Collective Pitch at 0.75 R (deg)	Half Peak-to-Peak Root Torsional Moment (in.-lb)
NH-3A/28	160.80	0.410	0.0730	-4.4	0.81	6.05	± 2360
NH-3A/39	164.60	0.420	0.0731	-5.0	-0.97	7.60	± 2675
NH-3A/43	185.97	0.474	0.0579	-3.4	1.74	5.23	± 4295
NH-3A/72	138.06	0.345	0.0854	Not Measured		4.60	± 5475
CH-53A/55	136.72	0.324	0.069	-1.3	-2.44	10.7	± 15,750
Model 51-11	100.5	0.504	0.081	0.1	0.1	12.0	± 24.3
Model 68-6	61.0	0.294	0.1056	0.5	0.5	11.0	± 18.5

TABLE X. COORDINATES AND WEIGHTING COEFFICIENTS FOR 10 POINT GAUSSIAN QUADRATURE

Station i	Normalized Coordinate ξ_i	Weighting Coefficient W_i	Actual Chordwise Location, Percent Chord
1	0.01305	0.033336	1.19
2	0.06747	0.074726	6.15
3	0.16030	0.109543	14.62
4	0.28330	0.134634	25.83
5	0.42557	0.147762	38.81
6	0.57443	0.147762	52.38
7	0.71670	0.134634	65.36
8	0.83970	0.109543	76.57
9	0.93253	0.074726	85.04
10	0.98695	0.033336	90.00

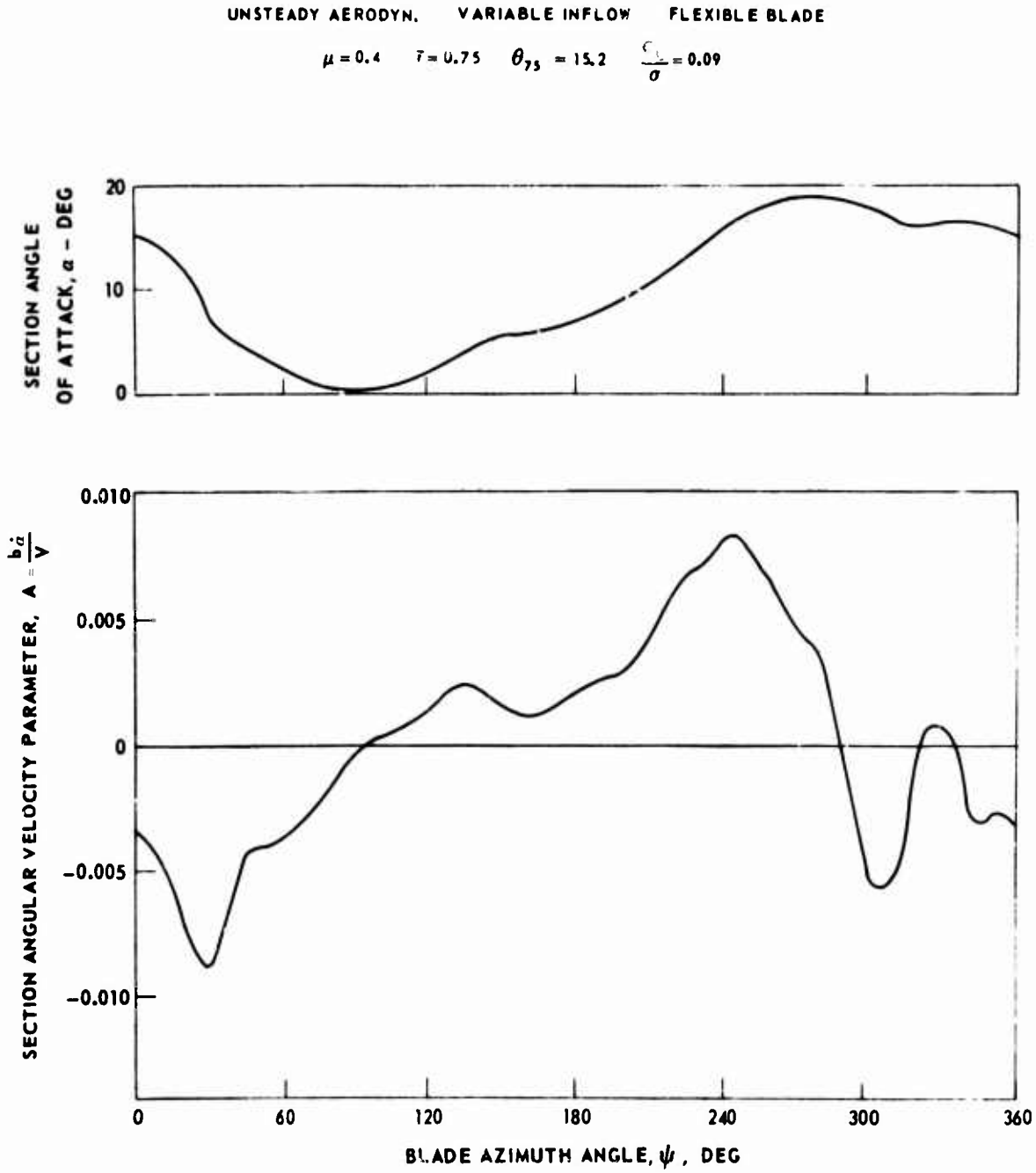

Figure 1. Typical Angle-of-Attack and Angular-Velocity-Parameter Variation With Azimuth Angle.

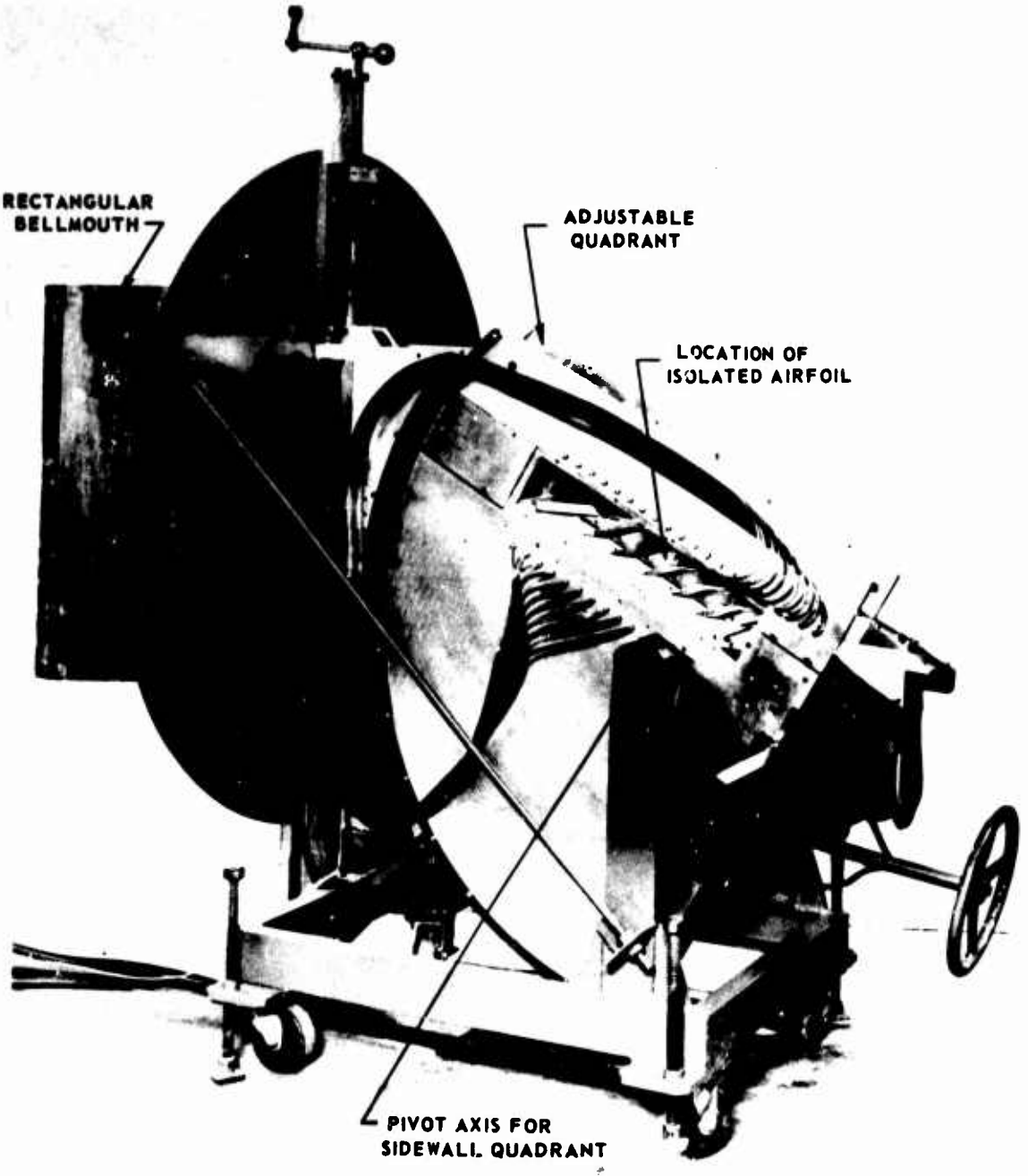

Figure 2. UAC Two-Dimensional High-Speed Cascade Wind Tunnel.

INTERIOR STRUCTURE OF AIRFOIL

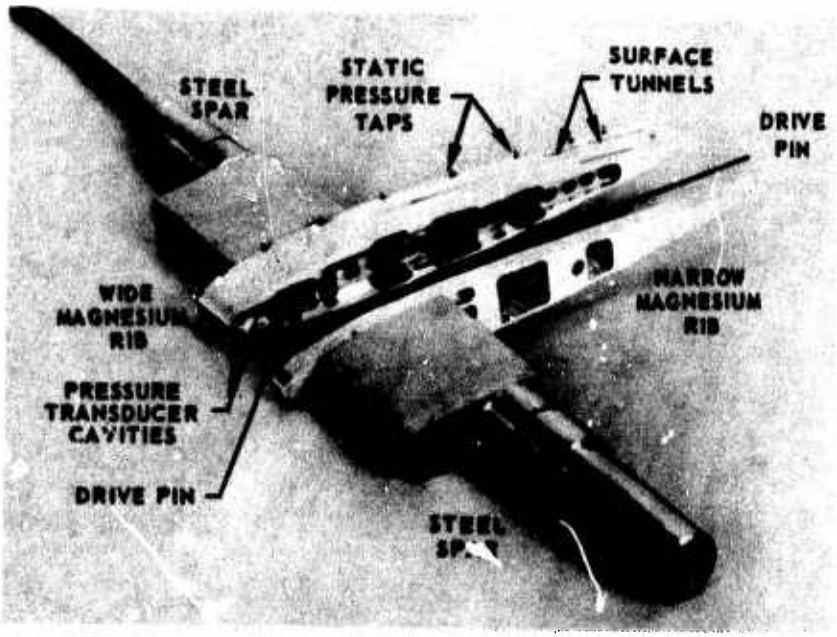

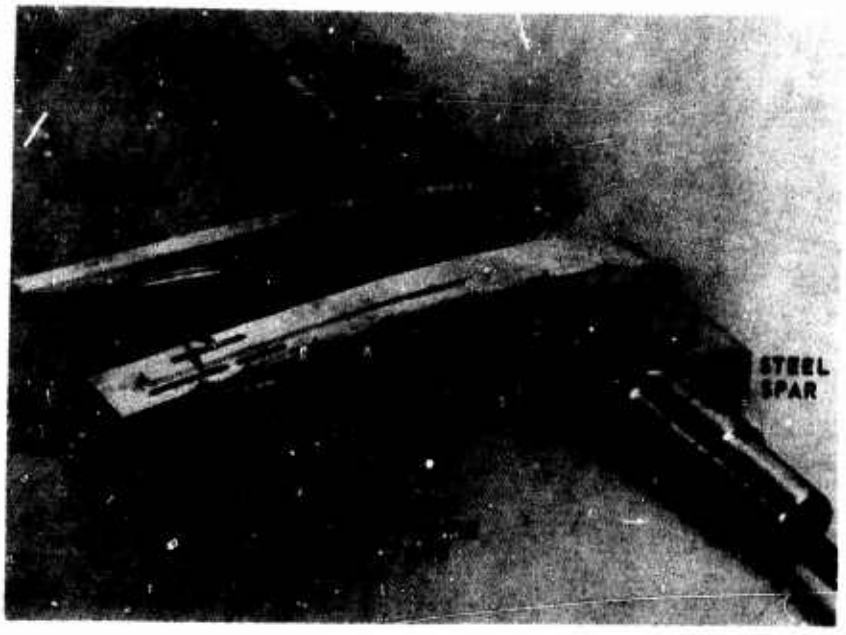

Figure 3. Airfoil Model Rib and Spar Assembly.

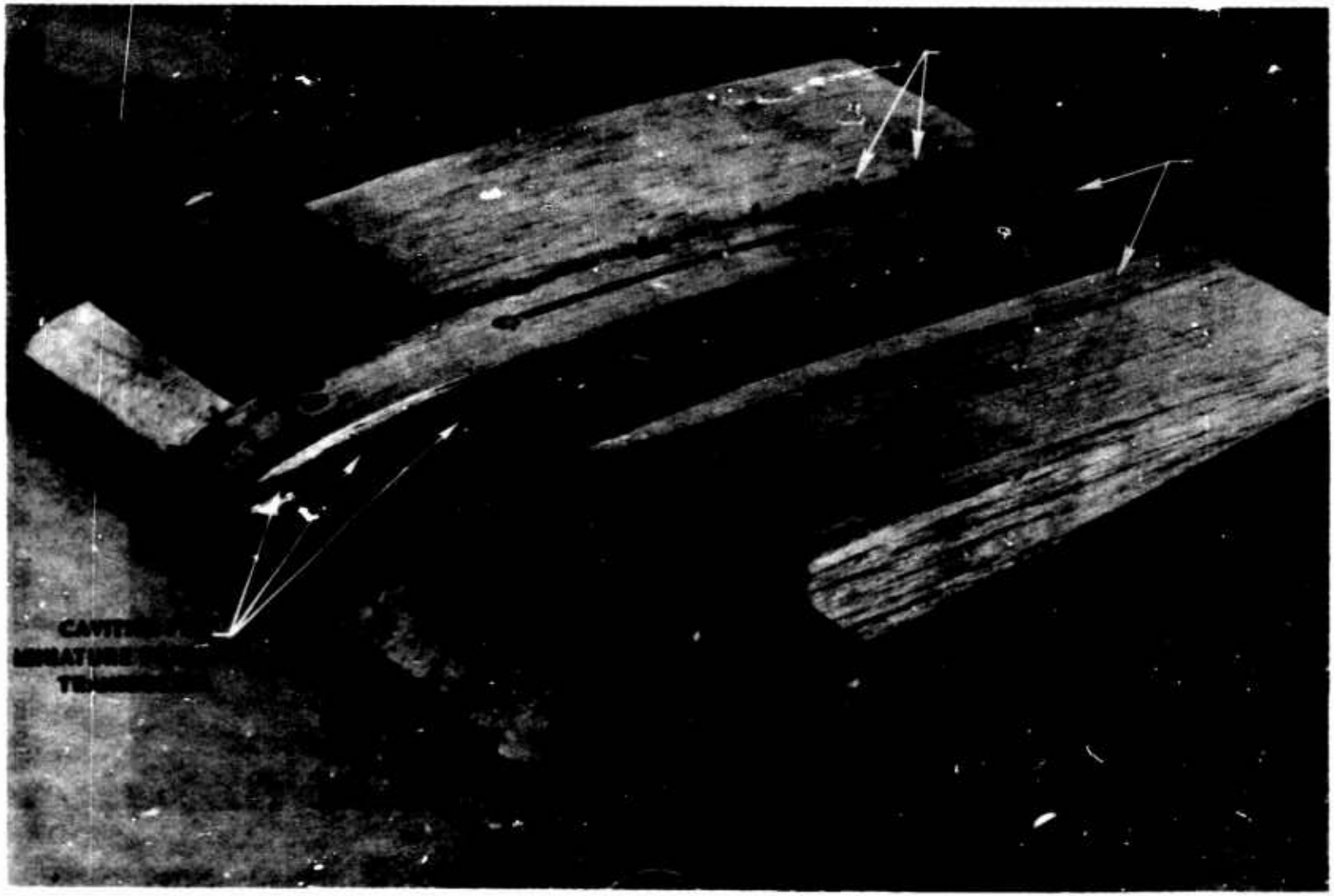

Figure 4. Airfoil Model Without Skin - Disassembled.

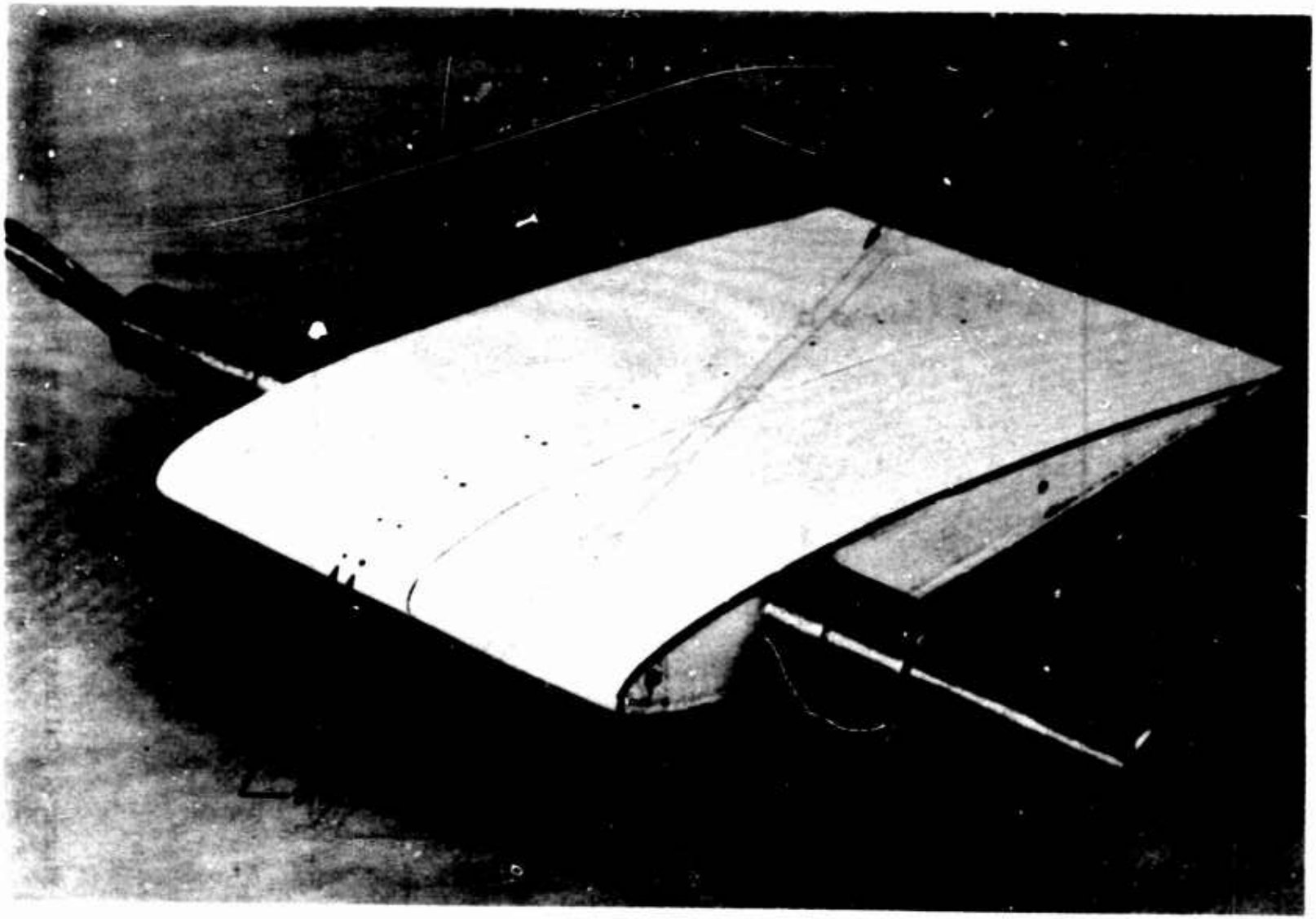

Figure 5. Airfoil Model - Assembled.

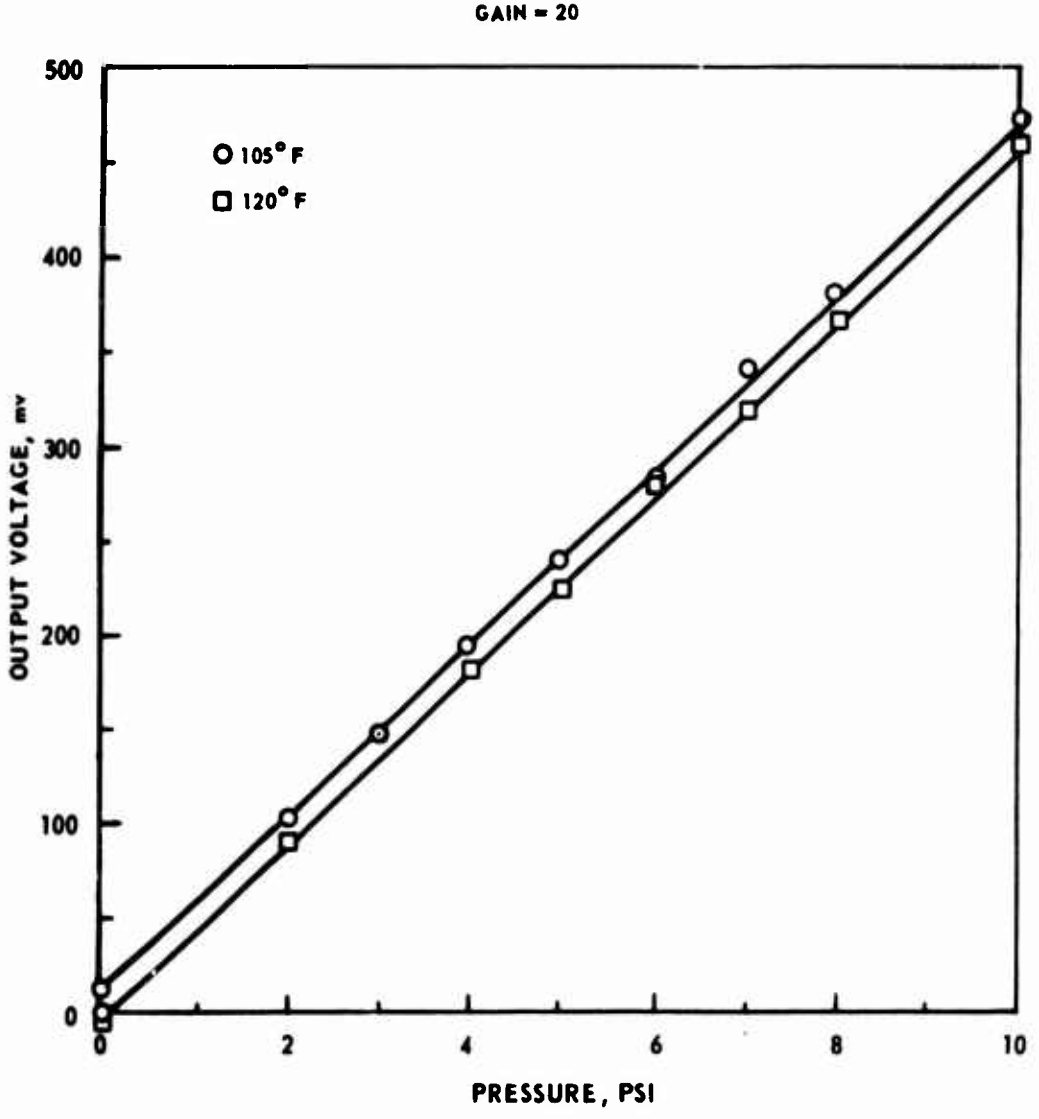

Figure 6. Calibration Curves of Miniature Pressure Transducer.

MINIATURE DIFFERENTIAL PRESSURE TRANSDUCER

TRANSVERSE SECTION VIEW THROUGH LARGE RIB, LOOKING AFT

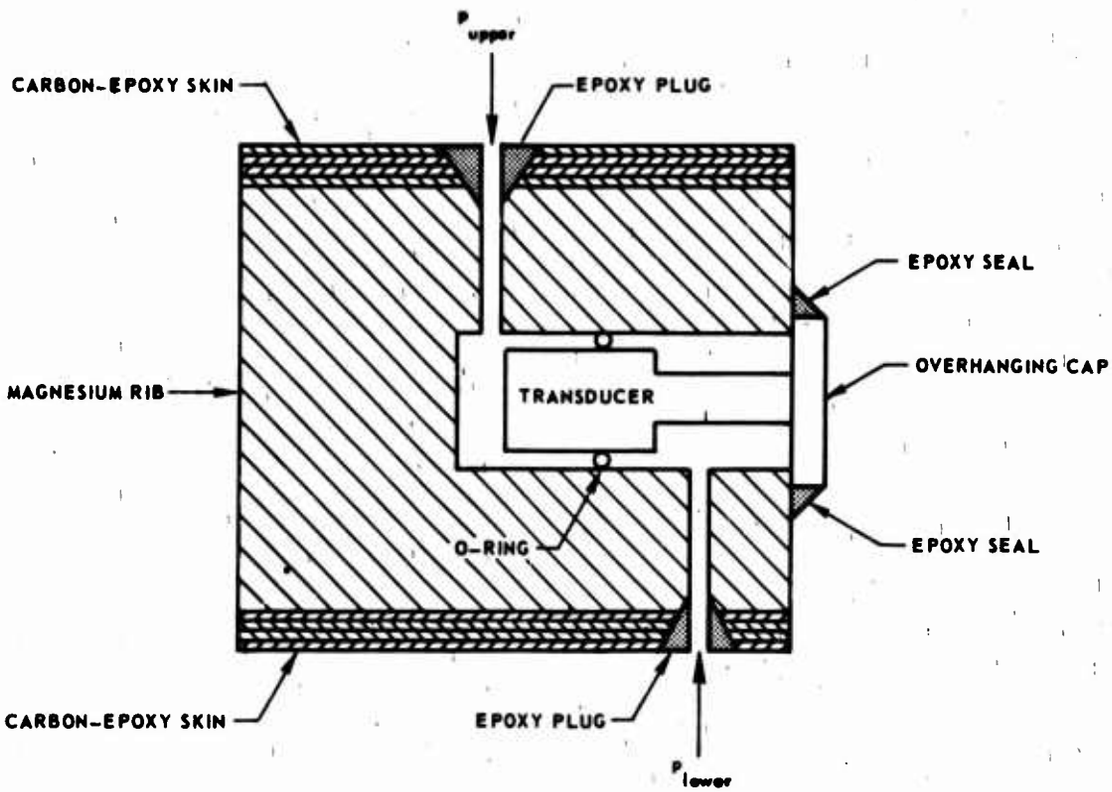

Figure 7. Miniature Pressure Transducer Installation.

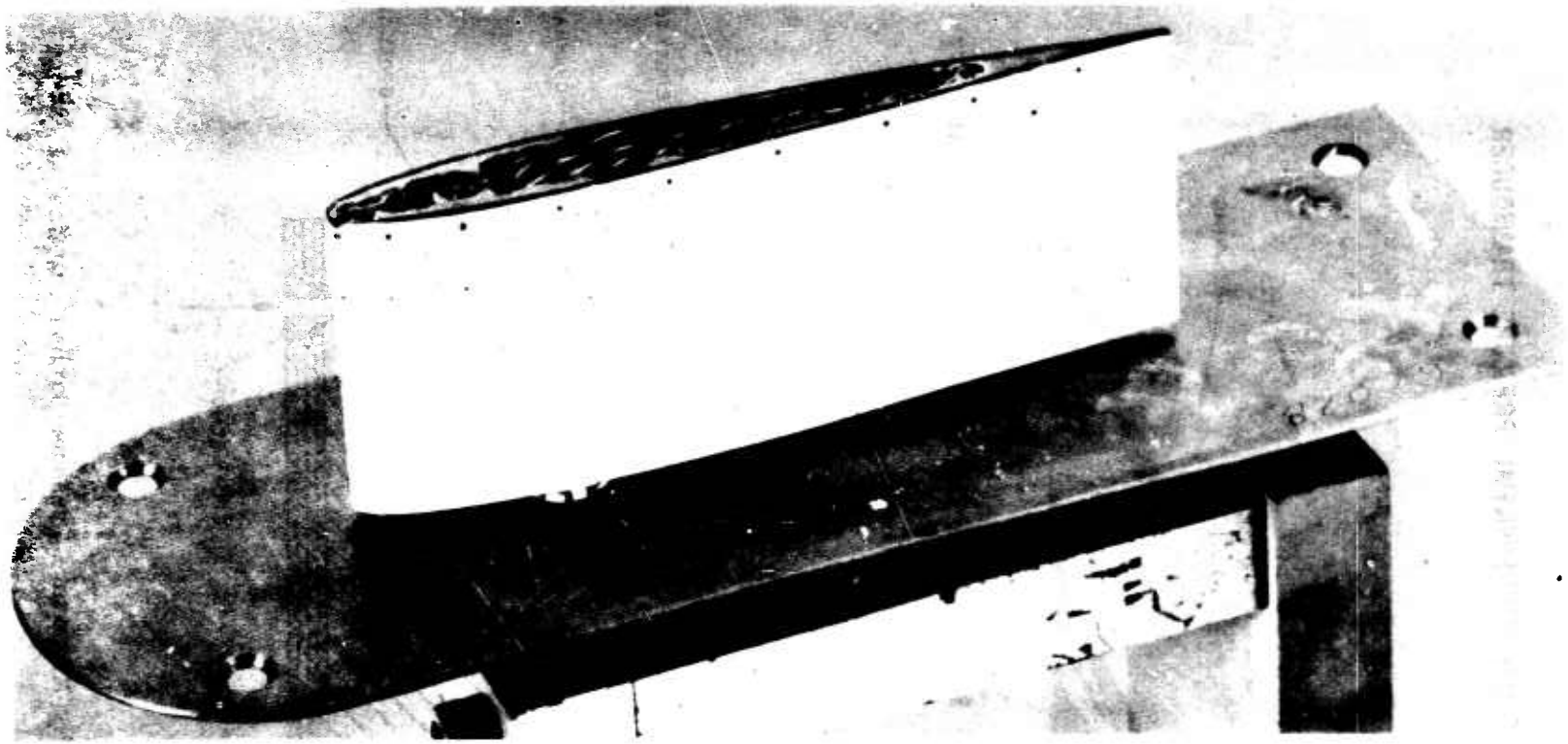

Figure 8. Instrumented Model With End Plate.

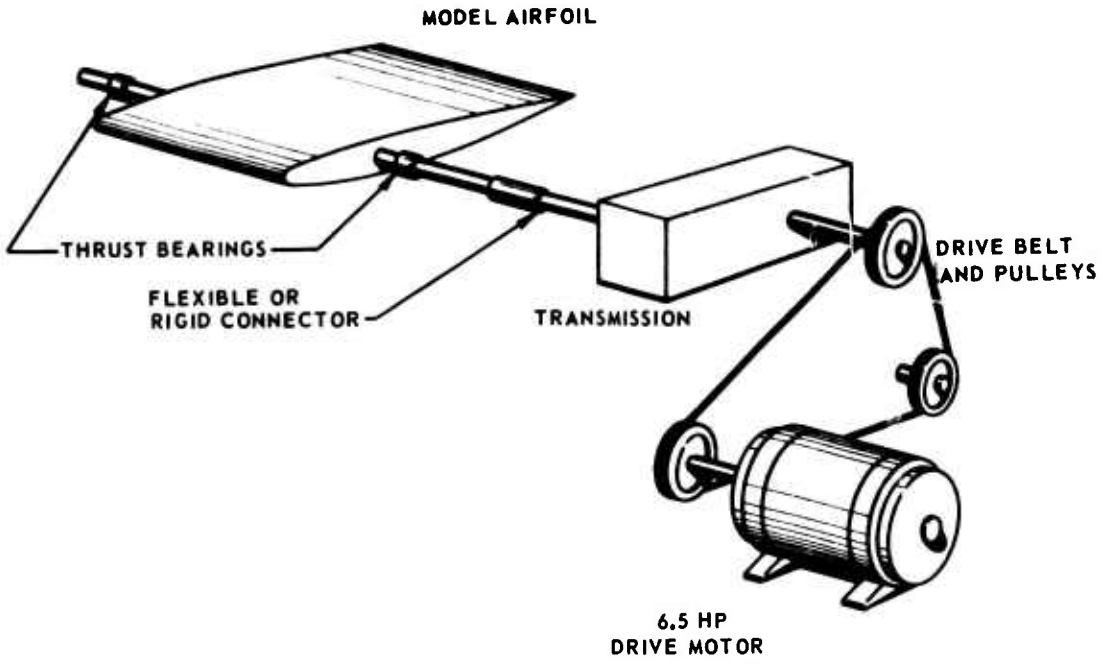

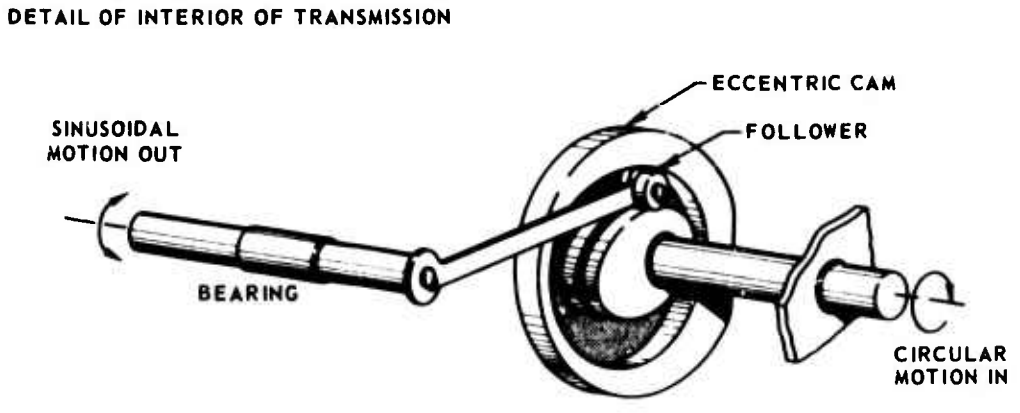

Figure 9. Model Drive System - Schematic.

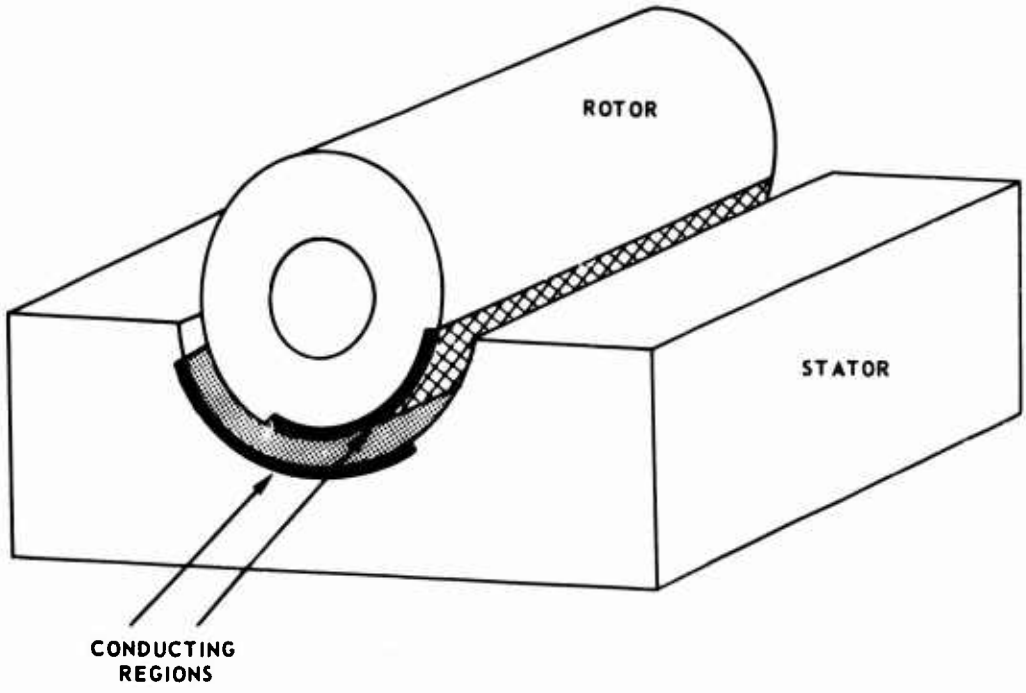

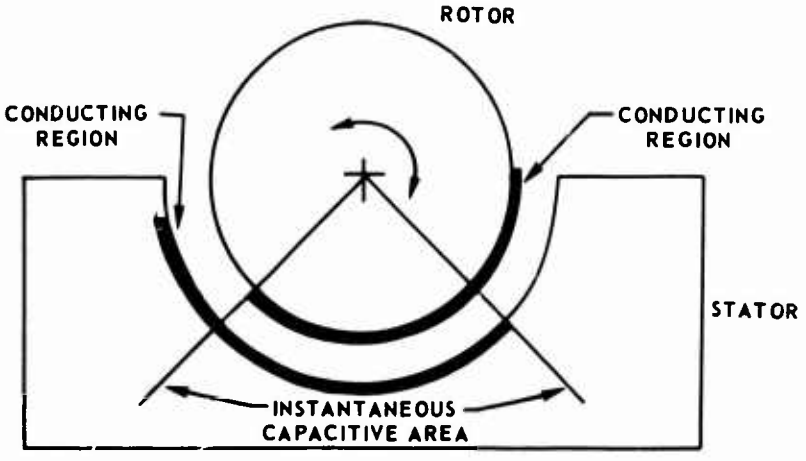

Figure 10. Capacitive Angular Transducer - Schematic.

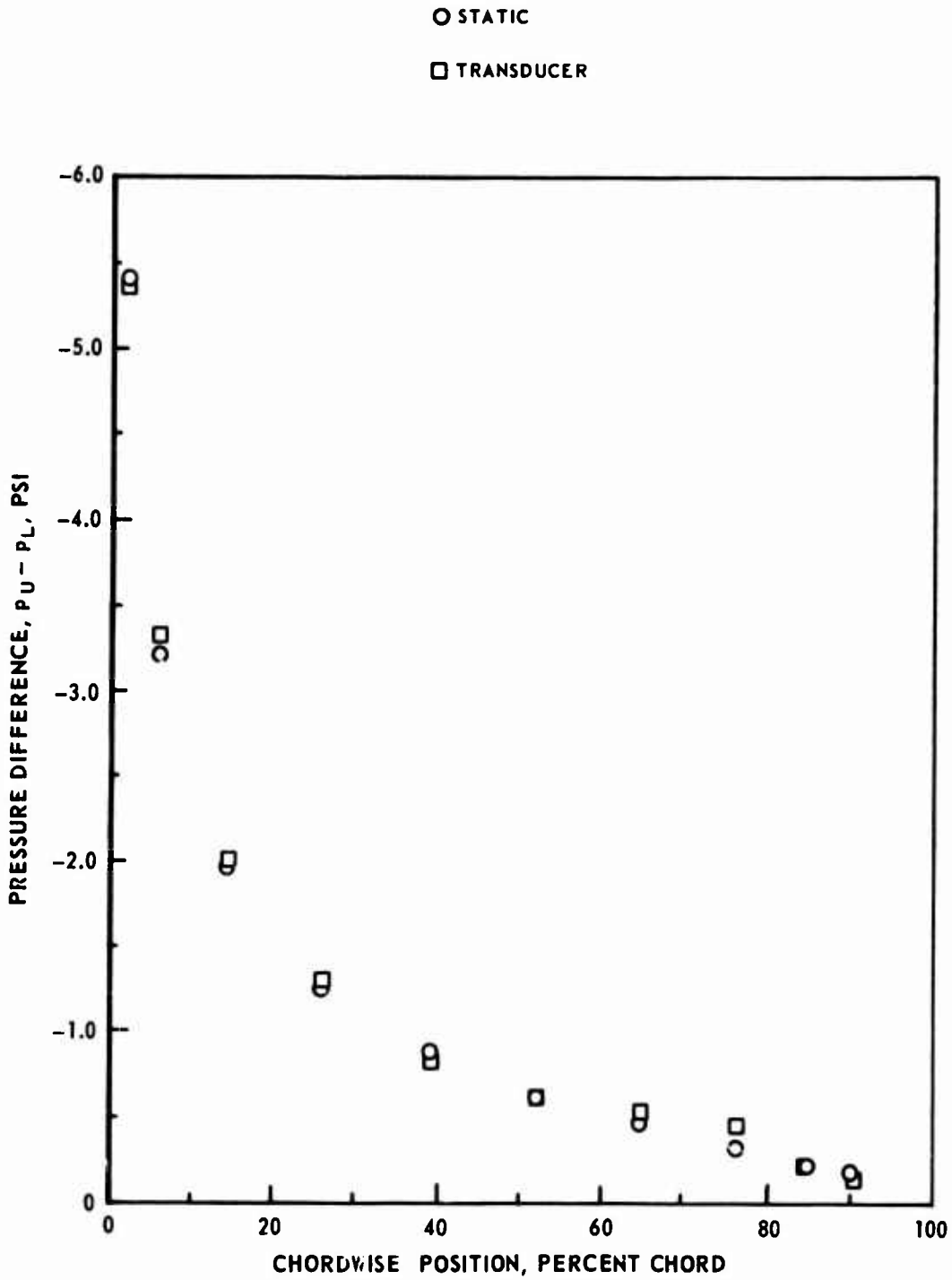

Figure 11. Comparison of Steady-State Pressures Obtained From Static Taps and From Differential Transducers.

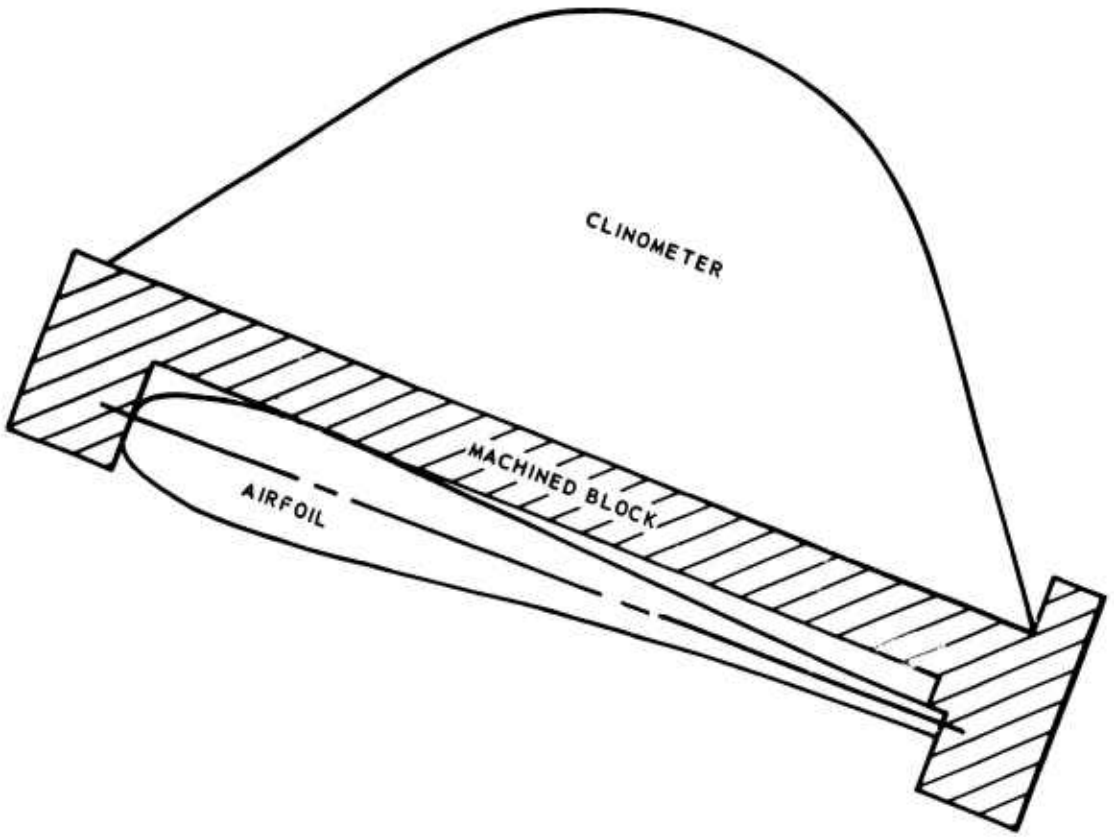

Figure 12. Airfoil With Angular Measuring Device - Schematic.

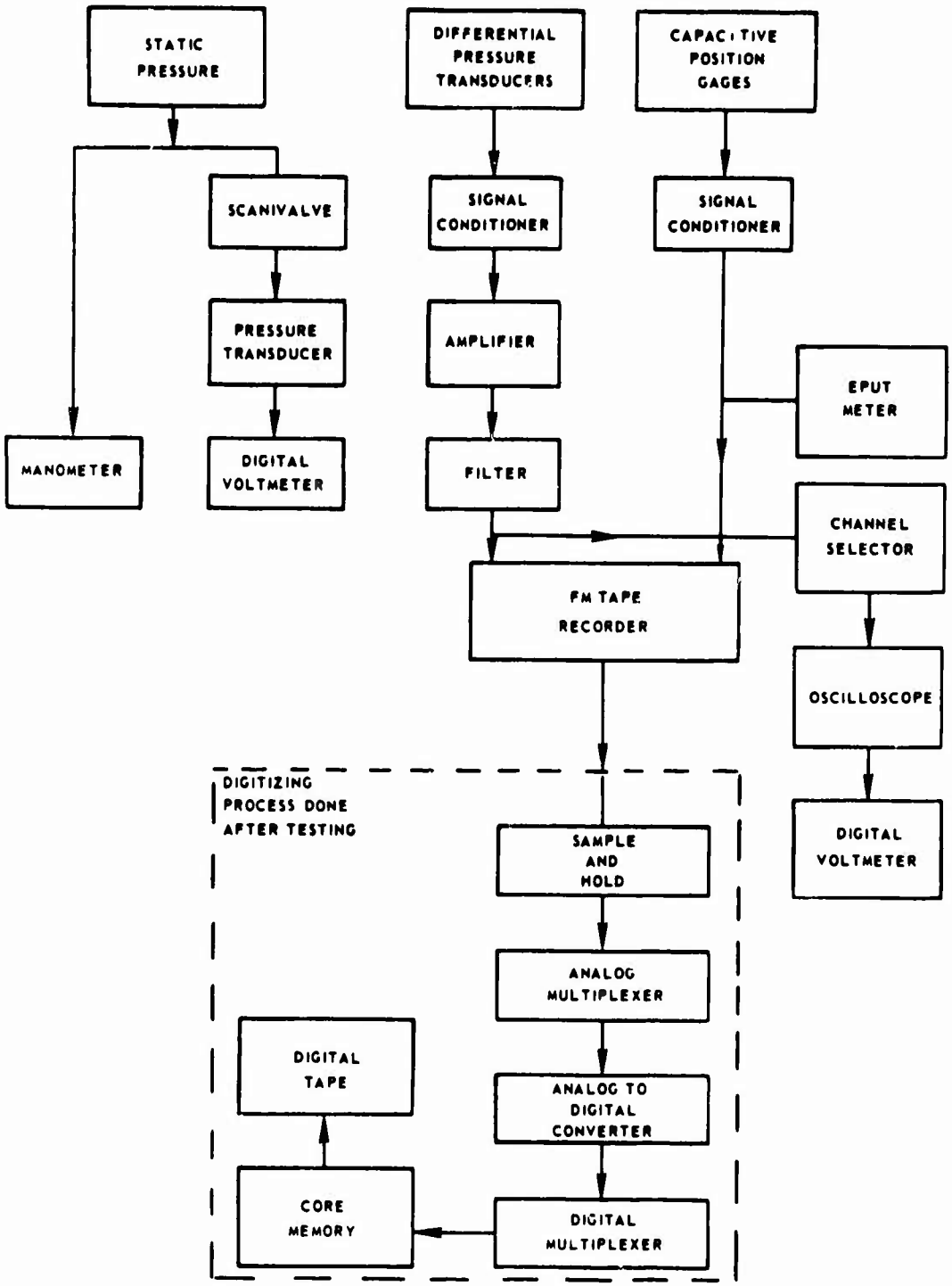

Figure 13. Block Diagram for Data Acquisition.

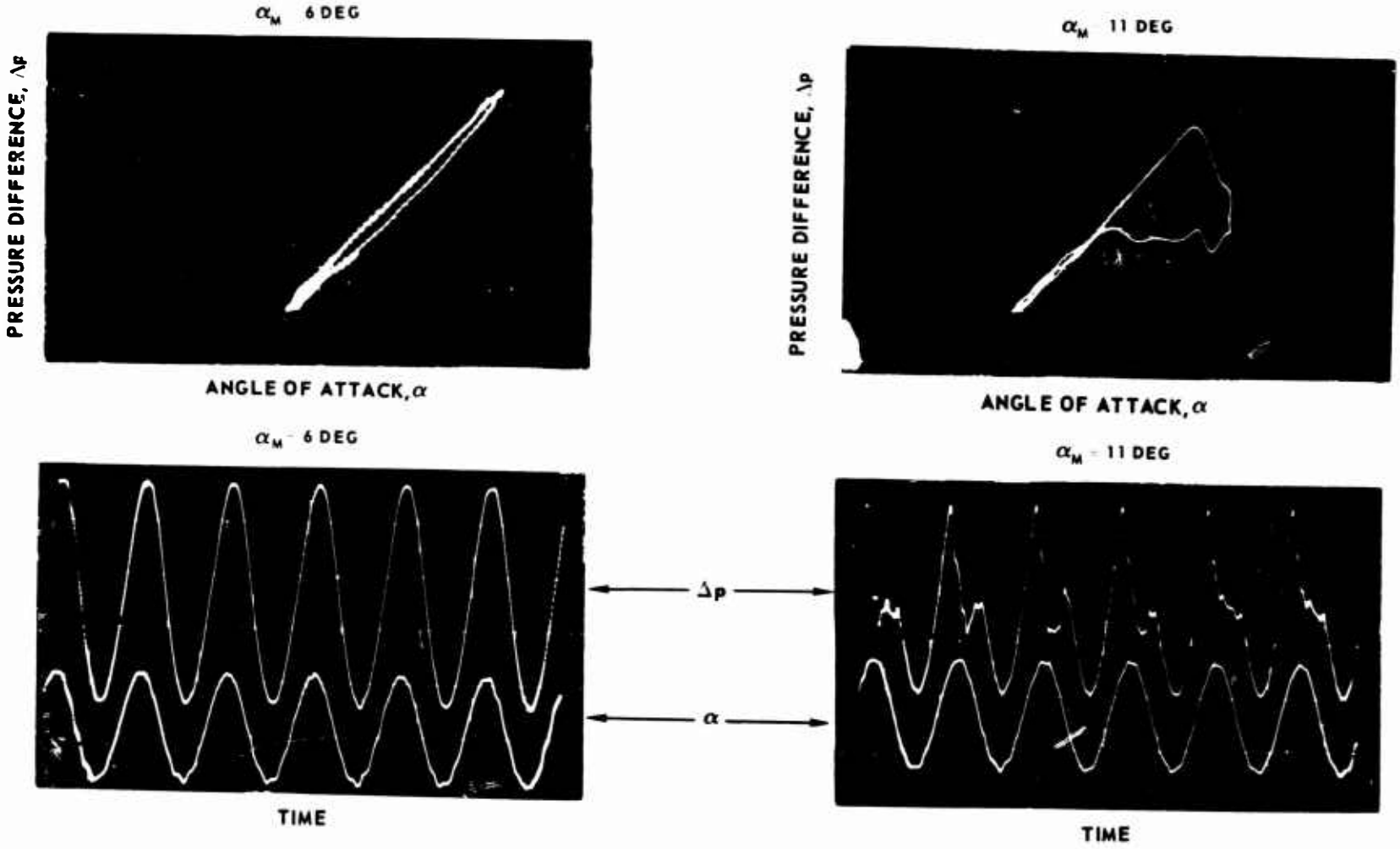

Fig re 14. Sample Oscillograph Traces of Pressure Difference Near Leading Edge vs. Time and vs. Angle of Attack.

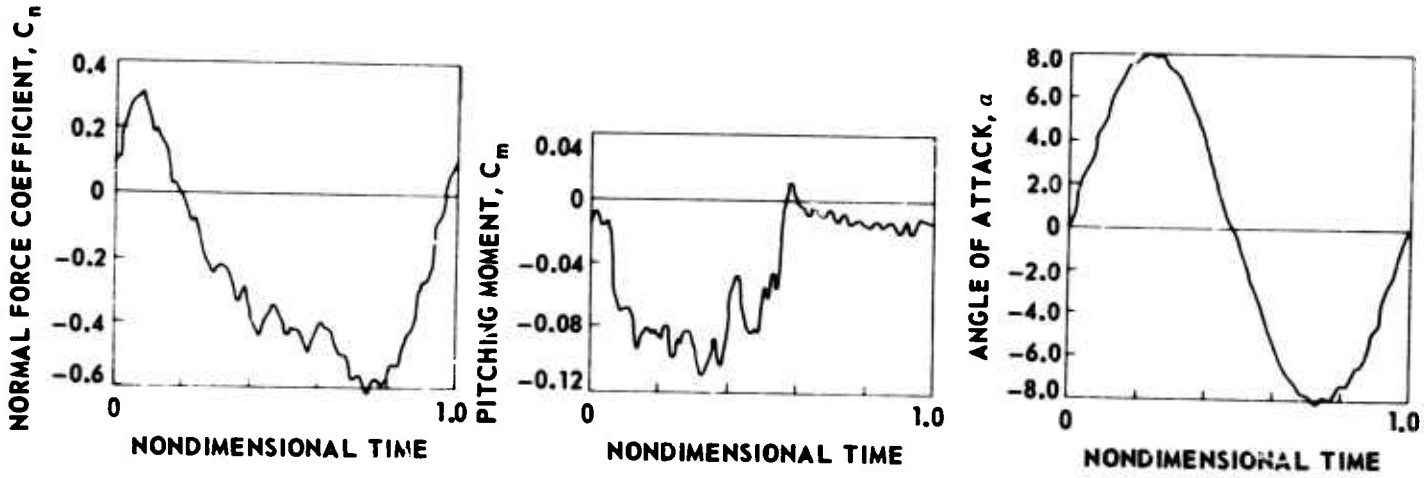

Figure 15. Typical Time History for a Single Cycle in Separated Flow.

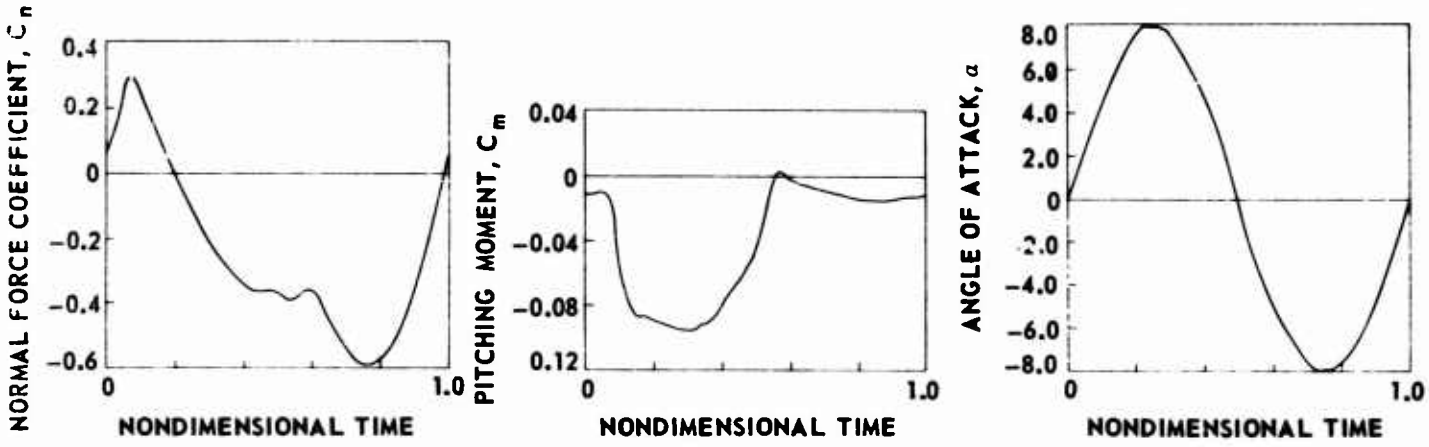

Figure 16. Typical Signal-Averaged Time History in Separated Flow.

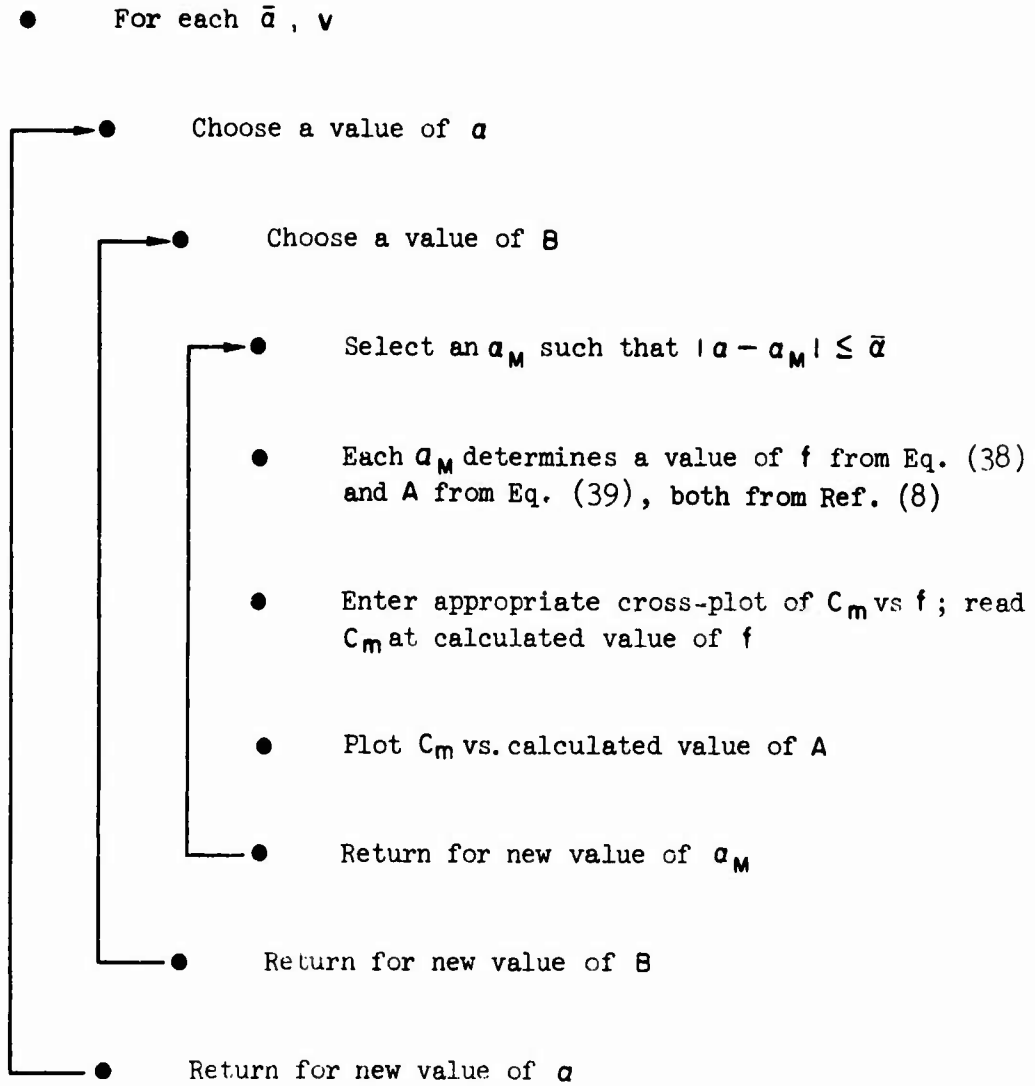

Figure 17. Flow Chart for Data Conversion to α, A, B Form.

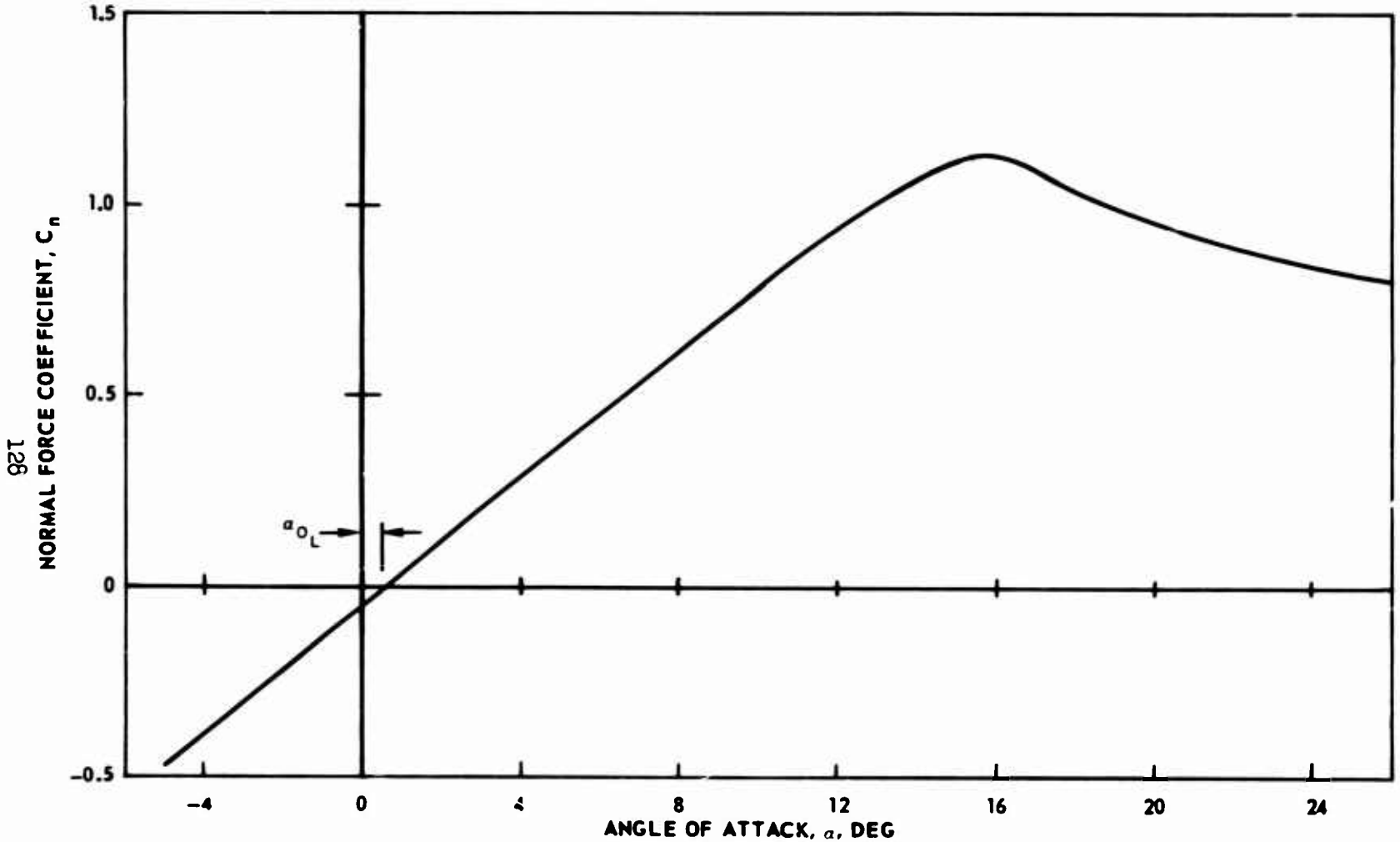

Figure 18. Steady-State Normal Force vs. Angle of Attack.

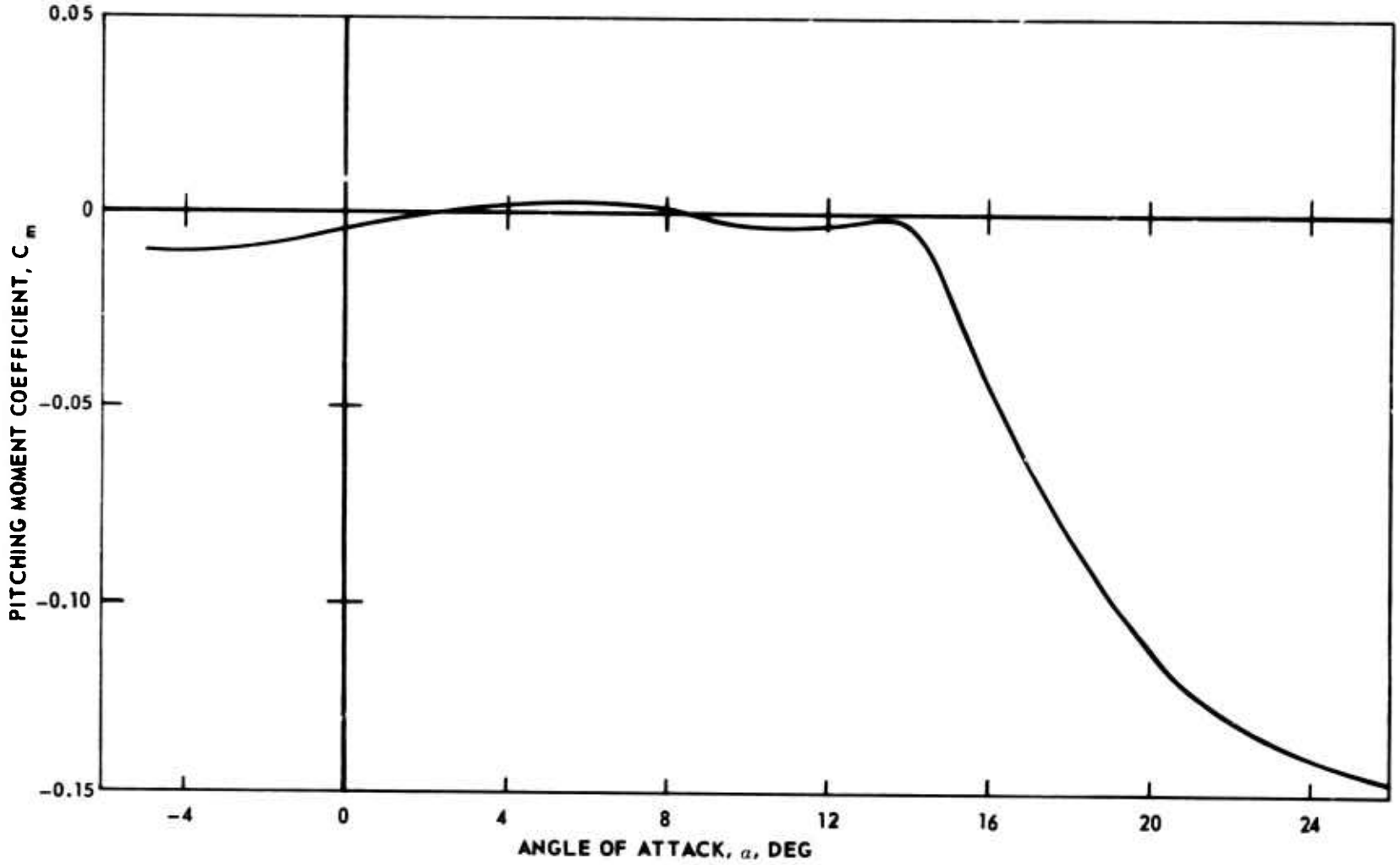

Figure 19. Steady-State Pitching Moment About Quarter Chord vs. Angle of Attack.

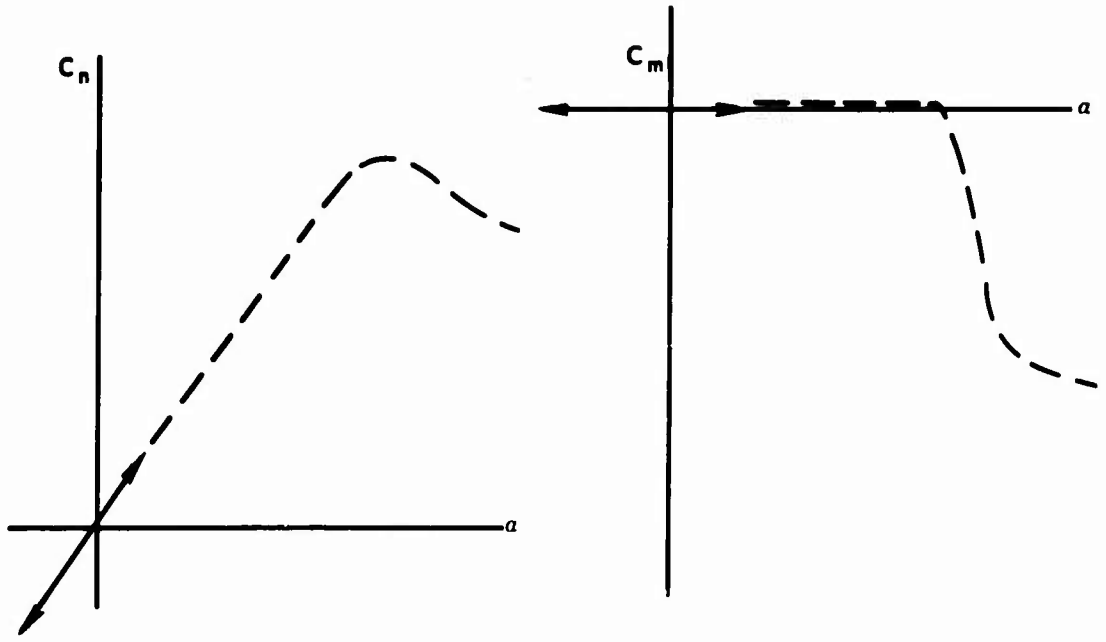

a) QUASI-STEADY MOTION

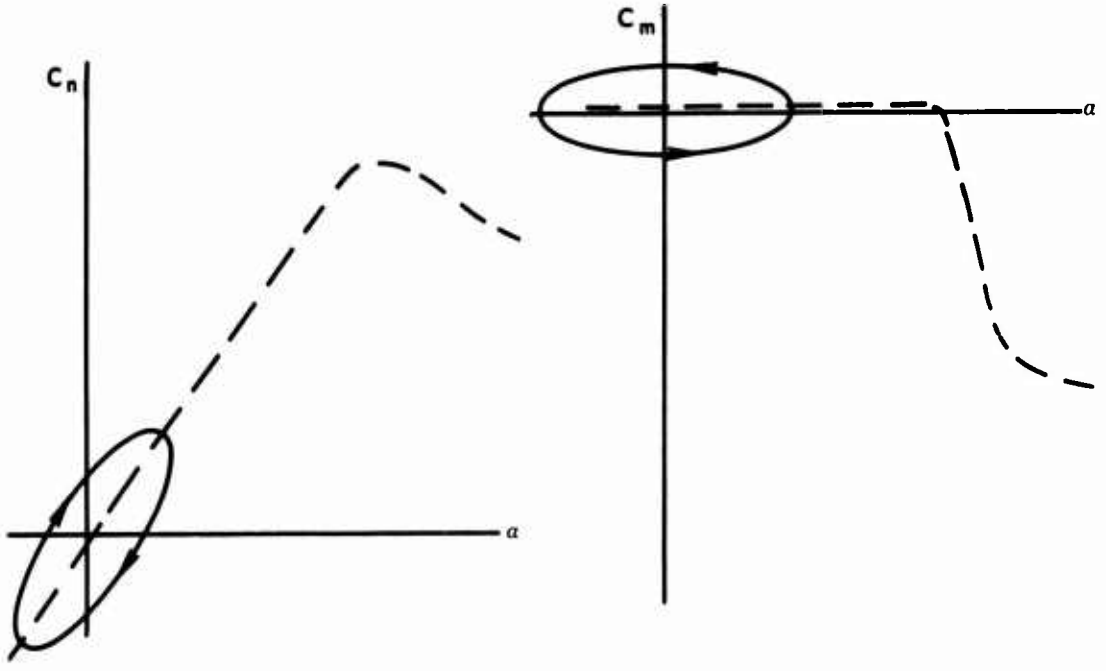

b) UNSTEADY POTENTIAL FLOW CONDITION

Figure 20. Schematic of Steady and Unsteady Normal Force and Moment Coefficients for Various Flow and Frequency Conditions.

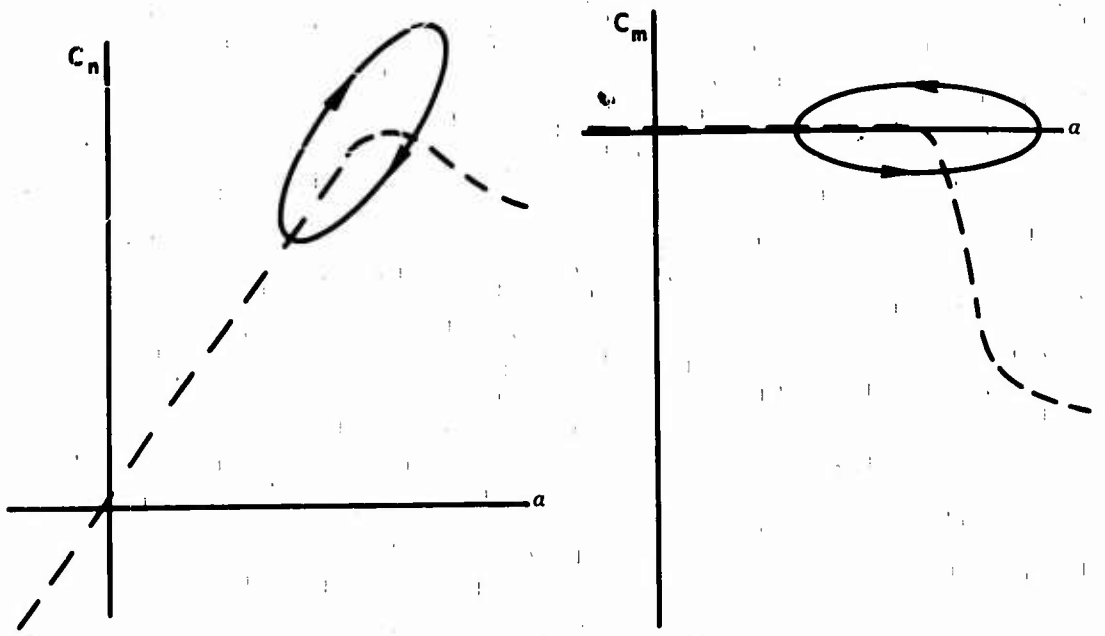

c) UNSTEADY HIGH ANGLE OF ATTACK WITHOUT DYNAMIC STALL

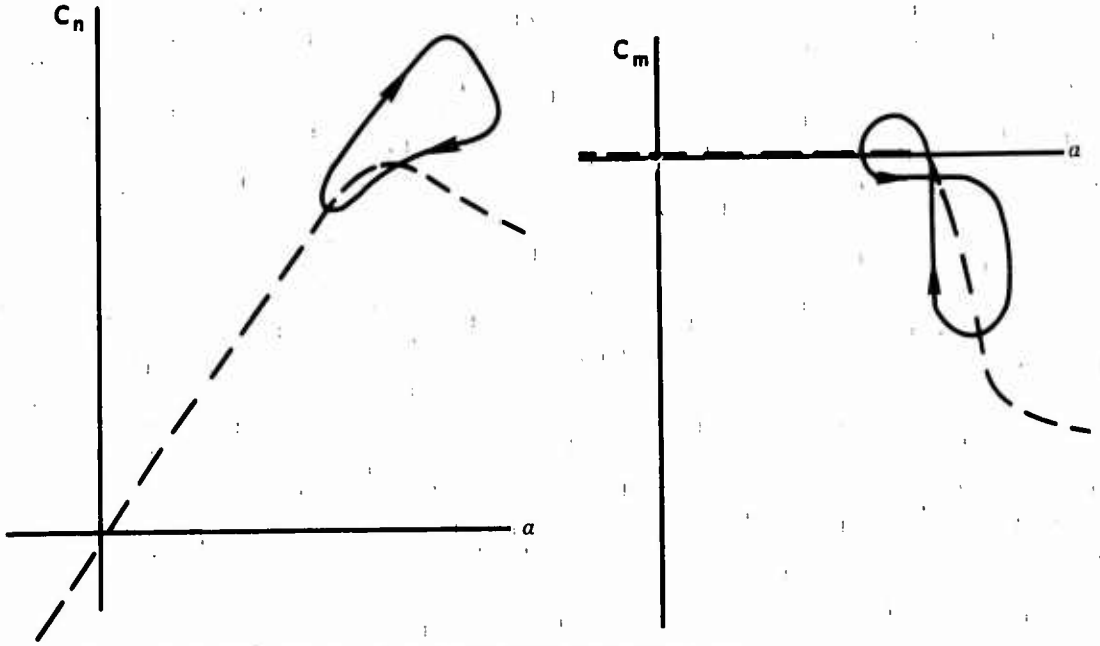

d) UNSTEADY HIGH ANGLE OF ATTACK WITH DYNAMIC STALL

Figure 20 - Continued.

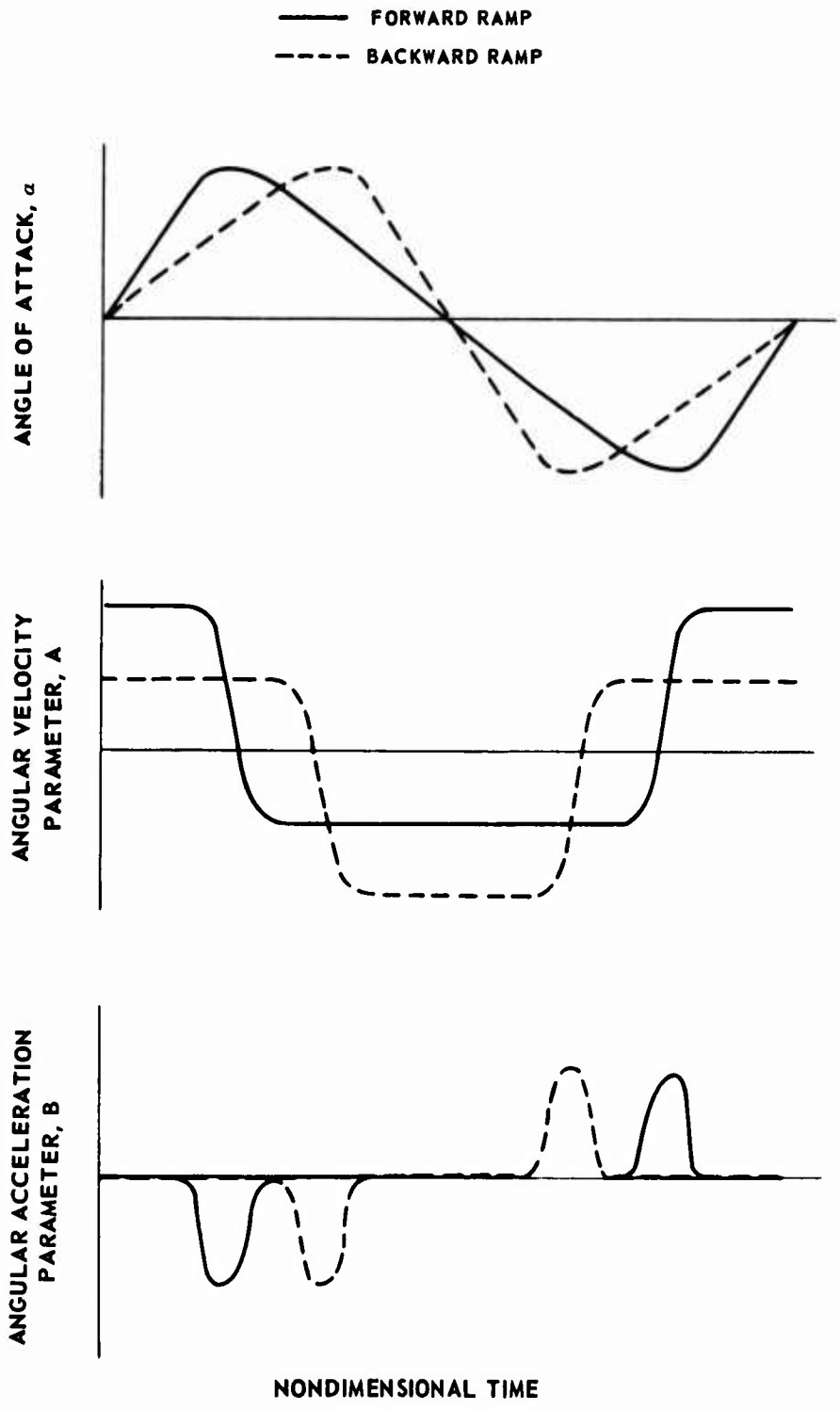

Figure 21. Variation of Angle of Attack, Angular Velocity Parameter, and Angular Acceleration Parameter With Time for Typical Ramp Motion.

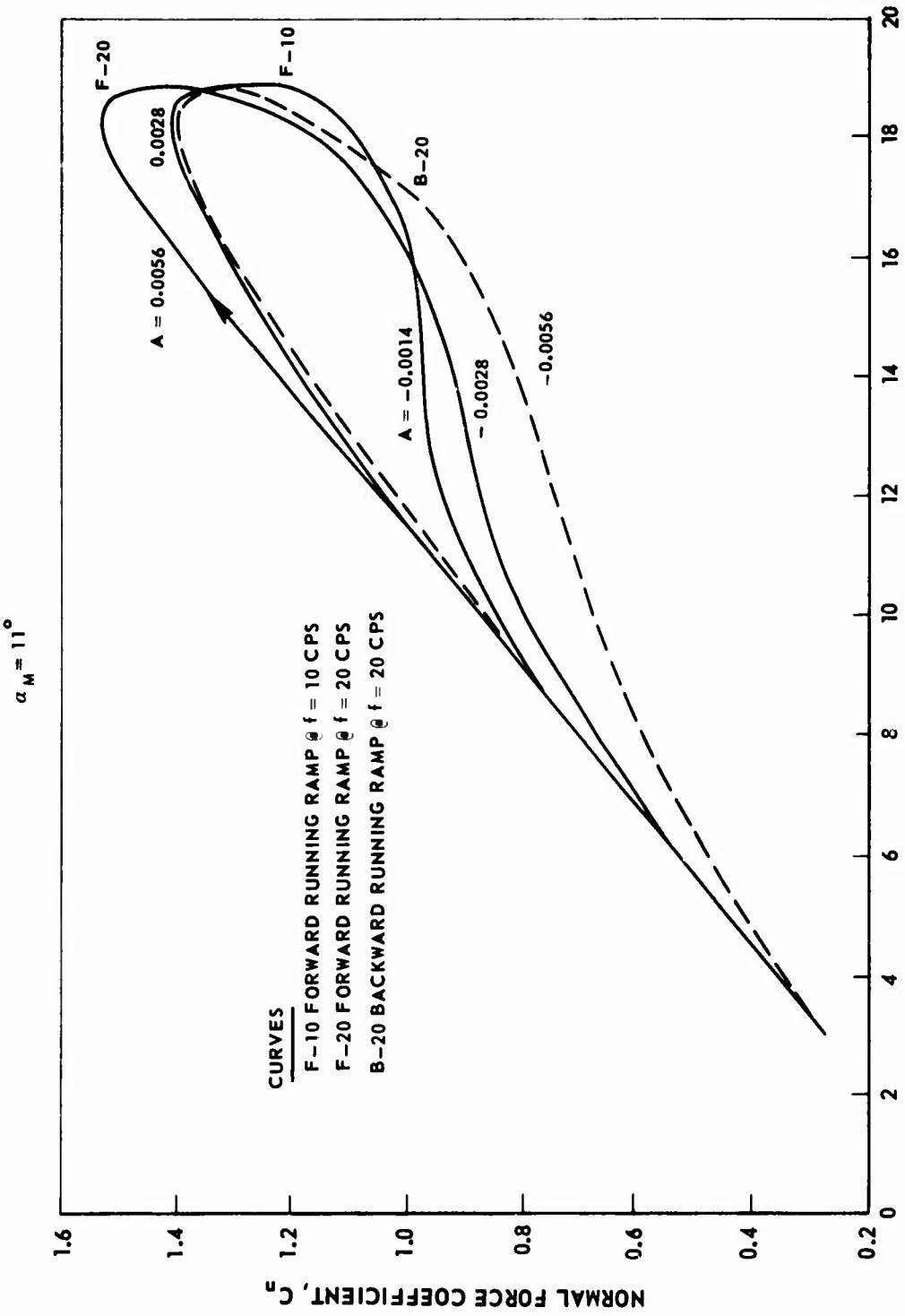

Figure 22. Normal Force Loops for Various Ramp Motions.

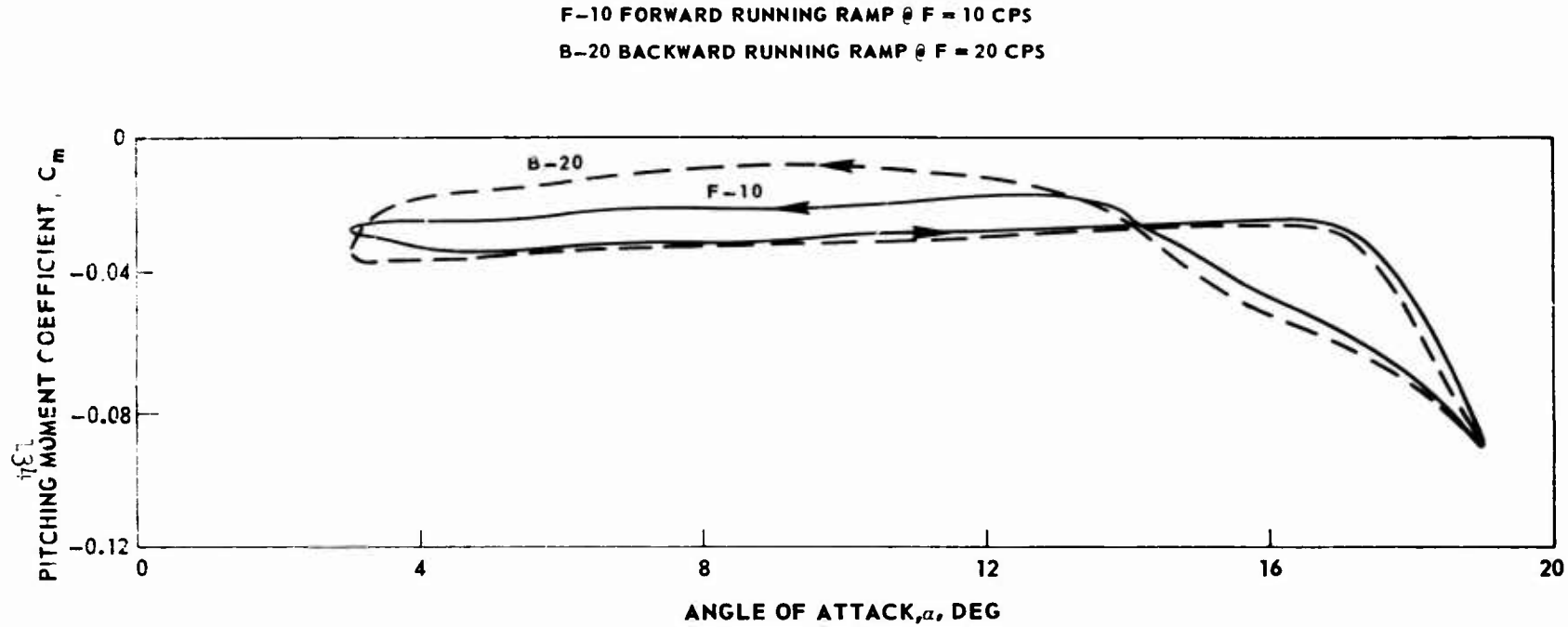

Figure 23. Moment Loops for Various Ramp Motions.

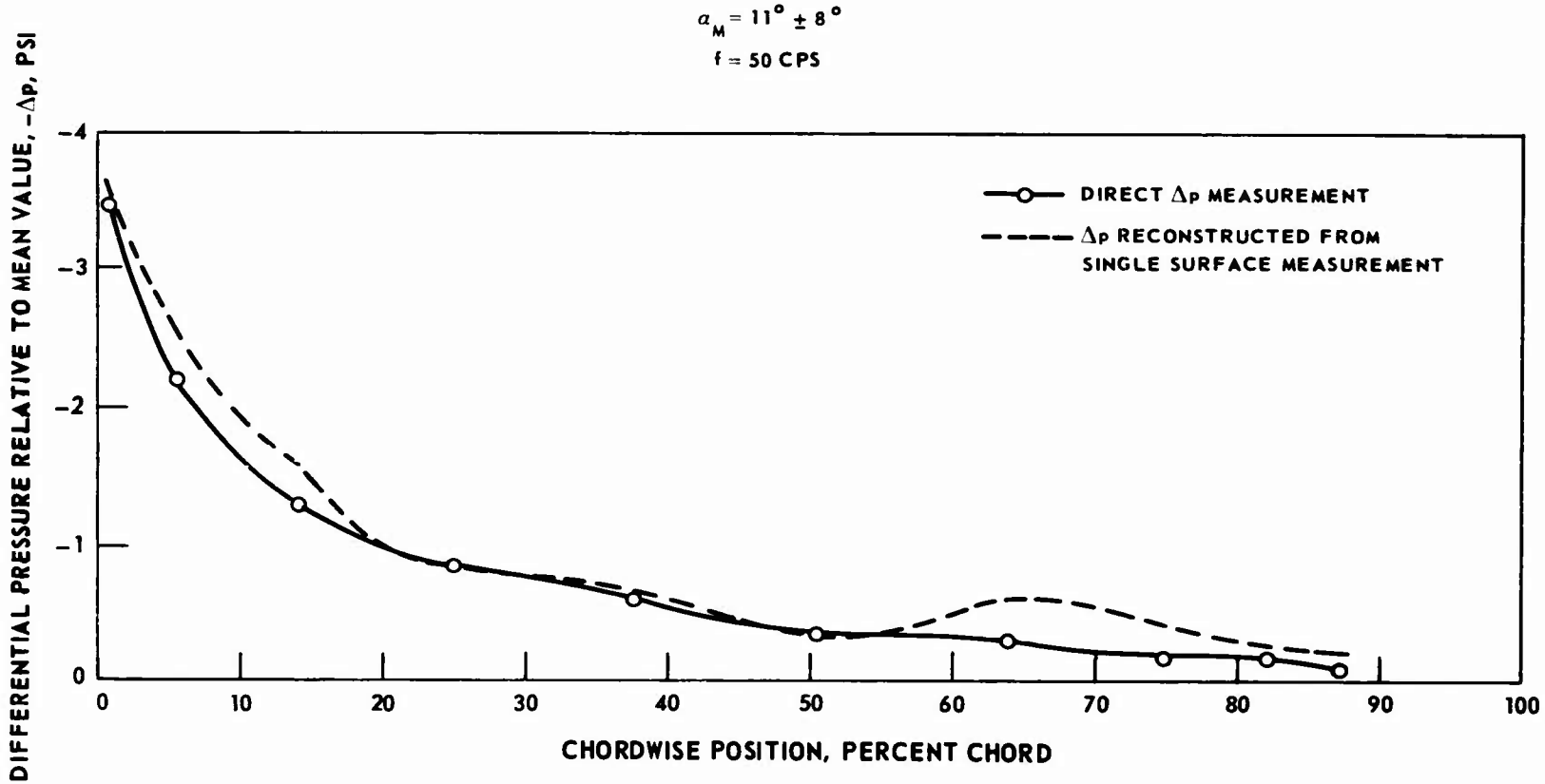

Figure 24. Oscillatory Chordwise Pressure Difference Distribution at α = 3 Degrees During a Sinusoidal Oscillation.

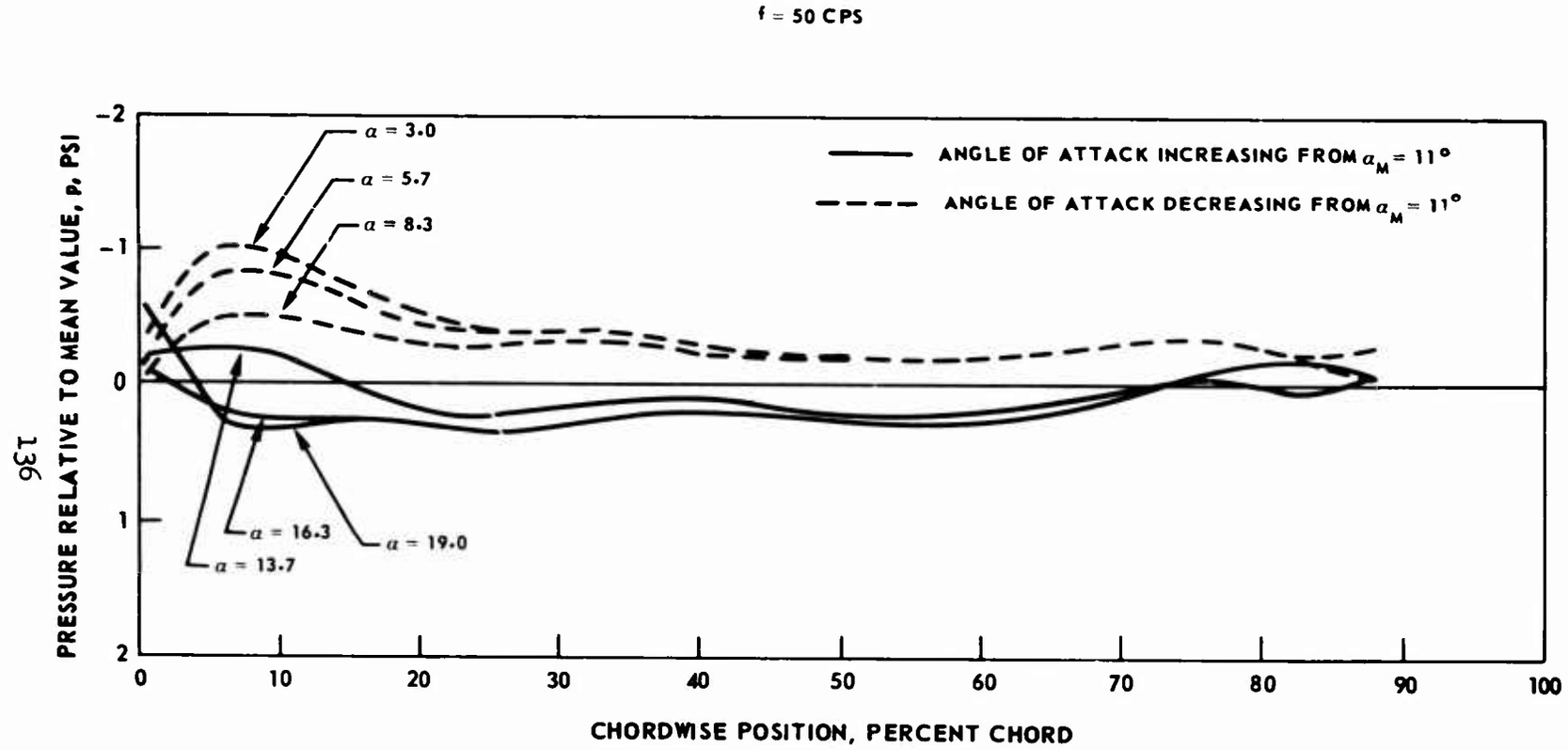

Figure 25. Instantaneous Chordwise Pressure Distribution on Pressure Surface During a Sinusoidal Oscillation.

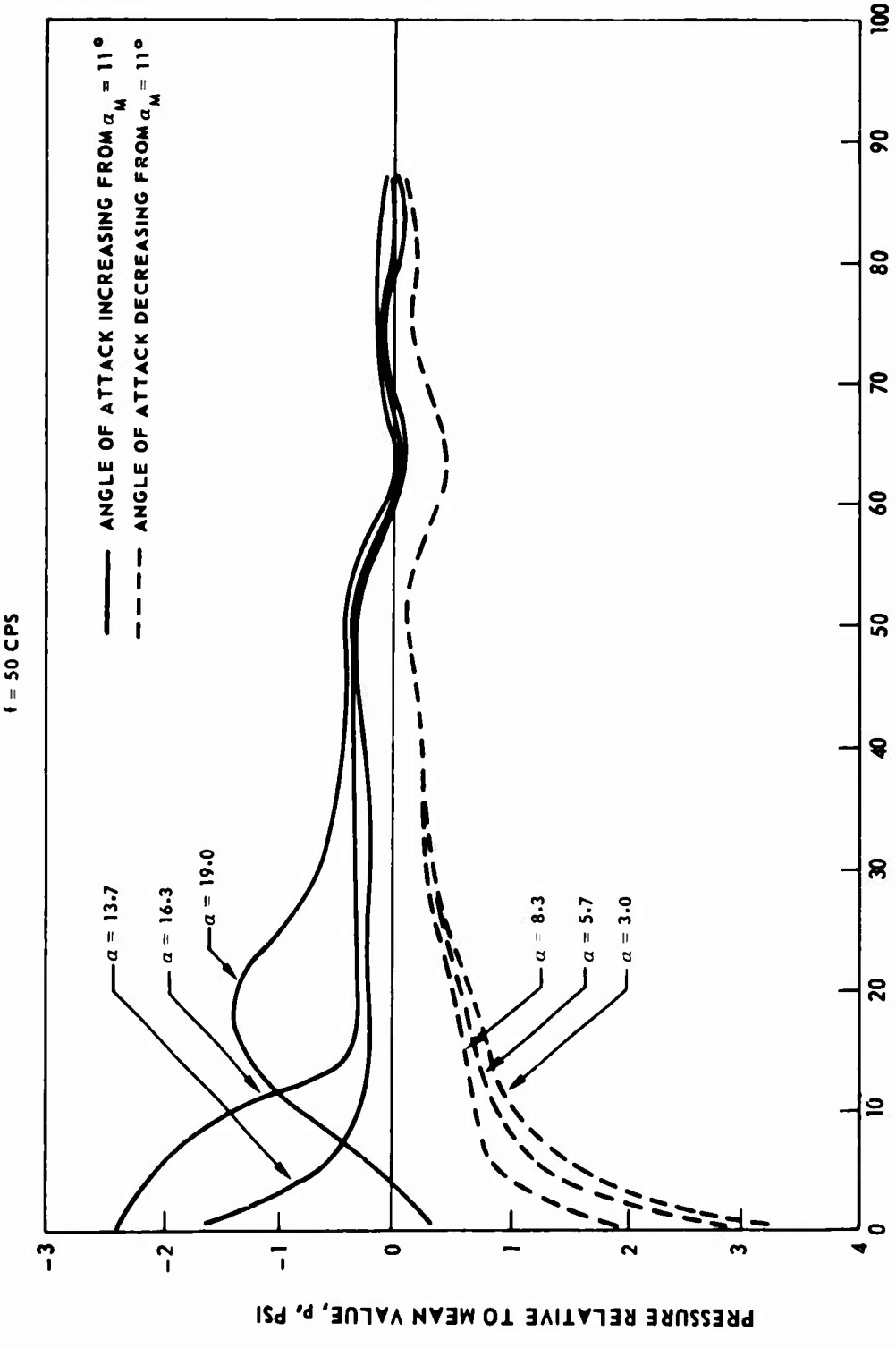

Figure 26. Instantaneous Chordwise Pressure Distribution on Suction Surface During a Sinusoidal Oscillation.

CURVE	MOTION
a	1P SINUSOID, ± 8°, HIGH ASPECT RATIO
b	1P SINUSOID, ±8°, LOW ASPECT RATIO
c	8P SINUSOID, ±4°, (STALL FLUTTER)
d	1P "RAMP" TYPE NONSINUSOIDAL, MAX FREQUENCY

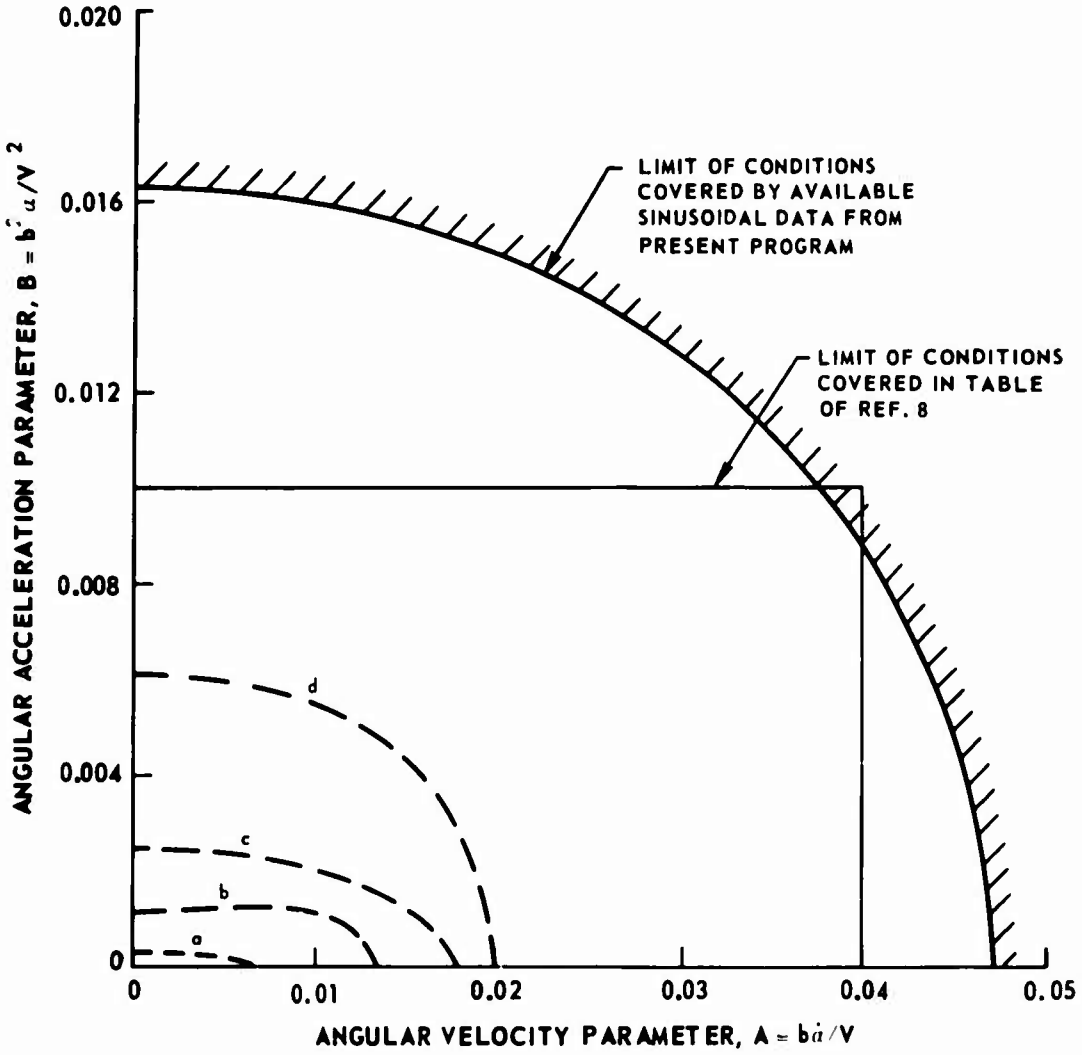

Figure 27. A-B Tabulation Limits Compared With Values for Various Motions.

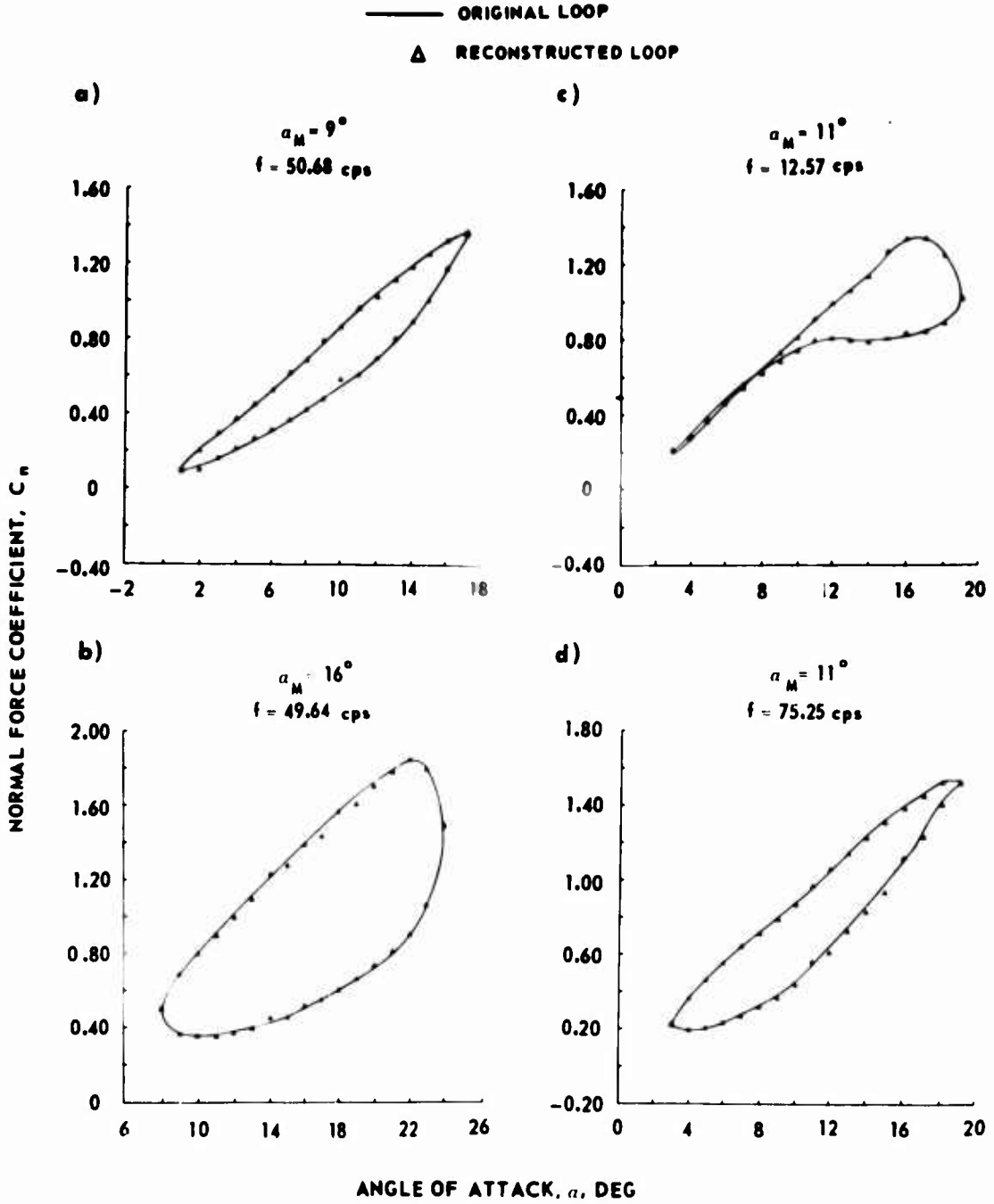

Figure 28. Comparison of Original and Reconstructed Normal Force Hysteresis Loops for Sirusoidal Motion at Various Frequencies and Mean Angles of Attack for $\bar{\alpha} = \pm 8$ Degrees.

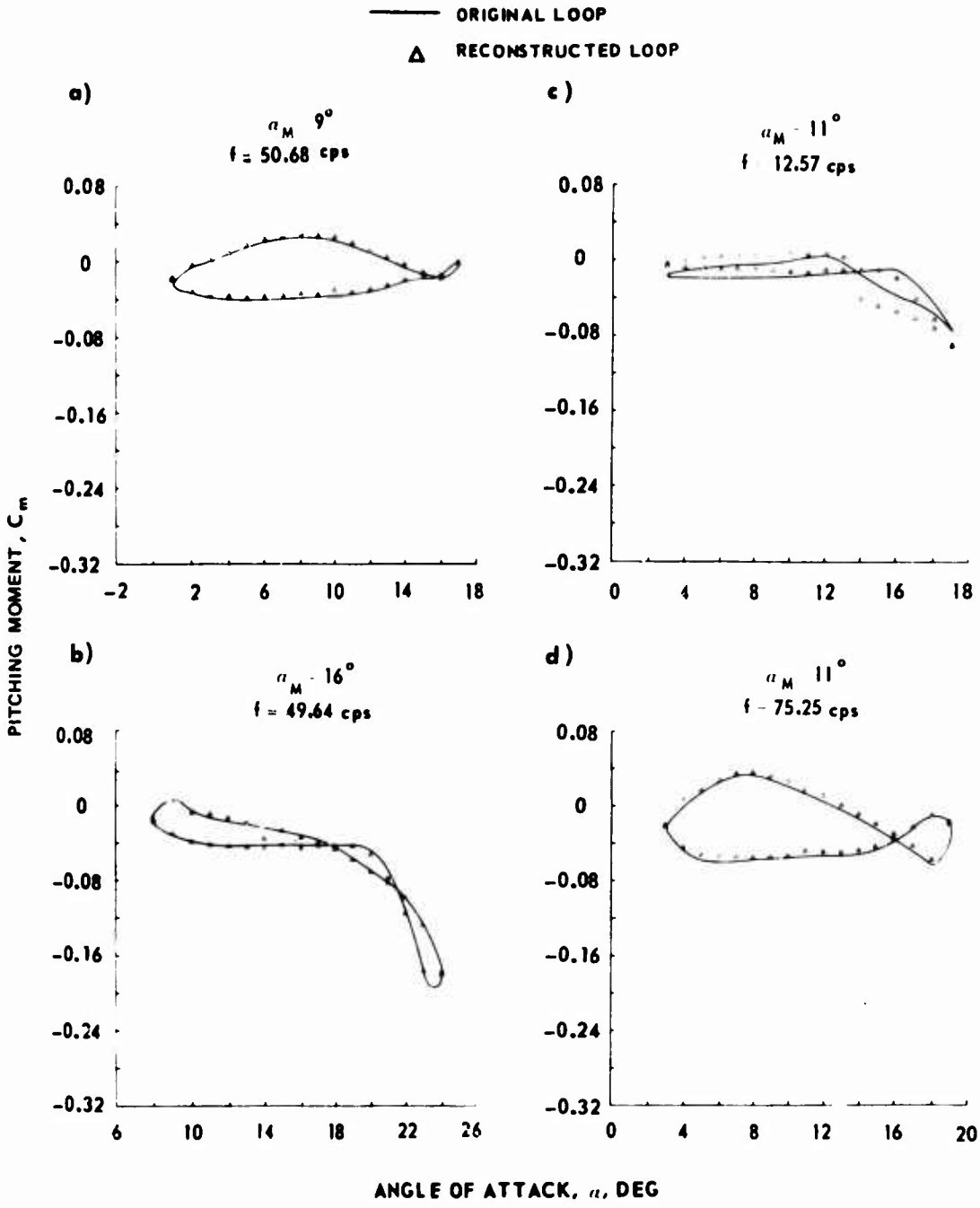

Figure 29. Comparison of Original and Reconstructed Pitching Moment Hysteresis Loops for Sinusoidal Motion at Various Frequencies and Mean Angles of Attack for $\bar{\alpha} = \pm 8$ Degrees.

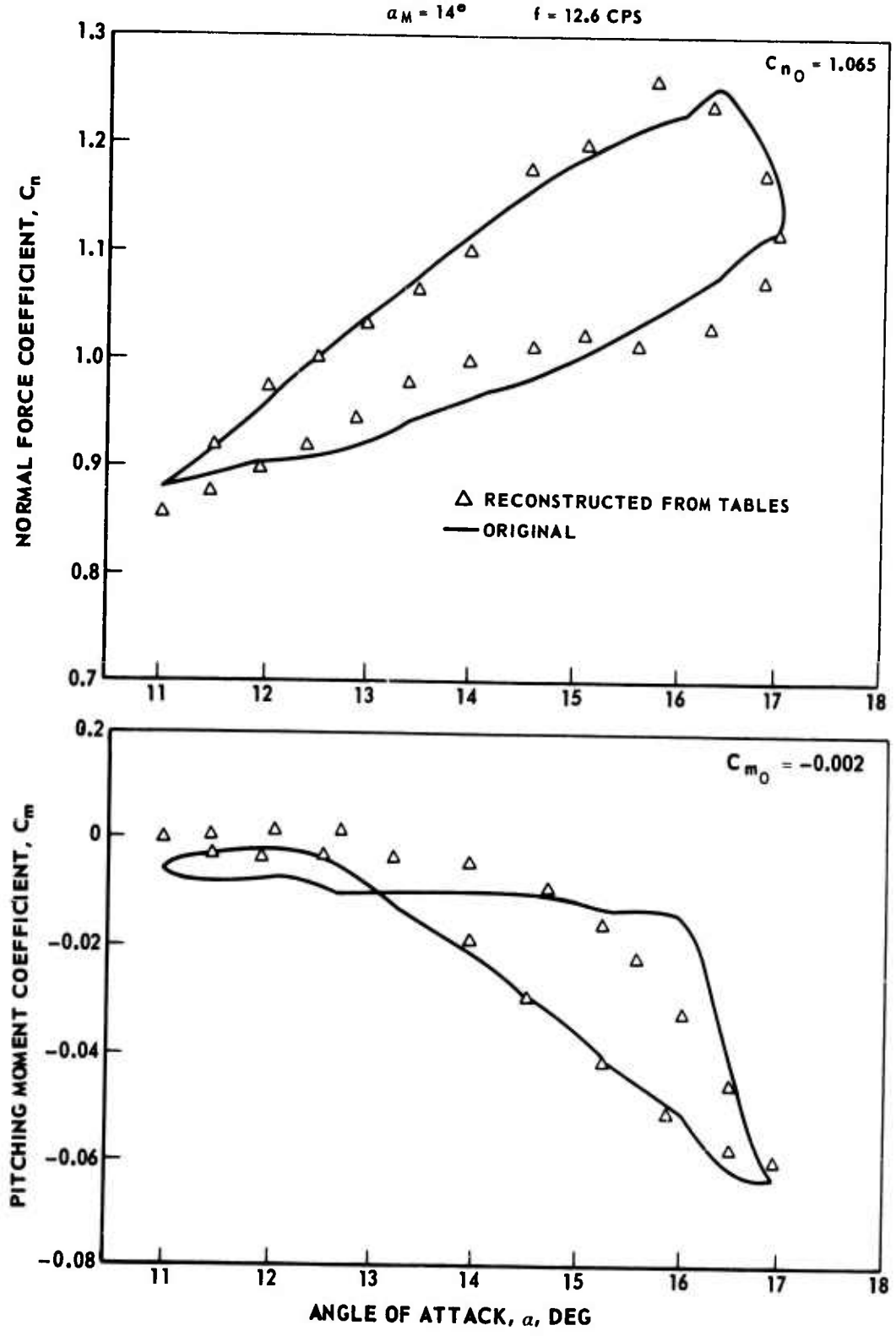

Figure 30. Comparison of Original and Reconstructed Normal Force and Pitching Moment Hysteresis Loops for ±3 Degrees Sinusoidal Motion.

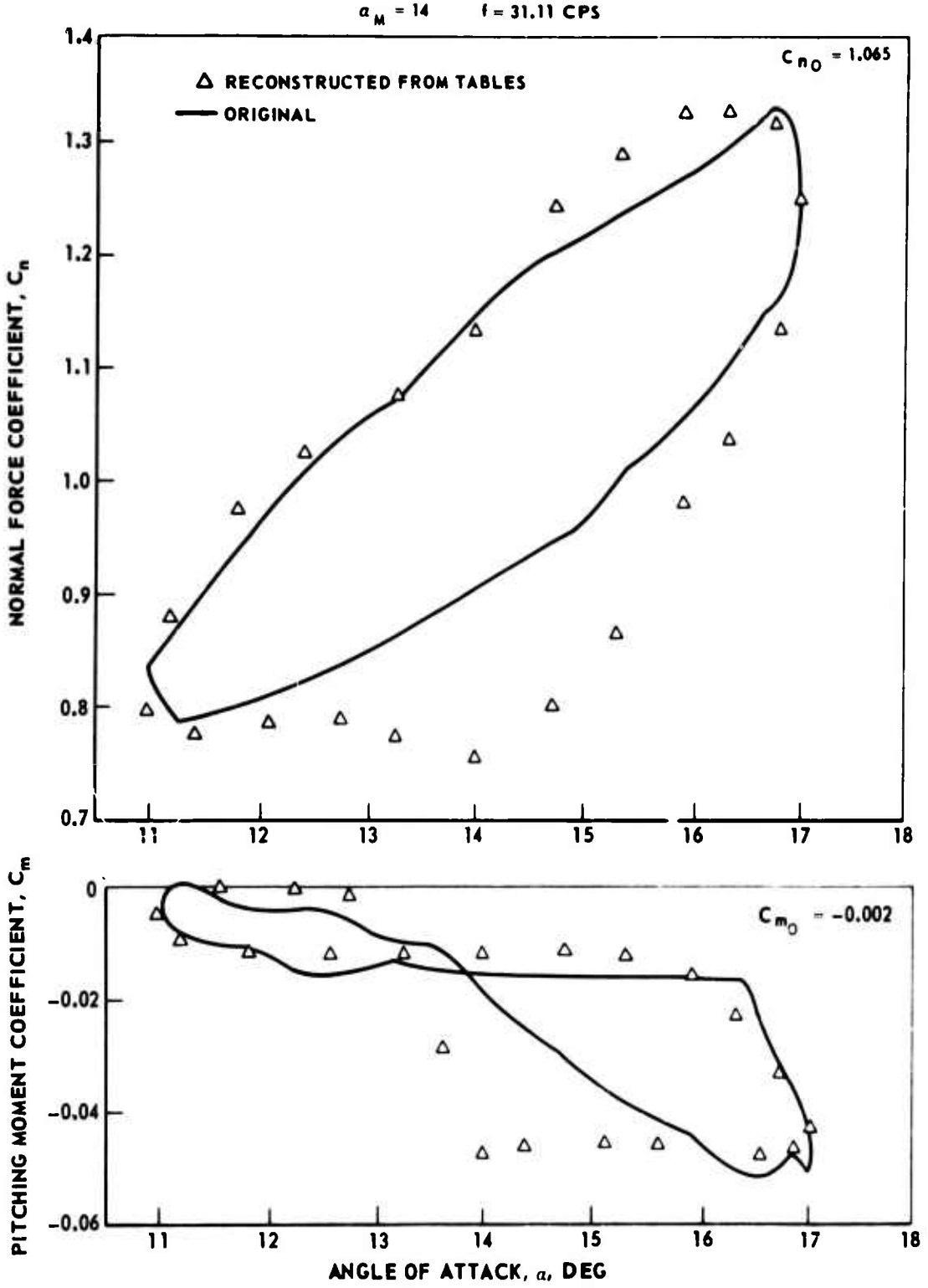

Figure 31. Comparison of Original and Reconstructed Normal Force and Pitching Moment Hysteresis Loops for ±3 Degrees Sinusoidal Motion.

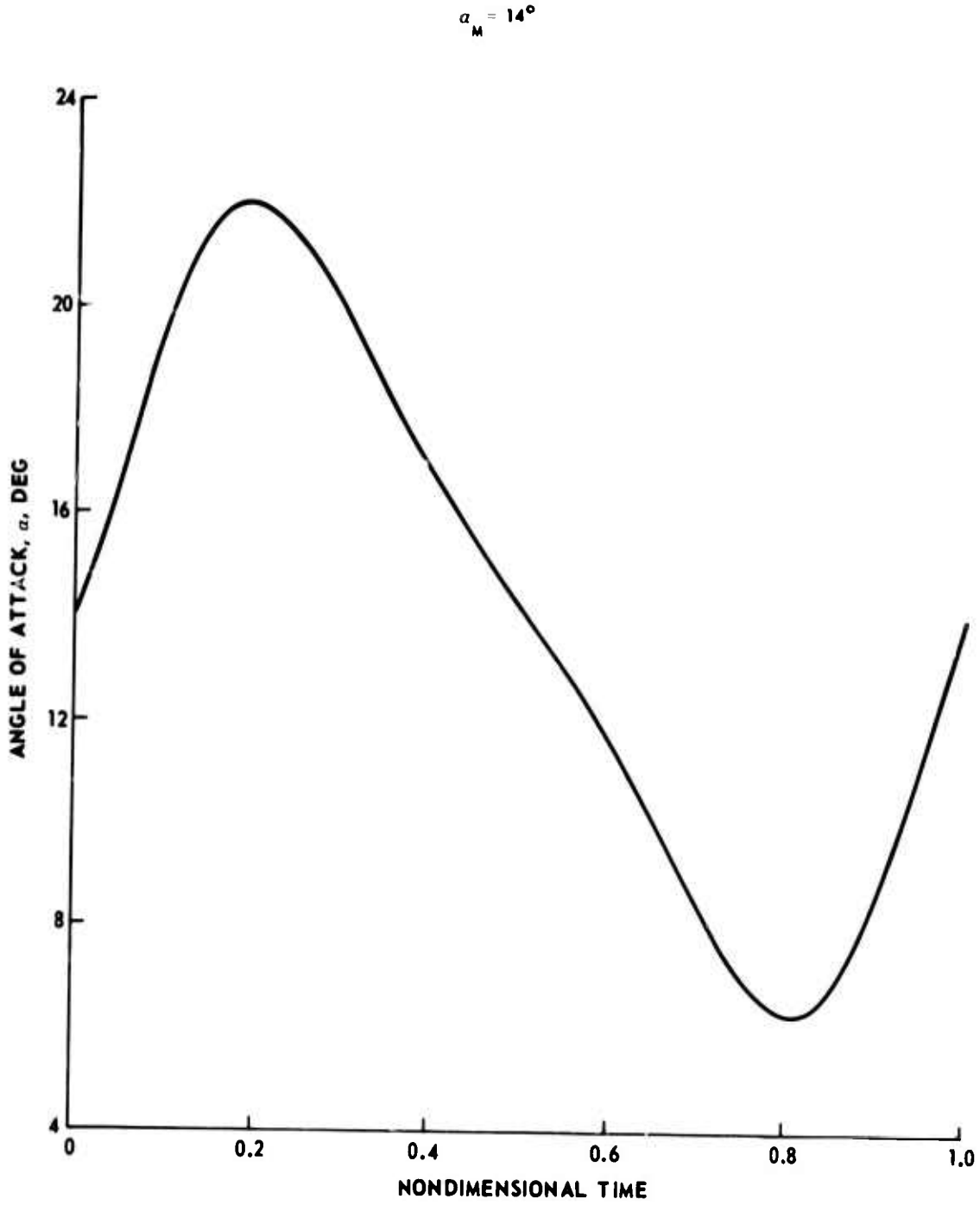

Figure 32. Angle of Attack vs. Nondimensional Time for Forward Ramp Motion.

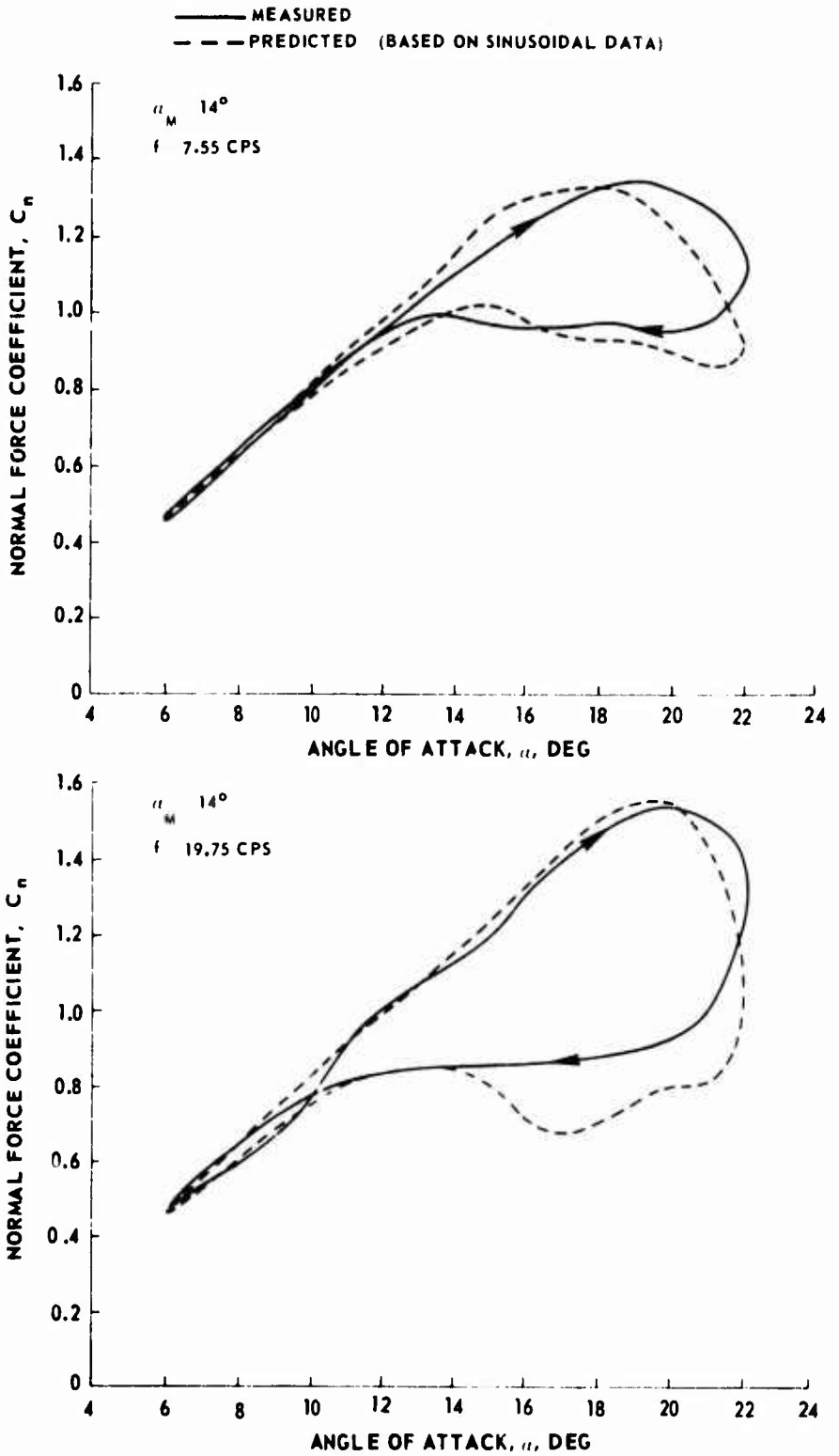

Figure 33. Normal Force for Forward Ramp Motion.

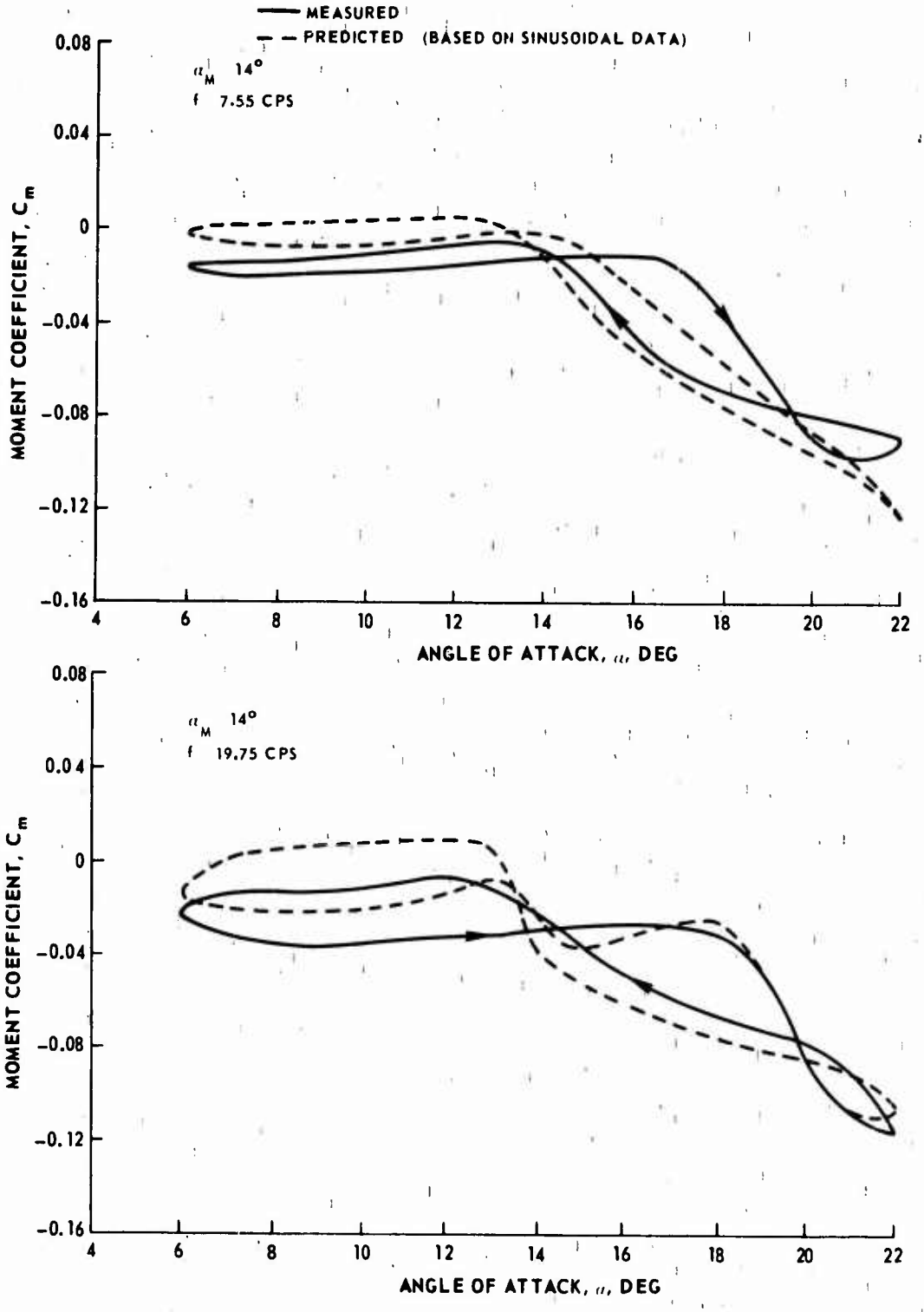

Figure 34. Moment for Forward Ramp Motion.

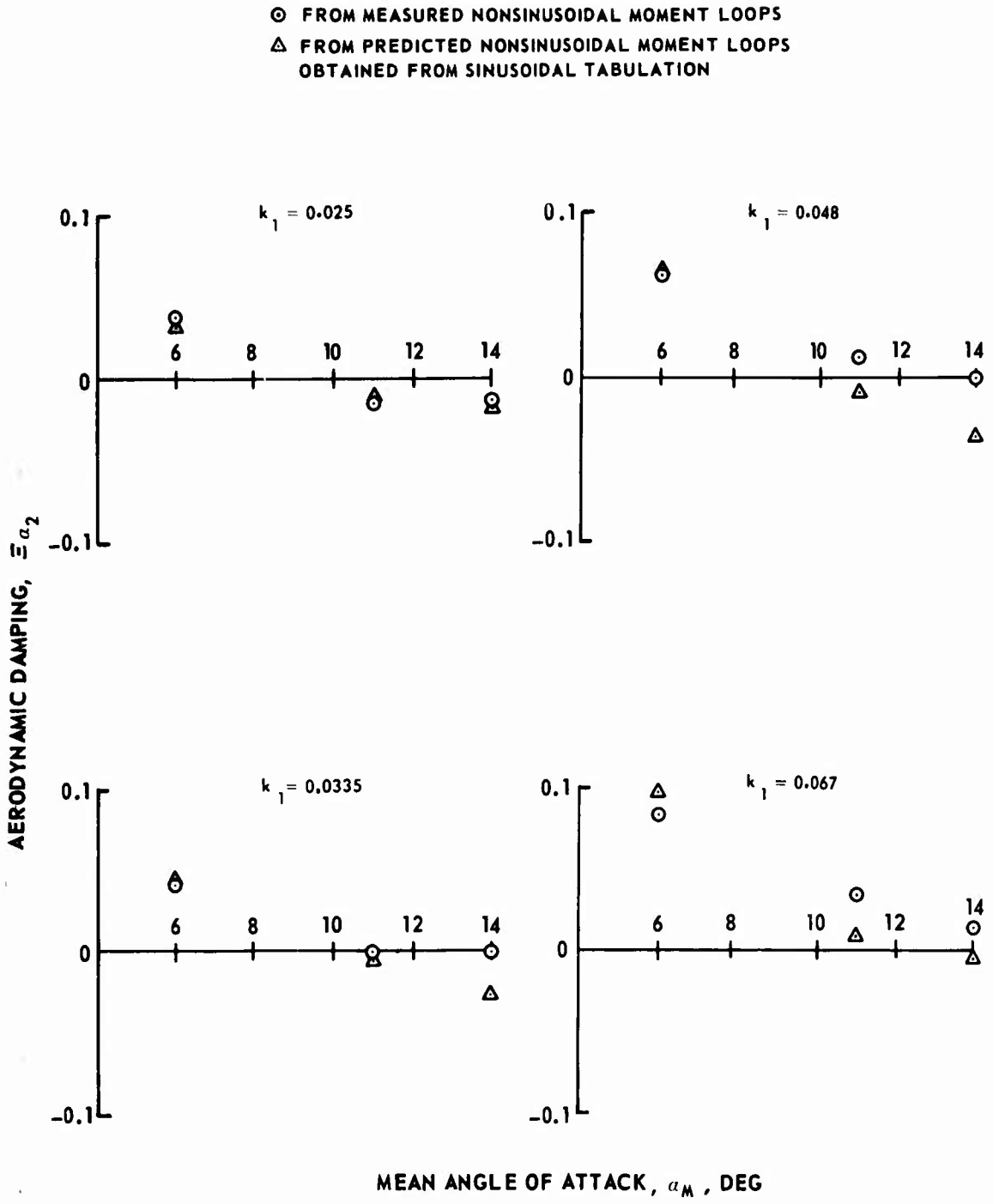

Figure 35. Two-Dimensional Aerodynamic Damping vs. Mean Angle of Attack at Various Reduced Frequencies for Forward Ramp Motion.

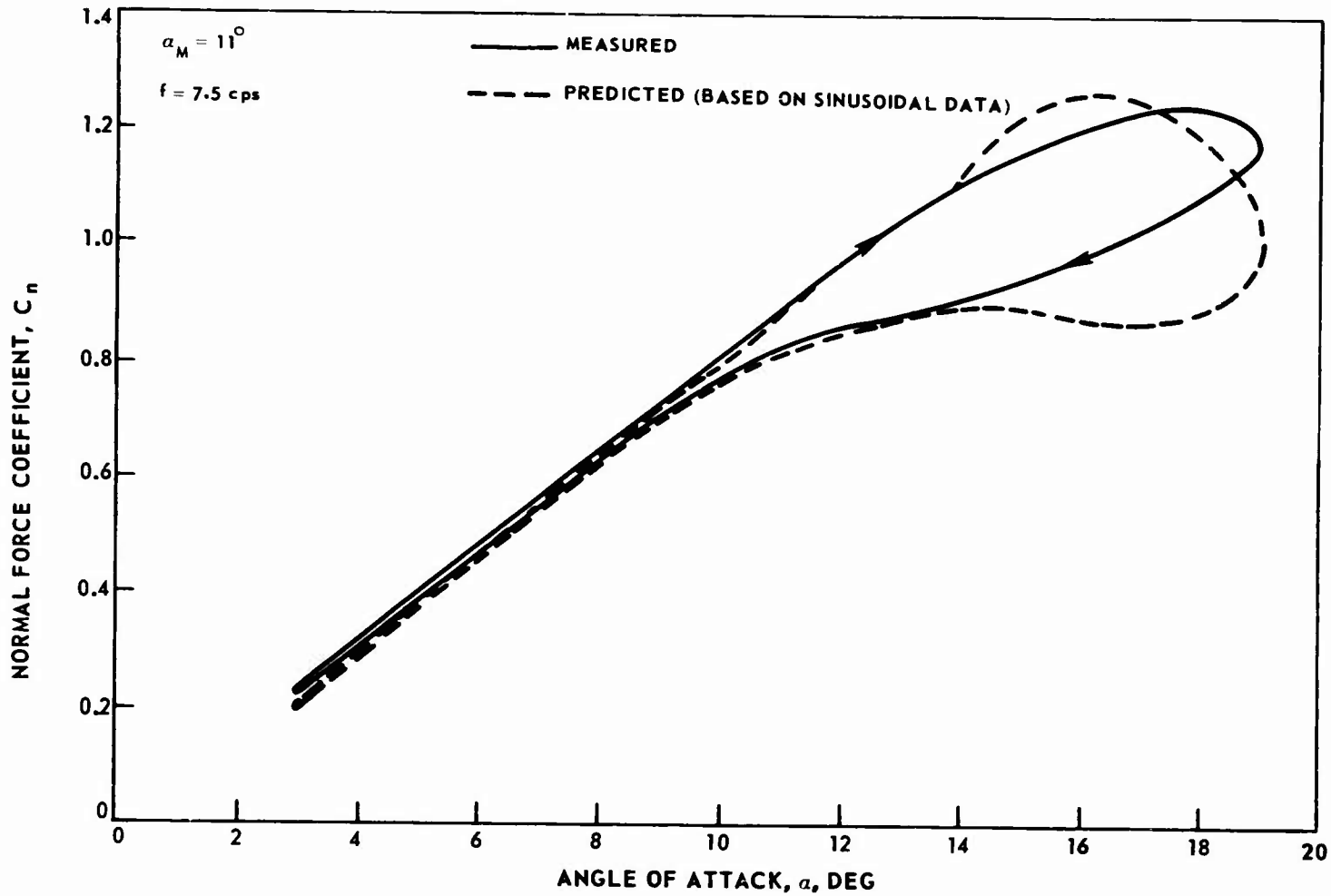

Figure 36. Normal Force for Backward Ramp Motion.

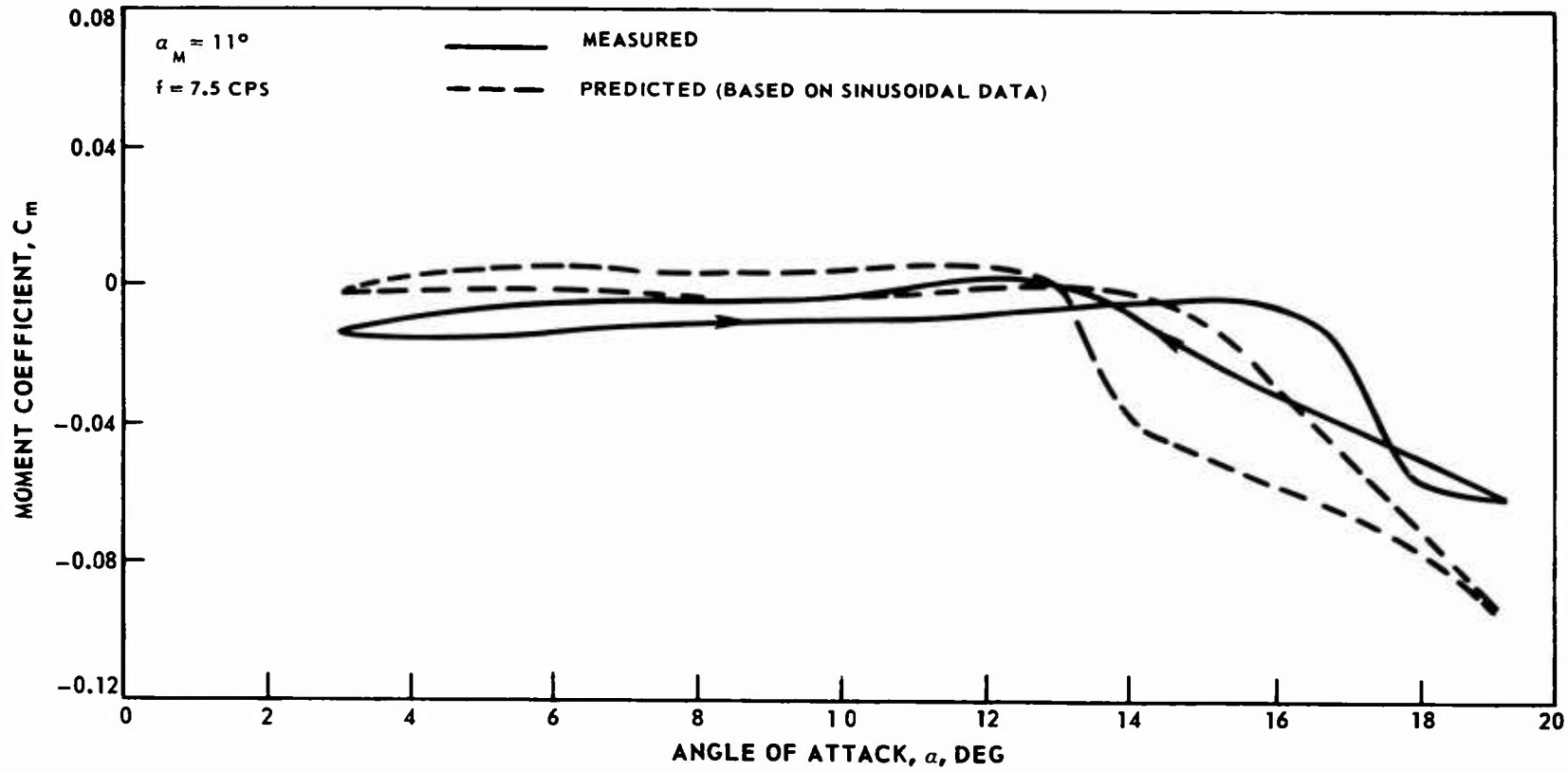

Figure 37. Moment for Backward Ramp Motion.

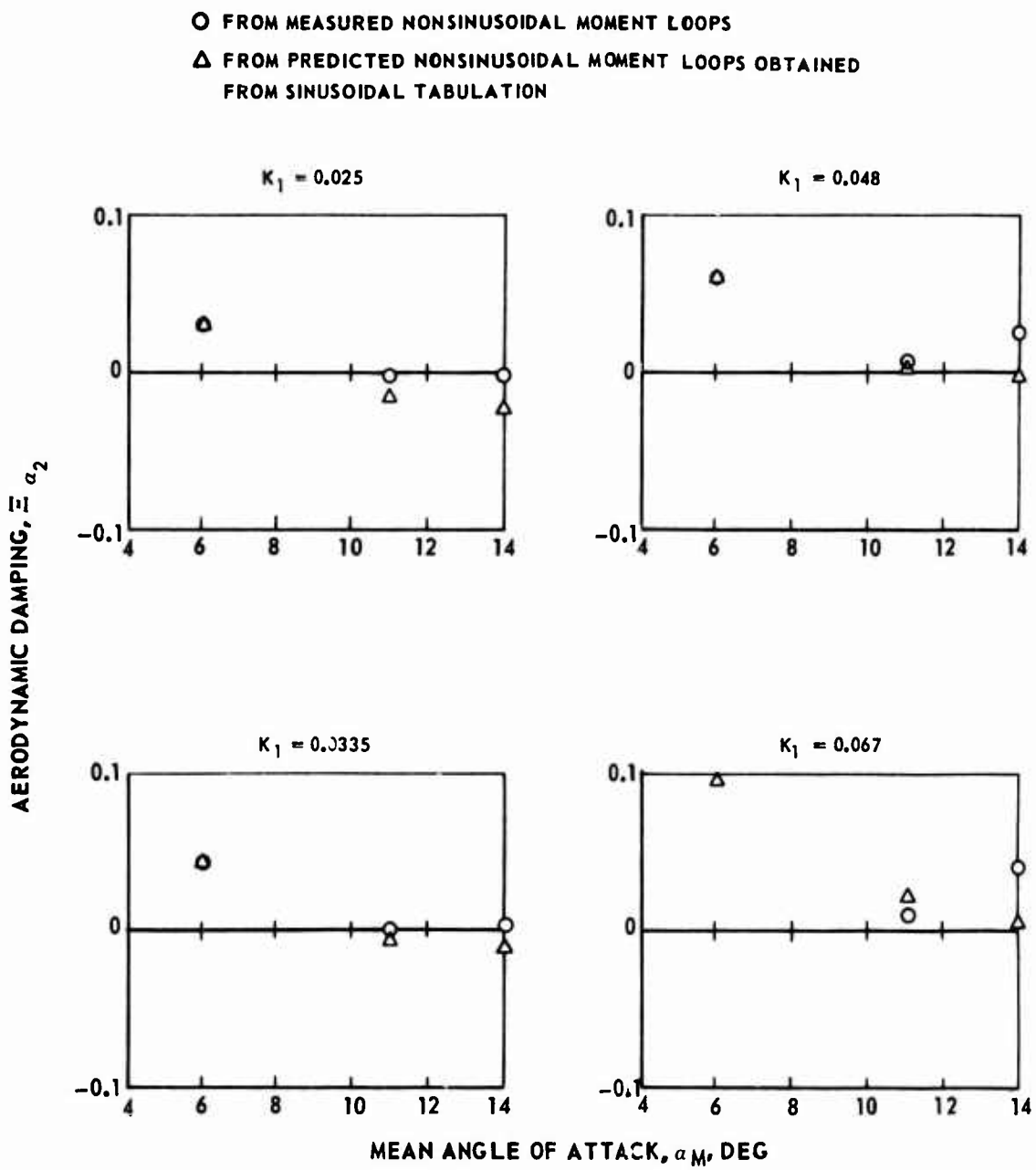

Figure 38. Two-Dimensional Aerodynamic Damping vs. Mean Angle of Attack at Various Reduced Frequencies for Backward Ramp Motion.

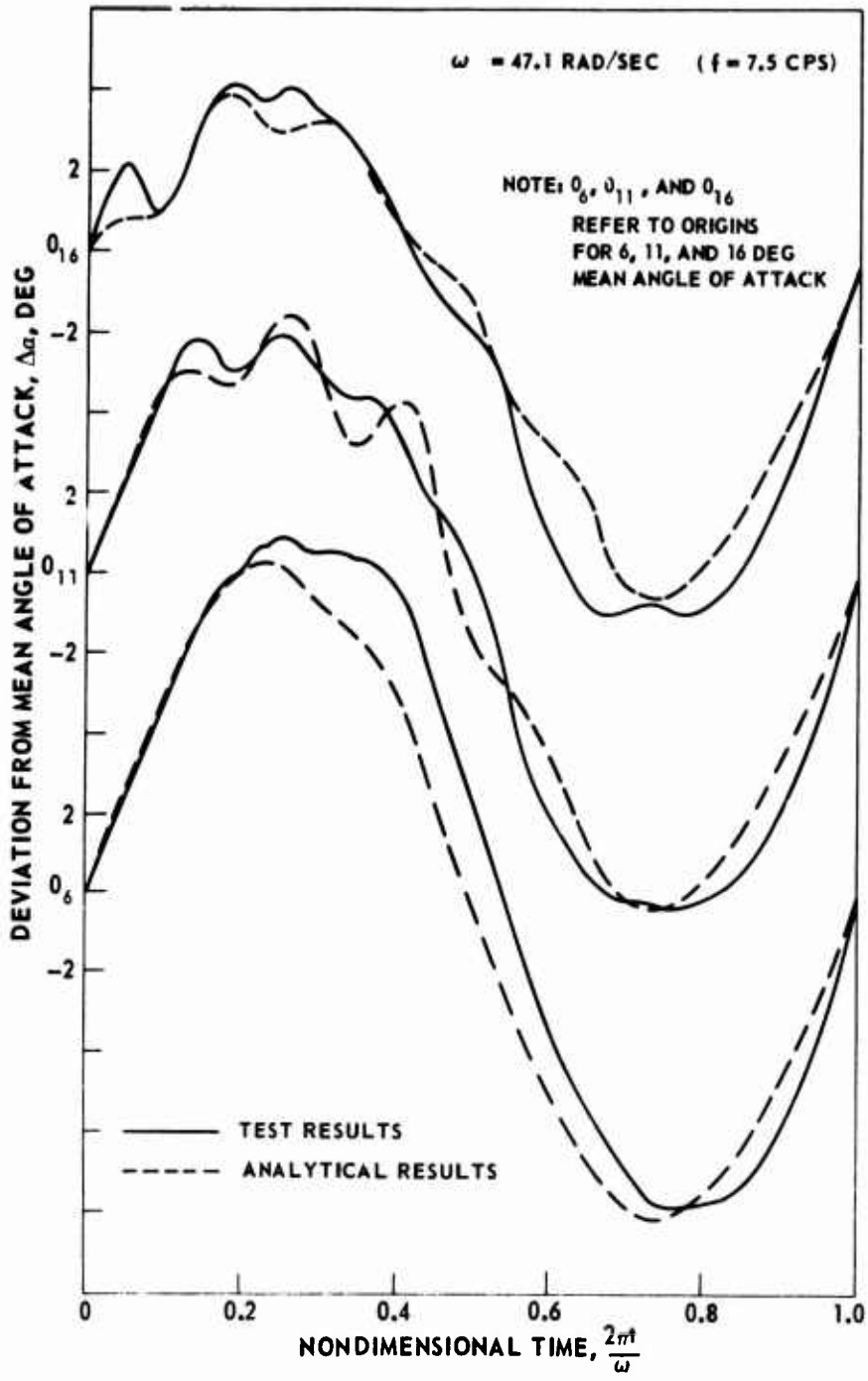

a)

Figure 39. Comparison of Experimental and Analytical Time Histories for Flexible Airfoil With f_α = 41.5 CPS.

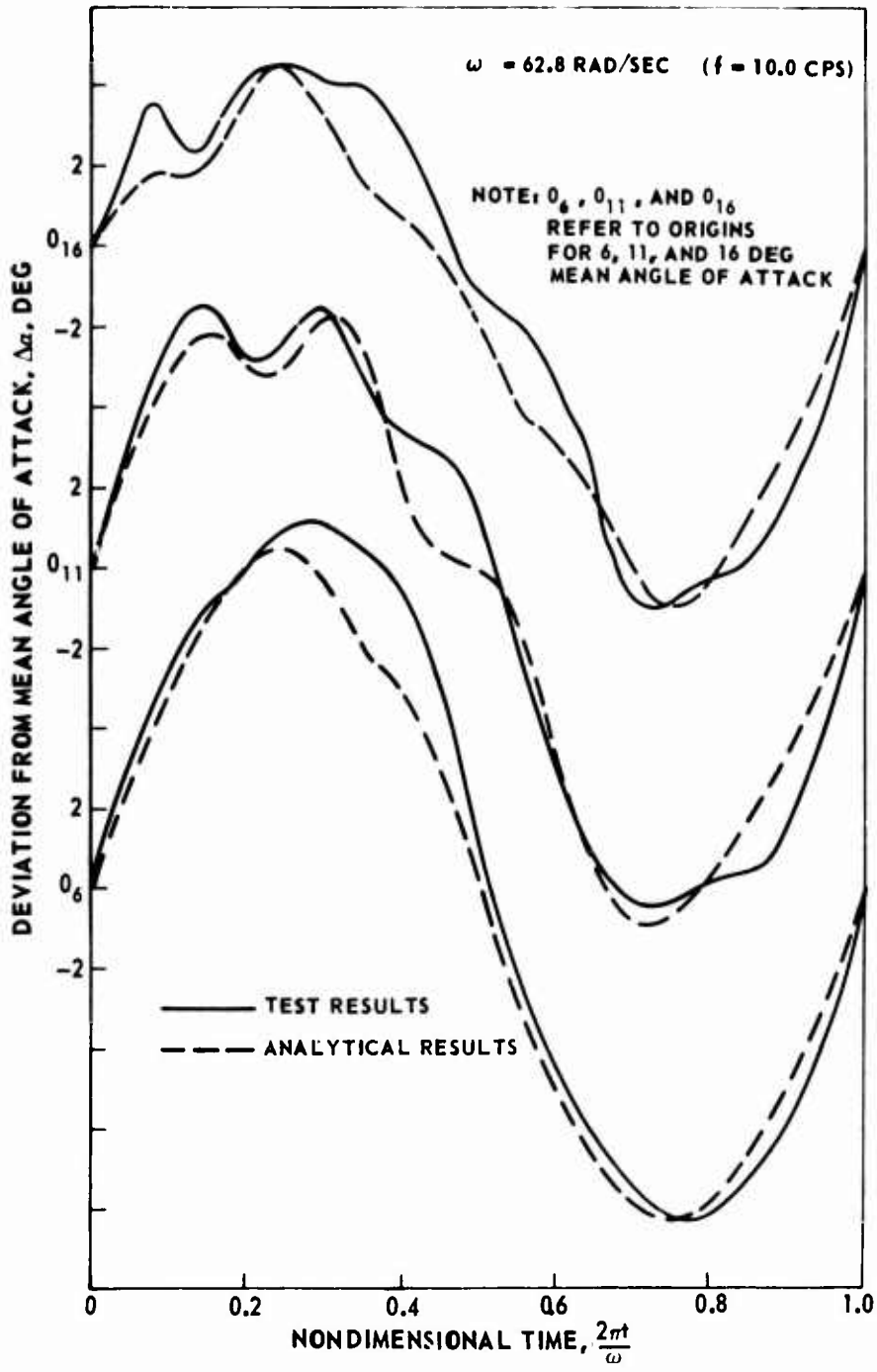

b)

Figure 39 - Continued.

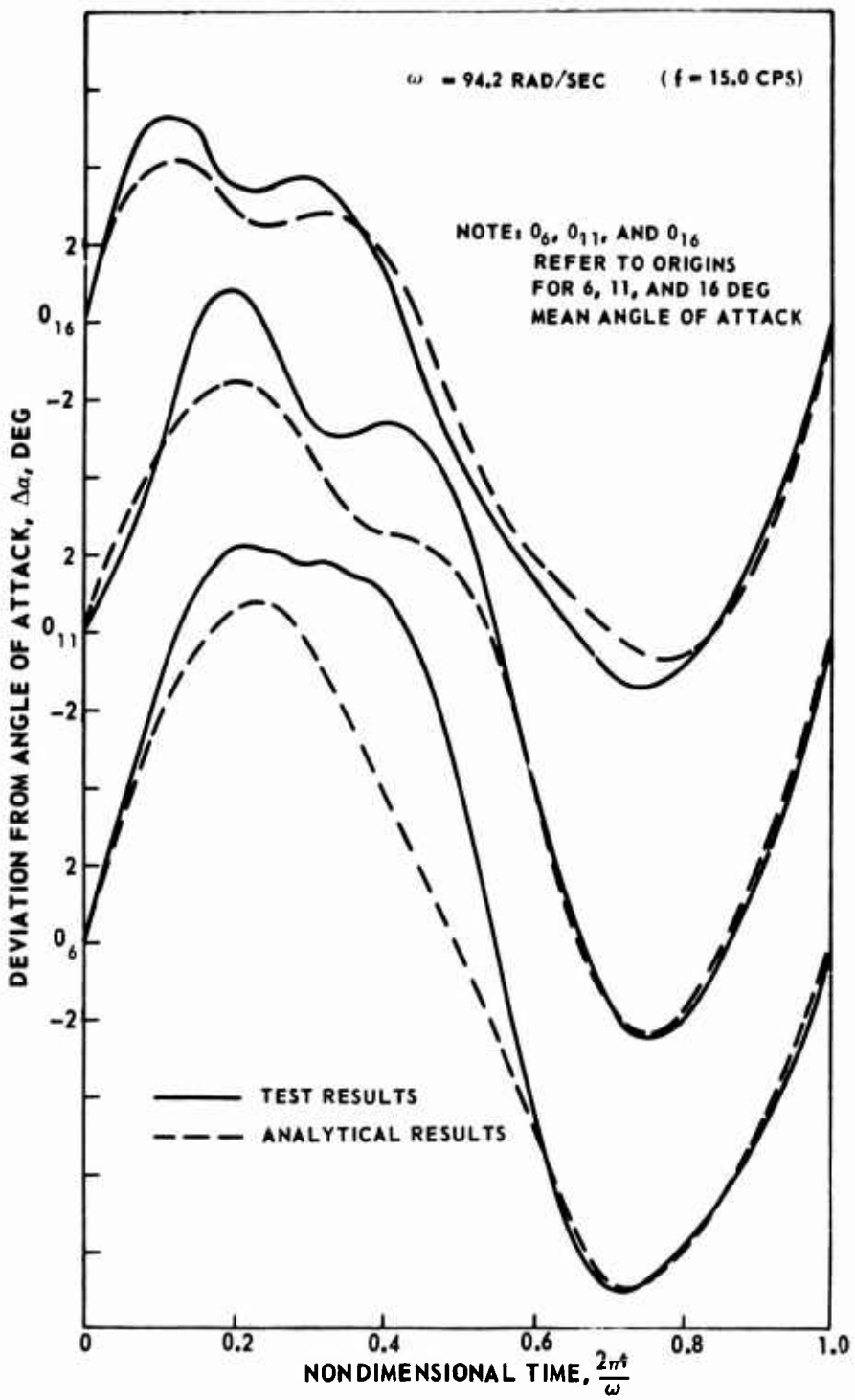

c)

Figure 39 - Continued.

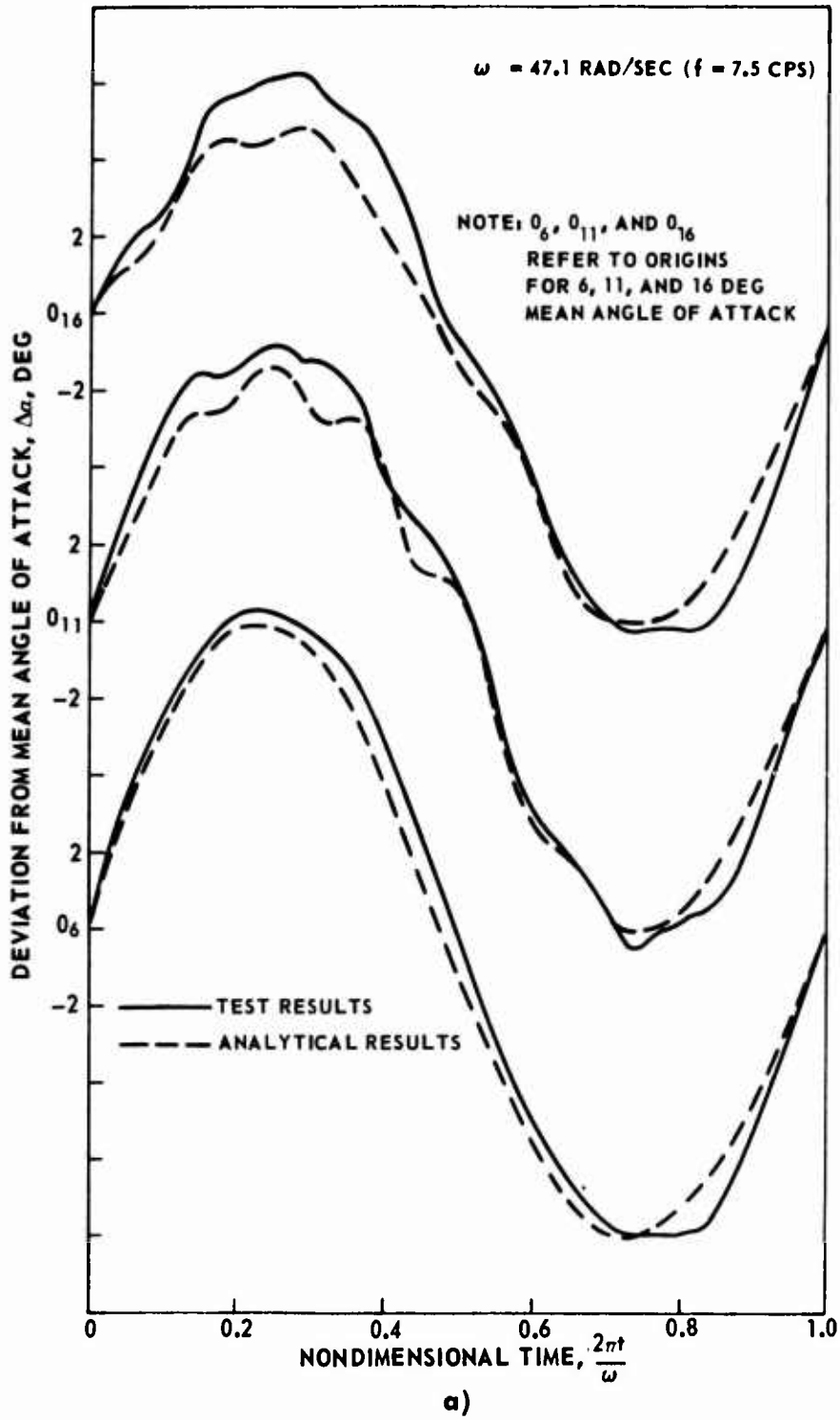

Figure 40. Comparison of Experimental and Analytical Time Histories for Flexible Airfoil With f_α = 52 CPS.

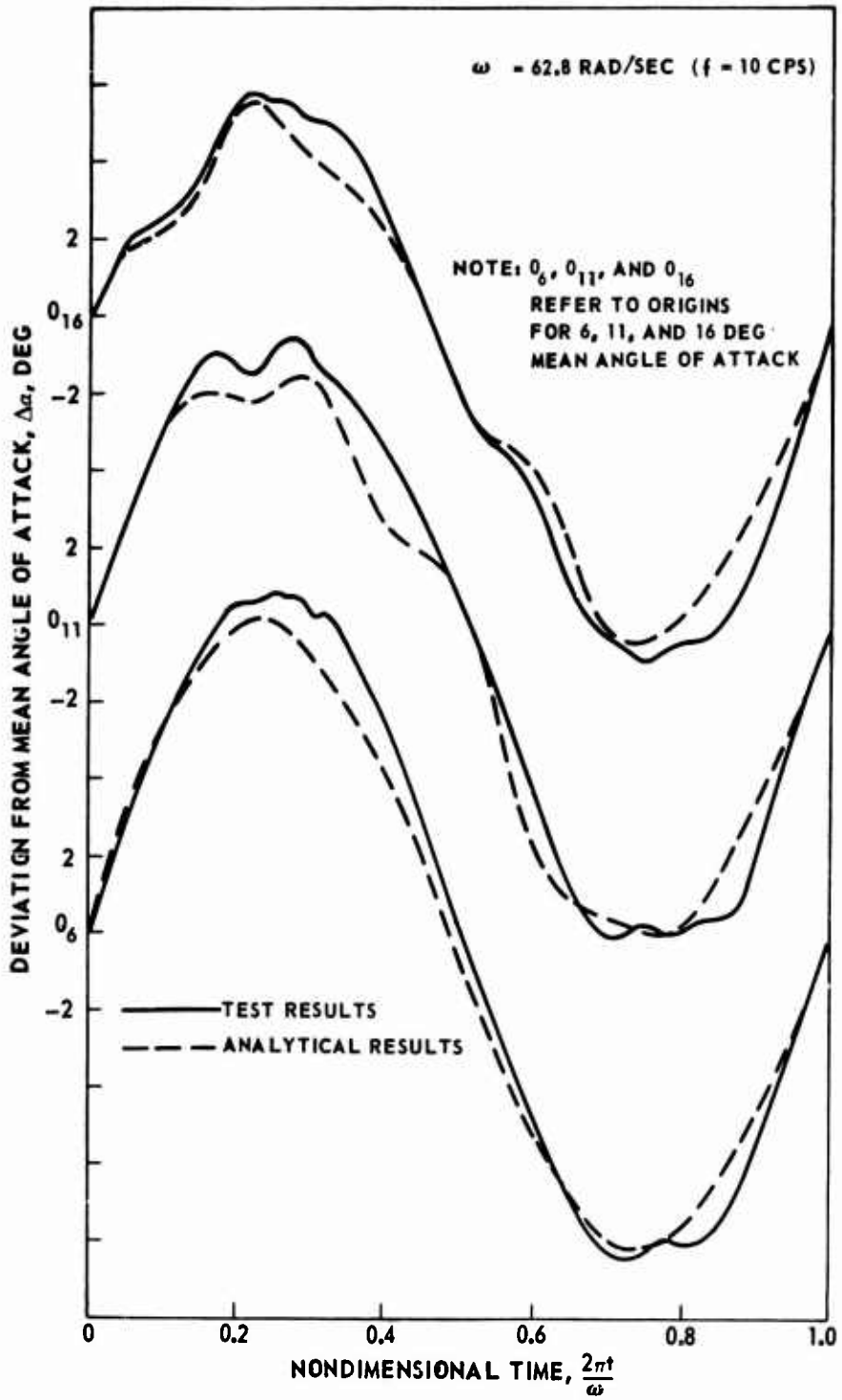

b)

Figure 40 - Continued.

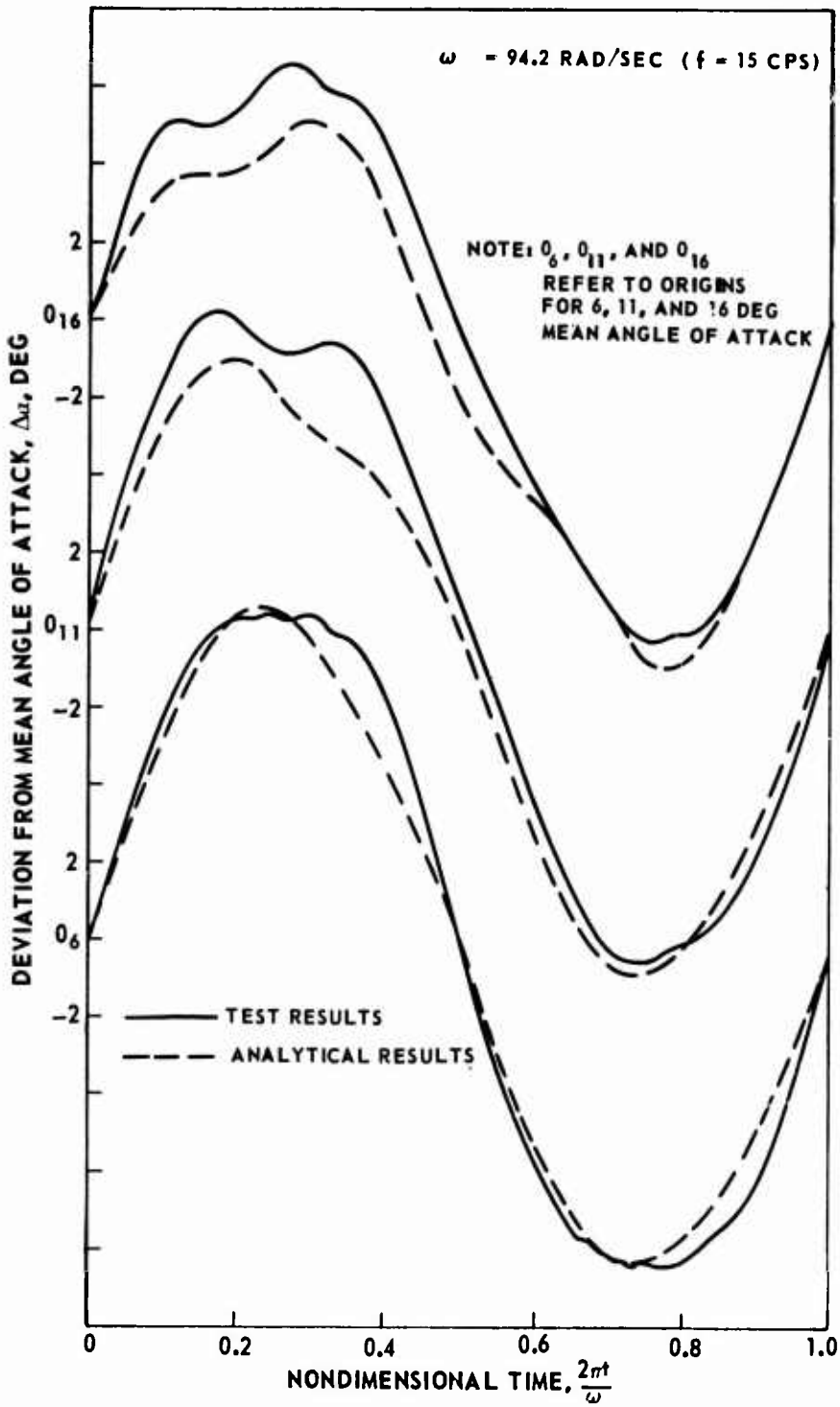

c)

Figure 40 - Continued.

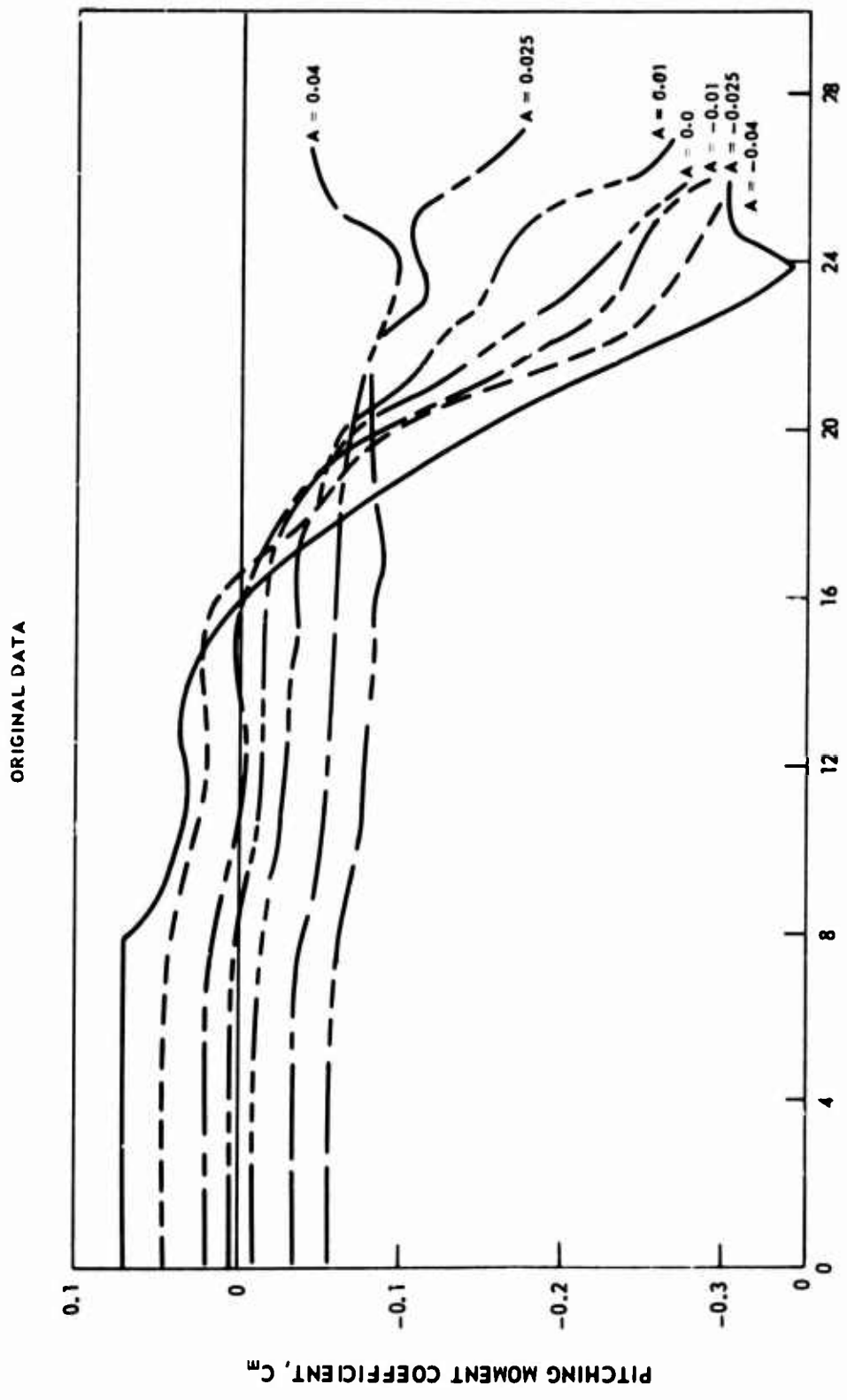

Figure 41. Comparison of Original and Smoothed Dynamic Moment Characteristics for B = -0.01.

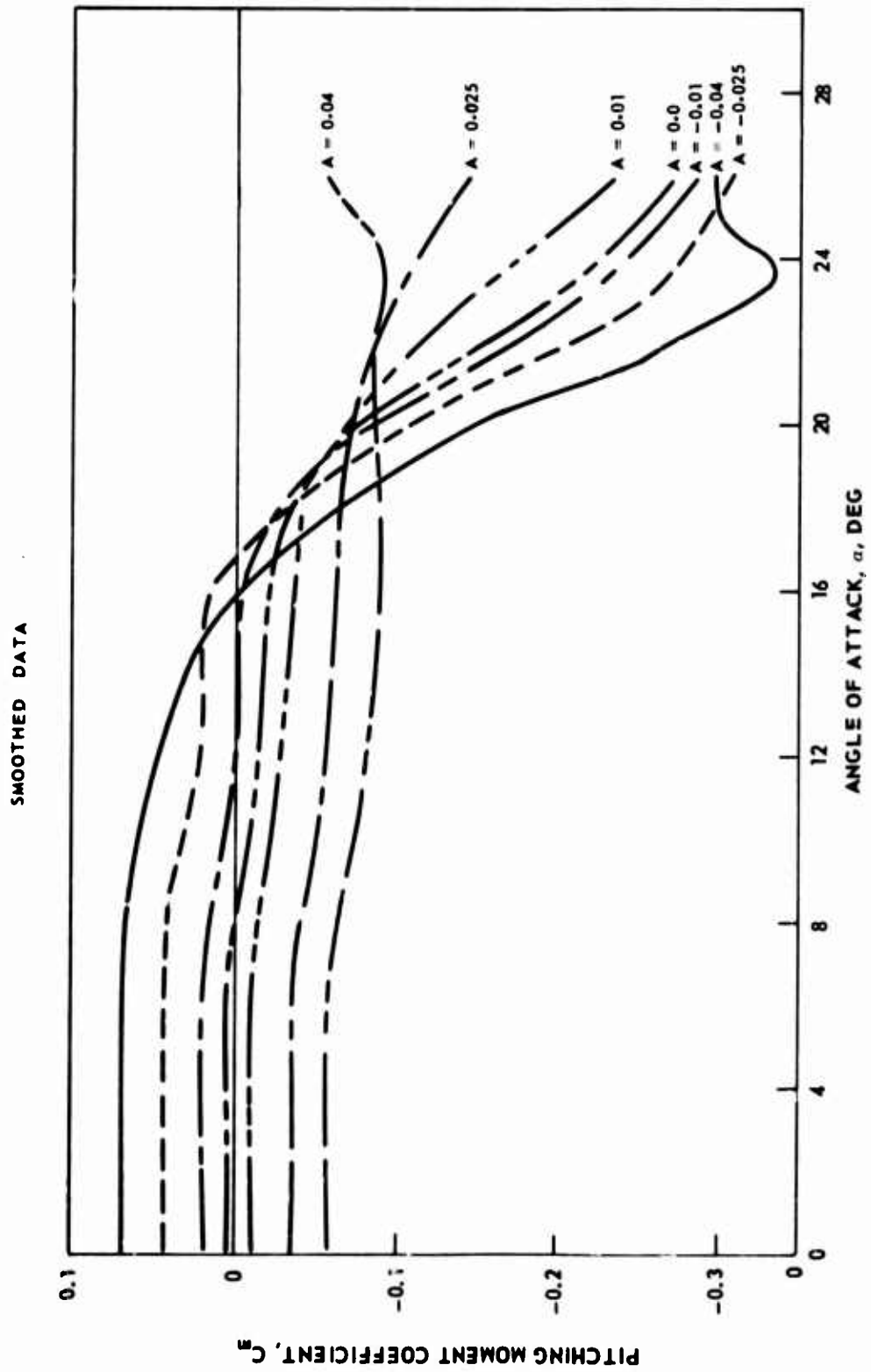

Figure 41 - Continued.

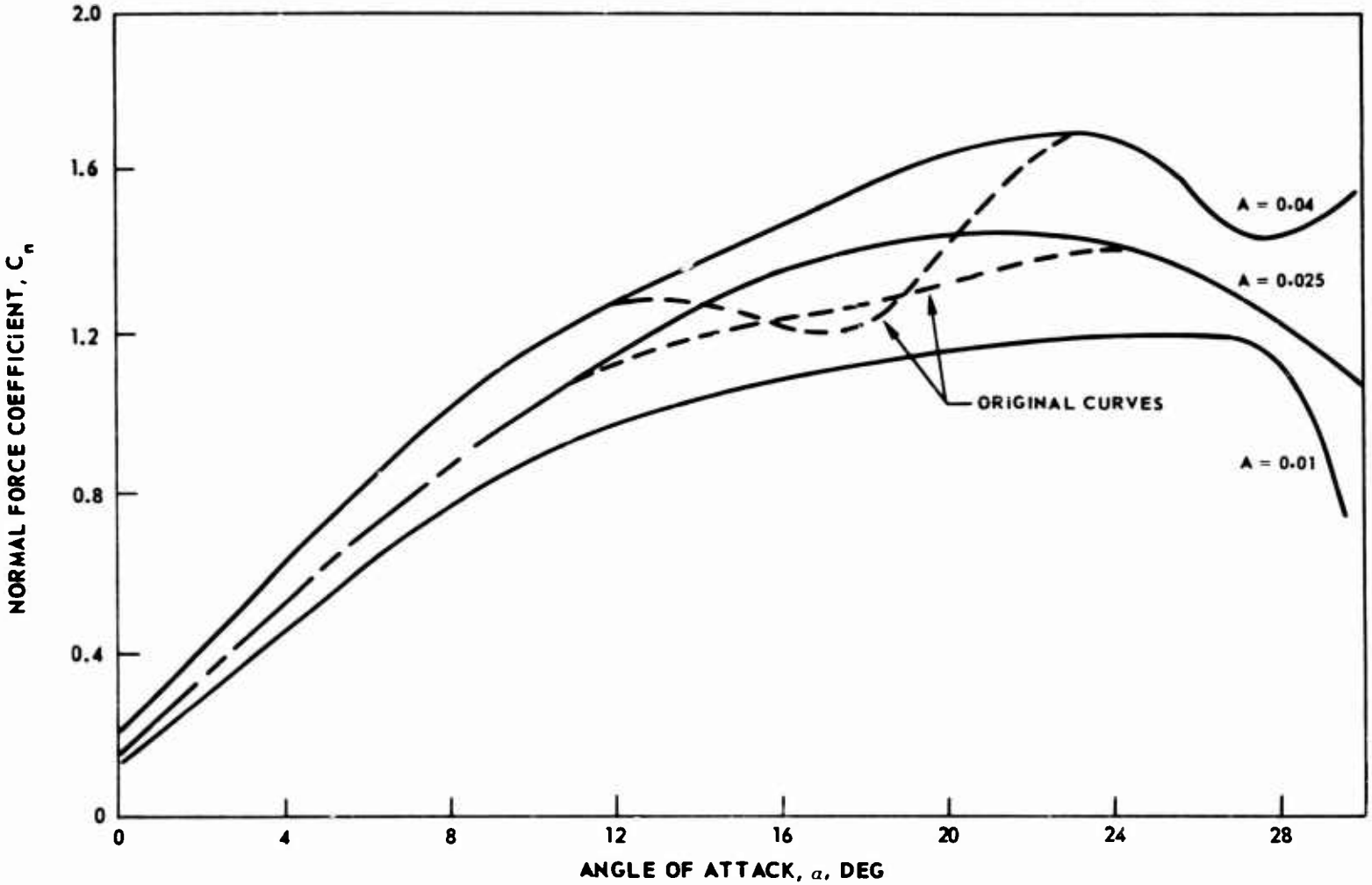

Figure 42. Comparison of Original and Smoothed Dynamic Normal Force Characteristics for B = 0.004.

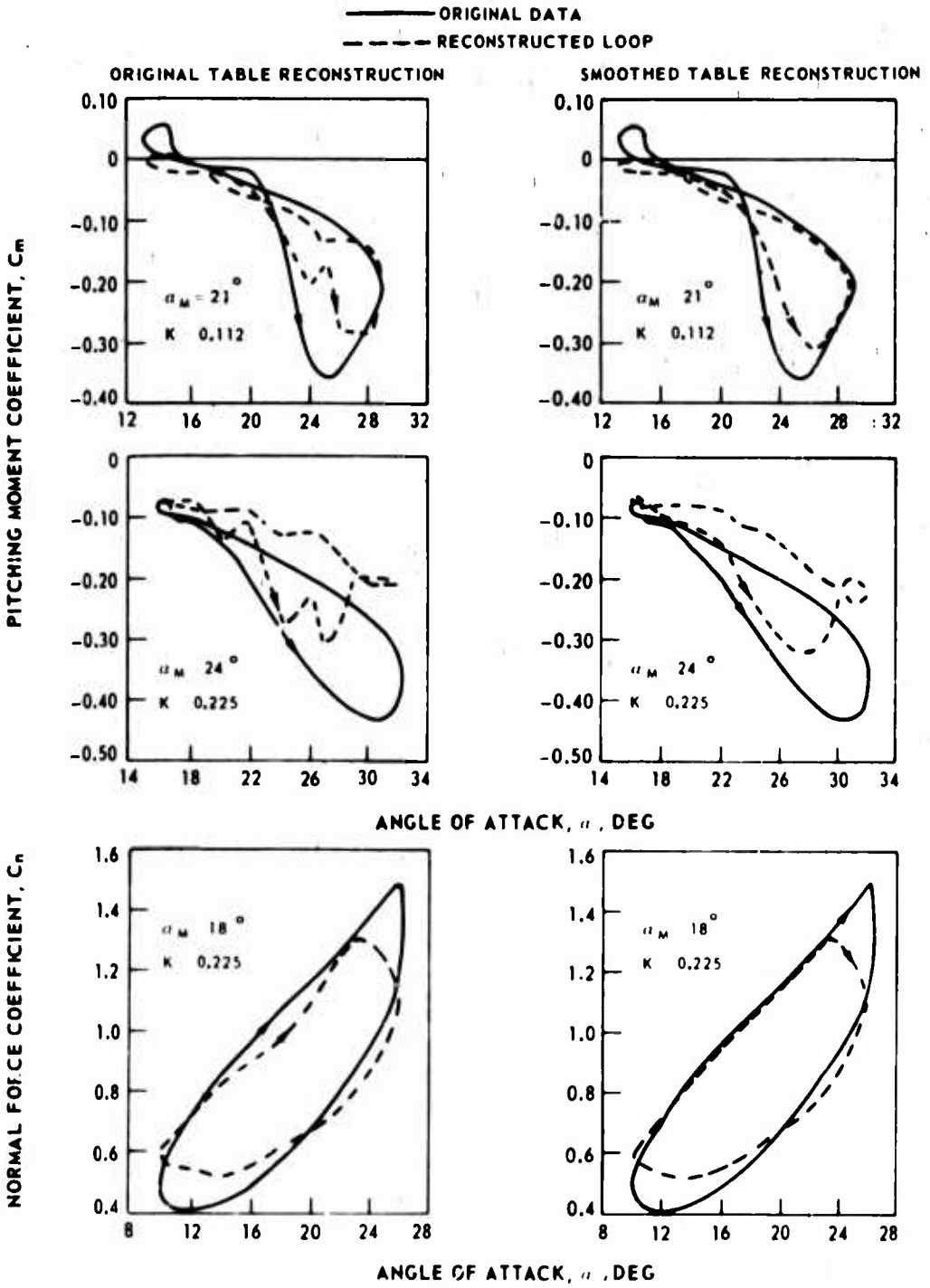

Figure 43. Comparison of Reconstructed Hysteresis Loops From Original and Smoothed Data Tables.

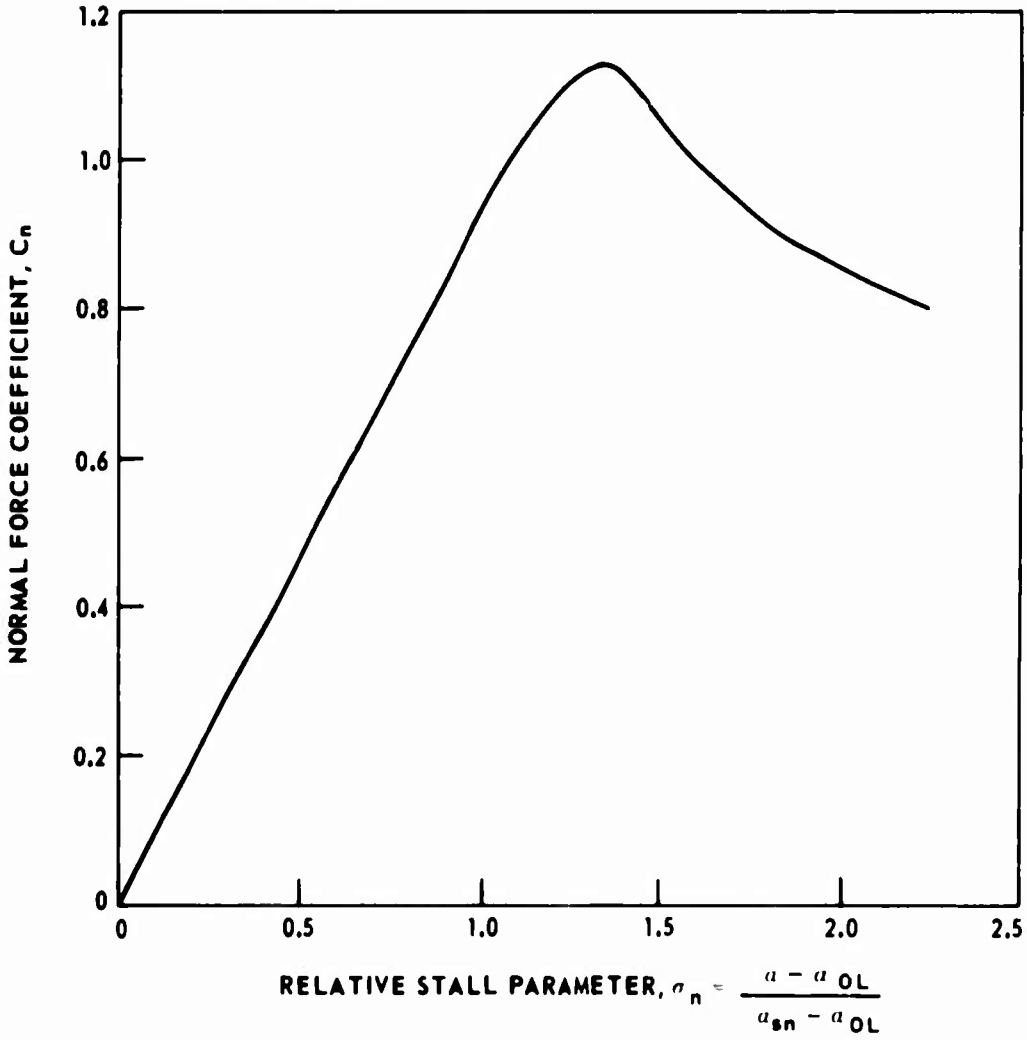

Figure 44. Normal Force Coefficient vs. Relative Stall Parameter, σ_n.

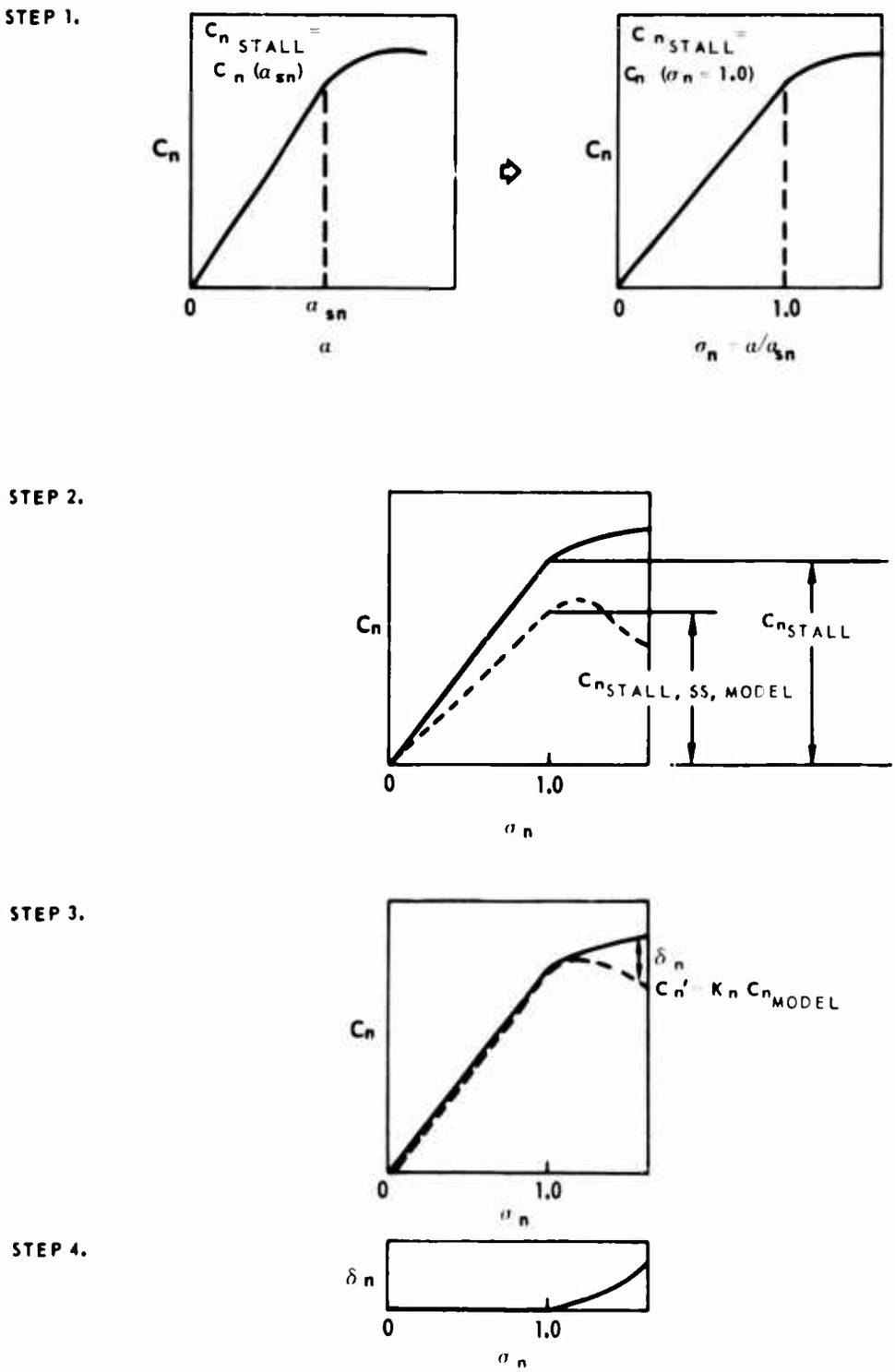

Figure 45. Derivation of the Parameters Needed To Scale Model Data to an Arbitrary Normal Force Curve.

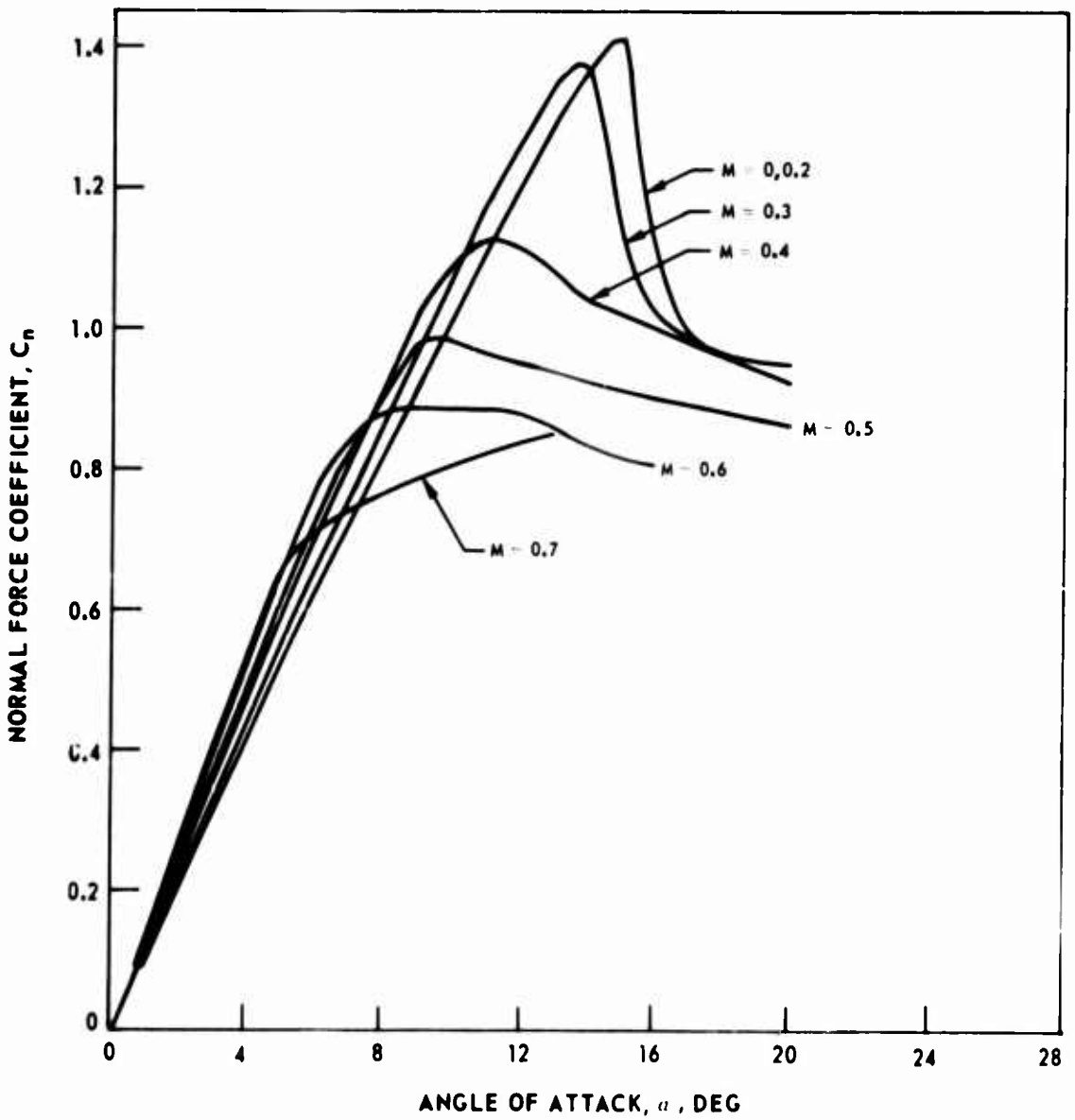

Figure 46. NACA 0012 Normal Force Characteristics.

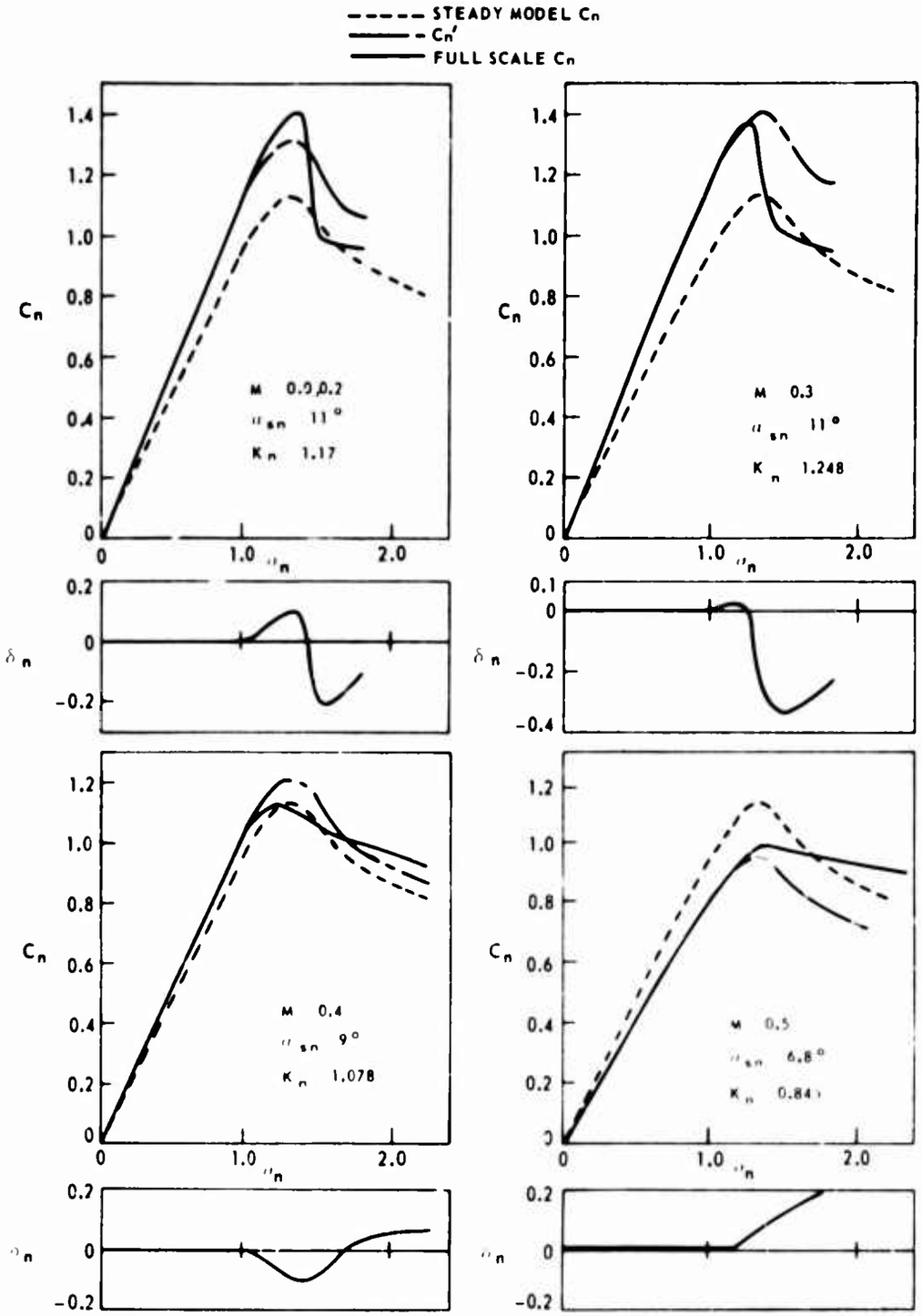

Figure 47. Normal Force Coefficient Scaling Curves.

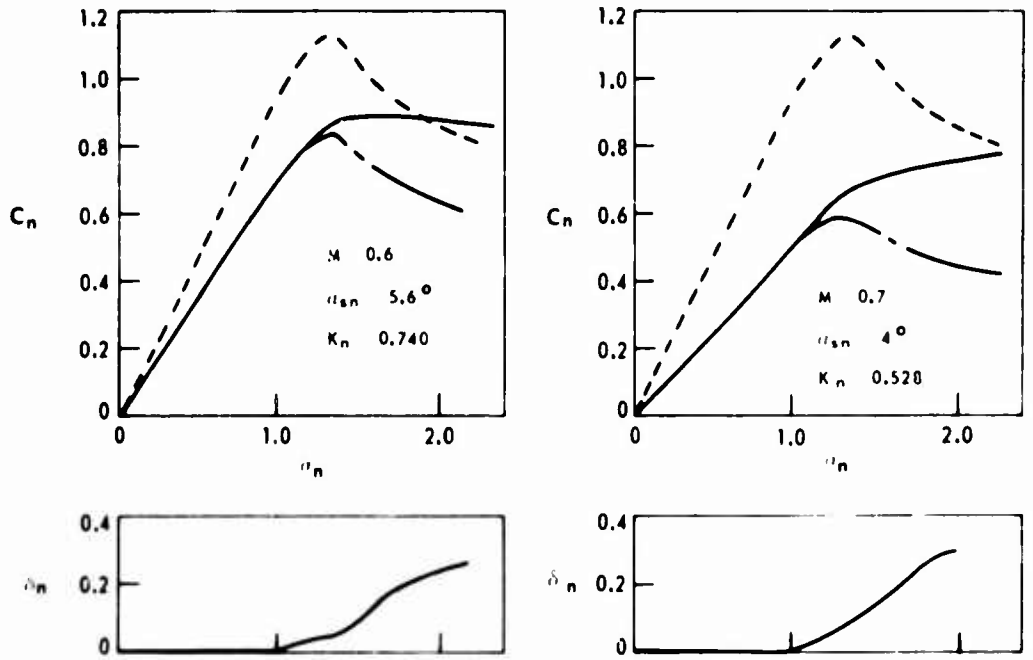

Figure 47 - Continued.

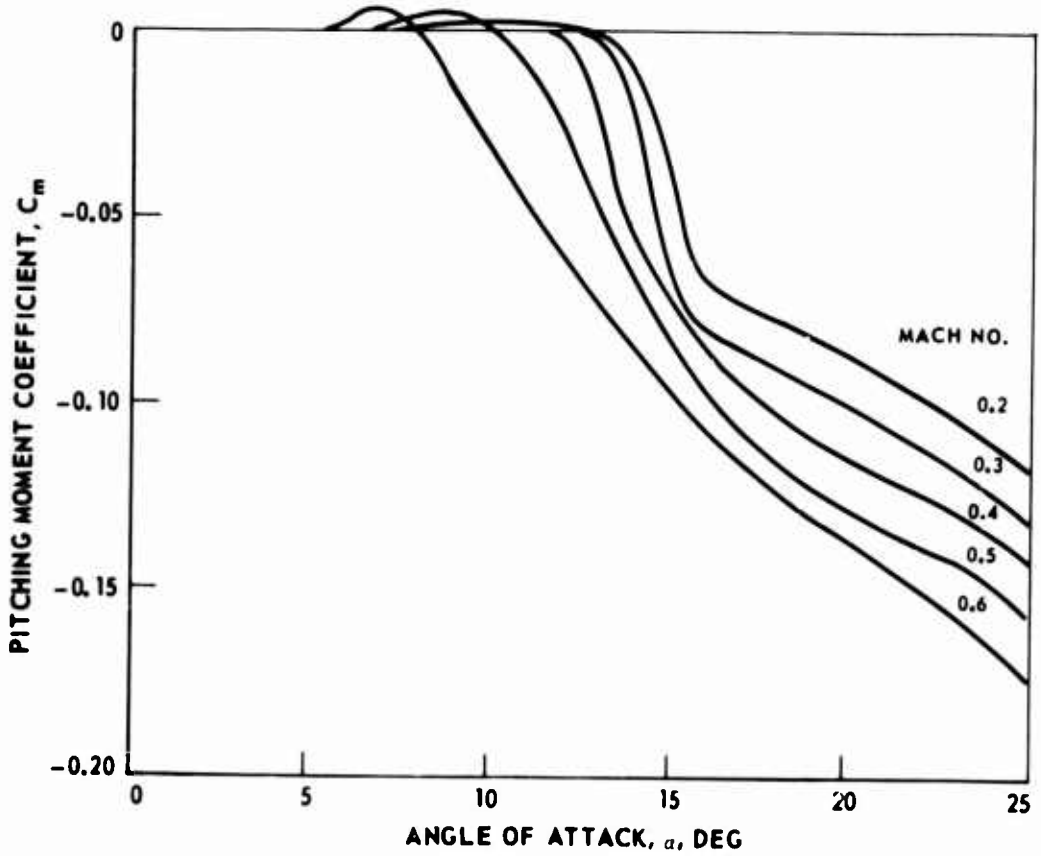

Figure 48. NACA 0012 Pitching Moment Characteristics.

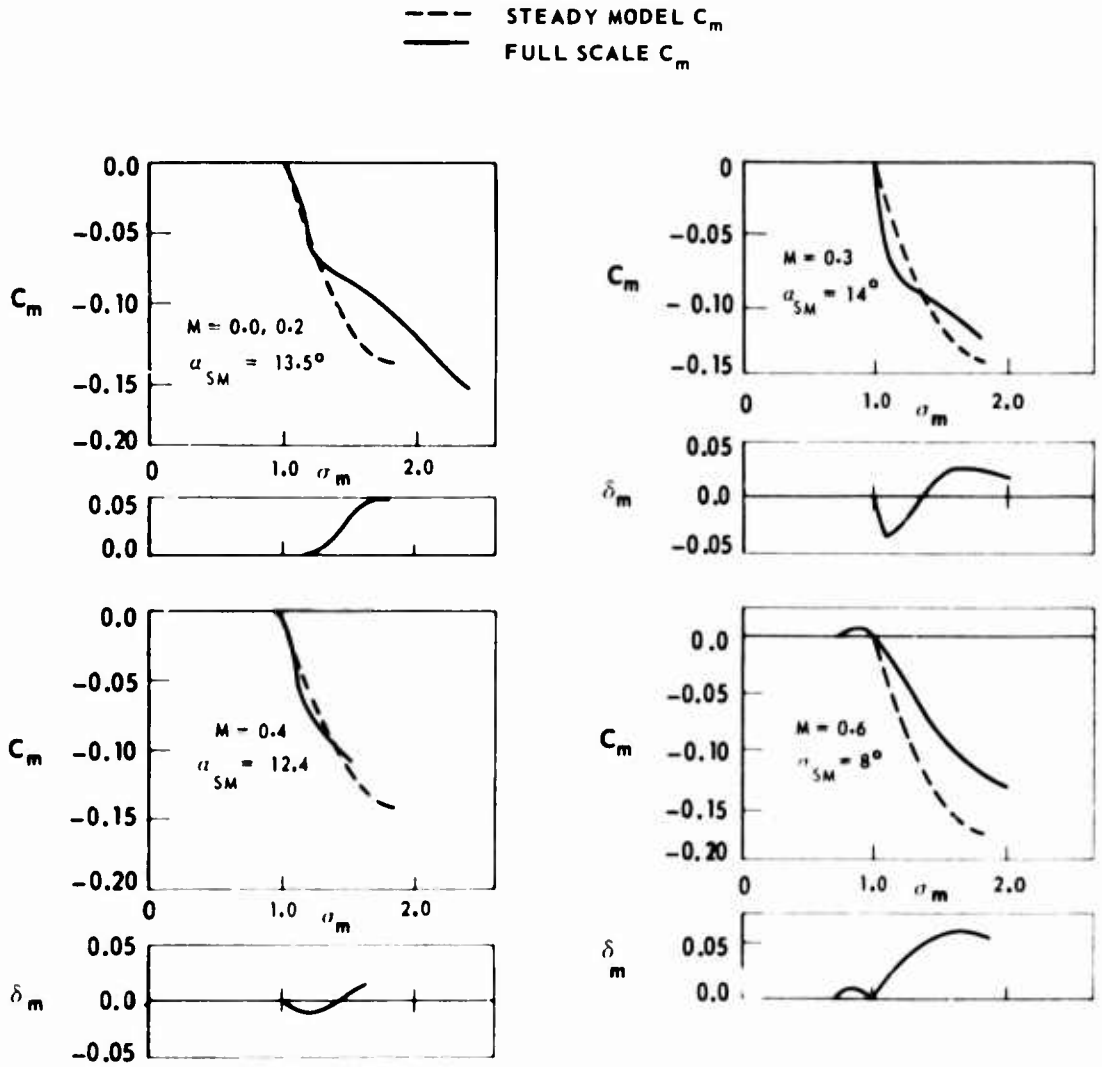

Figure 49. Pitching Moment Coefficient Scaling Curves.

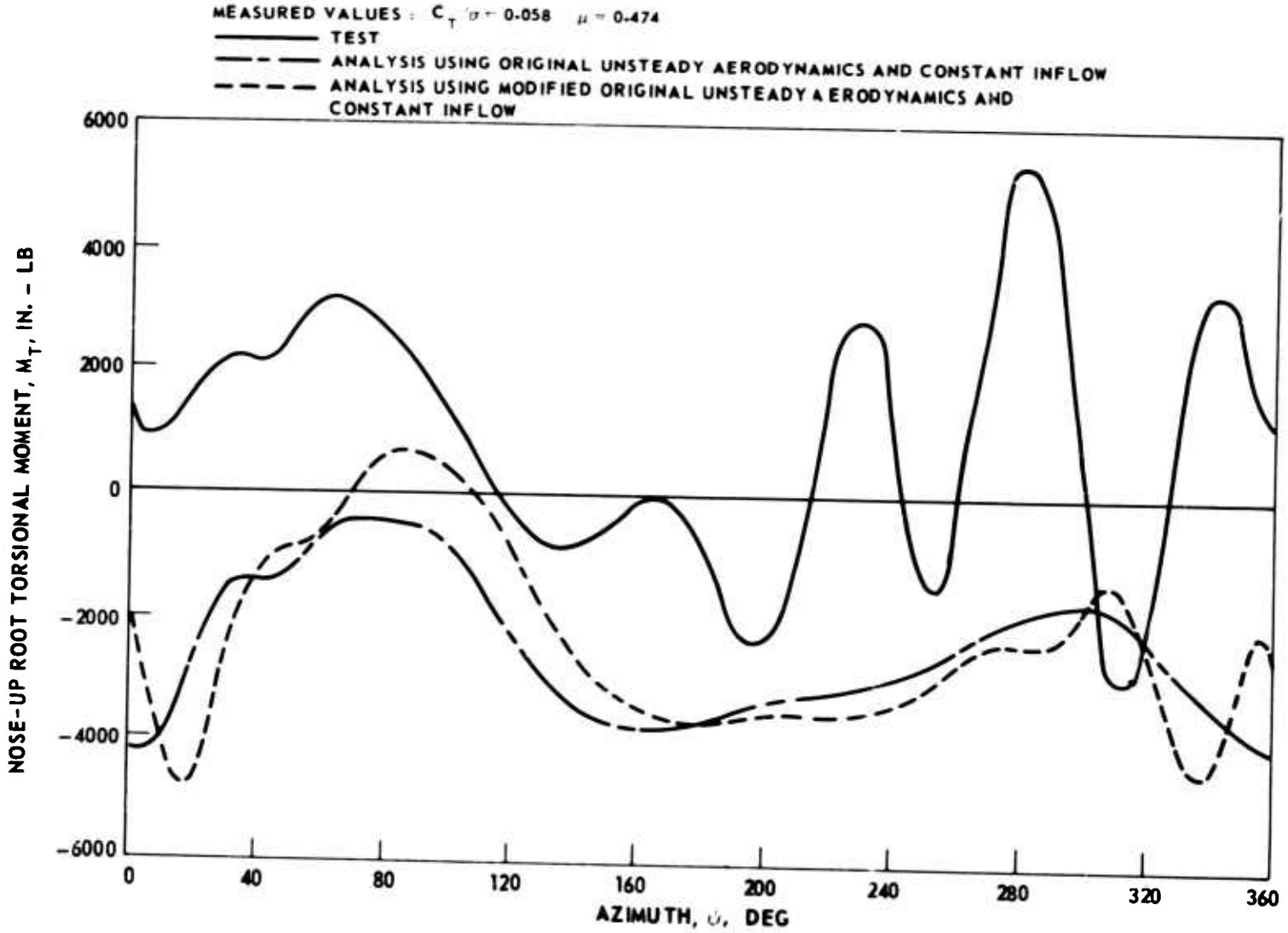

Figure 50. The Effect of Data Smoothing on Torsional Response Correlation - NH-3A Case 43.

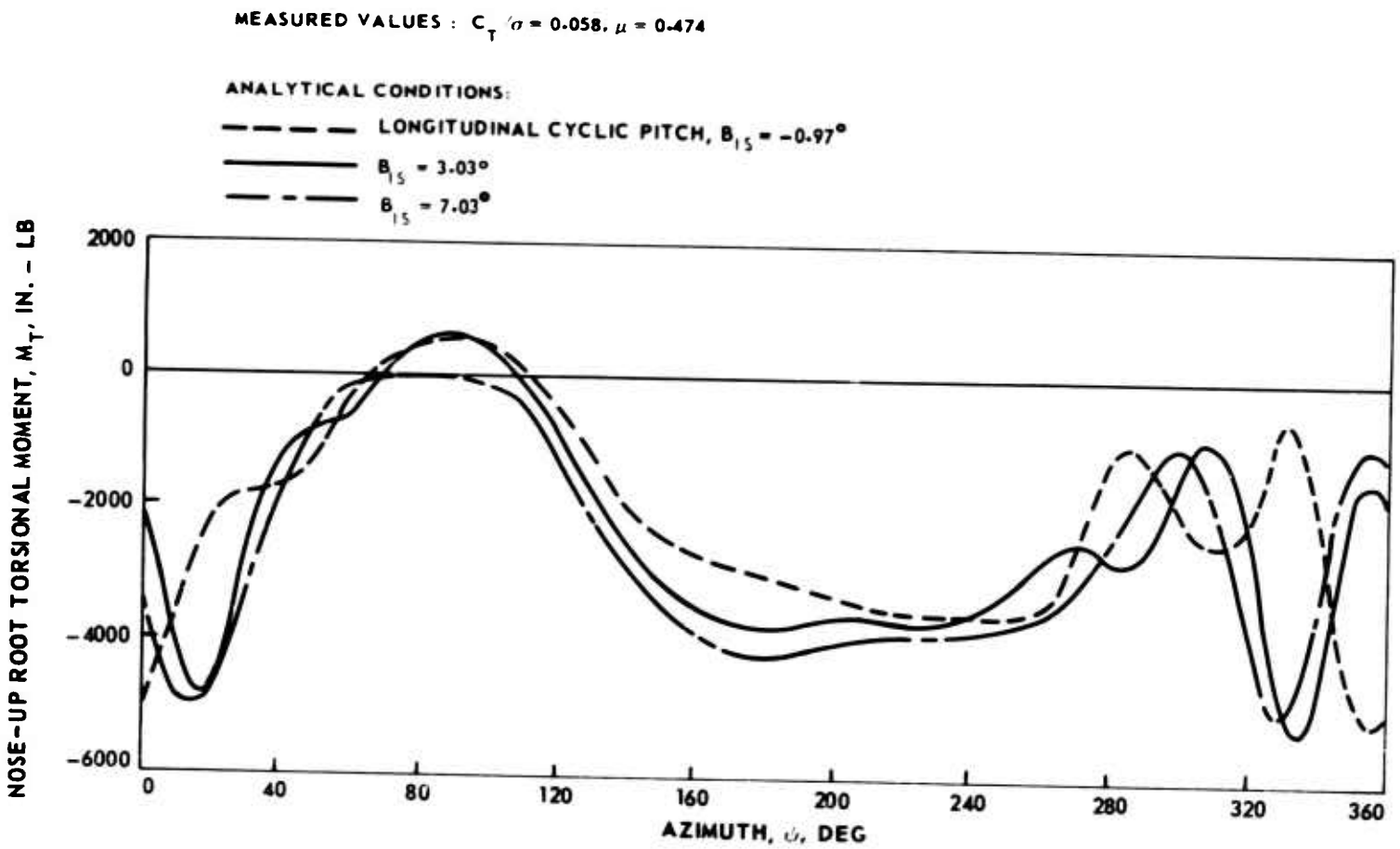

Figure 51. The Effect of Cyclic Pitch Variations on Calculated Torsional Response - NH-3A Case 43.

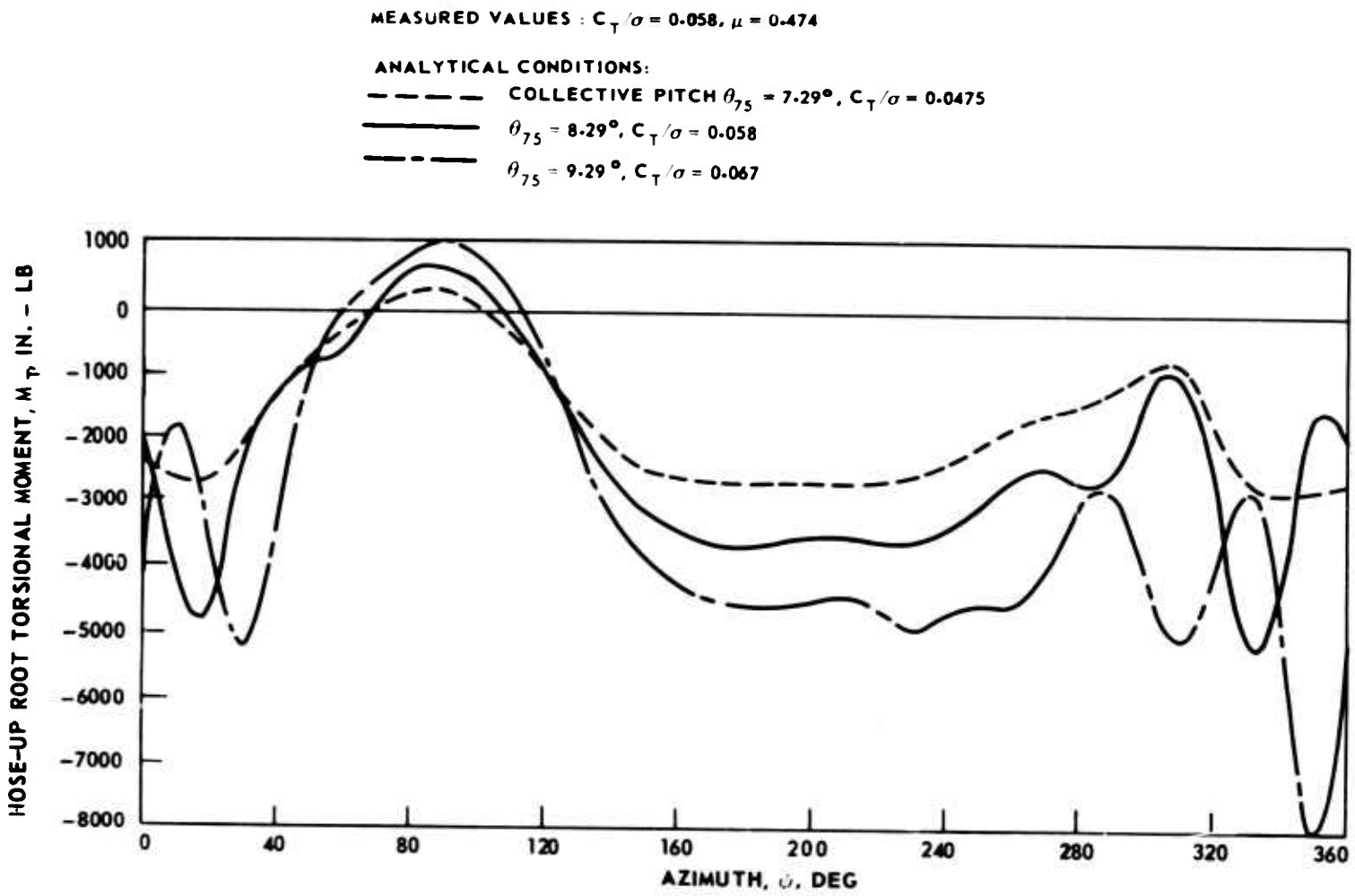

Figure 52. The Effect of Collective Pitch Changes on Calculated Torsional Response - NH-3A Case 43.

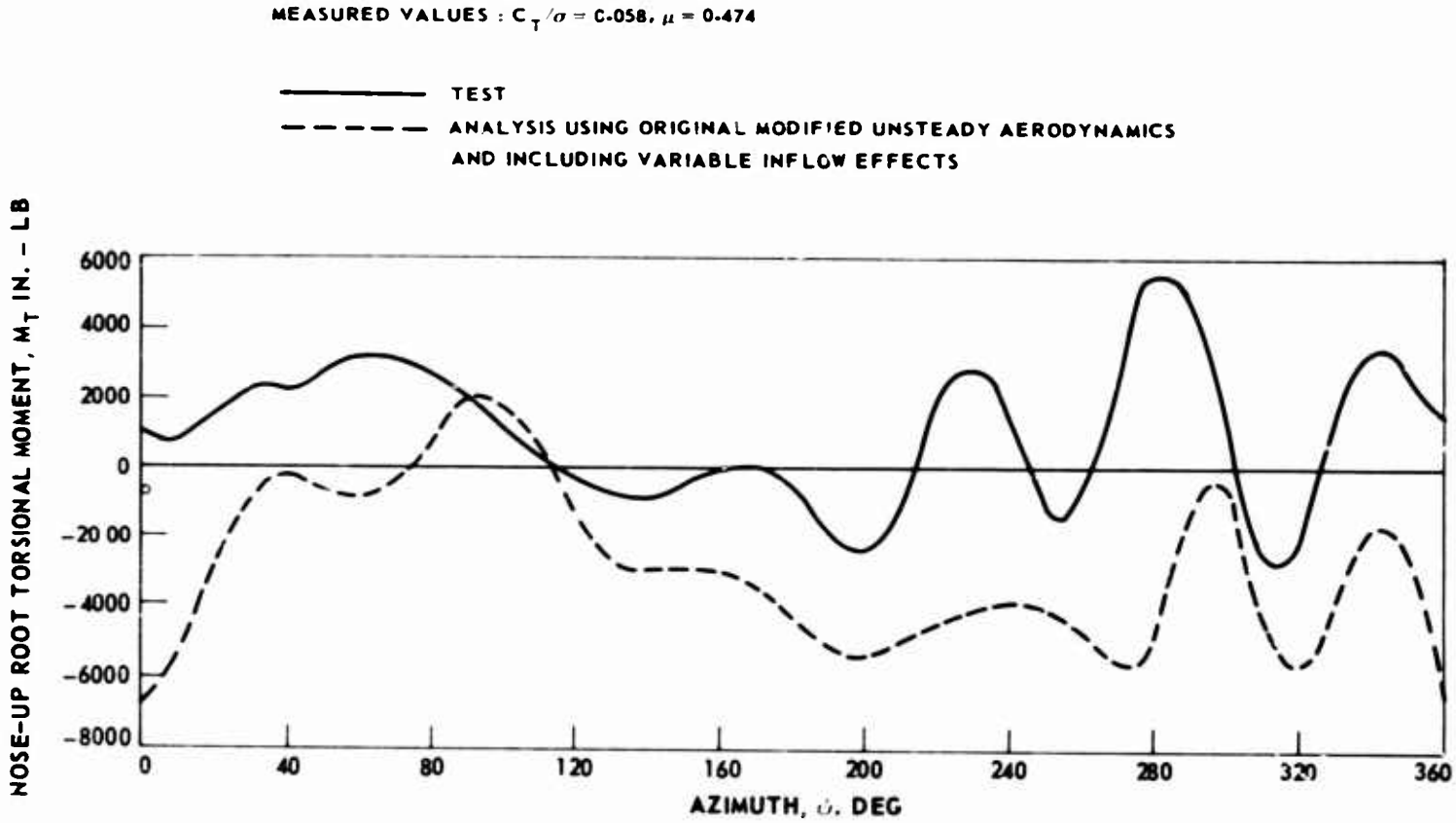

Figure 53. Torsional Response Correlation Using Original Unsteady Aerodynamics and Variable Inflow - NH-3A Case 43.

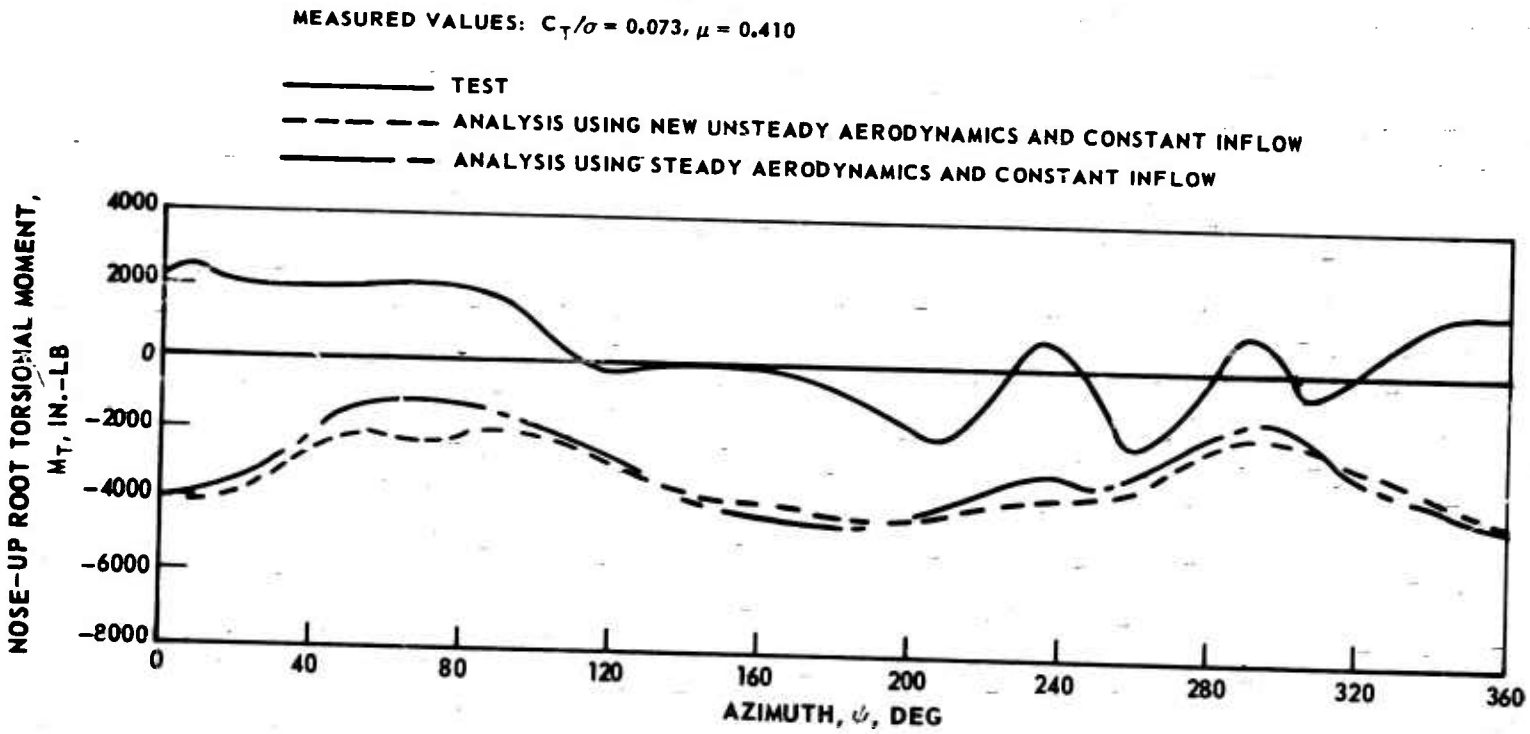

Figure 54. Torsional Response Correlation Using Steady and Unsteady Aerodynamics With Constant Inflow - NH-3A Case 28.

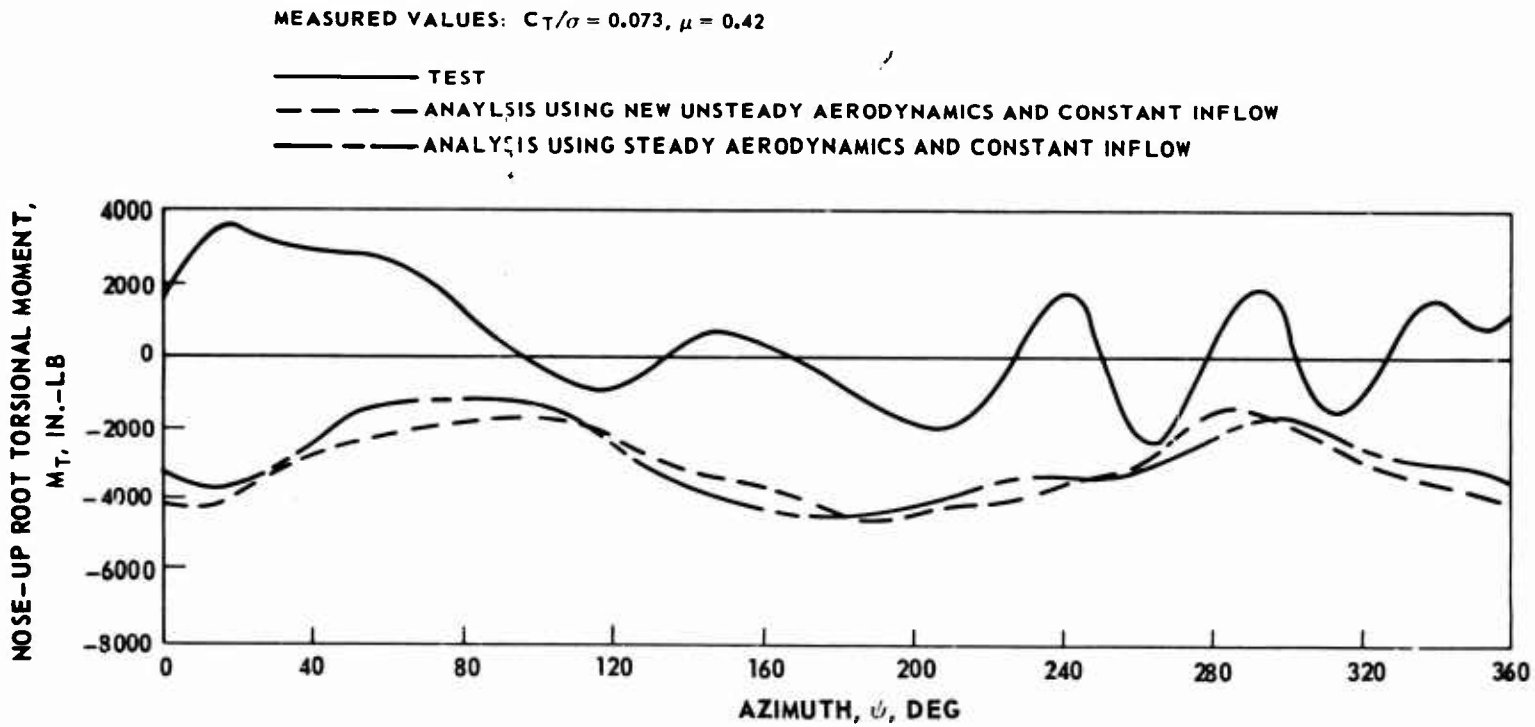

Figure 55. Torsional Response Correlation Using Steady and Unsteady Aerodynamics With Constant Inflow - NH-3A Case 39.

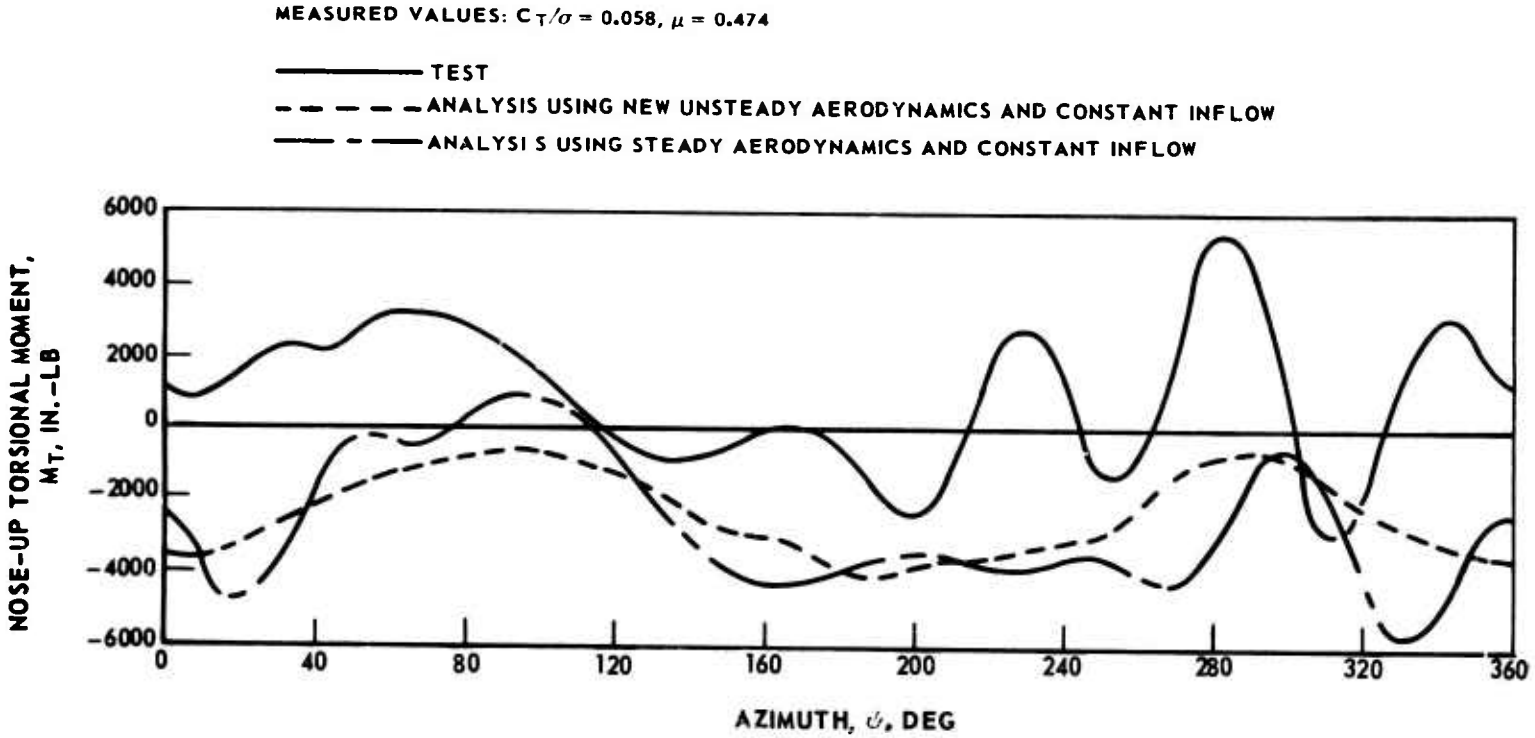

Figure 56. Torsional Response Correlation Using Steady and Unsteady Aerodynamics With Constant Inflow - NH-3A Case 43.

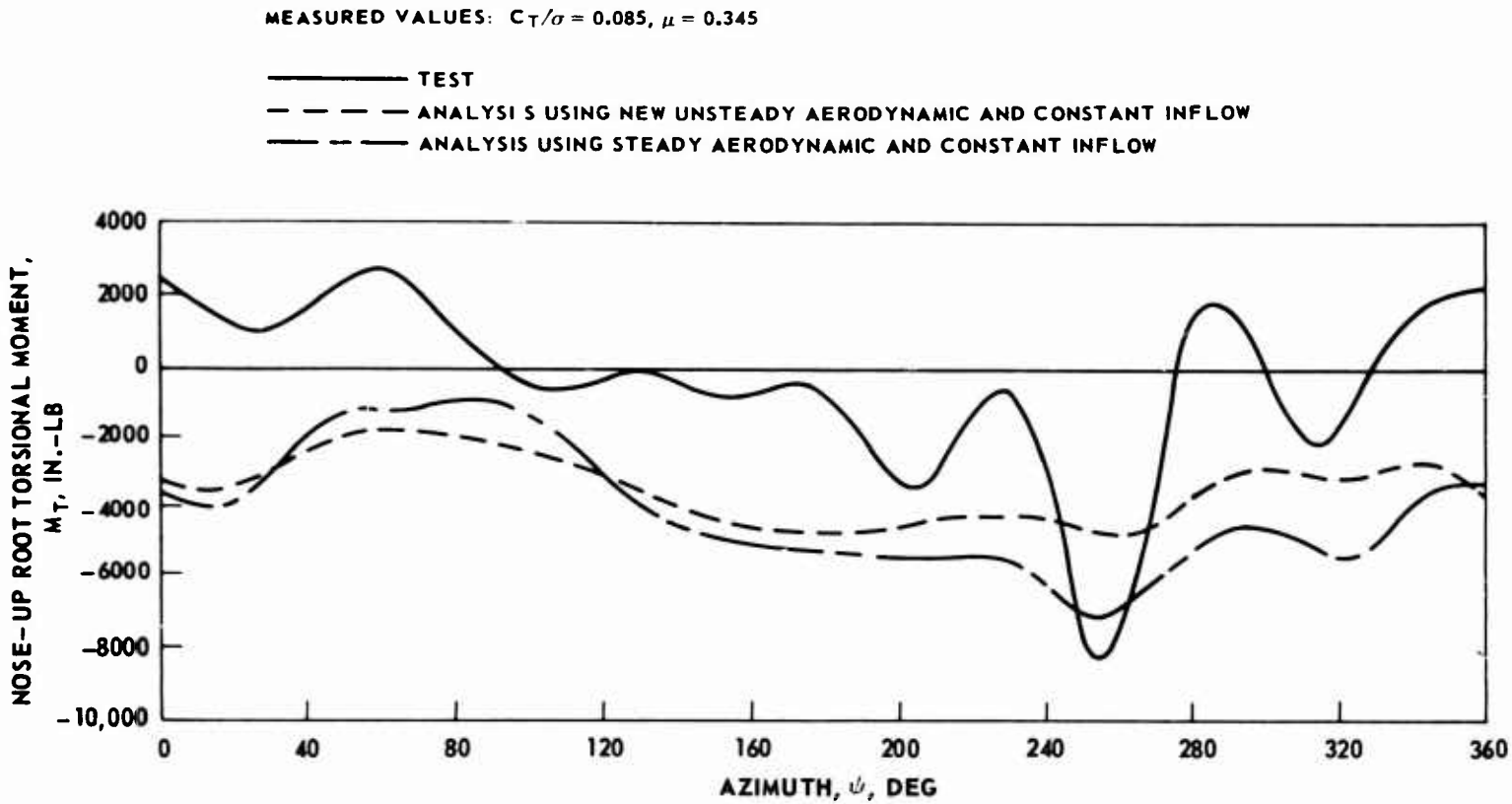

Figure 57. Torsional Response Correlation Using Steady and Unsteady Aerodynamics With Constant Inflow - NH-3A Case 72 - 60 Degree Angle of Bank, Right Turn.

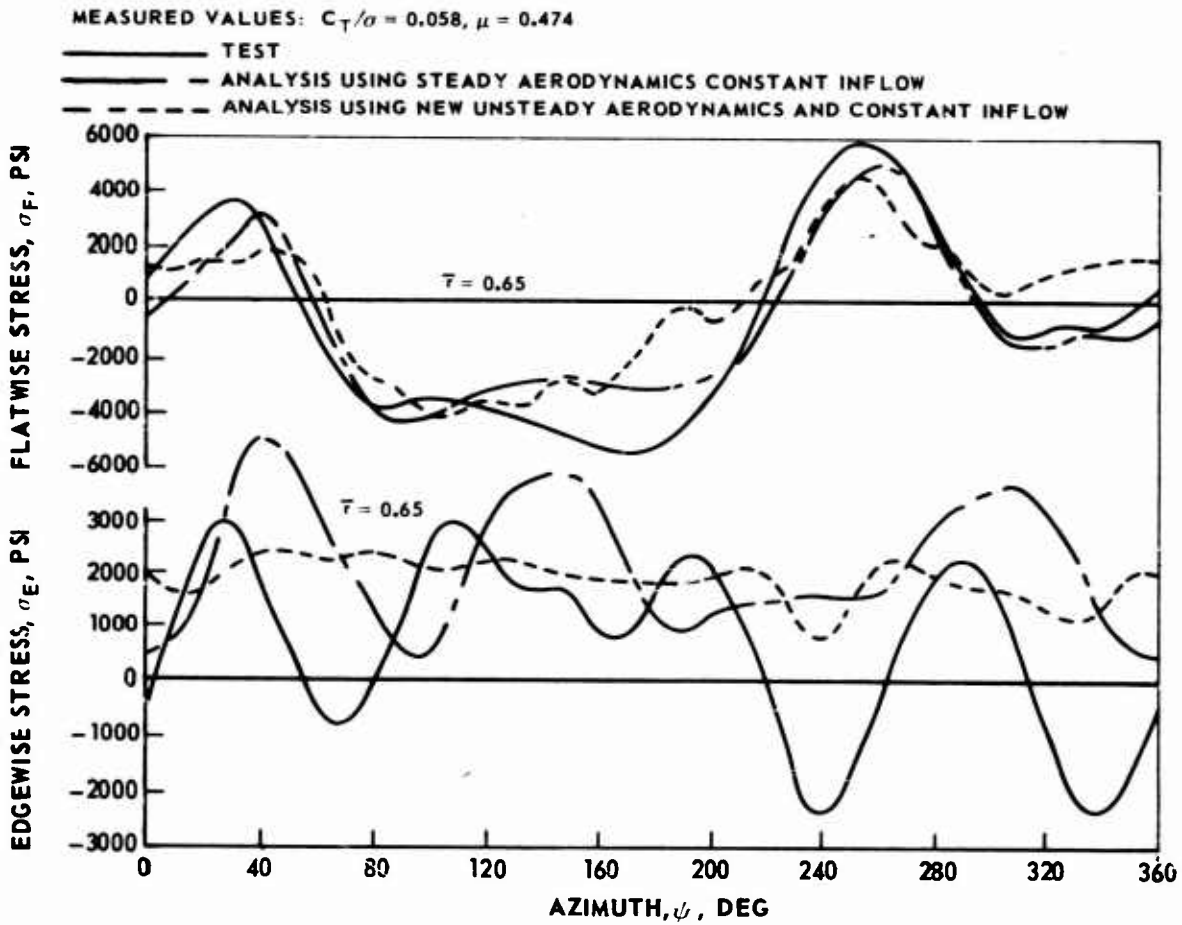

Figure 58. Correlation of Flatwise and Edgewise Stress Calculated Using Steady and Unsteady Aerodynamics With Constant Inflow - NH-3A Case 43.

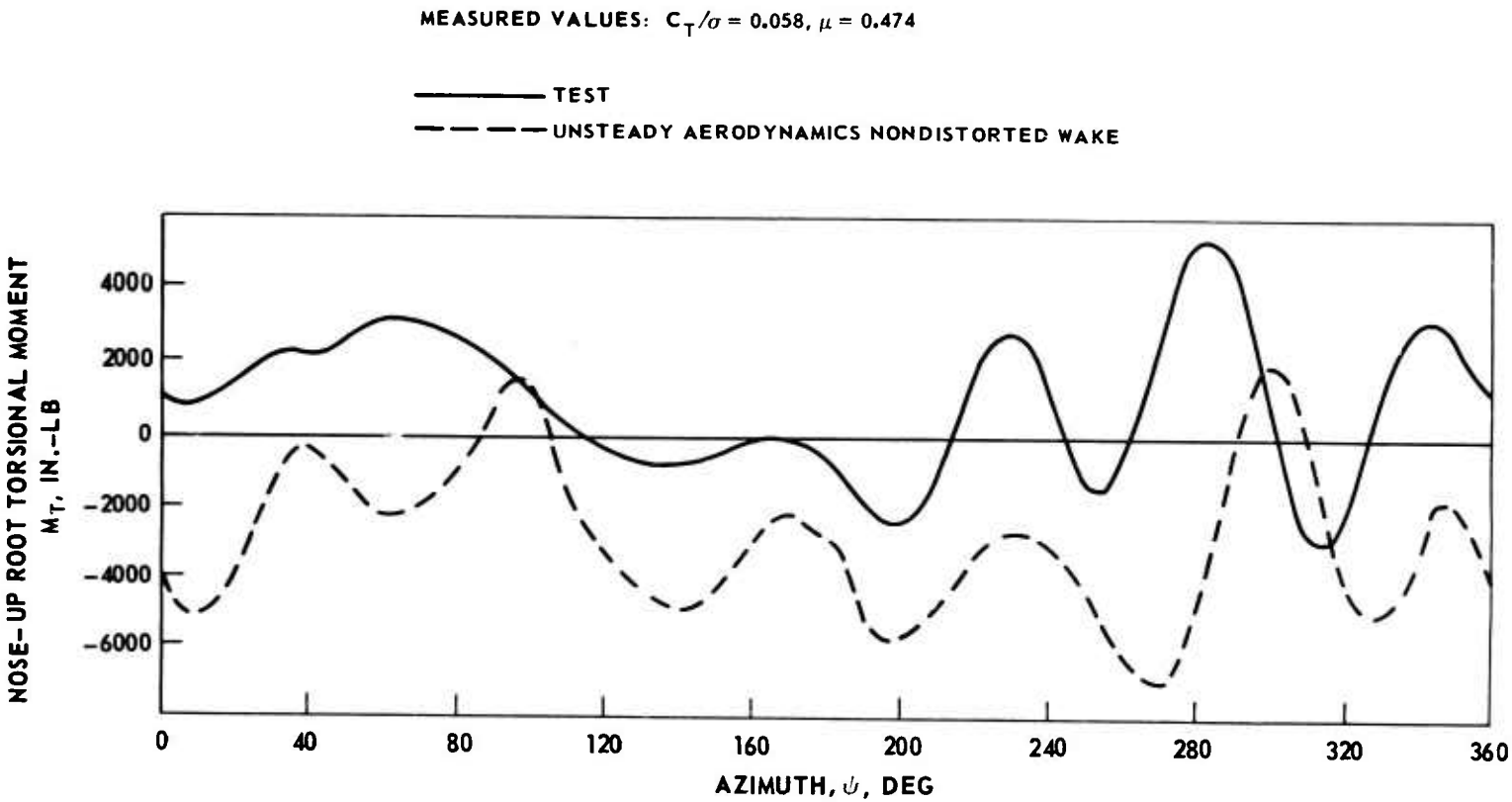

Figure 59. Torsional Response Correlation Using New Unsteady Aerodynamics and Nondistorted Wake Inflow - NH-3A Case 43.

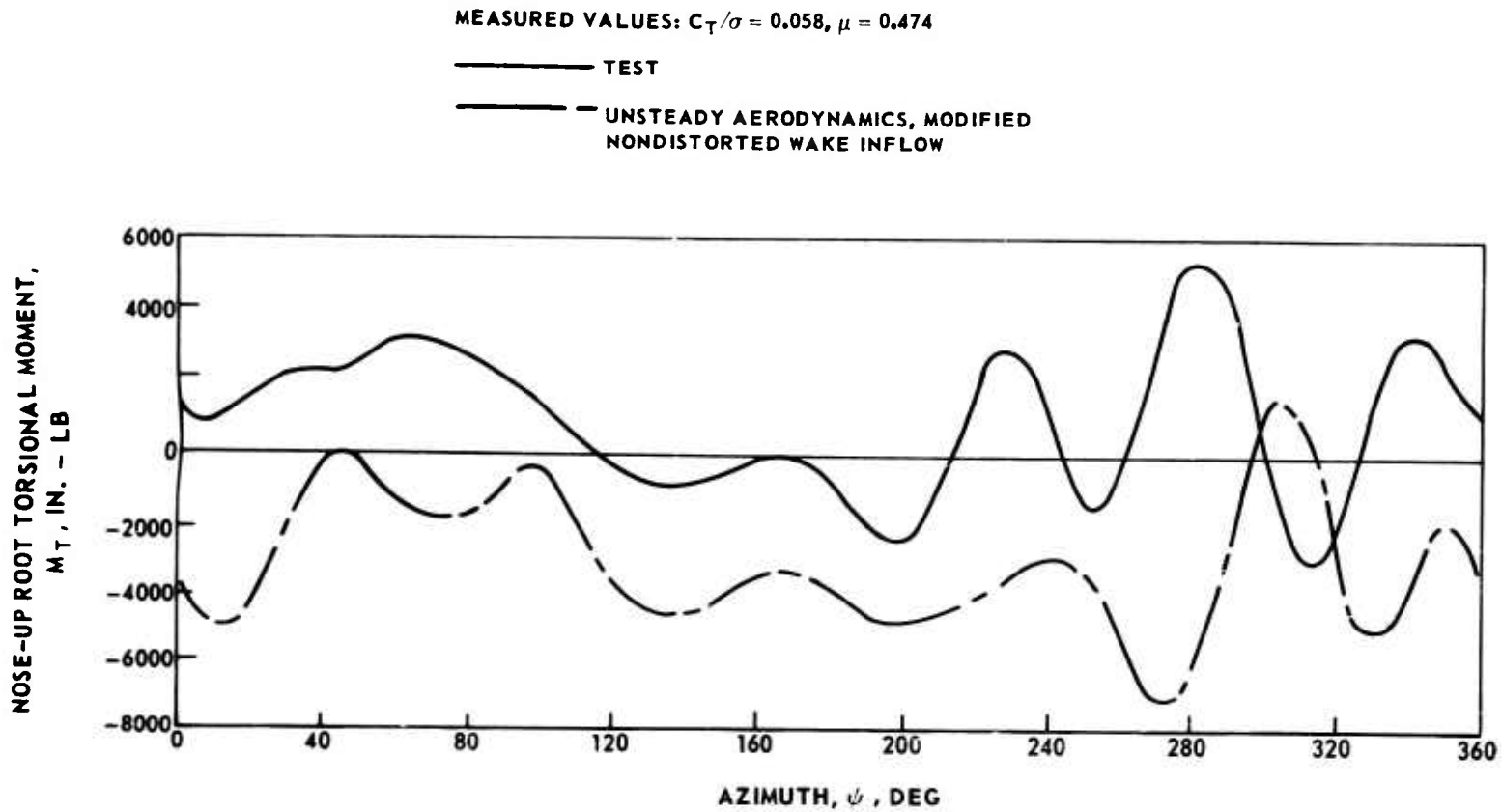

Figure 60. Torsional Response Correlation Using New Unsteady Aerodynamics and Modified Nondistorted Wake Inflow - NH-3A Case 43.

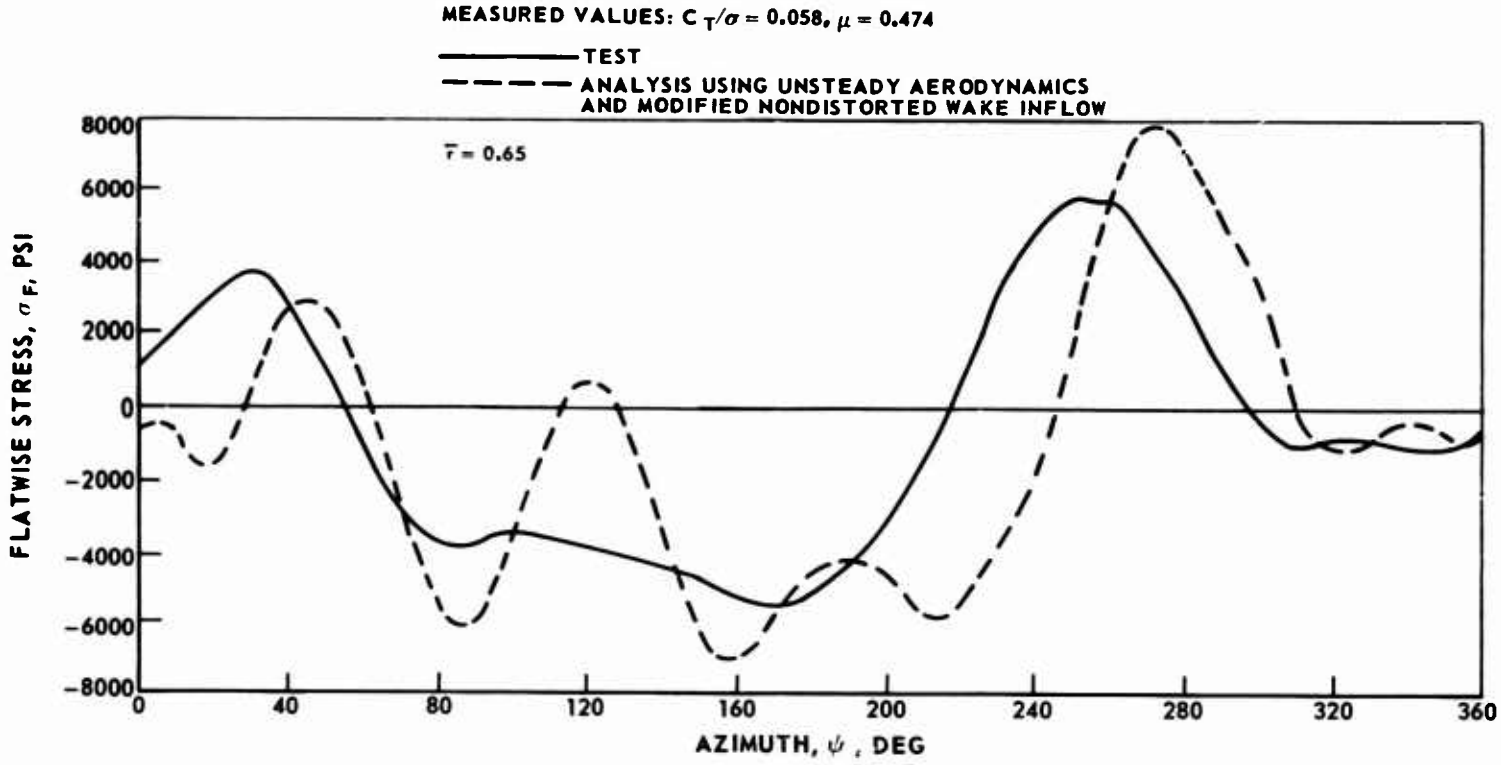

Figure 61. Correlation of Flatwise and Edgewise Stress Using New Unsteady Aerodynamics and Modified Nondistorted Wake Inflow - NH-3A Case 43.

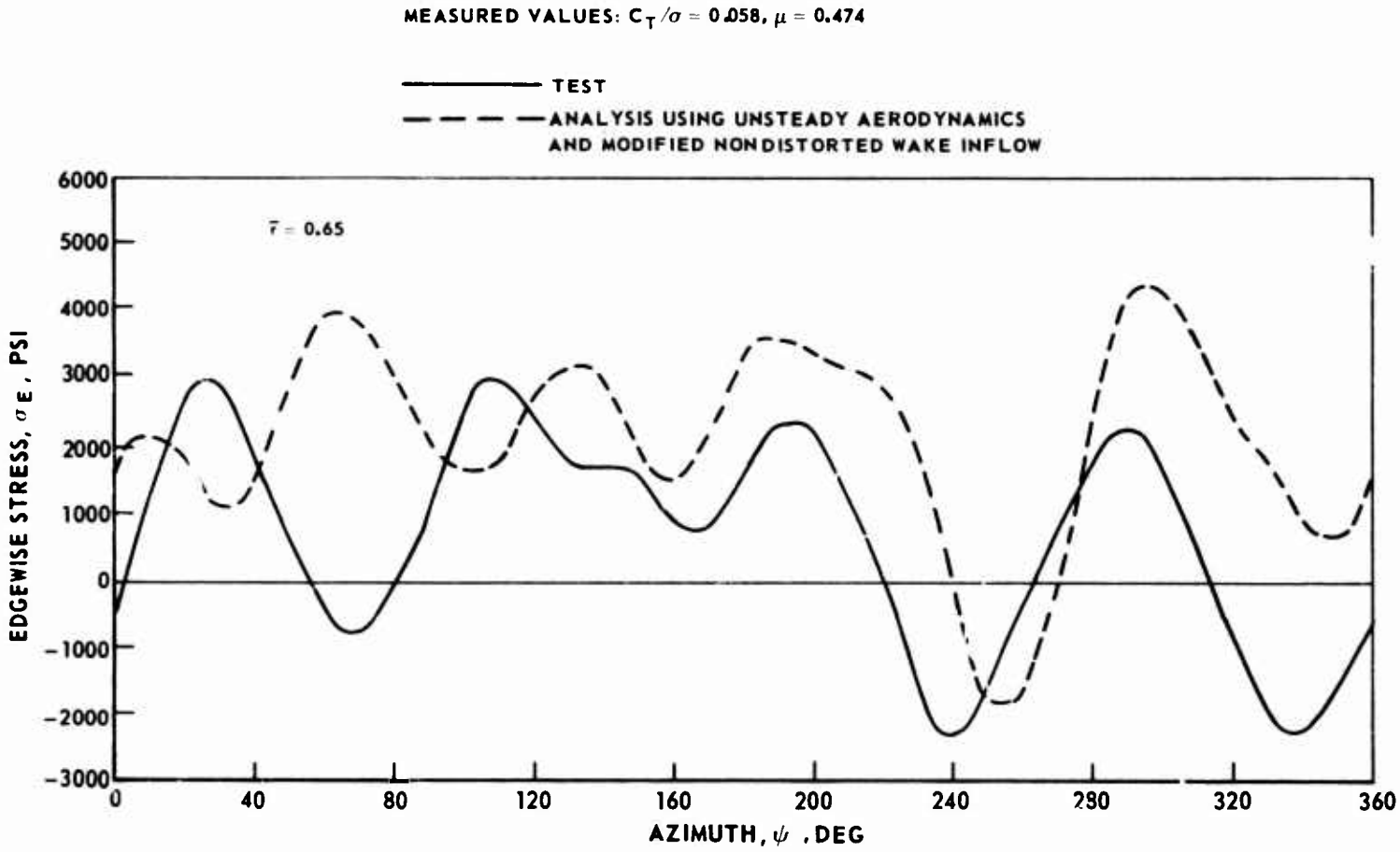

Figure 61 - Continued.

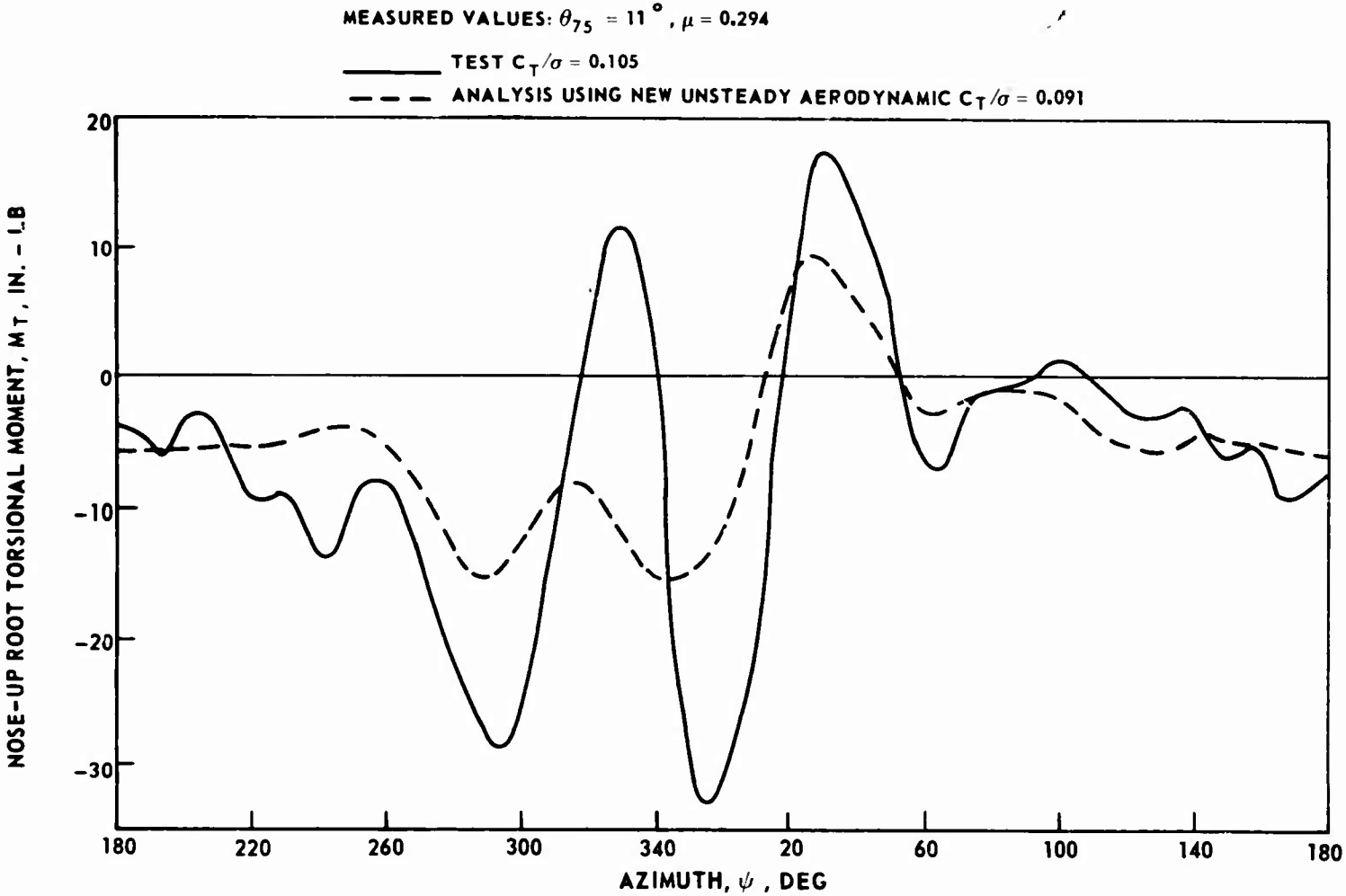

Figure 62. Torsional Response Correlation Using New Unsteady Aerodynamics - Model Rotor Case 68-6.

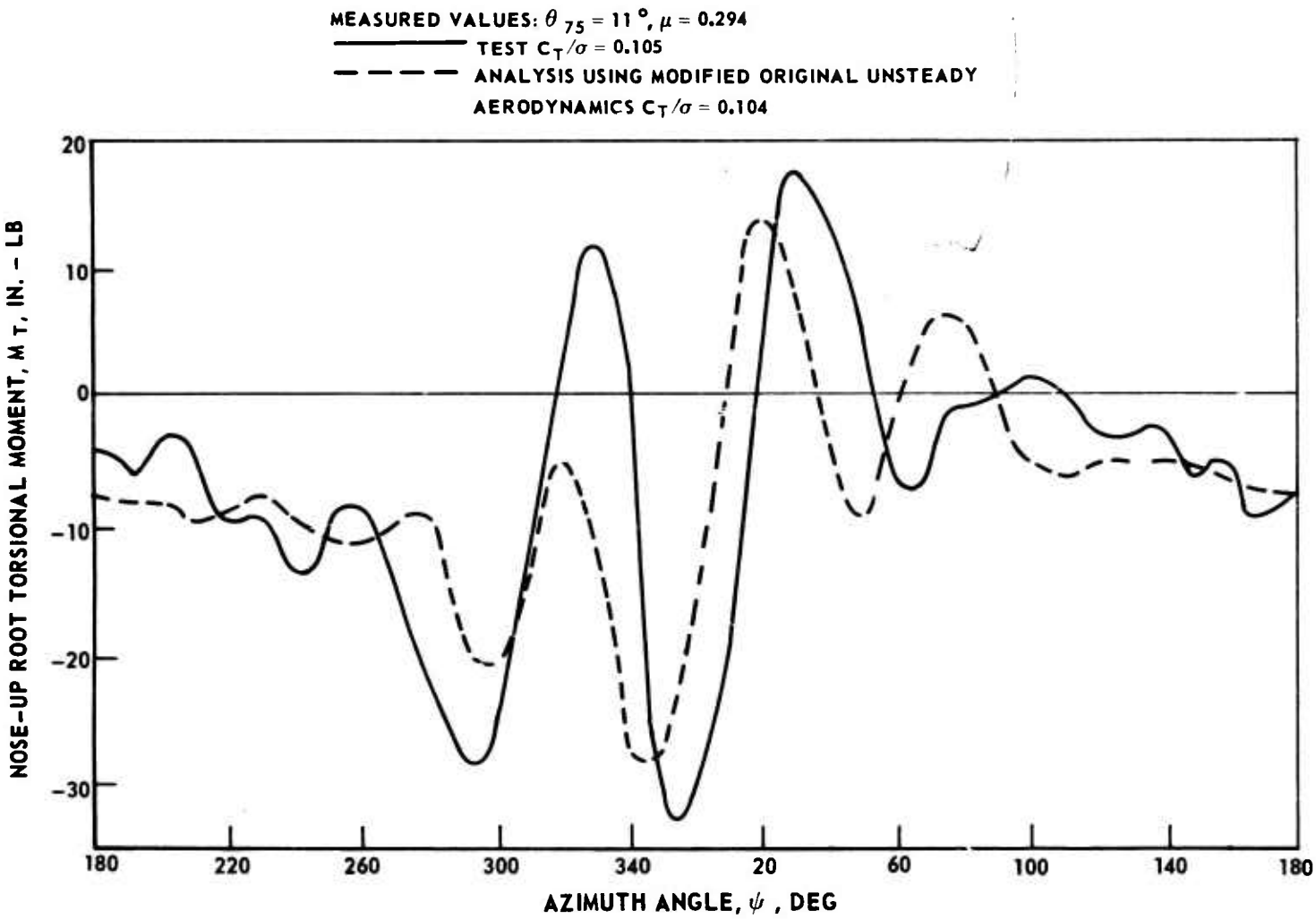

Figure 63. Torsional Response Correlation Using Original Unsteady Aerodynamics - Model Rotor Case 68-6.

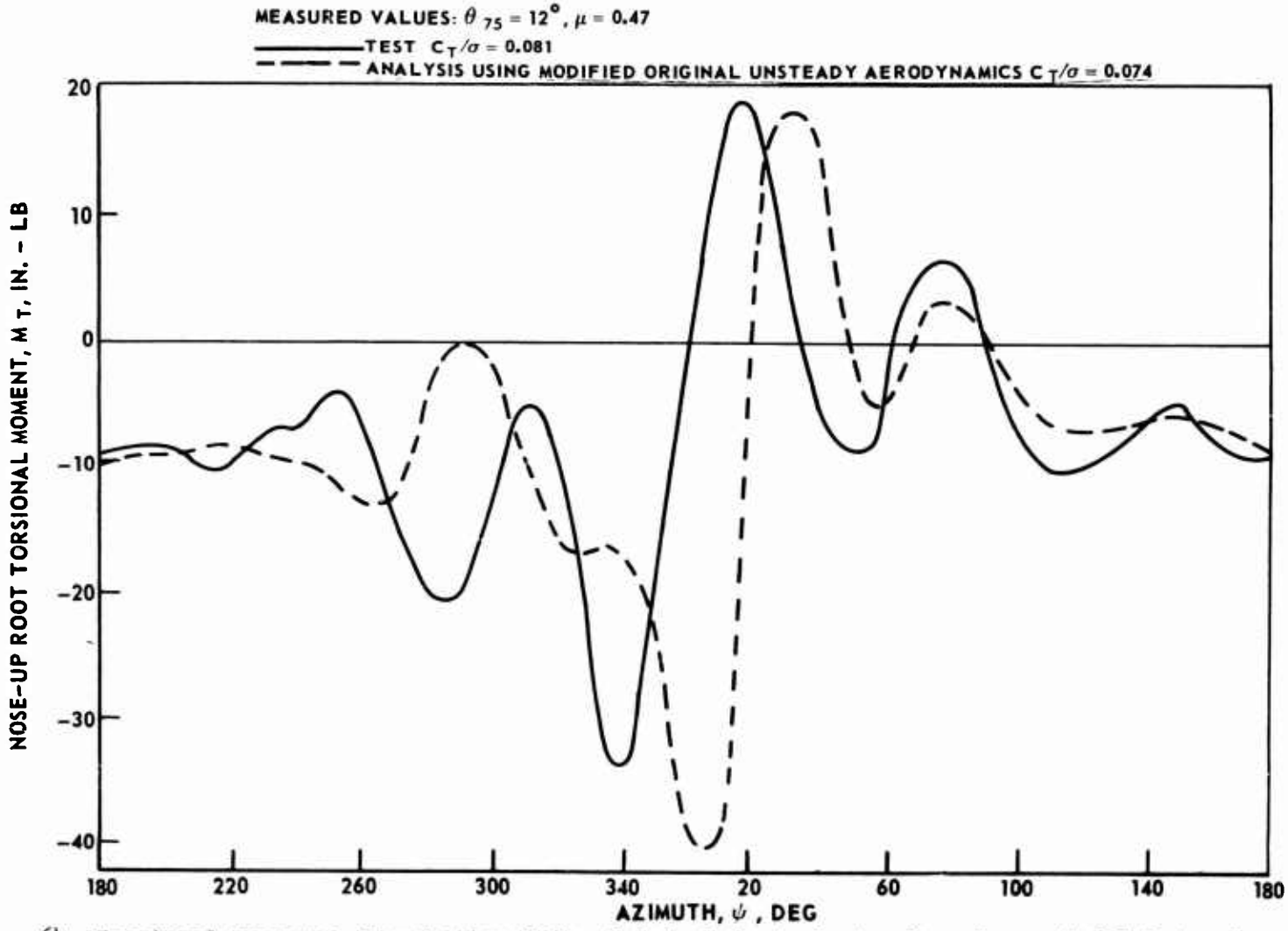

Figure 64. Torsional Response Correlation Using Original Unsteady Aerodynamics - Model Rotor Case 51-11.

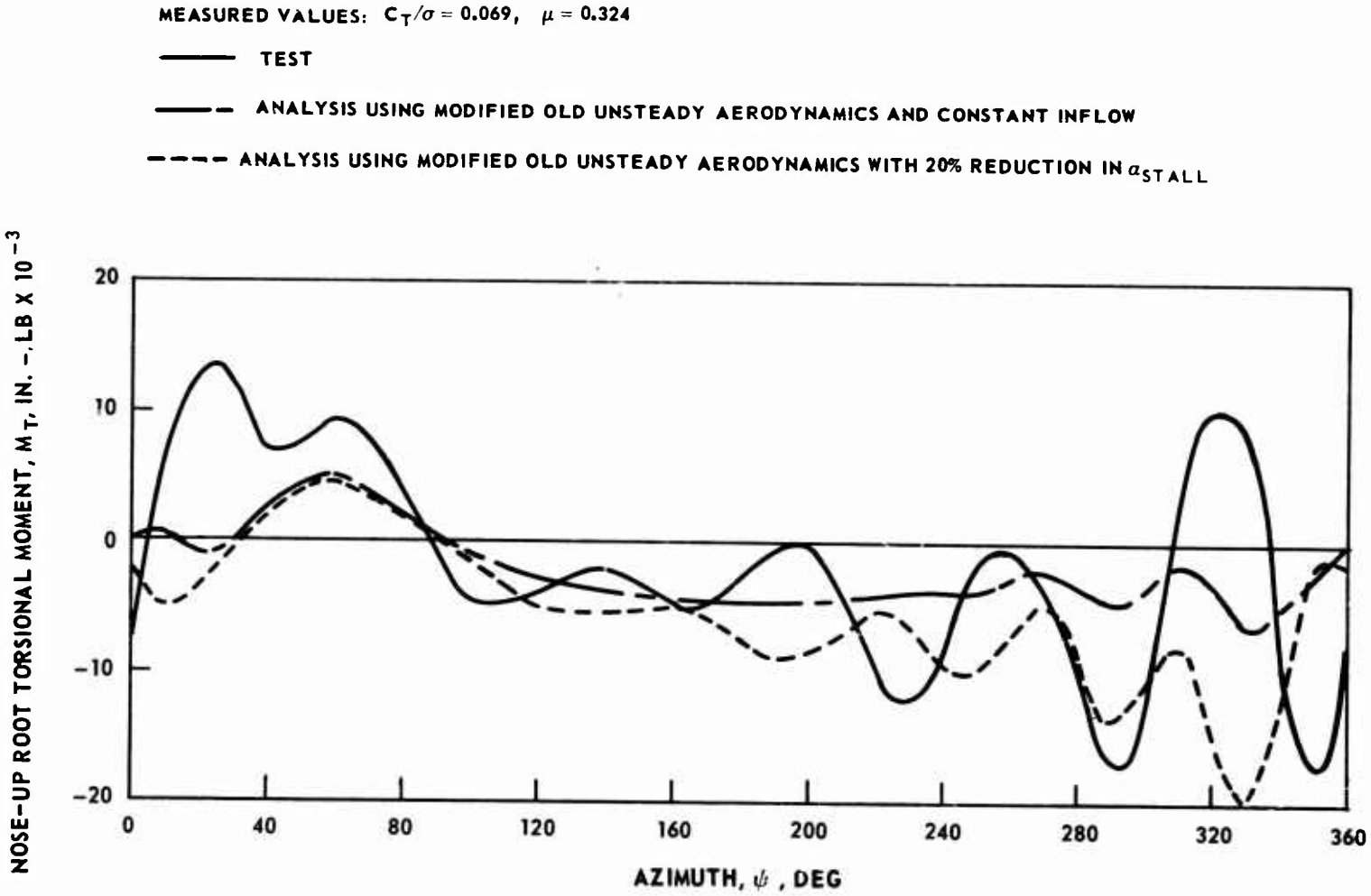

Figure 65. The Effect of Lowering Blade Stall Angle on Torsional Response Correlation - CH-53A Case 55.

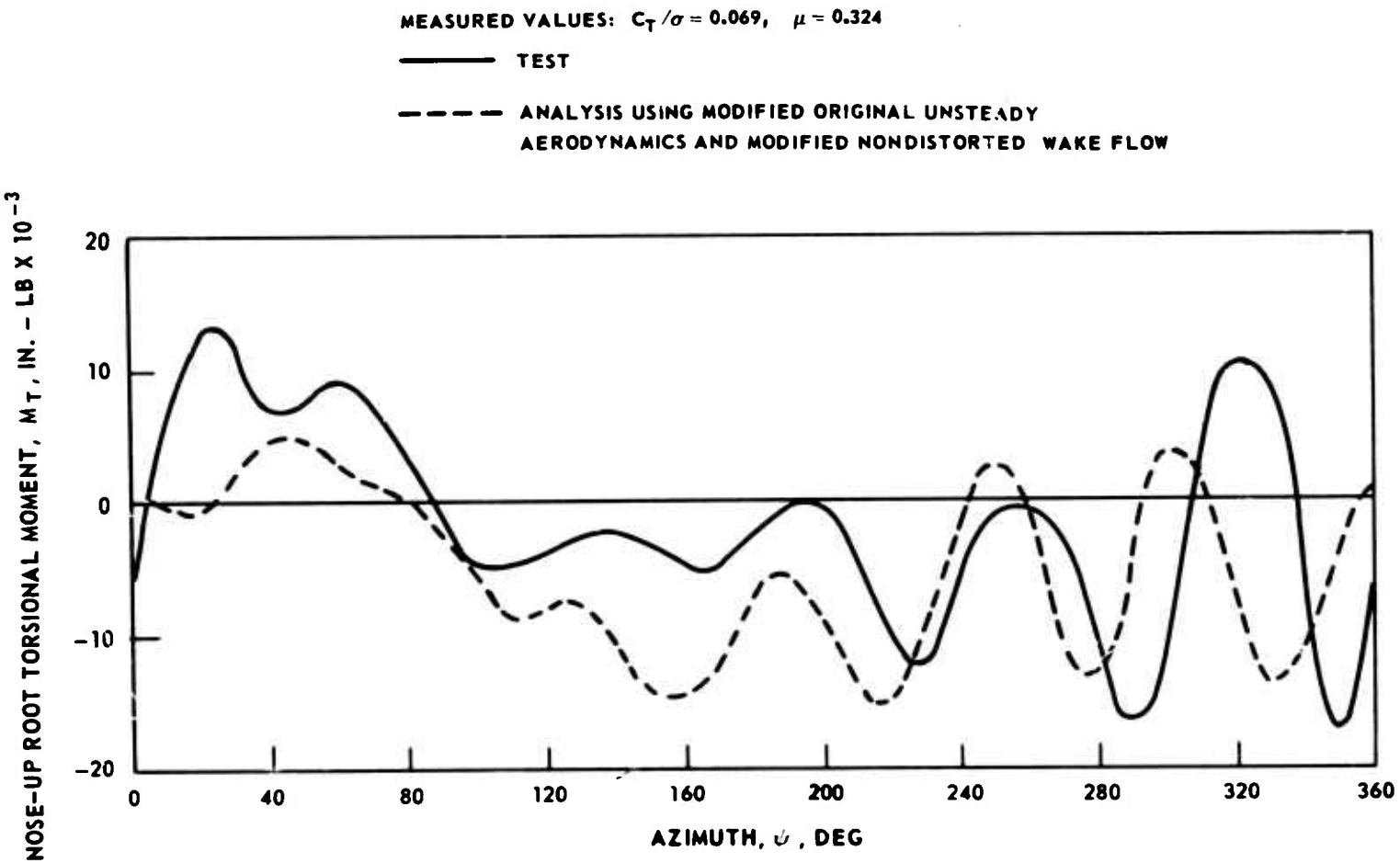

Figure 66. Torsional Response Correlation Using Original Unsteady Aerodynamics and Modified Nondistorted Wake Inflow - CH-53A Case 55.

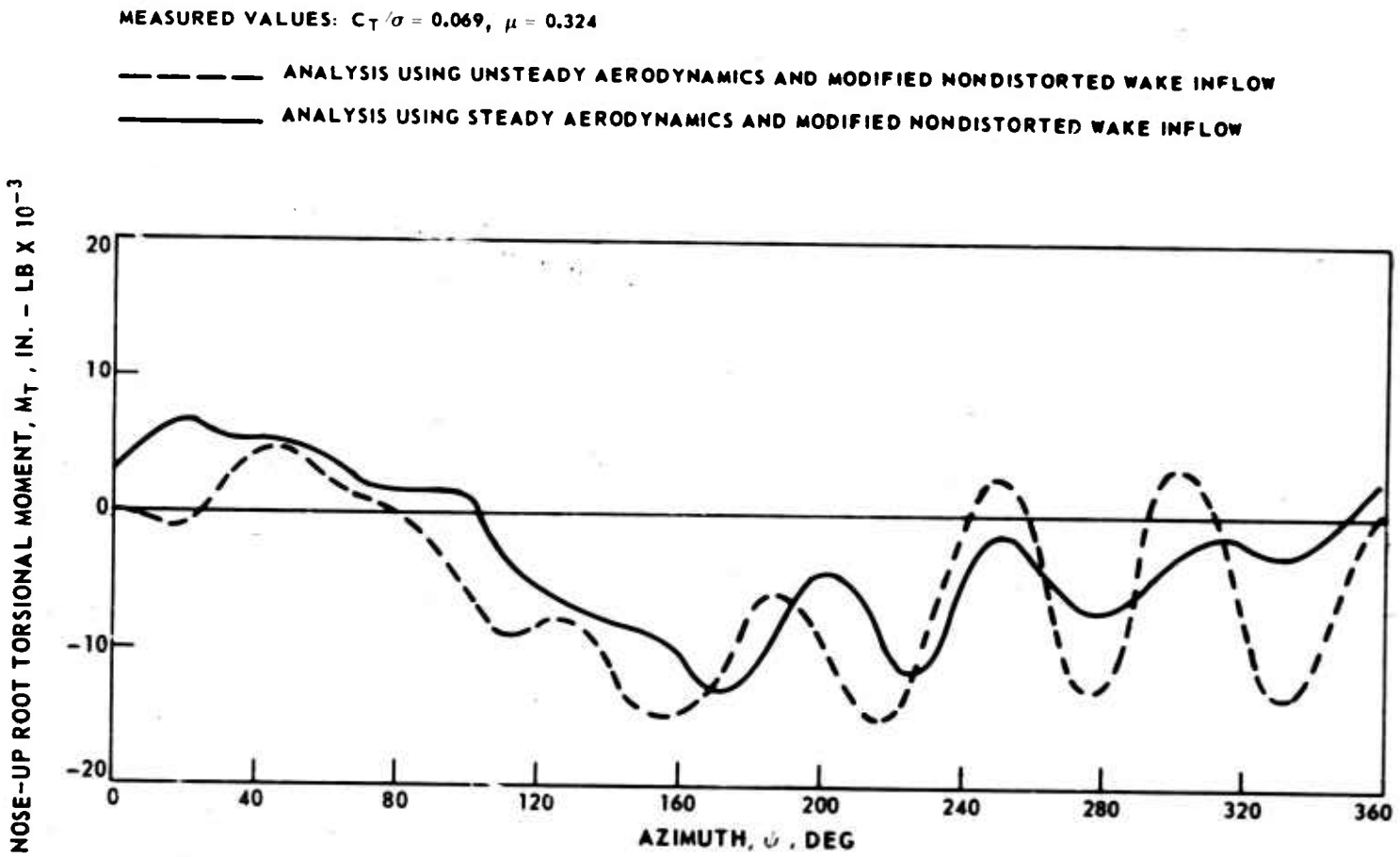

Figure 67. Torsional Response Calculated Using Steady and Unsteady Aerodynamics and Modified Nondistorted Wake Inflow - CH-53A Case 55.

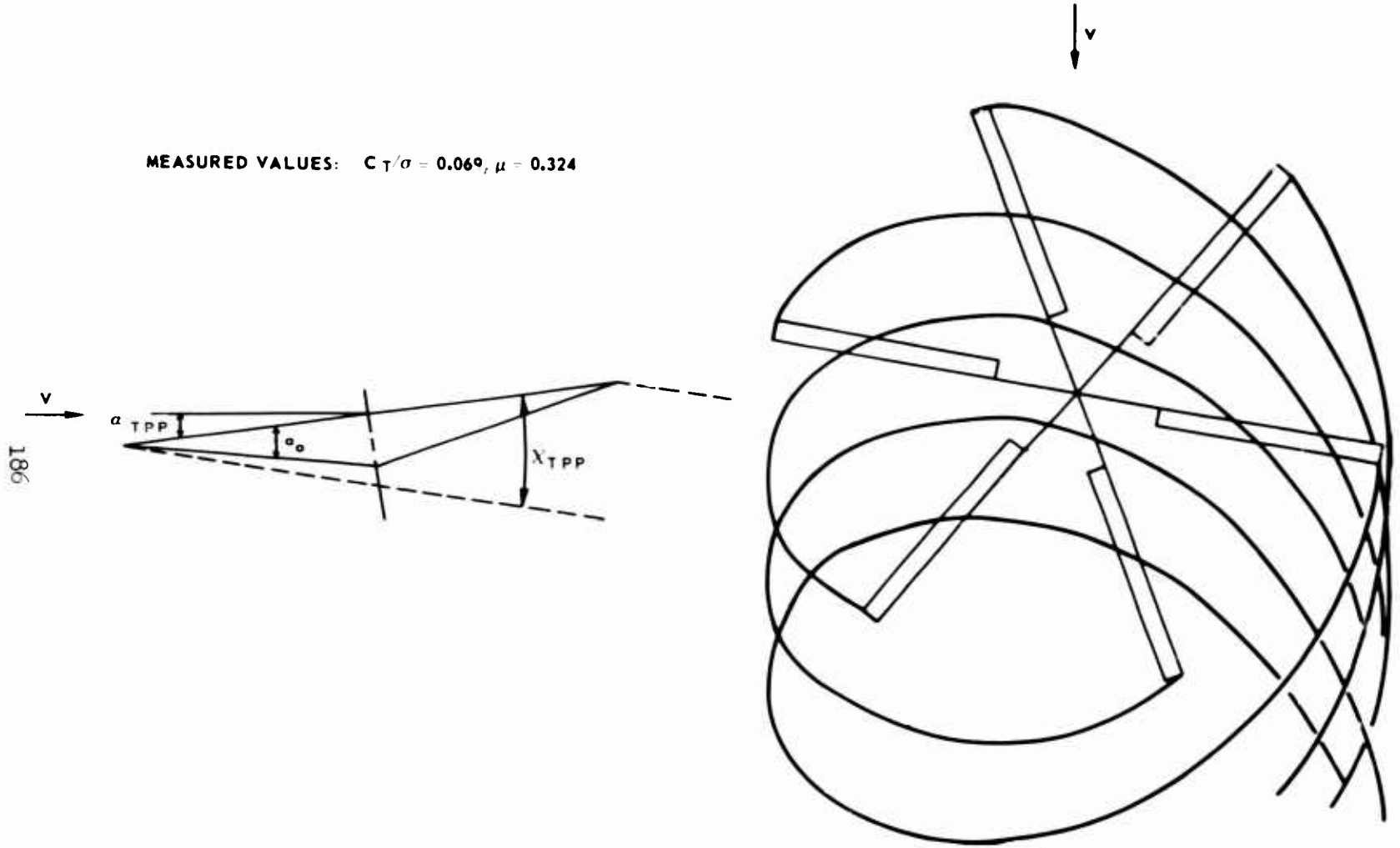

Figure 68. Wake Geometry - CH-53A Case 55.

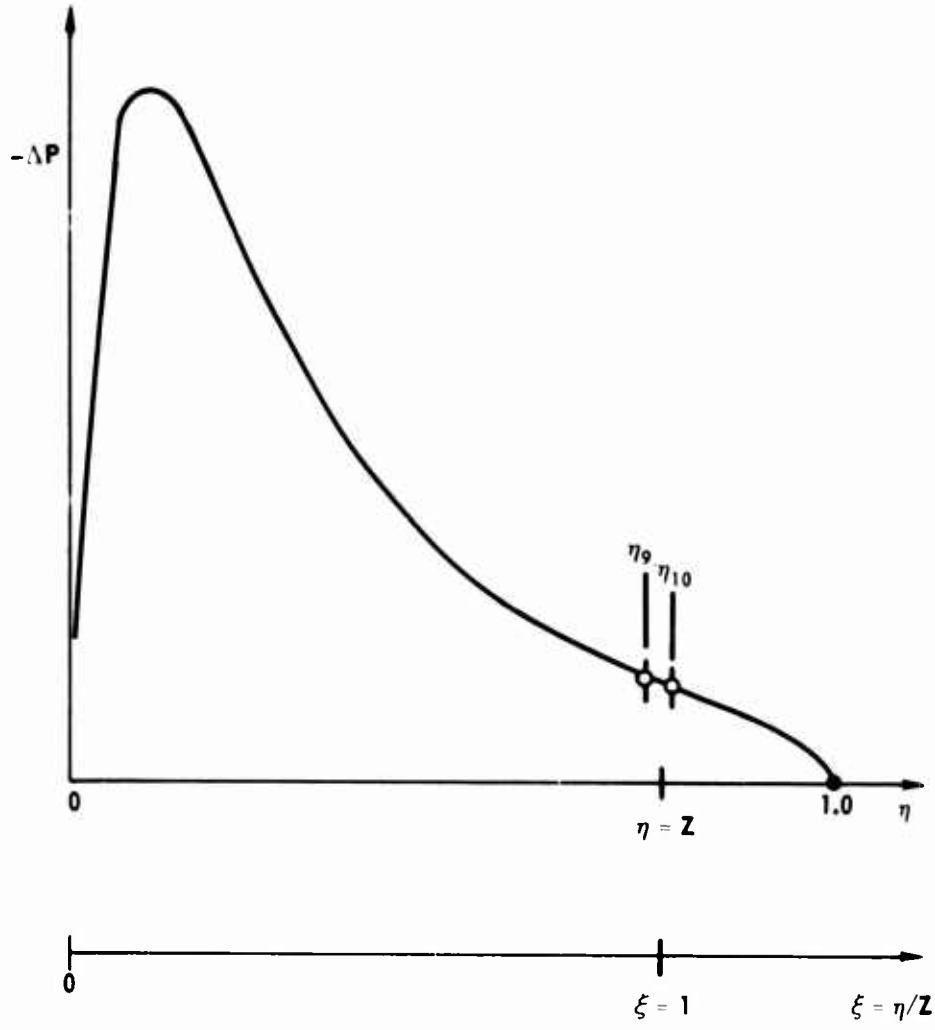

Figure 69. Schematic Representation of Numerical Integration Procedure.